The purification and *in vitro* motility analysis of *Drosophila melanogaster* ACT88F mutants.

Thesis submitted for the degree of
Doctor of Philosophy
by
Azam Razzaq, 1995.

Department of Biology,
University of York.

ABSTRACT

The indirect flight muscle (IFM) specific ACT88F actin isoform of *Drosophila melanogaster* was purified from flies on both a large and small scale. The development of a mini-actin purification protocol allowed the isolation of pure ACT88F actin from ten pairs of dissected IFMs in sufficient quantities, (approximately 5μg), for many *in vitro* motility assays. An actin preparation, starting with 10,000 flies, (10g), was also developed, using anion exchange chromatography to isolate the ACT88F isoform from the five other *Drosophila* isoforms. Milligram quantites of ACT88F, containing a 10% "contamination" of an unknown type III actin isoform, provide sufficient material for the future *in vitro* biochemical and kinetic characterisation of ACT88F mutants.

The *in vitro* motility of four ACT88F mutants, *G368E*, *E316K*, *E334K* and *E93K* was investigated using a rabbit skeletal muscle HMM. A significant 35% reduction in *G368E* filament velocity under standard assay conditions (SAC) was also seen when under various ionic and ATP concentrations. *E316K* only showed a significant 36% reduction in its filament velocity at limiting ATP concentrations. Under all conditions in the motility assay, *E334K* mutant filaments displayed no *in vitro* movement. Where wild-type (WT) actin washed off the surface at 50mM KCl in the motility assay, *E334K* actin dissociated at 30mM KCl. Three copolymers of *E334K* and WT actin, each representing a different proportion and distribution of mutant monomers in the cofilament, were all able to move under SAC. As the percentage fraction of *E334K* actin in the cofilament was increased, filament velocity decreased. Although *E93K* actin filaments washed off the surface under standard assay conditions, binding to, and movement of this mutant over the surface was seen at lower ionic strengths, albeit with a significant 50% reduction in filament velocity. These results are discussed with respect to the atomic structure of actin and the model of the actin-S1 reconstruction.

ACT88F was expressed in *Saccharomyces cerevisiae*. The expression of WT and six ACT88F mutants was confirmed by two-dimensional gel electrophoresis and/or Western blotting with actin specific antibodies. However, the levels of recombinant protein were not great enough to support *in vitro* biochemical studies.

For my Mam and Dad

Declaration

This thesis represents my own, unassisted work and has not been submitted for a previous degree or accepted for publication.

Acknowledgements

I would like to thank Dr. John Sparrow for giving me the opportunity to work in his laboratory and for all of his help and support during the course of this thesis. Additionally, I am extremely grateful to Dr. Justin Molloy for all of his helpful discussions, excellent ideas and spoonerisms. I am also indebted to Dr. Roger Karlsson and Professor Uno Lindberg for their kind hospitality during my stay in Stockholm. Thanks also to Anne Lawn for invaluable technical assistance, Dr. Nic Carter for making my life much easier during endless "tracking" and Dr. Marie-Christine Lebart for her suggestions on the affinity chromatography purification.

A very big thank you to Daniel Lawson, Nicky Rolley and Dr. Jo Bentley for all their help with references and figures. Finally, I would like to give special thanks to my mam and dad for all their help and support over the years.

CONTENTS

List of Figures

(the figures that are not on numbered pages are referenced with respect to the preceding numbered page).

List of Tables

(the tables that are not on numbered pages are referenced with respect to the preceding numbered page).

ABBREVIATIONS

A	Actin
Å	10^{-10}m (angstrom)
AB	Assay buffer
A_{cc}	Critical concentration for actin polymerisation
ACEX	ACtin EXtraction buffer
ADP	Adenosine triphosphate
ATG	Initiator methionine codon
APS	Ammonium persulphate
ATP	Adenosine triphosphate
ATPase	Adenosine triphosphatase
AUFS	Absorbance units full-scale
bp	Basepairs (of DNA)
BSA	Bovine serum albumin
cDNA	coding DNA
d	Step size
DEAE	Diethylamino ethyl cellulose
DLMs	Dorsolongitudinal muscles
DVMs	Dorsoventral muscles
DNA	Deoxyribonucleic acid
DNaseI	Deoxyribonuclease I
dNTPs	Deoxyribonucleotide triphosphates
dpsm	Dephosphorylated smooth muscle myosin
DTT	Dithiothreitol
ECL	Enhanced chemiluminescence
EDC	1-ethyl-3-(dimethyl aminopropyl)-carbodimide
EDTA	Ethylenediaminetetraacetic acid
EGTA	Ethylene glycol-bis(β-aminoethyl ether) N, N, N',N'-Tetraacetic acid
EM	Electron microscopy
EMS	Ethylmethanesulphonate
EPI	Ethanol-based protease inhibitor
f	Duty ratio
FITC	Fluorescein isothiocyanate
FPLC	Fast performance liquid chromatography
GAPH	Glyceraldehyde-3-phosphate dehydrogenase
HMM	Heavy mero-myosin
HPLC	High performance liquid chromatography
HRP	Horse-radish peroxidase
Hsc70	Heat shock cognate protein
IFM	Indirect flight muscle
IPTG	Isopropylthio-β-galactosidase
kb	Kilobase (1000 bp)
KDa	Kilodaltons

KRP	Kinesin related protein
LMM	Light mero-myosin
M	Myosin
MLF	Minimum length filaments
MOPS	3-(N-morpholino)propanesulphonic acid
mRNA	Messenger ribonucleic acid
MW	Molecular weight
N	Number of filaments
NEM	N-ethyl-maleimide
NP40	Nonidet P40
O.D.	Optical density
PAGE	Polyacrylamide gel electrophoresis
PCR	Polymerase chain reaction
PEGxxxx	Polyethylene glycol (xxxx MW)
PGK	Phosphoglycerate kinase
P_i	Inorganic phosphate
pI	Isoelectric point
PMSF	Phenylmethylsulphonyl fluoride
pPDM	N, N'-p-phenylenedimaleimide
psm	Phosphorylated smooth muscle myosin
rATP	ribose ATP
rpm	Revolutions per. minute
RNA	Ribonucleic acid
RSCU	Relative synonymous codon range
RT	Room temperature
S1	myosin head fragment
S2	myosin upper rod fragment
SAC	Standard assay conditions
SDS	Sodium dodecyl sulphate
sm	Skeletal muscle myosin
Tris	Tris(hydroxymethyl)amino methane
t_c	Duration of the ATPase cycle (total cycle time)
TEMED	N, N, N', N'-Tetramethylethylethylenediamine
TH1	Tail homology domain 1
tRNA	Transfer ribonucleic acid
t_s	Time spent in the strongly bound actomyosin state
UTR	Untranslated region
UV	Ultraviolet radiation
UYM	Ura^- medium
v_i	Limited filament velocity
v_0	Maximal filament velocity
v_f	*In vitro* filament velocity
(v/v)	Volume:volume ratio
WPI	Water-based protease inhibitors
WT	Wild type

(w/v)	Weight:volume ratio
X-gal	5-bromo-4-chloro-indoyl-β-galactopyranoside
YMG	York modified glycerol

CHAPTER ONE: INTRODUCTION

1.1 Molecular motors

Movement is a fundamental characteristic of biological organisms which adopts various guises ranging from whole cell motility, the intracellular translocation of organelles and vesicles, cytokenesis and muscle contraction. Three specialised groups of "motor" proteins, the myosins, kinesins and dyneins, are responsible for powering most, if not all, of these movements in conjunction with their complementary cytoskeletal polymers. Whereas myosins associate with actin filaments, the kinesins and dyneins are examples of microtubule based motors.

The gross quaternary organisation of these structurally and functionally diverse motor proteins contains analogous elements that conform to a general, consensus plan of domain arrangement. This is represented by an enzymatic domain attached to a unique and functionally specialised cargo domain. These cargo, or "tail", domains possess specific sites along their length, or attached to their extreme C-termini, which serve as adaptors, allowing motors to associate with many different structural components within the cell. The enzymatic "head" domain harbours a single site for binding ATP and one for the cytoskeletal polymer. Through the conversion of chemical energy, derived from ATP hydrolysis, into mechanical work, this domain generates a movement of the whole motor molecule with the attached cargo, along its complementary cytoskeletal "track".

The abundance of motile behaviours within a cell may be generated by the alternative arrangements of the motors and their respective cytoskeletal polymers. It was originally suggested that the variability in the cargo domains, in terms of their primary sequence, size and overall structure, defined the basis for the vast range of motility phenomena and that the enzymatic "motor" domains were simply interchangeable units. However, Goodson and Spudich (1993) have demonstrated through phylogenetic studies that since the head and tail domains in particular motors have

evolved in concert, motile properties are probably a consequence of a unique functionality of a particular tail coupled to that of its head.

Myosin, kinesin and dynein each represent a superfamily of proteins comprising a large and ever expanding number of classes. The subgroups within each superfamily exhibit a high degree of sequence homology in localised regions of their motor domains, emphasising the conservation of vital functions during evolution. These highly conserved mechanochemical domains have enabled the rapid discovery of new members of each superfamily by the molecular genetic analysis of existing mutations coupled to data base searches for homologous protein sequences, and PCR and antipeptide antibody based screens.

Despite the abundance of these motor protein families, the mechanism by which they convert chemical energy into mechanical force is still not fully understood. Myosin is the most studied of the motors and several models for its mode of action describe a conformational change in its enzymatic domain that drives the subsequent displacement of bound actin filaments (Huxley, 1969; Rayment *et al.*, 1993b). Although the myosins and kinesins are thought to interact specifically with their respective cytoskeletal polymers, the generality of the force producing mechanism for myosin may still apply to kinesin operations.

To achieve a complete comprehension of mechanochemical transduction, a number of fundamental questions concerning the action of single motor-polymer complexes have to be answered. The first regards the size of a single "working stroke" which represents the physical displacement of the motor-bound cytoskeletal polymer upon a single conformational change in the enzymatic domain. The second quantity regards the "step size". This is a measure of the physical distance moved by the motor molecule during a single ATP hydrolysis event. Although there has been a great conflict in the magnitude of these measurements in the past (Toyoshima *et al.*, 1990; Uyeda *et al.*, 1991; Harada and Yanagida, 1988; Harada *et al.*, 1990) the recent advances in biophysical technology are producing estimates that are in agreement with

the currently accepted structural model (Finer *et al.*, 1994; Ishijima *et al.*, 1994; Molloy *et al.*, 1995; Nature in press; Rayment *et al.*, 1993a, 1993b).

1.1.1 Microtubule based motors

The motor and tail units of the microtubule based motors, kinesin and dynein, exhibit an alternative arrangement into the consensus quaternary structure. Whereas the motor domain in kinesin is located at the N-terminus (Bloom and Endow, 1994) it resides at the C-terminus in dynein. Consequently, these two motors mediate movement in opposite polarities over the same cytoskeletal polymer, that of kinesin being directed to the plus ends (fast polymerising/depolymerising) of the microtubules and that of dynein being minus-end directed.

1.1.1.1 Kinesin

Conventional kinesin is a tetrameric protein consisting of two heavy chains and two light chains (Bloom *et al.*, 1988), (see figure 1.1). Electron microscopy revealed that it is a long, asymmetric molecule possessing a central 80nm rod that is associated with two 10nm globular heads at one end and a feathered tail at the other (Hirokawa *et al.*, 1989). Cloning and sequencing of the cDNA for the *Drosophila* kinesin heavy chain predicted structural features which, although limited to the primary sequence level, were consistent with those from electron microscopy (Yang *et al.*, 1989).

The kinesin heavy chain has three major structural domains. A highly conserved motor domain (50KDa), predicted to have a globular structure, is located at the N-terminus of the protein. Confirmation that it possesses both the ATP and microtubule binding sites was achieved after a bacterially expressed, head polypeptide was shown to support the *in vitro* sliding of microtubules (Yang *et al.*, 1990). This head domain is attached to a 50-60KDa hypervariable stalk which is expected to form an α-helical coiled-coil, as inferred from the primary sequence, and therefore enable the dimerisation of two kinesin heavy chains. The third structural domain is a tail region attached to the stalk at the opposite end to the motor domain. In kinesin, this

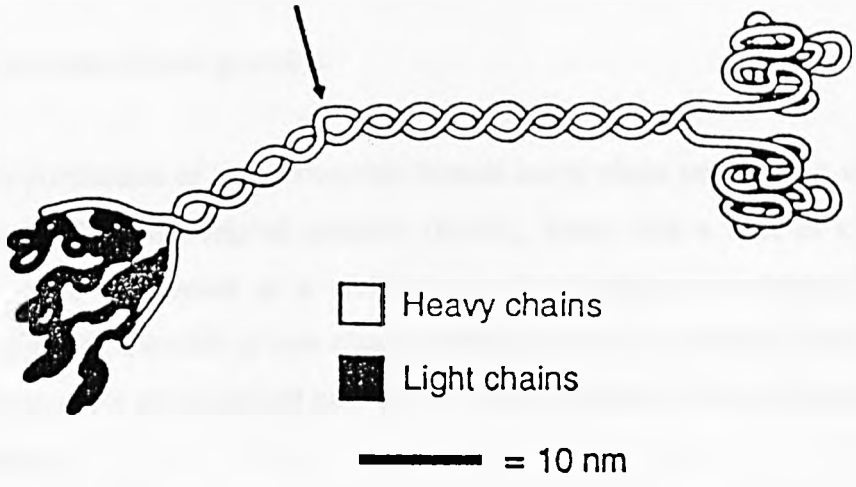

Figure 1.1. A proposed structural model for kinesin taken from Bloom and Endow, 1994. The model is not drawn to scale and is based on biochemical and EM data. The two N-terminal motor domains are drawn to the right hand side of the molecule. These are connected to the C-terminal light chains on the left by a long α-helical tail domain.

apparently globular structure is proposed to bind the light chains or a variety of membrane bound organelles.

1.1.1.2 Kinesin related proteins

Upon the publication of the *Drosophila* kinesin heavy chain sequence, a multitude of unconventional kinesin related proteins (KRPs), along with a host of conventional kinesins, were discovered in a wide range of organisms, inundating the kinesin superfamily with a wealth of new classes. Molecular genetic and biochemical analyses have subsequently characterised new KRP motors and their role in microtubule based karyokenesis.

The mechanochemical domains of each KRP generally possess a 320-340 amino acid region that exhibits a 35-45% sequence homology to the motor domain of conventional kinesin (Bloom and Endow, 1994). However, these motor proteins differ in terms of the arrangements of their three structural domains. Whereas some display a gross structure that is essentially the same as the *Drosophila* kinesin heavy chain arrangement, others such as Kar3 and ncd have an inverted structure in which the mechanochemical domain is located at the C-terminus and the tail domain at the N-terminus. These unusual domain arrangements were shown to confer minus-end directed movement upon the Kar3 (Endow, 1994) and ncd motors.

In association with the conventional kinesin motors which translocate membranous structures around the cell, the KRPs perform essential roles in chromosome and spindle movements during mitosis and meiosis (Sawin and Endow, 1993). Novel motors such as Kar3 and ncd demonstrate that the other motor superfamilies may possess equivalent extraordinary motors designed to tackle specialised motile processes.

1.1.2 Actin based motors

Myosins are the most abundant of the motor proteins and were first isolated from muscle tissue. The discovery of new members of this motor superfamily is progressing at an explosive rate. There are a number of criteria that are used to classify myosins and to identify new class members. These are defined by an ability to bind actin and the possession of an actin-activated ATPase activity. An additional ability to convey actin filament movement during the *in vitro* motility assay provides conclusive proof that the motor is myosin.

Primary sequence comparisons are also used to identify members of the myosin family. All myosins possess at least a single heavy chain which is predicted to have an N-terminal head domain and a C-terminal tail domain. Each heavy chain is also thought to be associated with at least a single light chain, which in some cases is represented by a calmodulin molecule. The binding site for these is recognised by the presence of IQ motifs in the heavy chain sequence. The enzymatic head domains possess a high degree of sequence homology that has served as a "molecular handle" for genetic and PCR-based approaches to detect new myosin classes. To date, there are thought to be at least ten major classes, (I-X), within the myosin superfamily that are classified according to their oligomeric state, functional properties and sequence homologies.

1.1.2.1 The conventional class II myosins

The skeletal muscle, non-muscle and cytoplasmic myosin II isoforms were the founding members of the myosin superfamily. Since the primary sequence of their tail domains exhibits a regular heptad amino acid repeating motif, two tails can associate through the formation of an α-helical coiled-coil structure to generate myosin heavy chain dimers. These myosins possess two N-terminal head domains and are subsequently denoted as the class II myosins. At low ionic strengths, these "conventional" heavy chain dimers can also self-assemble via their coiled-coil tails to form bi-polar, thick filaments that generally display a helical repeat of 140Å (Lowey *et al.*, 1969).

The C-terminal "neck" of each head domain in a class II myosin dimer associates with two light chains (Rayment *et al.*, 1993a) generating what is essentially a hexameric molecule. The two light chains are termed the essential and the regulatory light chains and are thought to directly regulate the actin activated myosin ATPase activity in some species (Sellers and Homsher, 1991). Analysis of the light chain primary sequences reveals homology to the calcium binding proteins, calmodulin and troponin-C (Collins and Matsudaira, 1991).

In addition to a well documented role in muscle contraction, class II myosin isoforms also play essential roles in cellular processes such as cell motility, cytokenesis, phagocytosis and cytoplasmic streaming, the latter being a phenomenon associated with the intracellular translocation of membranous organelles.

1.1.2.2 The unconventional myosins

The first "unconventional" myosin was indirectly discovered in the search for cytoplasmic myosins in *Acanthamoeba castellanii* (Pollard and Korn, 1973). Although this motor protein bound actin filaments in an ATP dependent manner and possessed an actin activated ATPase activity, it had a relatively low molecular weight, (140KDa), for a myosin. The latter was attributed to the virtual absence of the long α-helical tail, signifying that this myosin would exist as a single-headed monomer which would not be capable of self-associating into thick filaments. This motor was subsequently termed a myosin I in contrast to the two-headed, thick filament forming myosin IIs.

After the discovery of a second myosin I in the microvilli of chicken intestine epithelial cells (Matsudaira and Burgen, 1979), an abundance of new myosin subfamilies extended the classification of myosins beyond classes I and II (Cheney and Mooseker, 1992; Mooseker, 1993). The class I and V myosins represent two of the nine unconventional classes of myosin that have been characterised in greater detail and reflect a lot of the features that constitute the other members of this superfamily.

In addition to their presence in amoeboid and epithelial cells, class I myosins have been found in several mammalian brain tissues and are considered to be ubiquitous. They each possess a conserved head domain and short tail domains that are capable of multiple functions. The tails of *Acanthamoeba* 1A, 1B and 1C can be divided into three distinct homology domains (Pollard *et al.*, 1991; Hammer and Jung, 1991). Starting from the N-terminal head, a region of approximately 220, mainly basic, amino acids, constituting tail homology domain 1 (TH1), is thought to bind the acidic phospholipids in membranes (Adams and Botstein, 1989). Following TH1 is an unconserved region of sequence, the GPA domain, which comprises mostly glycine, alanine and proline residues.

The third domain, SH3, contains a region of fifty amino acids that resembles an SRC domain normally found in a large number of actin and membrane binding proteins. The combination of the SH3 and GPA domains defines a second ATP-independent actin binding site in the tail which is supplementary to the conventional binding site in the N-terminal motor domain. Other myosin Is, for example *Dictyostelium* 1A and 1E, only have the TH1 membrane binding domain incorporated into their tails and therefore do not possess the secondary actin binding site. Class I motors are generally thought to play a part in vesicle transport, phagocytosis and cell movements (Adams and Pollard, 1986).

The Class V myosin subfamily exhibits similarities to class I and II myosins. This class contains three distinct members which were each identified through the biochemical and genetic analysis of mutations. The mouse *dilute* motor has an N-terminal 215KDa motor domain which is highly conserved between Class V members and more closely resembles a cytoplasmic myosin II motor domain than that of a myosin I. As well as the neck of its motor domain possessing six putative calmodulin binding sites, *dilute* possesses a central tail domain containing sequence elements which promote an α–helical coiled-coil interaction. Although this region allows heavy chain dimerisation, the fact that it is shorter and less regular than the corresponding myosin II sequence probably renders it incapable of self-associating into thick filaments. This class of myosin V also resembles conventional kinesin in that it has a globular C-terminal

domain of around 400-500 amino acids. Although this sequence is highly conserved amongst the Class V myosins, its functional significance has not been determined.

Genetic analysis of myosin V mutants has revealed that this class of myosin motors, along with conventional kinesin and certain class I myosins, plays an important role in the vesicle trafficking system in the cell. Additionally, class V myosins may be involved in the transport of membranous organelles from the Golgi complex to the plasma membrane of nerve cells.

1.1.3 Molecular motors working in concert

Titus (1993) suggested that the choice of either a microtubule or an actin-based motor for vesicle transport is probably dependent upon the region of the cell in which the vesicle is located. Based upon the differential distribution of the two filament systems in the cell, she proposed that the kinesin/dynein motors would transport vesicles to the cell periphery along microtubule networks radiating outwards from the cell centre. The myosin motors would then take over and shuttle these vesicles to the plasma membranes along actin cable networks running directly beneath the plasma membrane.

Evidence for these two types of motors working in concert was demonstrated by the work of Kuznetsov (1992) where vesicles being transported in giant squid axons were seen to switch from a microtubule-based to an actin-based track. An additional demonstration that myosins and kinesins operate in conjunction was seen using a *SMY1* supressor for a yeast mutation, *myo2*. When sequenced, this suppressor was found to encode a KRP (Lillie and Brown, 1992). Although a *smy1* null appeared WT, a *myo2/smy1* deletion mutant resulted in host lethality. Clearly, these two motor proteins work together in a common process which is essential for host cell viability. Analysis of unconventional members of the myosin and kinesin families has revealed a great diversity in the types of movements mediated by, as well as the interplay between, these two types of motors.

In summary, a variety of structurally diverse motors are known to be expressed within a single organism, currently including plants, amoebae, yeast, *Drosophila* and mammals. *Dictyostelium* is postulated to have a single conventional myosin II motor and at least nine additional unconventional myosins (Hammer and Jung, 1991) whereas *Drosophila* possesses somewhere between six and thirty kinesin motors (Endow and Hatsumi, 1991). This vast repertoire of molecular motors, often within a single cell type, reflects the diversity in motility phenomena where one motor may have unique or overlapping functions with other motors. The newly recognised unconventional motors perform an array of motile functions that are subtly related to their mechanochemical potential, such as acting as crosslinkers between membrane proteins and the cytoskeleton in order to mediate the regulation of membrane channels. Evolution may have designed motor processes in cells that involve a number of different motors. Whereas any single one may not be entirely essential for movement, their concerted action may increase the biological efficiency of the whole process.

1.2 Skeletal muscle myosin

The conventional skeletal muscle myosin molecule is a combination of three gene products, a single heavy chain (220KDa) and two distinct light chains (15KDa and 22KDa), (Lowey *et al.*, 1969). The primary sequence of myosin predicts that a single heavy chain consists of an N-terminal globular head attached to a C-terminal α-helical tail. This was confirmed under electron microscopy where skeletal muscle myosin appears as a pair of globular heads that end in a long rod-like tail (Lowey and Cohen, 1962; Lowey *et al.*, 1969; Elliot and Offer, 1978).

Proteolytic digestion of the myosin heavy chain generates cleavage patterns that vary between different myosin isoforms (Lowey *et al.*, 1969; Applegate and Reisler, 1983; Harrington and Rodgers, 1984), (see figure 1.2). The limited tryptic digestion of the rabbit skeletal muscle myosin heavy chain cleaves away the globular heads from the tail. While the globular heads, each termed S1 (95KDa), are cleaved into three subfragments, the 25KDa, 50KDa and 20KDa head domains, the tail domain is itself cleaved into two subfragments named S2 (55KDa) and LMM (70KDa).

Figure 1.2. A diagrammatic representation showing the different proteolytic domains of myosin, (not drawn to scale).

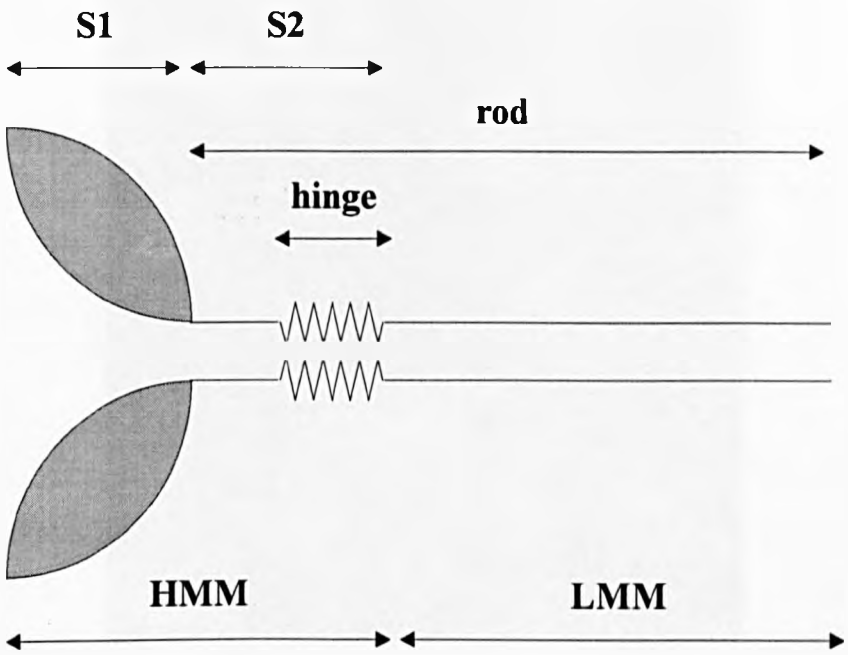

The S1 head is thought to be the mechanochemical domain, harbouring both the ATP and actin binding sites (Szilagyi *et al.*, 1979; Mornet *et al.*, 1981; Sutoh *et al.*, 1982). This was confirmed when S1 alone was shown to be capable of conveying motility *in vitro* (Toyoshima *et al.*, 1987).

1.2.1 The atomic S1 structure

Rayment *et al.* (1993a) solved the atomic structure of a chicken skeletal muscle S1 fragment, in the absence of ATP and actin, to a resolution of 2.8Å. The 95KDa S1 head is a highly asymmetric, elongated molecule with a length of 165Å, width of 65Å and a thickness of 40Å, (see figure 1.3). It consists of a globular segment harbouring both the ATP and actin binding sites and ends in a C-terminal "neck" dominated by an 85Å long α-helix that associates with the essential and regulatory light chains. The tryptic segments used to define the primary sequence do not represent discrete structural domains in the myosin crystal structure. As expected for the proteolytic cleavage sites, they lie on exposed surface loops in the structure that are presumed to

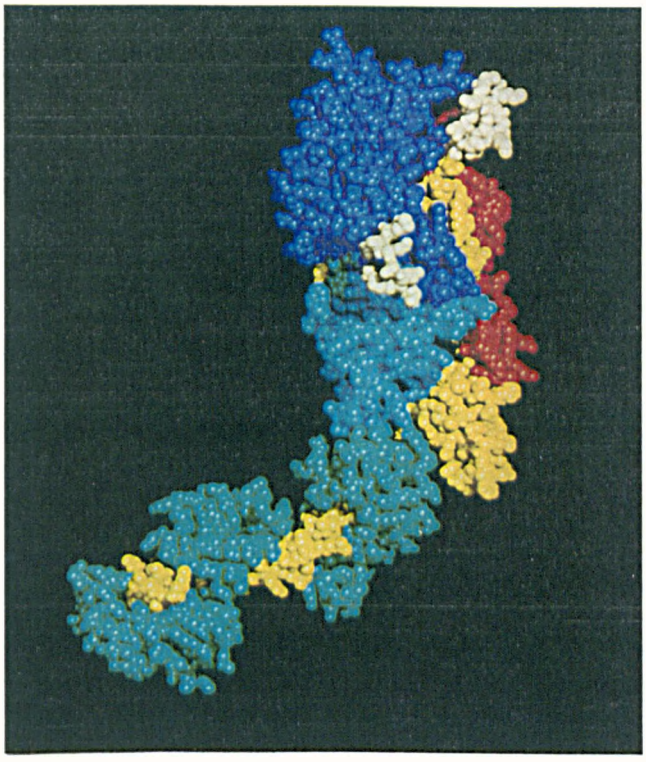

Figure 1.3. A space filling representation of the structural model for chicken skeletal muscle S1, (Rayment *et al.*, 1993a). The 25KDa, 50KDa upper, 50KDa lower and 20KDa domains are coloured in light blue, dark blue, red and yellow respectively. The essential and regulatory light chains are depicted in a blue/green and are situated towards the bottom half of the model. The white atoms represent surface loops, absent in the original Rayment model, that are remodelled from the *Dictyostelium* S1 primary sequence and inserted into the structure. The figure was prepared used the Quanta molecular graphics package.

be flexible because they represent regions of low electron density. Nevertheless, the crystal structure of myosin can be defined according to the three major tryptic domains.

There are two major clefts in the N-terminal globular domain that represent the binding sites for nucleotide and actin respectively. These are situated on opposite faces of the head and lie at a distance of 35Å from one another (Rayment *et al.*, (1993a). The nucleotide binding cleft was identified from the primary structure as a region of sequence G179-T186 containing the motif GESGAGKT. This is absolutely conserved in all myosins and shows a high degree of homology to sequence elements in other ATP binding proteins, eg. adenylate kinase and the Ras protein (Muller and Schulz, 1992; Pai, 1990). This ATP pocket is delineated mainly by residues from the 25KDa domain; Lys185-Ile199, Glu204-Gly216, Leu218-Gly233, Asp327-Ile340 and Thr667-Glu687. It has a diameter and a depth of 13Å and its two faces are inclined at an angle of ~40° with respect to one another (Rayment *et al.*, 1993a).

Immediately beneath the nucleotide binding pocket lie a pair of highly conserved α-helices, His688-Asn698 and Val700-Arg708, which harbour residues Cys697 (SH2) and Cys707 (SH1) respectively. Although these reactive thiol groups are 18Å apart in the crystal structure, they can be crosslinked to distances of 3-14Å in the presence of ATP (Burke and Reisler, 1977; Wells and Yount, 1982). These investigations therefore predict that upon nucleotide binding, the active site, seen in the "open" conformation in the Rayment structure, closes. On doing so, it initiates some form of conformational change that brings the two thiol groups closer together and propagates an intramolecular movement along the length of the heavy chain to the C-terminal end of the 85Å α-helix, producing a 50-60Å translation that defines the power stroke. In wrapping around the long α-helix, the two light chains are thought to stiffen it, ultimately maximising the length of the power stroke (Rayment *et al.*, 1993a).

The actin binding site lies on the opposite face of the myosin head, almost at a right angle to the nucleotide binding site. This interface represents contact sites in both the 50KDa and the 20KDa domains. The 50KDa domain is split into an "upper" and a

"lower" segment by the actin binding cleft that is probably in a more "open" conformation in this structure due to the absence of actin. The base of this cleft lies immediately underneath the nucleotide binding site in the region of the phosphate binding loop (Rayment *et al.*, 1993b). Their close proximity suggests that nucleotide binding to the active site may communicate with the actin binding cleft to modulate actin affinity and ultimately muscle contraction.

1.3 The cellular organisation, structure and function of actin

Actin represents a large superfamily of highly homologous proteins that are ubiquitously expressed throughout the eukaryotes. It plays a fundamental role in a diverse array of cellular processes, the majority of which are borne out of its association with members of the myosin superfamily. In non-muscle cells, actin and myosin constitute 10-15% and 1-2% of the total cell protein respectively (Pollard, 1981). Actin assembles into a filamentous cytoskeleton that provides the mechanical support necessary for the maintenance and generation of cell shape. Its arrangement into cytoskeletal "tracks" for myosin also enables it to participate in functions such as cytokenesis, vesicle/organelle transport and cell motility. In addition to these myosin mediated movements, actin based motility in non-muscle cells can be generated through the simple architectural transformation of actin filaments. The polymerisation or rearrangement of cellular actin generates phenomena such as the development of filopodia in platelet cells and the ruffling of leading lamellipodia of moving cells.

In muscle, actin and myosin represent 20% and 30% of the total cell protein respectively (Pollard, 1981) and are arranged into highly specialised structures termed sarcomeres, (see figure 1.4). Muscle consists of a number of myofibres, each made up of parallel arrays of many myofibrils. A single myofibril is formed from numerous tandem repeats of the functional unit of muscle, the sarcomere. The Z-discs demark the end of each sarcomere and are attached to thin filaments. The latter consist of an F-actin core complexed with a number of accessory proteins which include tropomyosin and the troponins. Together, these mediate the thin filament regulation of muscle contraction.

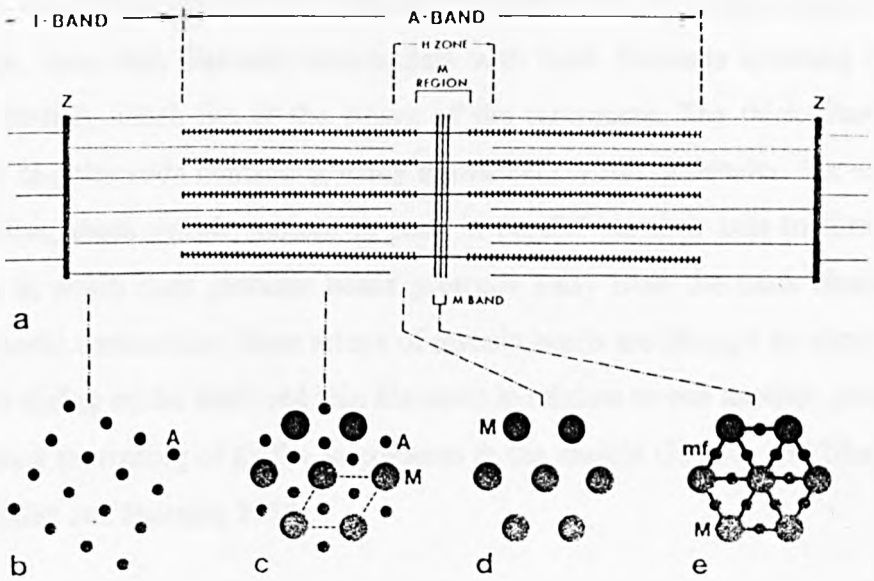

Figure 1.4. A schematic representation of the structure of a skeletal muscle sarcomere, taken from Squire, Muscle: design, diversity and disease, the Benjamin/Cummings Publishing company, Inc., (1986). (a) is a longitudinal view while (b), (c), (d) and (e) are different views along the length of the sarcomere. (b) represents the I-band region, (c) the region of overlap, (d) the H-zone and (e) the M-band. A and M denote actin and myosin filaments.

The thin filaments extend inwards from the Z-discs towards the centre of the sarcomere. Their pointed ends pass through a region called the I-band and into the A-band. Here, these thin filaments interdigitate with thick filaments spanning outwards from the M-line, which lies at the centre of the sarcomere. The thick filaments are essentially bi-polar rods containing many individual myosin molecules. On either side of the M-line, these myosin molecules pack in parallel via their tails to form a polar alignment in which their globular heads protrude away from the thick filament axis. During muscle contraction, these arrays of myosin heads are thought to attach to, and initiate the sliding of the thick and thin filaments in relation to one another, producing a simultaneous shortening of all the sarcomeres in the muscle (Huxley and Niedergerke, 1954; Huxley and Hanson, 1954).

1.3.1 Basic properties of actin

Most actin genes encode a protein with an apparent molecular weight of 42-43KDa. At low salt, actin exists as a monomer, denoted G-actin upon the basis of its globular structure (Korn, 1982; Pollard, 1986; 1990). Monomeric actin possesses a single high affinity binding site for both nucleotides (ATP or ADP) and divalent cations (Mg^{2+} or Ca^{2+}) along with several intermediate and low affinity sites that display indiscriminate binding to mono or divalent cations (Carlier and Pantaloni, 1986). The dissociation constants (K_d) are 0.1nM for ATP (Gershman *et al.*, 1986) and 2nM and 10nM for Ca^{2+} and Mg^{2+} respectively (Waechter and Engel, 1977). Although the primary divalent cation binding site has a higher affinity for Ca^{2+}, the approximate 5000 molar excess of Mg^{2+} over Ca^{2+} under physiological conditions predicts that this site will be occupied by Mg^{2+} *in vivo* (Sheterline and Sparrow, 1994).

The irreversible denaturation of actin upon removal of the closely associated nucleotide and divalent cation from their respective high affinity sites suggested that they may play a crucial role in the stabilisation of actin monomer conformation (Waechter and Engel, 1977). The identity of the bound nucleotide and divalent cation also influences actin polymerisation, the process by which individual actin monomers self-associate in high salt conditions to form filamentous actin, F-actin.

1.3.2 The atomic structure of actin

A vast genetic and biochemical characterisation has elucidated many properties and functions of actin (Sheterline *et al.*, 1995). This knowledge, coupled to its atomic structure, provides a greater overall view and subsequent understanding of the biology of this molecule. Initial attempts to elucidate the atomic structure of actin were hampered by the tendency of actin to polymerise into filaments at high salt. This hurdle was overcome by the co-crystallisation of monomeric G-actin in conjunction with actin binding proteins that obstruct its association into filaments.

Kabsch *et al.* (1990) first solved the crystal structure of α-skeletal muscle rabbit actin in complex with bovine pancreatic DNaseI (α:DNaseI) to a resolution of 2.8Å. A slight modification to the actin, involving mild tryptic digestion to remove the three C-terminal residues, facilitated crystallisation. The structure revealed that actin is a planar molecule which can fit into a cube of dimensions 55Å X 55Å X 35Å. It possesses two domains, historically known as the large and small domains, that are roughly equivalent in size and are separated by a cleft. This cleft harbours the binding site for the nucleotide and divalent cation, represented by ATP and Ca^{2+} in this structure, which holds the two domains together through a series of salt bridges and hydrogen bonds. Kabsch *et al.* (1990) also solved the structure for actin associated with ADP at the cleft to a resolution of 3Å.

The two major domains of actin can each be further sub-divided into two subdomains. These are labelled domains IA and IB, (representing the small domain), and IIA and IIB, (representing the large domain), using the same nomenclature that describes the structure of the 44KDa ATPase domain of the heat shock cognate protein Hsc70, (see figure 1.5). Although the primary sequence of Hsc70 only shows a 16% homology to that of actin, it displays a striking resemblance to actin's tertiary structure, illustrated by the superposition of 241 residues from each protein to a root mean square distance of 2.3Å (Flaherty *et al.*, 1991). A similar situation is seen in a comparison to the hexokinase b structure.

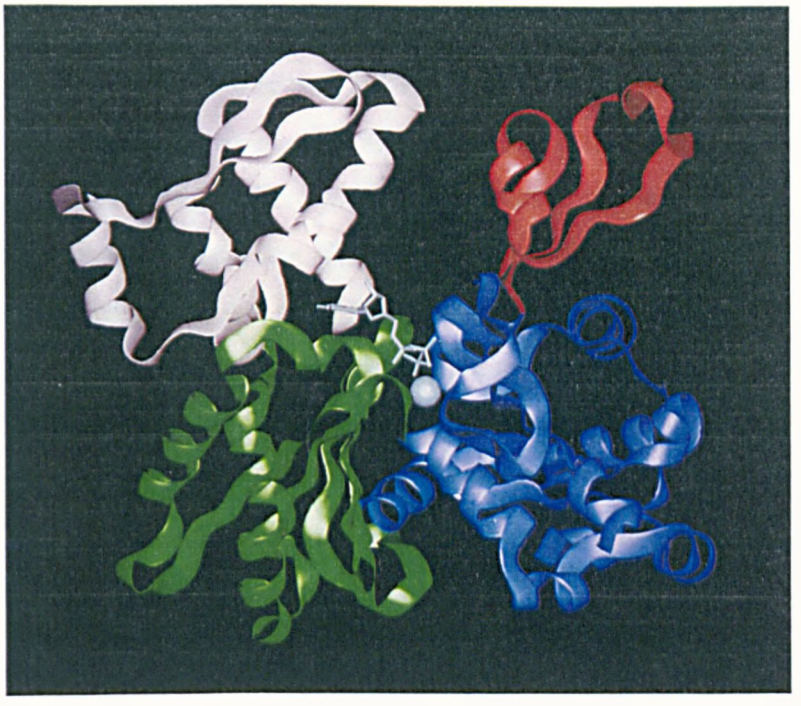

Figure 1.5. A ribbon representation of the structural model for a rabbit skeletal muscle actin monomer, Kabsch et al., (1990). The four subdomains IA, IIA, IB and IIB are coloured blue, red, green and pink respectively. The associated nucleotide, ATP, and divalent cation, Ca^{2+}, are depicted in grey.

Despite actin, Hsc70 and hexokinase b each performing different biological functions, they all possess the ability to bind and hydrolyse ATP through a common structural motif, the "ATPase fold" (Bork *et al.*, 1992). These structural similarities, coupled to the common mechanism for ATP hydrolysis, predict that these proteins may have evolved from a common ancestor (Holmes *et al.*, 1990). The observation that hexokinase b can be crystallised in an "open" or "closed" conformation, depending upon the absence or presence of bound nucleotide respectively, suggests the action of a putative "hinge" region at the base of its two major domains. The proposition that a similar element resides at the base of the actin cleft defines the basis for domain movements in actin, centred around this region, that may ultimately modulate nucleotide exchange *in vivo* (Kabsch *et al.*, 1990).

Further analysis of the actin structure revealed that both the N and C-termini of the polypeptide chain are located in subdomain IA. Additionally, subdomain IA and IIA both harbour five stranded β sheets, of which 75 residues from each can be superimposed to a r.m.s. (root mean square distance) of 2.8Å after a suitable translation and rotation. This similarity implies that the actin gene may have undergone a gene duplication event during its evolution, generating subdomains IA and IIA, with subdomains IB and IIB representing subsequent gene insertion events into IA and IIA respectively (Kabsch *et al.*, 1990).

In the crystal structure, DNaseI binds across the top of the monomer forming a major contact with residues Arg39-Lys50 (the "DNaseI binding loop") and Lys61-Ile64 in subdomain IB and a minor contact with residues 203 and 207 in subdomain IIB. Since DNaseI binds actin both rapidly and tightly in a 1:1 complex (Lazarides and Lindberg, 1974), doubts that it may distort the actin structure were put to rest upon the publication of the second major actin crystal structure.

The structure of rabbit skeletal muscle actin, complexed with segment I of gelsolin (α:gelsolin), was determined to a resolution of 2.55Å (McLaughlin *et al.*, 1993). The advantage of this study with regards to assessing the validity of the DNaseI and gelsolin based crystal structures was that whereas DNaseI binds across the top of the

monomer, the gelsolin interaction spans the bottom of subdomains IA and IIA. This subsequently enabled any conformational distortions induced by ligand binding to be identified. The superposition of the α carbon atoms of each structure to a r.m.s. of 0.9Å represented an excellent correlation between the DNaseI and gelsolin based actin structures. Two of the three main differences between the two structures were localised to regions involved in the binding of DNaseI and were therefore attributed to the tight binding of this ligand. The third anomaly regarded the absence of the extreme C-terminus in the α:DNaseI structure which was seen to fold into a hydrophobic cavity in subdomain I in the α:gelsolin structure.

Shortly after the publication of the α:gelsolin structure, Schutt *et al.* (1993) unveiled their crystalline structure of a bovine profilin:β-actin complex (β:profilin-actin). A novel feature of the β:profilin crystals was that unlike the isolated DNaseI and gelsolin derived crystals, these packed into a filamentous conformation known as the "ribbon lattice" (Schutt and Lindberg, 1992). It comprises individual profilin:actin units that form what resembles a one-start flattened helix. This exhibits actin:actin contacts that are not found in F-actin (see section 1.3.4) and are probably induced by the constraints applied by profilin in the ribbon structure.

A comparison between the β:profilin structure and those derived from DNaseI and gelsolin segment I co-crystals was complicated by the fact that whereas Kabsch *et al.* (1990) and McLaughlin *et al.* (1993) both employed an α-skeletal muscle actin isoform, Schutt *et al.* (1993) utilised a non-muscle β-actin isoform. Despite the primary sequence differences between these two isoforms, the three monomer structures showed a very good agreement.

The most obvious difference between the α: DNaseI and β:profilin structures was that upon an alignment of the large domains, a 5° rotation of subdomain IA relative to subdomain IIA was necessary in the latter to attain a respectable superposition. These domain rotations specifically involved two separate torsion adjustments at residues A138 and S338. These positions are highly significant because they pinpoint the location of the hinge region of the actin molecule which is thought to generate the

flexible domain movements described earlier. This suggests that whereas the domains in the α:DNaseI and α:gelsolin structures occupy a "closed" conformation, the profilin induced actin:actin contacts in the ribbon structure may favour a more "open" conformation of the actin monomers and subsequently explains the need for the domain adjustment in the β:profilin structure.

1.3.3 Actin isoforms

Most higher eukaryotes possess several actin genes which encode highly homologous but functionally distinct isoforms that are 374-375 residues in length. Although the human genome only has a single copy of each muscle actin gene, a multigene family of at least 20 β-actin and 16 γ-actin genes exists for the non-muscle isoforms. Despite these large numbers, only one copy of each appears to be expressed *in vivo* (Ng *et al.*, 1985; Ponte *et al.*, 1983; Vanderkerckhove and Weber, 1984). In contrast, the lower eukaryotes *Aspergillus nidulans*, *Saccharomyces cerevisiae* (Gallwitz and Sures, 1980; Ng and Abelson, 1980) and *Tetrahymena thermophila* (Cupples and Pearlman, 1986) each possess a single actin isoform which is the product of a single gene.

Multiple actin isoforms can be found within a single organism where they display a tissue specific expression pattern that is maintained across the species range, involving their localisation to alternative regions of the cell (Pardo *et al.*, 1983; Herman, 1993). Their tissue specific, as opposed to an intra-species specific, conservation suggests that each subset of related isoforms may possess individual specialised functions (Vanderkerckhove and Weber, 1978).

Mammals possess at least six different actin isoforms, four of which are muscle specific (α-skeletal, α-cardiac, α-smooth, γ-smooth) and two non-muscle specific (β and γ). The α, β and γ prefixes denote the relative migration of these actins on isoelectric focusing gels, where α represents the most acidic isoform and γ the most basic (Alonso *et al.*, 1986). Actin isoforms are also divided into two groups, the Class I and Class II actins (Rubenstein, 1990) depending upon how their amino-termini are post-translationally modified. The Class II or muscle specific α-actin isoforms generally

have longer primary sequences (375 residues) and are more acidic than their Class I non-muscle β/γ-actin counterparts (374 residues) due to their possession of an extra glutamic or aspartic acid residue at their N-termini.

Sequence comparisons of different actin isoforms can locate regions in the primary sequence that are conserved and subsequently provide a measure of the sequence identity and the evolutionary relationship between these isoforms (Hightower and Meagher, 1986; Meagher, 1991). These comparisons have revealed striking homologies between different actin isoforms. The most unrelated muscle isoforms, γ-smooth and α-skeletal actin differ from each other at only six positions in the polypeptide chain, generating a sequence identity of 98.4%. Even the two non-muscle actins, β and γ show an approximate 93% homology to the muscle actins (Rubenstein, 1990) and only differ from each other at four positions, producing a 1% divergence.

There are examples of divergent actin isoforms such as *Euplotes crassus* (Hennessey *et al.*, 1993) and *Tetrahymena pyriformis* (Hirono *et al.*, 1987) which have a 44.9% and 75% identity respectively. Overall, the observation that α-skeletal muscle and non-muscle β-actins in humans are identical to their counterparts in human, rat, mouse, cow and chicken confirms the earlier prediction that the high degree of sequence conservation between different actin isoforms is not species-specific.

A comparison of 123 unique primary actin sequences (Sheterline *et al.*, 1995) revealed that the majority of positions in most isoforms are represented by the same amino acid. Upon a more stringent comparison, only 49 of the 375 positions in all actins were absolutely conserved, generating a 13.1% invariability. This figure increased to 25.1% if the inclusion of single amino acid changes, the bulk of which represented conservative substitutions, was tolerated. Overall, these percentages will fall as new actin sequences are discovered.

Primary sequence comparisons of different protein isoforms can also be used to identify conserved regions within the molecule of interest that may represent unique, functional binding sites. The application of this method to the recognition of specific

sites in actin is problematical considering actin's extreme sequence conservation. However, this can be overcome by assigning regions of variability between actin isoforms as the sequence elements that potentially define isoform-specific functions. Subsequent isoform alignments revealed that consistently variable positions are scattered throughout the length of the polypeptide chain. Apart from extremely inconstant regions such as the N-terminus, and possibly residues 260-280, that can be identified by a run of consecutive variable positions in the primary sequence, no significant information regarding clusters of variable amino acids can be interpreted from these sequence alignments. Variability patterns can only be appreciated when the positions in the primary sequence are superimposed onto their respective positions in the atomic structure for actin (Kabsch and Vanderkerkhove, 1992; Clayton, thesis 1994).

Kabsch and Vanderkerckhove (1992) performed a variability search using an alignment of three actin sequences, α-skeletal muscle, β and γ non-muscle, to identify variable clusters in the monomer structure. Initial observations revealed a general sequence conservation in subdomains IB and IIB. Additionally, three clusters of variable residues were identified, the largest of which was centred around the bottom right hand corner of subdomain IA. This cluster was partially discernible from the primary sequence alignment, due to its harbouring the variable N-terminus and residues 103, 129, 364 and 357 which are thought to represent a region involved in the binding to myosin as well as a host of actin binding proteins (Sutoh *et al.*, 1982; Holmes *et al.*, 1991; Rayment *et al.*, 1993a; 1993b; Schröder *et al.*, 1993).

The second variable group resides in subdomain IIA and involves residues 153, 162, 176 and 298. This region is thought to bind the C2 and Iota toxins from *Clostridium botulinum* and *Clostridium perfringens* respectively (Aktories, 1989; 1990) and also phalloidin (Faulstich *et al.*, 1988; 1993; Lorenz *et al.*, 1993). Finally, the third cluster, which could also be vaguely identified from the isoform alignments alone, is defined by residues 225, 259, 266 and 271. This lies at the junction between subdomains IIA and IIB and forms the proposed "hydrophobic plug" that may form interstrand contacts in the F-actin helix, (Holmes and Kabsch, 1991), (see section 1.3.4).

A more recent study by Clayton (1994) generated a variability search from an alignment of 91 actin sequences. He identified 66 variable positions of which 34 were localised to surface regions of the monomer, a location that facilitates interactions with other ligands. In addition to the variable clusters discovered in the previous study, he was able to distinguish two other potential variable clusters. The first constituted residues 302-330 in subdomain IIA and the second, residues 38-52, which define the DNaseI binding loop (Kabsch *et al.*, 1991). The last two groups are surprisingly located in regions that coincide with actin:actin interfaces, areas which would be expected to show a high degree of sequence conservation. It was postulated that variability in this region may define the differential polymerisability and therefore functional properties between alternative actin isoforms. Conversely, the close proximity of these clusters when packed into the F-actin filament, for example the hydrophobic plug and DNaseI loop, may compensate for the individual variation in each and therefore bestow similar filament properties to unrelated actin isoforms. These variability studies may ultimately help to locate the very few regions in each isoform that contribute to the functional specificity of subsets of related isoforms.

1.3.4 The structure of F-actin

Although G-actin is capable of binding a multitude of actin-binding proteins, its polymerisation into F-actin generates the biologically active form of actin that provides the platform for the cytoskeletal structure and myosin based movements. Actin filaments possess a distinct polarity which can be visualised upon their decoration with the myosin subfragments S1 or HMM. This gives them an "arrow-head" appearance in which the top of the filament is termed the "pointed" end and the bottom of the filament the "barbed" end (Huxley, 1963).

The F-actin filament was originally viewed as a one-start, left-handed, "genetic" helix that traces a path through immediately adjacent monomers. In this model, the rotation and rise between neighbouring monomers was 166.2° and 27.5Å respectively, the latter specifying a helical pitch of 360Å in which 13 monomers reside in six left-handed turns (Egelman, 1985). Another model, using image reconstruction from cryoelectron

microscopy, favours the description of a two-start, right-handed, "long-pitch", double helix in which the two strands wind steeply around each other generating a half-helical pitch of 360Å and a filament diameter of 100Å (Milligan *et al.*, 1990). Variations in the long-pitch helix crossover distance between 340Å and 380Å were first identified by Egelman *et al.* (1982) and attributed to a random cumulative angular disorder. This is generated by the individual monomers within an actin filament possessing a torsional freedom of ±5° (Egelman and DeRosier, 1992) which subsequently results in an accumulated deviation from an ideal helical geometry with an increase in distance travelled from any one monomer.

Holmes and Kabsch (1991) presented the first model for an "atomic" structure of an F-actin filament by fitting the ADP-actin:DNaseI monomer structure (Kabsch *et al.*, 1990) into an 8.4Å resolution diffraction pattern of oriented gels of F-actin. Although this model failed to compensate for the conformational changes in the actin monomer associated with polymerisation and subsequent ATP hydrolysis (Carlier, 1989; Pardee and Spudich, 1982; Rich and Estes, 1976; Rouayrenc and Travers, 1981), a good alignment of the ADP-monomer was achieved by bestowing some rotational freedom upon the subdomains in the actin structure. This model enabled the orientation and packing of individual monomers into the filament structure to be visualised and confirmed the observations predicted by the undecagold labelling of cys-374 on monomers in the filament (Milligan *et al.*, 1990) and by several other studies (Milligan and Flicker, 1987; Bremer *et al.*, 1991). Each actin monomer fits into the helix with its long axis almost perpendicular to that of the filament axis such that domain I (small domain) is at a high radius to the filament axis and domain II (large domain) is at a low radius.

This atomic model suggests that the major intermonomeric contacts within the actin filament are along the long-pitch as opposed to the genetic helix. This was confirmed by image reconstructions from electron microscopy data of negatively stained filaments (Aebi *et al.*, 1986; Bremer *et al.*, 1991; Bremer and Aebi, 1992) and frozen hydrated filaments (Milligan *et al.*, 1990) which demonstrated that whereas there is a low electron density at the centre of the filament, each long pitch strand is associated with a

large mass of electron density. This intrastrand connectivity was also corroborated by the observation that long-pitch strands are sometimes seen to separate from one another (Bremer *et al.*, 1991). The predicted long-pitch bonds involve three major contact sites between subdomains IA, IIA and IIB whilst a single contact along the genetic helix links subdomains IA and IIB, (see table 1.1 and figure 1.6), (Holmes *et al.*, 1990).

Holmes *et al.* (1990) also defined a third "trimeric", hydrophobic contact that involves the insertion of a loop Pro264-Gly273, crossing the filament axis from a monomer on one long-pitch strand into a hydrophobic pocket between two monomers on the opposite long-pitch strand, delineated by residues Tyr166, Ala169, Leu171, His173, Cys285, Ile289, Gly63, Ile64 and His40-Val45. Although this loop is seen to partially extend from the surface of the monomer in the actin crystal structure, the energetically unfavourable proximity of the aromatic ring of Phe266 to the carboxylate group of Glu259 prompted Holmes to reorganise this loop into a four residue "hydrophobic plug" (residues 265-268) which is surrounded by two antiparallel β strands. This plug is proposed to bridge the filament axis producing a strong interstrand contact that is essential for filament stability.

Although images derived from electron microscopy of actin filaments are able to distinguish a region of interstrand density that corresponds to the position of the plug (Bremer and Aebi, 1992), Schutt *et al.* argue against the existence of the plug since they do not see any such region of density in the analogous region of their profilin:β-actin structure. This absence may however be due to the fact that the actin conformation in the ribbon structure is stabilised by its alternative actin:actin contacts.

Chen *et al.* (1993) investigated the effect of a mutation *L266D* in the hydrophobic plug and established that these mutants displayed a defective, cold-sensitive polymerisation. An additional mutation deleting or shortening the length of the plug resulted in host cell lethality in yeast (Chen and Rubenstein, 1995). Although these results do not prove the existence of the plug directly, they highlight the possible importance of this region in actin:actin interfaces.

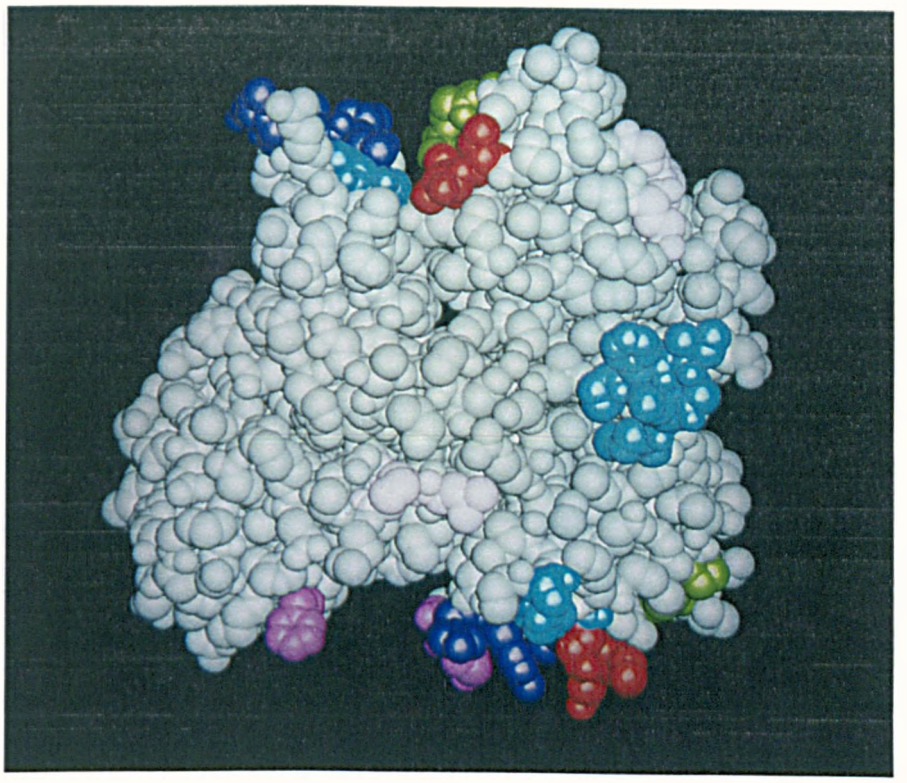

Figure 1.6. The actin-actin binding sites proposed by Holmes *et al.*, (1990), as shown on a single actin monomer. A view from directly behind the actin monomer depicts each of the three intrastrand and the single interstrand contacts in different colours. Also represented are the trimeric contacts which are shown as light blue, except in regions where they overlap with the intrastrand contacts, where they are subsequently depicted in dark blue. The colour of each intrastrand contact is listed in the order shown in table 1.1. The first intrastrand contact is coloured green, the second red and the third magenta. The single interstrand contact is shown in white.

	monomer 1	monomer 2
long-pitch intrastrand contacts	**IA** 322,325	**IIB** 243-245
	IIA 286-289	**IIB** 202-204
	IIB 166-169, 375	**IIA/IA** 41-45
interstrand contacts	**IA** 110-112	**IB** 195-197

Table 1.1 The following table highlights the residues, and the subdomains in which they reside, that are involved in intermonomeric actin contacts between adjacent monomers in an actin filament. The residues on one monomer, (the left hand column), are proposed to interact with the corresponding residues on a second monomer, (the right hand column). The groups highlighted also harbour a few residues which are also thought to define the "trimeric" actin contact site.

Image reconstructions from electron microscopy (Bremer *et al.*, 1991; Bremer and Aebi, 1992) have served to reinforce Holmes' model of the F-actin filament. However, one difference in this model concerns the presence of a region of electron density that is not observed in electron microscopy reconstructions and is attributed to the strong DNaseI binding which bestows this region with a greater degree of order. To compensate for this discrepancy, subsequent refinements of the existing F-actin model therefore involved the re-orientation of the DNaseI binding loop to a shallower radius (Lorenz *et al.*, 1993). This model of the F-actin filament is generally accepted and its coupling to the crystal structure of myosin S1 (Rayment *et al.*, 1993a) has enabled the identification of the docking site of the myosin head onto the actin filament, subsequently leading Rayment *et al.* (1993b) to propose a structural mechanism for muscle contraction.

1.3.5 Actin polymerisation

Polymerisation of G- into F-actin is one of the most vital properties of actin monomers and is generally used as an assessment of the integrity of mutant monomers. Actin exists as a monomer up to a minimal threshold level termed the critical concentration for polymerisation (A_{cc}). Above this, polymerisation is initiated and proceeds until a steady-state level is achieved. In this situation, actin filaments co-exist with a critical concentration of monomers, in addition to a small number of actin dimers and trimers, which represent intermediate steps in the polymerisation process.

Polymerisation is defined by essentially four stages: monomer activation, nucleation, elongation and the steady state level. Monomer activation is the process by which the actin monomer changes conformation upon the binding of mono and divalent cations at its medium and low affinity binding sites (Pardee and Spudich, 1982; Rich and Estes, 1976). The identity of the cation at these sites affects the monomer conformation, nucleotide binding and subsequently polymerisation (Strzelecka-Golaszewska *et al.*, 1993). The activated monomer is able to self-associate into unstable dimers and subsequently trimers which serve as nuclei that seed the elongation process. The formation of dimers is energetically unfavourable and is the rate-limiting step for

polymerisation. Trimers produce a stabilised nucleus on which the rapid addition of ATP-monomers leads to elongation. Kinetic studies have shown that polymerisation follows a sigmoidal curve with an initial lag phase during nucleation and a log phase representing a rate of elongation that is directly proportional to the actin concentration (Kasai *et al.*, 1962).

After the incorporation of an ATP-monomer into an elongating filament, the bound ATP is hydrolysed to ADP at a rate of 0.02/s. Although the hydrolysed phosphate is transiently retained at the end of the filament (Carlier *et al.*, 1984; Carlier, 1991b) it is subsequently released at a dissociation rate of 0.006/s (Carlier *et al.*, 1987). Due to the critical concentration for assembly, and therefore disassembly, being higher for the pointed end than the barbed end, the rate constants for exchange are 20 times faster at the barbed ends (Pollard, 1986; Sheterline and Sparrow, 1994).

The pointed ends exhibit ATP-actin assembly at a rate which is five times slower than that at the barbed end and additionally show a slight preference for disassembly of ADP-actin. Therefore, monomers are incorporated into the barbed end at a higher rate compared to the pointed end. This continues until a steady state situation is reached in which a net growth of subunits at one end of the filament occurs simultaneously with a net loss at the opposite end. This phenomenon is known as "tread-milling" (Wegner, 1976; Selve and Wegner, 1986). Since the probability of ATP hydrolysis is higher than phosphate release in an assembling filament, it will consist of an ADP-actin segment at its pointed end which is preceded by a region of ADP.Pi subunits and capped at the barbed end by a small number of ATP-actin monomers.

1.4 Muscle contraction

The conventional swinging crossbridge theory (Huxley, 1969) describes the currently accepted model for muscle contraction. It proposes that actomyosin based movements are generated by a repeated cycle of the sequential attachment of a myosin head to an actin filament, a conformational change in the head which alters the attachment angle of the crossbridge, and subsequent release. The change in conformation of the head is

proposed as the force producing event that drives actin filament displacement and sliding. The energy for each power stroke event during a single contractile cycle is thought to be derived from the concomitant hydrolysis of a single ATP molecule (Cooke, 1986).

Kinetic studies have demonstrated that a single crossbridge cycle comprises a number of discrete intermediate stages in which the actomyosin complex undergoes conformational transitions that are determined by the chemical state of the nucleotide residing in the active site of the myosin head (Taylor, 1979; Adelstein and Eiselberg, 1980; Geeves, 1991; Lymn and Taylor, 1971), (see figure 1.7). During a crossbridge cycle, actin and myosin spend the majority of the time in a detached state, where they are involved in extremely rapid, weak attachments and detachments to one another. During a brief period of time when they are strongly attached, the myosin head undergoes the conformational change that drives the sliding of its tightly bound actin filament.

The individual sequential events that make up the crossbridge cycle can be considered to begin with the rigor complex in which actin and myosin are strongly associated in the absence of ATP. This complex is decidedly weakened upon the binding of Mg^{2+}-ATP to myosin and the subsequent, rapid dissociation of actin triggers ATP hydrolysis to generate a stable state, M.ADP.Pi. Reassociation of actin with this state produces a weakly bound intermediate, A.M.ADP.Pi that undergoes an isomerisation event to a strongly bound conformation, A.M*.ADP.Pi (Eisenberg and Green, 1980). The release of the phosphate from this complex is thought to initiate the power stroke (Lymn and Taylor, 1971; Goldman, 1987) and subsequent dissociation of ADP from the A.M.ADP complex completes the cycle, leaving actin and myosin once more in a rigor state.

Many structural and biophysical studies have attempted to observe the conformational change in the myosin head that represents the power stroke, but so far with only limited success. Although the strongly bound rigor state occupies only a brief fraction of the time during a contractile cycle in muscle, it is the easiest actomyosin complex to

Figure 1.7. The Lymn-Taylor kinetic representation of the actomyosin ATPase cycle.

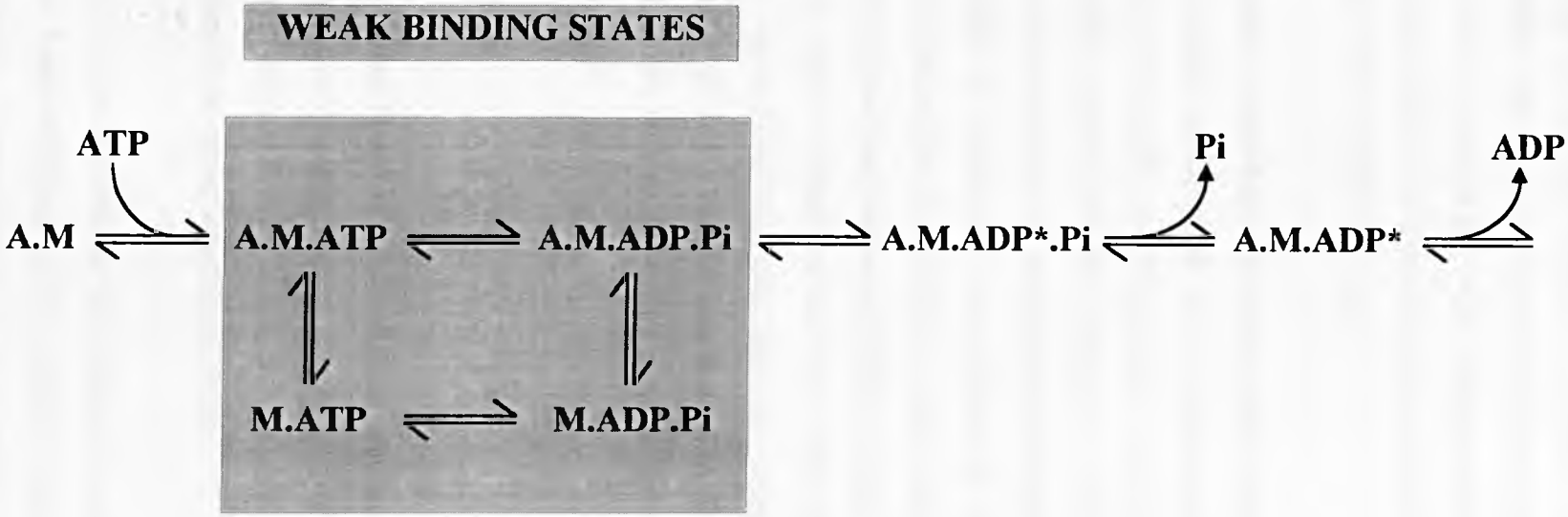

recreate and observe experimentally. Its visualisation by electron microscopy reveals that the myosin heads attached to the actin filament are inclined at an angle of approximately 45° to the filament axis, pointing towards the centre of the sarcomere (Huxley, 1963; Reedy *et al.*, 1965; Moore *et al.*, 1970; Milligan and Flicker, 1987). This state is thought to represent the end of the power stroke, in which the head has rotated from an attached angle of 90° to the filament axis.

Direct observation of the weaker, intermediate crossbridge states is more difficult to achieve due to the rapid transitions taking place over a microsecond time scale. However, electron microscopy of chemically cross-linked acto-S1 and also cross-linker free acto-HMM complexes in the presence of ATP (Craig *et al.*, 1985; Frado and Craig, 1992) illustrated that the few heads bound to actin filaments were attached at a variety of angles. This diversity in attachment was attributed to the alternative actomyosin conformations that define the intermediate, weakly bound crossbridge states. Frado and Craig (1992) reported that their acto-HMM complexes seemed to be attached to the filaments at angles centred around 90°. This infers that the conformational change in the myosin head manifests itself as a transition from an A.M.ADP.Pi crossbridge bound at 90° to the filament axis to an A.M.ADP crossbridge bound at 45°, thus driving the actin filament through a distance determined by the chord length of the myosin head.

1.4.1 The actomyosin interface

The first model of a molecular motor bound to its cytoskeletal substrate at the atomic level was produced by Rayment *et al.* (1993b). The subsequent structural organisation of a rabbit skeletal muscle actin : chicken skeletal muscle S1 complex concurred with the structural implications derived from earlier biochemical studies.

The actomyosin atomic complex was constructed by firstly fitting the refined model of an actin filament, derived from X-ray diffraction data of oriented F-actin gels (Lorenz *et al.*, 1993) into a ~30Å resolution, electron density envelope of S1 decorated F-actin obtained from cryo-electron microscopy image reconstructions (Milligan and Flicker,

1987; Milligan *et al.*, 1990). The "docking" of the S1 crystal structure (Rayment *et al.*, 1993a) into the density map produced a good alignment, with the globular motor domain of the S1 head situated at a short radius to the actin filament. One region of ambiguity in this fit concerned a collision of the proximal portion of the S1 head with an actin monomer. However, this was not so surprising considering that the S1 structure used in this alignment represented a state lacking both nucleotide and actin. Since this region of overlap could be avoided by causing the 50KDa actin binding cleft to close, it was inferred that some conformational change in actin and/or myosin might occur upon binding.

Immediately after this structure was published, Schröder *et al.* (1993) unveiled an atomic model for an F-actin filament decorated with *Dictyostelium* S1. By fitting the rabbit F-actin (Lorenz *et al.*, 1993) and the chicken S1 (Rayment *et al.*, 1993a) atomic models into a cryo-electron microscopy based image reconstruction of rabbit F-actin decorated with recombinant *Dictyostelium* S1, a close agreement to the Rayment structure was obtained. Minor differences in the actomyosin interfaces of these two structures were explained by a variability between the primary sequences of chicken and *Dictyostelium* myosin isoforms. These differences are highlighted below. Although these acto-S1 complexes allow general features to be established, the exact interaction between individual amino acids cannot be confidently assigned due to unaccounted domain movements in actin and myosin as well as the freedom of flexible surface loops which are not seen in the X-ray diffraction data.

The actin interface on the myosin head involves residues located in both the upper and lower 50KDa domains and the 20KDa domain. A single myosin head exhibits hydrophobic and ionic interactions with two adjacent actin monomers in an actin filament. These comprise three "primary" contacts with one actin monomer and a single "secondary" contact with the monomer immediately below along the long-pitch helix. Each of the primary and the secondary contact site combine to form the strong actomyosin rigor complex. The actomyosin interaction derived from the Rayment and Schröder structures are highlighted in table 1.2 and illustrated for the former in figure 1.8.

The first of the primary interactions is predicted to involve an ionic contact between a flexible, disordered loop Tyr626-Gln647, located at the junction of the 50KDa and 20KDa domains in myosin, and residues in the N-terminus of actin. This electrostatic interaction is thought to represent the initial weak binding component that enables the myosin head to bind actin in a wide variety of orientations. Whereas Rayment *et al.* (1993b) describe this actin contact as including Asp1-Glu4, Asp24 and Asp25, Schröder *et al.* (1993) also include residues Glu99 and Glu100. This inclusion of the latter residues is surprising since the primary sequences of chicken β and *Dictyostelium* S1 exhibit only a single charge difference in this region where E361 in the former is replaced by N361 in the *Dictyostelium* sequence (Schröder *et al.*, 1993). These ionic contacts in the N-terminus confirm those previously identified by proteolysis, cross-linking and biochemical studies (Mornet *et al.*, 1981; Sutoh, 1982).

The major primary binding site is the main component of the strong rigor contact (Schröder *et al.*, 1993) and involves extensive hydrophobic contacts between highly conserved residues in actin and myosin. These involve the binding of two α-helices in the lower 50KDa domain of myosin, Gly516-Phe542 and Asp547-His558, to two exposed hydrophobic regions in actin, Ile341-Gln354 and Ala144-Thr148. Additionally, residues Asn552-His558 in one of these myosin α-helices is thought to come into contact with residues His40-Gly42 that lie on the actin monomer immediately below along the long-pitch helix.

The third primary contact site is also predicted to be hydrophobic in nature and involves a strong contact between residues Arg405-Lys415 from a flexible loop in the upper 50KDa region of myosin and residues Pro332, Pro333 and Glu334 in subdomain IIA of actin. A final component of the primary contact involves the residues Gln647-Lys659 in the 20KDa domain of myosin which bind actin in an unspecified region (Rayment *et al.*, 1993b).

The secondary actomyosin interaction is thought to be ionic in nature and may stabilise the initial, weak binding of actomyosin. It involves an exposed loop, Lys567-His578, located in the lower 50KDa domain of myosin, that interacts with the actin monomer

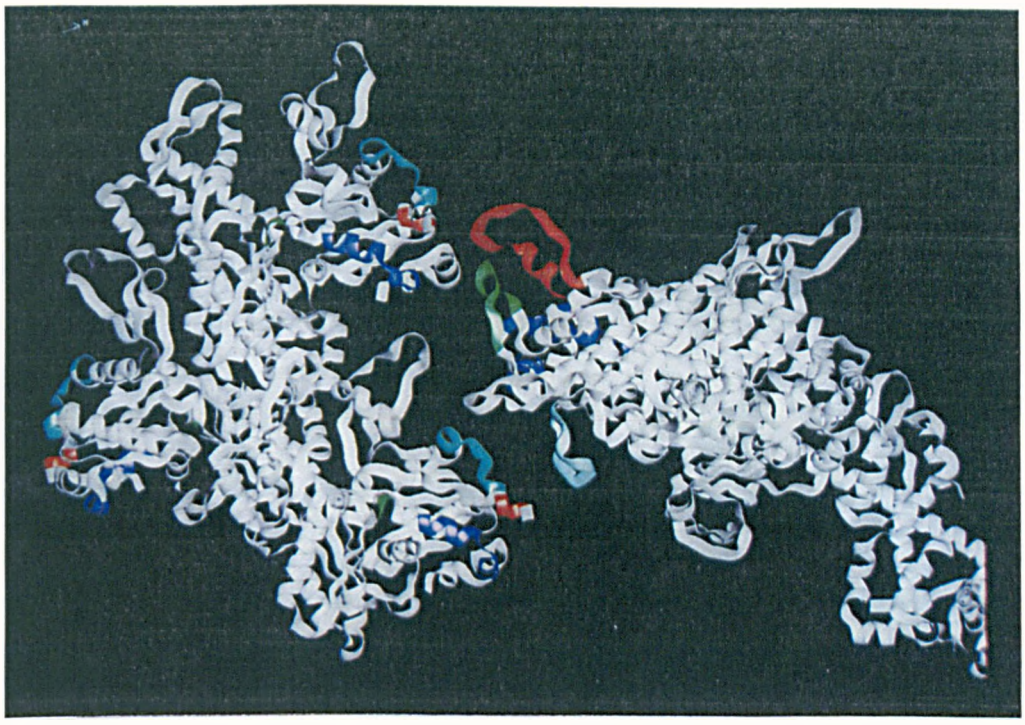

Figure 1.8 A representation of an S1 myosin head in close proximity to three actin monomers in an F-actin filament. The three monomers were compiled from the coordinates of the unrefined monomer structure, Holmes *et al.*, (1990). The myosin S1 head is derived form the coordinates of the chicken skeletal muscle S1structure, Rayment *et al.*, (1993). The surface loops originally missing in this S1 structure were modelled from a *Dictyostelium* myosin sequence and superimposed onto the chicken S1 structure. The proposed actomyosin binding sites, Rayment *et al.*, (1993b), are highlighted in different colours and will be described with respect to the myosin domains in table 1.2; the primary ionic contact is red, the upper 50KDa domain hydrophobic contact is dark blue, the lower 50KDa hydrophobic contact is green and the secondary contact is light blue. (sd=subdomain).

	myosin	bond	actin
Primary contacts	Tyr626-Gln647 flexible loop 50KDa/20KDa junction	ionic	Asp1-4, Asp24, Asp25 actin N-terminus sd IA
			Glu99, Glu 100 loop sd IA
	Gly 516-Phe542 Asp547-His558 Asn552-His558 α-helices lower 50KDa	hydrophobic	Ile341-Gln354 Ala144-Thr148 His 40-Gly42 sd IA, junction sd IA/IIA and sd IB respectively
	Arg405-Lys415 flexible loop upper 50KDa	hydrophobic	Pro332-Glu334 sd IIA
			Pro332-Pro333 sd IIA
Secondary contact	Lys 567-His578 flexible loop lower 50KDa	ionic	Tyr91-Glu100 loop sd IA
			Trp79-Asn92 sd IA

Table 1.2 The actomyosin contacts proposed by Rayment *et al.*, (1993b), from the docking of a chicken skeletal muscle S1 head into an electron density envelope of S1 decorated F-actin. The three primary and single secondary contacts between actin and myosin are shown. For each contact, the residues involved, and their location in the respective domains of actin and myosin are listed. The proposed nature of bonding for each contact is also specified. Highlighted are the differences in the actin contact sites seen between the chicken and *Dictyostelium* S1 heads.

below the one involved in the primary contacts. Whereas Rayment *et al.* (1993b) suggested that this region could contact residues Tyr91-Glu100 in subdomain IA of actin, Schröder *et al.* (1993) proposed a contact with Trp79-Asn92 in the *Dictyostelium* model. These alternative binding sites are not so surprising in light of the sequences of *Dictyostelium* and rabbit myosin showing a variation in the distribution of charged residues in this exposed loop.

1.4.2 A structural model for muscle contraction

Coupled to the classical crossbridge theory (Huxley, 1969) the insights gained from the atomic reconstruction of actomyosin led Rayment *et al.* (1993b) to propose a structural model for muscle contraction, (see figure 1.9). The kinetic prediction of several intermediate crossbridge states, each possessing a particular actomyosin affinity, was incorporated into this model by the suggestion that rigor complex formation is a sequential process in which each successive, intermediate state constitutes an increasing fraction of the proposed actomyosin binding sites.

Starting with the rigor state, actin and myosin are strongly associated with each of their primary and secondary sites in occupation. Subsequent nucleotide binding at the myosin active site is proposed to be a two step process that diminishes actomyosin affinity. The initial stage involves only a fraction of the nucleotide in which the triphosphate complex and the ribose ring form a contact with the phosphate binding loop at the base of the nucleotide binding pocket. This somehow influences the opening of the adjacent 50KDa actin-binding cleft, weakening the affinity of myosin for actin. The second step of nucleotide binding involves a closure of the active site around the whole of the nucleotide moiety. This tight binding is proposed to "cock" the 85Å helical arm of myosin by an approximate 50Å translation of its C-terminal end with respect to the actin-binding site. The release of actin from this "primed" state initiates ATP hydrolysis to generate the stable products complex M.ADP.Pi. This metastable state then rebinds actin in a sequential multi-step manner.

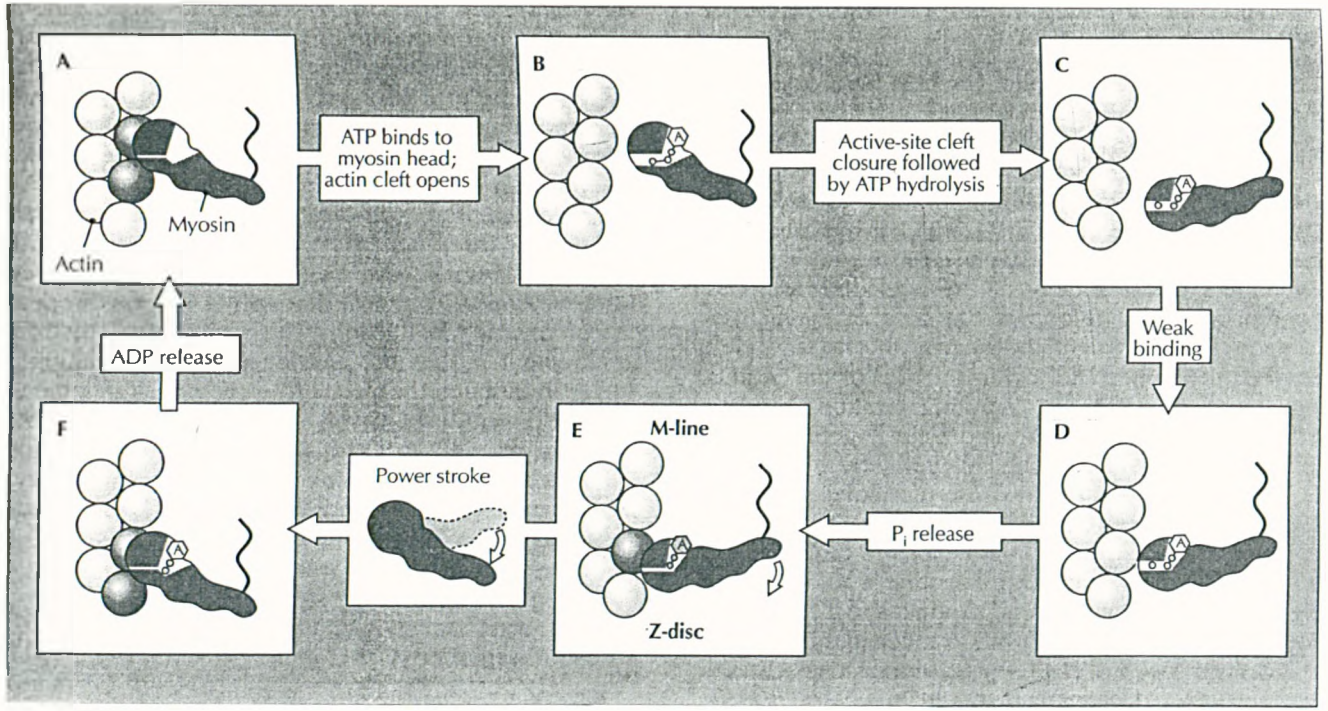

Figure 1.9. A cartoon representation of the interaction of actin and myosin at each step in the crossbridge cycle, leading up to the power stroke.

This rebinding involves an initial "docking" of acin and myosin which is mediated by the weak, primary, ionic interaction and possibly stabilised by the secondary ionic interaction. The association of the stereospecific, hydrophobic contacts reconstitutes a strong actomyosin link that is braced by the binding of the loop in the upper 50KDa domain of myosin to subdomain IIA of actin. The rejuvenation of the strong actomyosin contact reduces the affinity of the active site for the bound phosphate. Its release is proposed to trigger the power stroke in which the "cocked" C-terminal tail returns to its relaxed position, with the concomitant translocation of the tightly bound actin filament through a distance of 50Å. Figure 1.10 provides some idea of how the movement of the myosin tail, in relation to the actin filament, (and also with reference to the sarcomere), would produce a displacement. Phosphate release also prompts a re-opening of the active site which subsequently liberates ADP, thus generating a short-lived rigor state in muscle in which the 50KDa actin-binding cleft is closed and the ATP cleft is open.

The crux of this model lies in the close proximity of the base of the nucleotide binding site to the apex of the actin binding cleft that divides the 50KDa domain into an upper and lower segment. The binding of ATP at the active site is proposed to modulate the opening and closing of the 50KDa cleft, and ultimately the affinity for actin. This model is consistent with a wide range of biochemical studies and although it has not been proved as yet, it provides a visual framework for future studies of actomyosin.

Recently (Fisher *et al.*, 1995), a structure of the *Dictyostelium* S1 head with and without ADP-BeF_3-Mg^{2+}, (a state thought to resemble that of bound ATP), associated at its active site was revealed. Although these structures were derived from a truncated S1 head that was crystallised without the need for reductive dimethylation of its lysine residues, their overall tertiary structures were very similar to each other as well as to that of the chicken skeletal S1 isoform. These findings suggested that nucleotide-bound and nucleotide-free S1 are unexpectedly similar, a feature that was emphasised by the size of the nucleotide cleft only closing by a few Angstroms in the bound state. Additionally, significant conformational changes between the nucleotide-bound and nucleotide-free structures were seen in the C-terminal segment of the heavy chain.

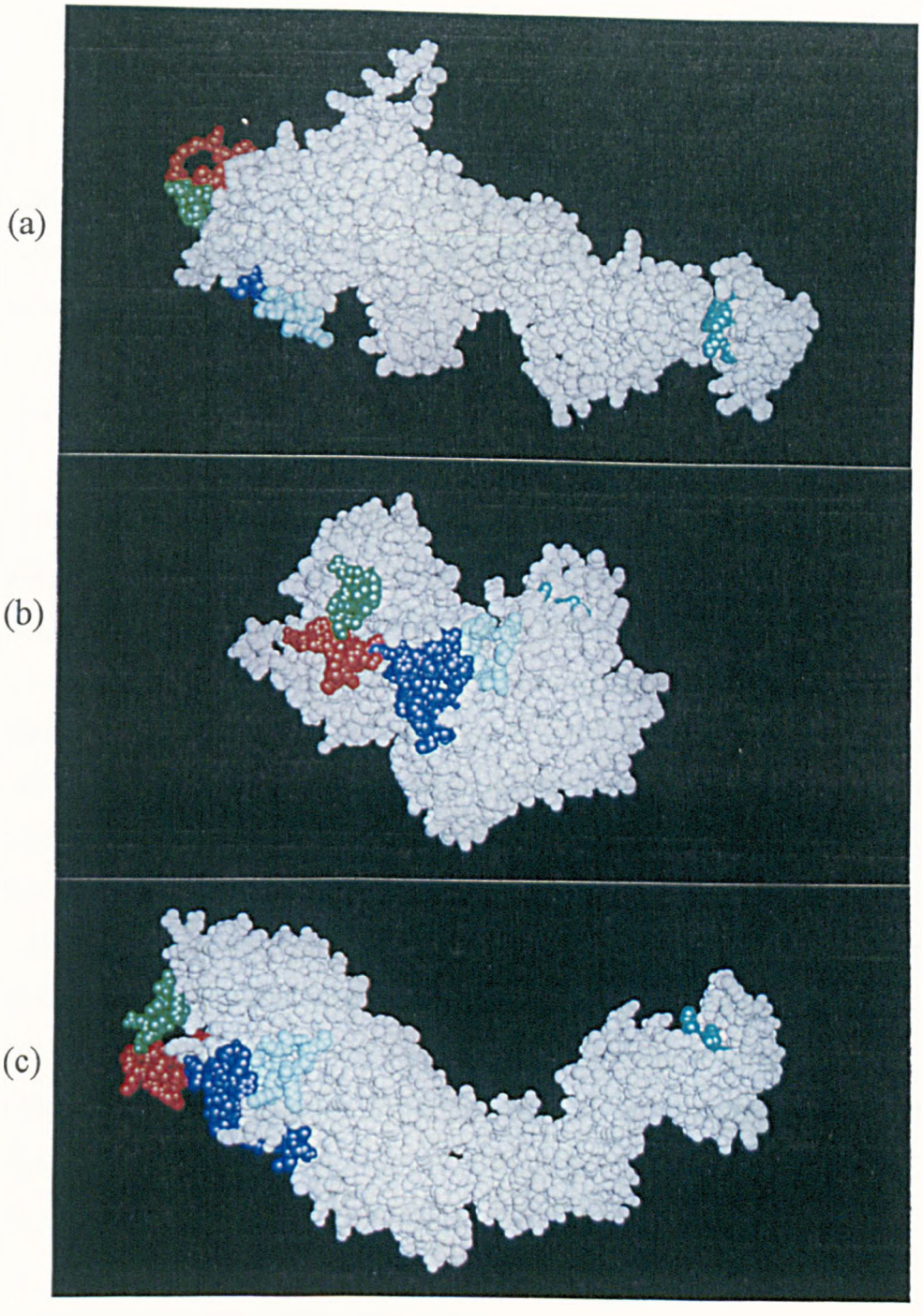

Figure 1.10 Three alternative orientations of the chicken skeletal muscle S1 myosin head, with its actin binding sites coloured as described in figure 1.8. (a) represents a view from the side, ie. perpendicular to the actin filament axis, where the myosin is roughly poisitioned in a manner in which it would interact with the actin filament. (b) is a view looking outwards from the centre of the actin filament axis, directly at the front face of the S1 head. (c) looks down from the pointed end of the actin filament onto the top of an interacting myosin head. In each case, a short C-terminal helix, Pro830-Lys839, is depicted in turquoise. This is oriented at an angle of approximately 20° with the actin filament axis and points to the M line if this model were oriented according to its location in the sarcomere.

These were proposed to originate in the region of the two sulphydryl groups, SH1 and SH2.

Although these observations do not corroborate Rayment's structural theory for muscle contraction, which would expect a large closure of the active site in the nucleotide bound form, they lead to a hypothesis that a conformational domain arrangement, this time around the region containing the sulphydryl groups, may still define the basis for actomyosin motility.

1.5 The systems used for the mutational analysis of actin

The alliance of biochemical and genetic approaches has long been employed to dissect functional protein interactions. The most commonly employed strategy aims to relate the properties of a particular mutated protein *in vitro* to its effects on cellular events *in vivo*, such that its overall functional character can be assessed. For a host organism to be considered an ideal system for the study of actin mutations, it has to have a well defined molecular and genetic character. These features facilitate *in vivo* mutant analysis by enabling the introduction of mutations engineered *in vitro* into the host as well as the recovery and identification of mutant genotypes that have been induced *in vivo*. For most organisms that possess the aforementioned attributes, the endogenous or recombinantly expressed mutant actins can be purified from host cells and used for *in vitro* biochemical investigations. The following sections will describe some of the host organisms that are used for the *in vivo* and *in vitro* examination of mutant actin. Comprehensive reviews of the study of actin mutants are available in several recent reviews, Hennessey *et al.* (1993), Sheterline and Sparrow (1994).

1.5.1 The *in vivo* study of actin mutants

In vivo study has advantages over *in vitro* study in that it examines the performance of a protein in its physiological environment where its functions are optimised under the influence of numerous stabilising co-factors. As well as yeast and *Drosophila*, there are

other less well developed systems that have allowed the characterisation of actin mutants (Hennessey *et al.*, 1993; Sheterline and Sparrow, 1994).

1.5.1.1 *Dictyostelium discoideum*

The ease of the molecular genetic manipulation of the slime mould, *Dictyostelium discoideum*, has rendered it a powerful host for the extensive mutational analysis of myosin, enabling the characterisation of functionally important regions of the molecule as well as probing the mechanism of the actomyosin interaction (Kubalek *et al.*, 1992; Ruppel *et al.*, 1994; Uyeda *et al.*, 1994). The advantage of *Dictyostelium* for myosin study is that it possesses a single conventional myosin heavy chain that can be removed and/or replaced by homologous recombination (De Lozanne and Spudich, 1987) In contrast, the use of this organism for the study of actin is complicated by its possession of 17 actin genes (Vanderkerckhove and Weber, 1980) that encode five actin isoforms (Romans and Firtel, 1985) and subsequently hinder genetic manipulation. To date, no actin mutations have been recovered in *Dictyostelium* by selecting for disrupted phenotypes.

1.5.1.2 *Caenorhabditas elegans*

Mutations that have been isolated in the nematode, *Caenorhabditis elegans*, (Waterston *et al*, 1984) display an uncoordinated locomotion, (*unc*). Many of these mutations disrupt muscle structure and some have been localised to a region of the genome that contains three of the four nematode actin genes (Files *et al.*, 1983). However, the exact genotype of these mutants has not been established.

1.5.1.3 *Saccharomyces cerevisiae*

The well defined classical and molecular genetics of the yeast, *Saccharomyces cerevisiae*, coupled to its ease of manipulation, makes it a model system for the study of the *in vivo* effects of actin mutations on the cytoskeleton. Yeast actin is the product of a single actin gene, *Act 1*$^{+}$ (Gallwitz and Sures, 1980; Ng and Abelson, 1980) and

exhibits extensive primary sequence homology to vertebrate skeletal and cytoplasmic actin isoforms. This high degree of interspecies sequence conservation is mirrored by most other genes encoding components of the yeast cytoskeleton and suggests that the cytoskeletal structures assembled by yeast and higher eukaryotes may be similar and therefore perform analogous functions *in vivo*.

The essential nature of *Act1*$^+$ was demonstrated when its disruption resulted in host cell lethality (Shortle *et al.*, 1982). This suggested that any actin mutants studied in yeast have to be either co-expressed in the presence of *Act1*$^+$, or be capable of maintaining host cell functions upon the replacement of this allele. A commonly employed strategy for mutant analysis involves the *in vitro* mutagenensis of a cloned actin gene, followed by its integration into the host genome via one or two homologous recombination events, thus disrupting or replacing the endogenous WT copy respectively. The desired integrants can be verified and selected for by the joint transfer of a closely linked auxotrophic marker.

Shortle *et al.* (1984) used this procedure to screen for temperature sensitive diploids that had been transformed with an integrative plasmid possessing an actin gene with a specified mutation and a truncated 3' end. Two conditional lethal mutants that were temperature sensitive for growth were isolated. Under non-permissive conditions, these mutant cells displayed randomly distributed actin patches instead of localised structures, increased cell volumes and lysis. These features implicated a role for actin in defining the polarity of cell surface growth, and also in osmoregulation which involves the organisation and secretion of materials to and through the plasma membrane (Novick and Botstein, 1985). The disorganised actin phenotype may reflect an impairment of normal actin polymerisation/depolymerisation, caused either by defective actin monomers or by a loss/aberration in an interaction with an actin-binding protein (Novick and Botstein, 1985). Incidentally, similar phenotypes were observed in yeast cells containing mutations in other cytoskeletal components, suggesting a common disorder; tropomyosin (Liu *et al.*, 1989), profilin (Haarer *et al.*, 1990), Cap2p (Armatruda *et al.*, 1990).

Johannes and Gallwitz (1991) and Cook *et al.* (1991) followed a strategy in which a mutant actin gene replaced one of the genomic alleles by homologous recombination to generate diploids heterozygous for the mutation. Actin mutations could be rapidly screened for by inducing the sporulation of these diploids and establishing through tetrad analysis whether the mutations were recessive or conditional lethal, or if they had any effect at all. As mentioned above, the major drawback of this system is that the choice of actin mutations are limited to those that will hopefully maintain host cell viability. Shortle *et al.* (1984), Johannes and Gallwitz (1991) and Wertman *et al.* (1992) were able to recover a higher percentage of viable, conditional actin mutants which displayed similar phenotypic consequences upon the cytoskeleton to those found by Shortle *et al.* (1984).

Finally, Karlsson *et al.*, (1991) used an alternative system in which a diploid host, possessing one intact and one disrupted copy of *Act1*$^{+}$, was transformed with an expression vector harbouring a chicken β acin gene. This expression vector was maintained extrachromasomally upon host cell transformation and was inherited by haploid ascospores due to its possession of sequences that mediate stable segregation during mitosis and meiosis. Following sporulation, the finding that haploid ascospores, lacking an intact *Act1*$^{+}$ allele, were viable due to a complementation by the recombinant β-actin demonstrated that the heterologous actin is capable of fulfilling host functions normally provided by the endogenous isoform.

1.5.1.4 *Drosophila melanogaster*

The genome of *Drosophila melanogaster* hosts six actin genes, of which four encode muscle specific actins and two cytoplasmic actins (Fyrberg *et al.*, 1983), (see table 1.3).

All of these genes have been sequenced (Sanchez *et al.*, 1983; Mahaffey *et al.*, 1985). The differential expression of these genes during development was demonstrated by probing the alternative actin mRNA species present in various parts of the *Drosophila* body and life cycle with DNA probes specific for the unique 3' untranslated regions of

each gene (Fyrberg *et al.*, 1983). Although all six actin isoforms are found in adults, ACT88F expression is localised solely to the indirect flight muscles, (IFMs), (Fyrberg *et al.*, 1983; Hiromi and Hotta, 1985). The IFMs power the flight of the flies through the antagonistic action of two sets of asynchronous muscles, the dorsoventral (DVM) and the dorsolongitudinal (DLM) flight muscles. These are termed "indirect" flight muscles because they are attached to the cuticle as opposed to directly to the wings. These raise and lower the wings by generating deformations of the thorax.

Table 1.3 A list of the six actin genes found in *Drosophila melanogaster* with the stages during development in which they are expressed (Fyrberg *et al.*, 1983). Also shown are the adult tissues in which these actin gene products are located (Fyrberg *et al.*, 1983).

actin gene	developmental expression	location in adult tissue
Act88F	adults	IFMs
Act79B	adults	thorax
Act42A	embryo, pupae, adults	abdominal wall, ovaries
Act5C	embryo, pupae, adults	abdominal wall, ovaries
Act87E	embryo, larvae, adults	head, abdominal wall, leg, ovaries
Act57A	larvae, adults	abdomen, abdominal wall

The ACT88F isoform is the sole actin isoform found in the IFMs (Ball *et al.*, 1987). Since these muscles are not essential for the viability and fertility of flies, the effects of ACT88F mutations upon IFM structure and function can be studied *in vivo*. *Act88F* mutants can be isolated by whole genome mutagenesis which involves exposing flies to a mutagen eg. EMS (ethylmethanesulphonate), and subsequently selecting for an abnormal behavioural phenotype such as flightlessness (Ball *et al.*, 1987; Cripps *et al.*, 1994). Although mutations are recovered in a number of genes, those that map within the 88F polytene region of chromosome 3 can be designated as being *Act88F* specific. A mutation, *E93K*, was isolated in this way (Ball *et al.*, 1987).

A more efficient method for generating *Act88F* mutations involved the random *in vitro* mutagenesis of the 3' end of a cloned *Act88F* gene (Drummond *et al.*, 1991a). By cloning mutated versions of the whole gene into P-element vectors, these mutant alleles could be transfected into the fly germline via P-element mediated transformation (Rubin and Spradling, 1982; Spradling and Rubin, 1982). A *KM88* mutant strain was used as the transformation host since it possesses a base substitution in its *Act88F*

coding sequence that converts codon 79 to a stop codon. Since these flies therefore lack endogenous ACT88F, their subsequent transformation with mutant *Act88F* alleles enables the effects of the latter upon IFM structure and function to be assessed.

After a round of random *in vitro* mutagensis, sequencing revealed that only 7 out of 100 mutagenised clones were characterised by a single amino acid substitution. These 7 missense mutant alleles, *G368E*, *E316K*, *E334K*, *E364K*, *R372H*, *G366D* and *V339I*, were subsequently introduced into flies. Only three of these mutants were able to form a discernible muscle structure. Whereas *G368E* and *E316K* generated relatively normal structure with only minor defects, *E93K* and *E334K* had a more disrupted muscle structure that lacked Z-discs (Drummond *et al.*, 1991a; Sparrow *et al.*, 1991b). Further details of the *in vivo* properties of these mutants will be discussed in chapter 5.

Although the above procedure for isolating and examining mutants has allowed valuable insights into the roles of particular amino acids in determining actin function, analysis relies heavily upon the ability of these mutant actins to assemble into muscle. The inefficiency of this system is highlighted by the recovery of only 2 mutants that can accumulate functional muscle. The severe disruption shown by the mutants may not be unexpected judging from the fact that most of these mutants studied involved charge changes. A greater recovery of mutations could be achieved by site-directed mutations engineered with the knowledge of the atomic structure for actin, (Kabsch *et al.*, 1990), a luxury that was not afforded by Drummond *et al.*.

Through the construction of more subtle mutants in regions that are not in "core" areas vital for the folding of the proteins, but in surfaces that may delineate binding sites, this system can be used effectively for studying actin mutations. Although it is not as efficient as yeast for the rapid recovery of viable mutants, it is a powerful technique that enables the effect of mutant actins upon muscle to be studied.

1.5.2 Expression systems for the *in vitro* study of mutant actins

An essential requirement for the *in vitro* biochemical and biophysical analysis of actin mutations is the recovery of at least milligram quantities of protein. Unfortunately, the traditional protein expression systems have not proved entirely suitable for the expression of actin. The next section will briefly review the different systems that have been, or are currently used to cultivate recombinant actin.

1.5.2.1 *Escherichia coli*

Eschericia coli has proved a powerful tool for studying the structural and functional relationships of many proteins. The advantage of expressing actin in *E.coli* is that unlike other eukaryotic systems, the recombinant protein does not have to be purified away from other endogenous isoforms. Actin expressed in *E.coli* forms insoluble inclusion bodies that are thought to arise through the aggregation of the recombinant protein with the outer membrane components of host cells (Frankel *et al.*, 1990; McNally *et al.*, 1991). These insoluble aggregates are often seen when proteins are expressed at high levels in *E.coli*, eg. the *Dictyostelium* myosin light chain kinase and the head domains of *Drosophila* kinesin and rat cardiac myosin (McNally *et al.*, 1991).

A sarkosyl detergent (N-laurylsarcosine) utilised at low concentrations in an extraction procedure was able to solubilise recombinant actin away from the insoluble membrane components. This actin was deemed to be native, as assessed by its ability to polymerise into filaments, bind to S1 in an ATP dependent manner and also bind to DNaseI. However, the yields were limited to only 30μg/ml (McNally *et al.*, 1991), suggesting that very large numbers of cells would have to be cultivated in order to generate only a few milligrams of protein. More recently, a β-actin isoform expressed in *E.coli* was solubilised by denaturation and then refolded into a native state using an *in vitro* reticulolysate system supplemented with a cytoplasmic chaperonin (Gao *et al.*, 1992). Despite these efforts, the need to denature actin prior to its biochemical characterisation questions the authenticity of the final protein.

1.5.2.2 *Dictyostelium discoideum*

Actin expression in *Dictyostelium discioideum* is complicated by this organism's possession of multiple actin genes which encode a number of isoforms (Vanderkerkhove and Weber, 1980). Nevertheless, the expression and purification of mutations in the *Dictyostelium 15* actin gene has been established (Sutoh *et al.*, 1991). The major drawback of this system is that any mutations engineered *in vitro* by site-directed mutagenesis have to incorporate a charge change such that upon expression, the recombinant actins can be isolated from the endogenously expressed WT isoforms by anion exchange chromatography. The *in vitro* biochemical analysis of mutations expressed using the *Dictyostelium* expression system are described in section 5.1.5, (Sutoh *et al.*,1991; Johara *et al.*,1993).

1.5.2.3 *Saccharomyces cerevisiae*

Two strategies can be adopted for the expression of actin in yeast. The first involves isolating actin from null host strains complemented by the integration of a heteologous actin gene, (see section 1.5.1.3). Recombinant actin can be purified from these cells without the need for its separation from the endogenous actin isoform (Shortle *et al.*,1984; Johannes and Gallwitz, 1991; Cook *et al.*, 1991; Karlsson *et al.*, 1991; Cook *et al.*, 1992). The second procedure involves the transformation of host cells with a mutant gene that is expressed in concert with *Act1*$^{+}$, either after integration into the host genome, or during stable maintenance upon extrachromasomally localised expression vectors. The range of mutations studied in this system is also limited in the same way as the current *Dictyostelium* expression system mentioned above. Only heterologous gene products having a charge differential with respect to that of yeast actin can be isolated from this endogenous isoform after expression (Karlsson, 1988; Aspenström and Karlsson, 1991; Aspenström *et al.*, 1992a; 1992b; 1993).

Initial reports suggested that the overexpression of recombinant actin in yeast resulted in host cell lethality (Shortle (unpublished); Huffaker *et al.*, 1987; Magdolen *et al.*, 1993). This was not so surprising in light of findings that the overexpression of genes

encoding other yeast cytoskeletal proteins also proved lethal to the host. These observations suggest that essential cytoskeletal assembly and function is governed by a precise stoichiometry between actin and a complex system of actin-binding proteins. Mutation or overexpression of any one of these cytoskeletal components may upset this delicate balance and subsequently disrupt vital host cell functions.

This statement was substantiated by Magdolen *et al.* (1993) who demonstrated that the deleterious effects generated by overexpressing actin could be suppressed to some extent by the co-overexpression of yeast profilin. The sequestration of excess actin by excess profilin probably acts to rebalance the stoichiometric levels by reducing actin assembly, thus bestowing these cells with a phenotypically near normal actin microfilament system. Karlsson (1988) adopted a more subtle approach to express actin in yeast and his system is described in chapter 3.

1.5.2.4 *Drosophila melanogaster*

To date, the isolation of ACT88F from mutant strains of *Drosophila melanogaster* is complicated by the presence of the five other endogenous actin isoforms. Anson *et al.* (1995) performed the kinetic and *in vitro* motility analysis of two actin mutants using material purified from whole flies, (see section 5.1). Despite these preparations containing the other endogenous isoforms, mutant effects were still discernible. The development of this organism as a system for providing milligram quantities of pure mutant protein for biochemical analyses is described in chapter 4.

1.6 Motility assays

The presence of actin and myosin in non-muscle, as well as muscle cells supports the prediction that a common elementary actomyosin interaction defines the basis for a variety of cellular motile behaviours such as cytokenesis, exocytosis, cytoplasmic streaming and muscle contraction. However, despite extensive research into muscle actomyosin, the molecular mechanism of mechanochemical transduction has yet to be elucidated. The *in vitro* motility assays described below allow the direct, real time

visualisation of movements which are due to an interaction between actin and myosin molecules alone.

The glass-surface based assays of Kron and Spudich (1986) are now used routinely as an alternative approach for assessing the functions of actin and myosin mutants. Assays incorporating the current advances in optical trap technology (Finer *et al.*, 1994; Ishijima *et al.*, 1994; Molloy *et al.*, 1995) in conjunction with various features from the standard motility assay, permit the realisation of forces and displacements produced by single actomyosin crossbridges. The next section describes the development of the motility assay from the direct observation of movement in the giant green algal cells of *Chara* and *Nitella* to the present day where the nano-manipulation of actin and myosin are being used to elucidate the mechanism of mechanochemical transduction.

1.6.1 The early qualitative *in vitro* motility assays

The rotational cytoplasmic streaming first discovered by Corti (1774) in giant *Characean* cells is driven by a motive force which produces an active shearing at the interface between the stationary cytoplasmic cortex and the outermost layer of the flowing endoplasm. Embedded into the cortex are rows of chloroplasts which run parallel to the direction of streaming and are lined with subcortical fibrils on their endoplasmic-facing edges. Decoration of these fibrils with skeletal muscle HMM revealed an F-actin composition which was postulated to interact with putative myosin molecules in the endoplasm to generate streaming (Chen and Kamiya, 1975). HMM decoration of these fibrils (Kersey *et al.*, 1976) produced arrowheads pointing upstream, demonstrating that the actomyosin interaction during cytoplasmic streaming in *Nitella* and *Chara* has the same polarity as that during skeletal muscle contraction.

Initial *Nitella* based *in vitro* assays attempted to reproduce the interaction driving cytoplasmic streaming by using a cell free system. If an internodal cell of *Nitella* is cut open, its cytoplasm can be carefully squeezed out onto a shallow glass cuvette containing an ATP activating solution to form an endoplasmic droplet. Kamiya and Kuroda (1956) were able to observe rapid, independent, axial rotation of chloroplasts

in this *in vitro* system using phase contrast microscopy. This rotation may involve actin filaments attached to the chloroplast surface interacting with putative endoplasmic myosin by the same molecular mechanism that produces the shearing force responsible for cytoplasmic streaming. The only difference between these two processes is that in cytoplasmic streaming, chloroplasts are anchored along the cell cortex whilst during rotation, they are free in the cytoplasm.

Kuroda and Kamiya (1975) were able to puncture the surface membrane of these endoplasmic droplets using a fine glass needle, thus dispersing the cytoplasmic extract into the activating medium. Chloroplasts in this demembranated *in vitro* system were shown to rotate almost as actively as before the surface membrane was removed. Kuroda and Kamiya (1975) were able to inhibit chloroplast rotation with NEM, a treatment which prevented cytoplasmic streaming of the endoplasm of living internodal cells (Chen and Kamiya, 1975). The subsequent reactivation of *in vitro* chloroplast rotation by addition of skeletal muscle HMM to the medium was one of the first *in vitro* demonstrations that chloroplast rotation, and consequently cytoplasmic streaming *in vivo*, is generated by the interaction between actin and myosin in the presence of Mg-ATP.

Higashi-Fujime (1980) used this same demembranated *in vitro* system to show, by phase contrast microscopy, that chloroplast chains linked together by invisible cytoplasmic fibrils move at a rate of 10μm/s for 5-10 minutes. Dark field microscopy of the same *in vitro* cell also revealed that movement of free cytoplasmic fibrils followed curved tracks. These fibrils never reversed their direction of movement and often formed ringed or polygonal structures which rotated at the same velocity as the free fibrils. Decoration of moving fibrils with rabbit skeletal muscle HMM revealed a polarity in which the direction of sliding movement *in vitro* was the same as that during endoplasmic streaming.

Although direct observation of *in vitro* motility was made possible using these initial systems, the presence of contaminating cytoplasmic components, analogous to the presence of accessory sarcomeric proteins in studies using single demembranated

muscle fibres, may influence the overall actomyosin interaction and complicate subsequent interpretations. A number of the following investigations therefore utilised totally defined biochemical systems where the direct observation of movement between purified proteins revealed for the first time that actin and myosin alone were capable of generating movement.

Superprecipitation, first demonstrated by Szent-Gyorgyi (1951), effectively represents a reconstruction of the basic interaction involved in muscle contraction. This is initiated upon the addition of ATP to a test tube containing purified actin and myosin at low ionic strength. Higashi-Fujime (1982) observed the events involved in superprecipitation under dark field microscopy. After an initial increase in the turbidity of the protein mixture, large aggregates of actomyosin fibrils appeared and attached to the glass surface. These aggregates then dispersed, resulting in the spontaneous appearance and disappearance of fibrils displaying forward and backward sliding-like movements of around 30μm/s. This bi-directional movement was attributed to the parallel and antiparallel arrangement of polar actin filaments in the bundles of F-actin and myosin filaments, and closely resembled the *in vitro* movement of cytoplasm in an endoplasmic droplet.

Whereas this latter investigation displayed actomyosin fibril motility, a subsequent analysis by Higashi-Fujime (1985) demonstrated the unidirectional movement of short myosin filaments over polar bundles of F-actin at a velocity of 6μm/s. These bundles were generated spontaneously using a modification of the conditions used in the previous investigation which involved superprecipitation in the presence of a high concentration of $MgCl_2$. Some myosin filaments were seen to change their direction of movement along their axes over dispersed single actin filaments free in suspension. The change in direction of these bipolar myosin filaments corresponded to their exchange between actin filaments of different polarities. Nagashima (1986) also described the bi-directional movement of synthetic myosin filaments in an actomyosin system at an ionic strength of 130mM KCl, where superprecipitation does not occur.

Actomyosin generated movements were also reconstituted in a novel, artificial system (Yano, 1978; Yano *et al.*, 1978). This recreated a steady unidirectional streaming in a circular slit filled with a HMM solution supplemented with ATP. The circulating flow was due to the direct interaction between the HMM in suspension and specifically oriented F-actin that was coated onto the sides of the chamber. This movement exhibited similar properties to cytoplasmic streaming, and as demonstrated by most of the aforementioned investigations, represented pointed-end forward directed motion which is analogous to that seen in skeletal muscle actomyosin.

1.6.2 The quantitative *in vitro* motility assays

1.6.2.1 The *Nitella* bead assays

In vitro assays endow a greater control over the number and type of contractile proteins involved in the interaction as well as the local chemical environment. The *Nitella* bead assay of Sheetz and Spudich (1983), subsequently redefined in Sheetz *et al.* (1984), represented the first major *in vitro* system in which movement could be routinely quantified. It manipulates the aforementioned polar actin cables which line the cytoplasmic face of cortex embedded chloroplasts in *Nitella* cells. There are approximately five actin cables for each chloroplast file, each cable being 0.2μm in diameter and consisting of hundreds of actin filaments all possessing the same polarity.

By surgically splitting open a giant internodal cell of *Nitella*, and washing away the cytoplasm and endogenous mobile elements, the bared actin filaments were used as an organised substratum for myosin coated beads where ATP dependent movement was observed under fluorescent light microscopy. The fluorescent beads used in this assay were 0.7μm in diameter and covalently crosslinked to rabbit skeletal muscle myosin. Any beads that came into contact with the bared actin filaments ceased Brownian motion and displayed stable, unidirectional movement with the same polarity that cytoplasmic flow would occur in an unopened cell. Although myosin filaments were bound to beads in random orientations, the directed motion was determined by actin filament polarity. Velocities ranged from 0.5-10μm/s with an average of 2.5μm/s.

Hynes *et al.* (1987) suspected that the preferred attachment site of myosin to the beads used in the above assays was via the head. This predicted that the previously demonstrated movement using HMM (Sheetz *et al.*, 1983) or myosin (Sheetz *et al.*, 1984) substrates was probably mediated by aggregates of HMM or myosin which ensured that some heads projected off the bead surface, allowing an interaction with actin. Hynes *et al.* (1987) subsequently substituted these beads with formalin-fixed *Staphylococcus aureus* cells which possess protein A upon their surface. The latter binds antibodies to which myosin or its subfragments can be attached. This method, in which myosin or HMM was bound specifically and with a better defined geometry, generated more reliable movement with velocities greater than 1μm/s.

These assays generate reproducible quantitative movement data which are comparable to the relative rates of sliding of actin and myosin filaments in muscle. Although the effects of different myosin species could be investigated in the *Nitella* system, the versatility of this assay is limited by the biochemically undefined composition of the actin filament bundles which may also contain cytoplasmic components of *Nitella* and unknown stabilising factors.

1.6.2.2 The glass surface based assays

In a modification of the *Nitella* assay, Spudich *et al.* (1985) substituted the undefined *Nitella* actin cables with an array of polar aligned actin filaments of known composition. This was achieved by irreversibly binding biotinylated *Dictyostelium* severin to actin filaments at their barbed ends, thus enabling their immobilisation onto an avidin coated substrate. Application of flow subsequently orientated bound filaments with their free pointed ends directed downstream. When myosin coated beads were placed onto this array, they were seen to move upstream against the flow of the buffer at rates of movement similar to those measured in the original assay, thus allowing a reliable quantitative measurement of movements produced by purified actin and myosin. The problem with this particular assay was that as well as the force generating interaction still involving a number of accessory molecules, many of the beads attached to the avidin substratum without moving.

The glass surface based assays were devised soon after Yanagida *et al.* (1984) demonstrated that single fluorescent actin filaments labelled with rhodamine-phalloidin could be visualised in solution using video enhanced light microscopy. The phalloidin conjugate stabilises actin filaments by a tight binding and vastly reduces the critical actin concentration required for polymerisation, therefore preventing filament depolymerisation during dilute assay conditions. Alternatively, Honda *et al.* (1986) observed fluorescent actin filaments by labelling with fluorescein isothiocyanate (FITC) which binds covalently to Cys374 on each monomer in a phalloidin stabilised actin filament.

These glass-based assays overcome the problematic requirement for large arrays of actin of known polarity by inverting the *Nitella* system so that purified myosin represents the immobilised substrate. The movement of fluorescent actin filaments upon a glass fixed myosin substrate was first reported by Kron and Spudich (1986). Although myosin filaments directly attached to the glass surface were randomly arranged as in the *Nitella* assay, the specific binding of actin to myosin resulted in a continuous, directional sliding at velocities of about 6μm/s, rates which are consistent with those obtained from muscle fibre experiments and *Nitella* assays.

Under fluorescence microscopy, actin filaments free in solution are observed to bend, rotate and sway under Brownian motion. These movements suggest that actin filaments are analogous to semi-flexible rods (Yanagida *al et.*, 1984). These filaments also display a number of characteristics in the *in vitro* motility assay which were noted by Kron and Spudich (1986), and encountered by subsequent investigators. Fluorescent actin filaments display a great variation in length, ranging from 5-40μm long. Under rigor conditions, they bind tightly to the immobilised substrate surface and cease Brownian movements. Motility is initiated upon the addition of a standard assay buffer containing 2mM ATP and filaments exhibit random unidirectional motion along winding paths up to distances of 50μm.

During smooth movement, the posterior end of each actin filament will follow the same path as that led by the anterior end, such that the shape of a filament at any one time

can be superimposed upon the track of movement that it followed. This suggests that an actin filament interacts with particular myosin heads which are able to convey its movement from the anterior to the posterior end at a uniform rate. Sometimes, filaments wash off the surface during movement whilst others free in solution diffuse down onto the surface and begin moving.

Although the majority of the motion exhibited is smooth, some filaments display erratic movement during which periods of motility are interspersed with static intervals. This latter behaviour is probably caused by the presence of inactivated myosin "dead heads" on the substrate surface which lose their ability to dissociate from actin filaments, even in the presence of ATP, possibly generating a rigor-like state. A modification to the substrate prior to surface decoration is able to eliminate these dead heads. This is achieved by mixing the myosin substrate with unlabelled F-actin, in the presence of ATP, and then performing high speed centrifugation. Any inactivated myosin molecules will pellet with the F-actin, leaving the supernatant with a high percentage of active heads that are able to dissociate from actin in the presence of ATP. These produce an ideal myosin plane which conveys the smooth movement of actin filaments.

Another characteristic of the motility assay is that long filaments undergo severe fragmentation into shorter filaments which each continue sliding in the same direction as the original filament, but along different tracks. A densely packed substrate surface generating an excess of head interactions, low ATP or low ionic strength are all factors which may impart a great mechanical stress upon actin filaments, thus promoting their breakup. Filament disintegration is also facilitated by high temperatures and oxidation by free radicals in the assay buffers. High temperatures are generated under prolonged exposure to a light source but can be overcome through the employment of temperature regulated microscope stages and heat filters.

Quenching of the excited states of fluorescent groups by molecular oxygen results in free radical generation that contributes to the photodestruction of actin-bound rhodamine-phalloidin. This causes a reduction in actin filament stability that manifests itself as a loss of filament sliding, photobleaching and filament fragmentation. Kishino

and Yanagida (1988) limited the degree of photodestruction by designing a novel system in which an enzymatic reaction mops up all the free radicals in solution, (see section 5.2.4.1). All of the aforementioned improvements prevent filament fragmentation, prolong the intensity of the fluorescence image and virtually eliminate intermittent movement which is an essential requirement for quantitative velocity measurements.

1.6.3 Myosin attachment to the substrate surface

The modifications of the original glass surface based assay of Kron and Spudich (1986) by Toyoshima *et al.* (1987) are generally employed by most motility researchers to date. In contrast to using a bare glass surface, a glass coverslip coated with 0.5% nitrocellulose in water (Toyoshima *et al.*, 1987), subsequently modified to 0.1% nitrocellulose in amyl acetate (Uyeda *et al.*, 1990), was used to achieve movement of actin filaments over randomly distributed monomeric myosin, myosin filaments, HMM and S1. Whereas filament velocities on monomeric and polymeric myosin were comparable to those obtained from the original glass surface based assays, HMM mediated movement was faster and that of S1 greatly reduced.

It was suggested that the difference in the rates of movement over S1 and HMM could be attributed to their alternative modes of binding to the nitrocellulose film. Sheetz *et al.* (1984) and Sellers *et al.* (1985) discuss the problems of coating polystyrene beads with myosin or HMM, stating that myosin heads could become attached to the bead surface equally as well as the rod portion of the molecule. Toyoshima *et al.* (1987, 1993) illustrated that S1 and HMM were bound to the nitrocellulose surface in a number of specific configurations. Through proteolytic digestion of myosin subfragments whilst they were attached to the nitrocellulose and subsequent analysis of the subfragment species released or remaining bound to the film, they showed that both S1 and HMM attached either via their heads or tails, or sometimes both in the case of HMM, to the surface. Additionally, they surmised that only those subfragments that bound via their tail portions, which represented 10% of the total number bound, were capable of conveying actin filaments. Therefore, despite this heterogeneity of binding

configurations, directed movement was probably only produced by a small proportion of suitably bound myosin molecules.

1.6.4 Identification of the minimal motor domain

The *in vitro* motility assay can be used to identify the minimal functional domains of myosin required to generate a motive force that drives sliding. The *Nitella* based assay of Sheetz *et al.* (1984) demonstrated that whole myosin was capable of supporting bead movement. Hynes *et al.* (1987), using his modified version of the *Nitella* assay, addressed the search for the motor domain by demonstrating movements mediated by myosin and its subfragments HMM and short HMM. Investigation of the latter established that neither thick filament formation nor the hinge region at the end of the S2 tail were required for sliding. Additionally, Harada *et al.* (1987) questioned whether cooperation between the two heads in a myosin molecule was required for sliding, and consequently muscle contraction, by using a glass surface based assay similar to that of Kron and Spudich (1986). They demonstrated that a single headed myosin was capable of producing actin filament motility, but at slightly lower velocities than intact myosin, thus illustrating that single myosin heads are capable of generating force and movement.

In order to pinpoint the force generating domain of myosin, Toyoshima *et al.* (1987) showed that S1 alone could support actin filament movement. Thus, the *in vitro* motility assay (Kron and Spudich, 1986), subsequently modified by Toyoshima *et al.* (1987), has enabled important conclusions regarding the myosin molecule and its mode of action during sliding to be made. It has been used to identify the minimal motor domain and to show that no portion of the rod domain is required for movement *in vitro*.

1.6.5 Myosin head flexibility

Much evidence indicates some degree of torsional freedom in actomyosin, most probably in the region of the myosin head. Kinosita *et al.* (1984) suggested that the

myosin head rotates rapidly along its long axis over distances of tens of nanometres every microsecond in search of a favourable binding site on actin. Although this "wobbling" occurs in random orientations, its high frequency ensures efficient binding. To generate movements of this magnitude, Kinosita concluded that there must be a large amount of rotational freedom about an S1.S2 hinge as well as between the S2.LMM pivot. This statement was corroborated by Winklemann and Lowey (1986) and Miyanishi *et al.* (1988) who argued that a variation in the binding position of antibodies specific to the 25KDa and 50KDa domains of the myosin head was due to the rotational flexibility at the S1.S2 hinge region. Reedy *et al.* (1989) and Sparrow *et al.* (1991b) also confirmed flexible movements of myosin heads by demonstrating that in *Drosophila* flight muscles of two different mutants of the *Act88F* actin gene, reverse rigor bridge angles, due to myosin heads binding actin filaments of opposite polarity, could be seen.

Clear demonstrations of the flexibility of myosin heads was achieved by two sets of *in vitro* motility assays. The first (Toyoshima *et al.*, 1989) showed that a single "HMM track" could convey actin filaments in either direction, the direction depending solely upon the polarity of the filament. The track used in this assay was constructed by coating a nitrocellulose film with HMM-decorated actin filaments. Upon the addition of ATP, the bound filaments slid off the track leaving behind an alignment of individual HMM molecules at an optimal periodicity for interaction with actin filaments. This was reflected in the constant velocities obtained using these tracks. In contrast, most motility assays generate a great degree of variability in filament velocities due to imperfections in the nitrocellulose surface. Although the randomly bound myosin heads are flexible enough to mediate movement through 180°, variations in the periodicity of adjacent myosin heads constitutes a sub-optimal surface which results in a reduction of the maximal filament velocity.

The second *in vitro* assay system, in which the bi-directional movement of fluorescent actin filaments was seen, involved movement over native, molluscan smooth muscle thick filaments, both towards and unexpectedly away from the central bare zone (Sellers and Kachar, 1990). Observed velocities were approximately ten times greater

towards the centre of the myosin filament than away from it, suggesting both that myosin molecules are flexible enough to interact with actin through 180° and that filament velocity depends upon the myosin head orientation.

The main discrepancy between these two sets of *in vitro* assays concerns the fact that the velocity of actin filaments is the same in both directions over the HMM track but not the myosin filament substrate. The determining factor for velocity may reside in the difference between the constraints placed upon the myosin heads in nitrocellulose-bound HMM and native thick filaments. The HMM track consists of individual HMM molecules that are deposited onto the nitrocellulose in a correct orientation and register such that the myosin heads may be able to rotate freely about their S1.S2 hinge and generate maximal velocity. In thick filaments, although myosin heads can bind actin filaments in unfavourable orientations (Reedy *et al.*, 1989; Sparrow *et al.*, 1991b; Craig *et al.*, 1980), their flexibility may be constrained by the tight specific packing into filaments. This may subsequently reduce the freedom around the S1.S2 hinge and slow actin filament movement in the unfavourable direction.

1.6.6 Filament velocity and step size during the *in vitro* motility assay

The classical crossbridge model proposes a tight mechanochemical coupling between each force producing cycle and ATP hydrolysis event (Huxley, 1969). It also implies that the step size, defined as the working stroke distance conveyed by one crossbridge during a single ATP hydrolysis event, should be no greater than 40nm. This distance represents the maximum possible stroke size that can be achieved by a myosin head, of chord length 20nm, swinging through an arc of 180°, though the current consensus is that the head probably moves through a maximum of 90°. Alternatively, Rayment *et al.*, (1993b), (see section 1.4.2), proposed from their solution of the S1 atomic structure that a conformational change in the myosin head could transmit movement through the extended coiled-coil portion of the myosin head to produce a 5nm stroke displacement upon single ATP molecule hydrolysis.

Attempts have been made to determine the step size, (**d**), from *in vitro* motility assays (Harada and Yanagida, 1988; Harada *et al.*, 1990; Toyshima *et al.*, 1990; Uyeda *et al.*, 1990; Uyeda *et al.*, 1991). The following premises regarding the number of heads involved during sliding, in relation to the ATPase cycle, had to be considered in these investigations. As described in section 1.4, the duration of the actomyosin ATPase/crossbridge cycle (t_c) can be split into two phases corresponding to periods of time in which actin and myosin are essentially detached, undergoing rapid association and dissociation events, and attached, where the myosin head is strongly bound to the actin filament, (see figure 1.11). Uyeda *et al.* (1990) estimated that the duration of the strongly bound state (t_s) represents only a small fraction of the total ATPase cycle time and is approximately equal to 0.05.

Figure 1.11. A diagrammatic representation of the ATPase cycle for a single myosin head. The grey shaded areas represent the proportion of the crossbridge cycle, (not drawn to scale), where actin and myosin are weakly attached, undergoing rapid association and dissociation events, (t_c). The blackened segment represents the small fraction of time, (not drawn to scale), where actin and myosin are strongly attached, (t_s). The end of this phase represents the power stroke event.

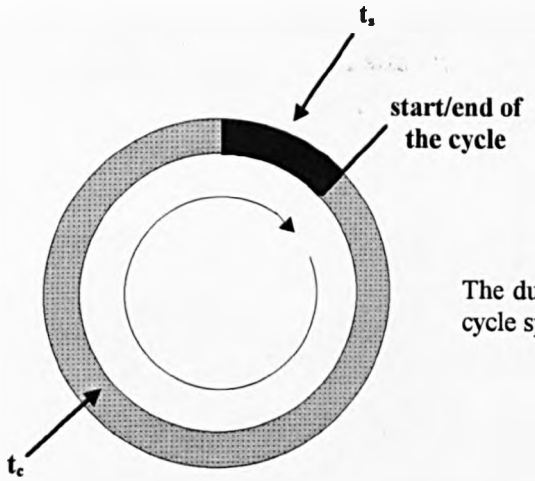

The duty ratio, (**f**), represents the fraction of the ATPase cycle spent in the strongly bound state.

$$f = t_s / t_c \quad (1)$$

When f is small and only a few myosin heads are bound to an actin filament, then the probability that more than one head is bound in a force generating state is very low. Considering tight mechanochemical coupling, a single, strongly bound head will only undergo a power stroke after each release of ADP hydrolysis product (an ATP hydrolysis event). Consequently, filament velocity (v_i) will be kinetically limited by the duration of the ATPase cycle, where

$$v_i = d / t_c \quad (2)$$

Assuming that myosin heads stroke asynchronously and at constant speeds, the velocity component generated by two heads would essentially be additive and therefore double the velocity mediated by a single head, ($2.v_i$). This velocity would again be limited by t_c. When the number of heads interacting with a filament is increased, a quantity is reached where the probability of the force generating states of different heads overlapping is higher than with a limiting number of heads. At this point, filament velocity (v_0) is no longer limited by t_c but by the dissociation of the strongly bound state (t_s), such that

$$v_0 = d / t_s \qquad (3)$$

Attempts to determine step size through the employment of motility assays yielded conflicting estimates. Some are in accordance with the current model and propose a 7-28nm range in the step size (Toyoshima *et al.*, 1990; Uyeda *et al.*, 1990; Uyeda *et al.*, 1991) whereas others estimate displacements of up to 130nm (Harada and Yanadiga, 1988; Harada *et al.*, 1990). Most of the investigations used the following formula to calculate step size, d.

$$d = v_0 . t_s \qquad (4)$$

An ideal calculation for step size would measure the stroke displacement, (estimated from the filament velocity during the motility assay), for a single ATP hydrolysis event. However, the estimation of step size during the *in vitro* motility assays is complicated by the fact that filament sliding is mediated by many strongly bound heads undergoing asynchronous power strokes, and consequently multiple hydrolysis events.

Toyoshima *et al.* (1990) and Harada *et al.* (1990) observed that for any saturating density of heads, the actual number interacting with actin is determined by filament length. Actin filaments of all lengths bind tightly to a myosin coated surface in rigor. However, upon the addition of ATP, the probability of a very short actin filament having a continuous contact with at least one force generating head is much lower than that for a long filament and subsequently implies that this short filament will spend

periods of time where it is only weakly bound to the surface. During this time Brownian motion will facilitate its dissociation from the substrate surface.

To minimise the number of heads interacting with an actin filament, the use of minimum length filaments (MLF) was introduced. These allow a measurement of the activity mediated by one or a few strongly bound heads which are sufficient to prevent actin filament dissociation from the substrate surface. These filaments therefore generate a sliding velocity limited by t_s. Where Toyoshima *et al.* (1990) described a step size of 8±2nm, Harada *et al.* (1990) estimated a step size greater than 100nm, a value which is inconsistent with the tight coupling crossbridge model and demands multiple cycles of myosin head attachment and detachment for each ATP hydrolysed. The discrepancy between these two sets of data may reflect the variation in the estimates of the number of attached heads and also that Toyoshima *et al.* utilised HMM whereas Harada *et al.* employed native myosin filaments in their respective motility assays (Huxley, 1990; Burton, 1992).

Uyeda *et al.* (1991) calculated step size by measuring the velocity of filaments shorter than the minimum length moving over a surface sparsely coated with S1. Since these filaments would not be in continuous contact with a strongly bound, stroking head, spending the majority of time in weak binding interactions, their dissociation from the surface by lateral Brownian motion would be expected. This was prevented by the inclusion of 0.8% methylcellulose in the ATP buffer. Subsequently, these filaments spent long stretches of time exhibiting axial Brownian motion interspersed with periods of very slow constant sliding. This "unitary velocity" nv_i, (n representing the number of bound heads), probably generated by one or two heads, was much slower than the maximal sliding velocity and was limited by t_c. Therefore,

$$d = v_i \cdot t_c \qquad (5)$$

From this study, a step size of 5-20nm was predicted, a value which is in accordance with the current crossbridge theory.

The *in vitro* motility of actin filaments at high ionic strengths observed by Takiguchi *et al.* (1990) supports the loose coupling model described by Yanagida *et al.* (1985). Under these conditions, filaments exhibited unstable movement which appeared to be produced by interactions with the surface at one or a few points. The latter were thought to represent single, strongly bound heads which conveyed movement for a few μm over a brief period of time, thus reflecting a step size of 100nm. A single myosin head moving an actin filament through such a large distance would need to maintain some sort of continuous interaction with the actin filament which prevents its dissociation from the surface. It was therefore postulated that the myosin head would remain attached to the filament in a weak binding state analogous to that of the dynein-microtubule ADP-vanadate weak binding complex which exhibits one dimensional diffusion along the long axis of the microtubule over large distances (Vale and Fumio, 1990).

A controversy still exists as to whether the step size measured from the above studies conforms to the limits set by the classical crossbridge theory. The *in vitro* motility assay may not represent the most suitable means for determining this quantity because it measures velocity under virtually unloaded conditions, which are not an accurate representation of sliding in muscle. It has been proposed that ATP hydrolysis, and therefore step size, may be dependent upon the load in a system. Consequently, during unloaded conditions, there may be numerous power strokes for each ATP hydrolysis event whereas at higher loads, a tight 1:1 coupling between these two processes may occur. The next section describes how the measurement of the actual working stroke displacement is made possible.

1.6.7 Single molecule force and working stroke measurements

Through refinement of existing *in vitro* motility assays, two groups participated in the race to observe force and displacement events generated by single myosin molecules. Ishijima *et al.* (1994) adopted a system devised by Kishino and Yanagida (1988) and employed by Ishijima *et al.* (1991) to detect piconewton range forces produced by the interaction between a small number of myosin molecules and an actin filament. It

involved the attachment of one end of a fluorescently labelled actin filament to a fine glass microneedle, and manipulation such that the other end was lowered over a myosin substrate. Upon attachment, myosin induced force and displacement events were manifested as a bending of the microneedle. Since the stiffness of these needles had been precalibrated and the position of the needle could be determined with nanometre accuracy using a sensitive photodiode detector, this technique enabled the simultaneous measurement of force and displacement.

Ishijima *et al.* (1994) addressed the problem that a randomly oriented myosin substrate may reduce the efficiency of force production and displacement by using myosin filaments in the assay. To ensure single molecule events, synthetic myosin cofilaments containing varying ratios of intact myosin monomers and myosin rod domains were generated. A 1:32 myosin:rod cofilament displayed a normal bi-polar structure except for the predicted sparse distribution of myosin heads upon the filament surface. Ishijima *et al.* used glass microneedles of various stiffnesses, to measure force transients at conditions analogous to high and low load.

Finer *et al.* (1994) approached the measurement of forces and displacements by constructing an optical trap system similar to the one used to detect single events mediated by kinesin molecules (Svoboda *et al.*, 1993; Svoboda and Block, 1994). Unlike Ishijima *et al.*, Finer *et al.* adhered more closely to the conditions of the original *in vitro* assays by using 1μm silica beads, coated with randomly orientated HMM molecules, as docking platforms onto which actin filaments were lowered. A sparse distribution of HMM molecules on the bead surface, coupled with its curvature, limited the number of heads that could interact with the actin filament and subsequently increased the likelihood that any observed events were caused by single motor molecules. Manipulation of actin filaments using optical traps involved attaching a single, 1μm diameter, polystyrene bead, covered with NEM-HMM, to each end of a fluorescently labelled actin filament.

To measure single molecule displacements or forces, each of the beads was caught in an optical trap, the actin filament between them pulled taut, and this assembly was then

lowered into position over the bead surface. Compliant optical traps, originally thought to be stiff enough to reduce Brownian motion, were used to measure single molecule events under conditions of low load. Sensitive photodiode detectors monitored the position of one of the actin bound beads and thus enabled a measure of any displacement with nanometre accuracy. To measure force at higher loads, stiffer traps were used in conjunction with a feedback system. The latter applied a displacement to the optical trap by an amount proportional to the myosin induced force and subsequently retained the bead in the centre of the trap. The magnitude of the trap displacement therefore provided a measure of myosin-induced forces acting upon the actin filament under conditions representative of isometric force.

Whereas the system employed by Ishijima *et al.* enabled measurement of force and displacement simultaneously, that of Finer *et al.* determined these parameters separately. At high load conditions, Ishijima *et al.* (1994) observed forces and displacements of 5 ± 2.3pN and 4.7 ± 1.8nm respectively. Under conditions more indicative of isometric tension, Finer et al. (1994) were able to display single force transients over three different ATP concentrations ranging from 1μM, 10μM and 2mM ATP. The magnitude of the average force was 3.4 ± 1.2pN, with a range of 1-7pN, and the duration of the force increased as the ATP concentration was lowered.

Under conditions of low load, Finer *et al.* (1994) detected 11-12 nm displacements over the three specified ATP concentrations, with the duration of these displacements also increasing with a decrease in the ATP concentration. It was suggested that each transient could be due to a single ATP hydrolysis event and that at low ATP concentrations, duration was limited by ADP release. Observations at sub-saturating HMM concentrations revealed that although displacements were larger than those at lower HMM concentrations, the beads spent periods of time at discrete levels which were 11nm apart. It was suggested that these multiple steps were due to a small number of HMM molecules sequentially attaching to and moving the actin filament. Svoboda *et al.* (1993) postulated that by measuring displacements at low ATP concentrations in this system, a kinesin motor generating many steps for each ATP hydrolysed would exhibit periods of time at zero displacement interspersed with

clusters of multiple steps. Finer *et al.* stated that the displacement steps seen at low load and ATP concentrations in his investigation were discrete and unclustered, suggesting a 1:1 coupling between ATP hydrolysis and force generation.

The measurements made by Ishijima *et al.* were complicated by Brownian noise at conditions of low load. Despite this, discrete force spikes of reduced force and displacement, compared to those at high load, were still apparent. At zero load conditions, the force transients were very sharp and displayed clustering. This non-linearity of the effect of load on force and displacement led Ishijima *et al.* (1994) to question the conventional theory, as previously proposed in Ishijima *et al.* (1991), which suggests that each power stroke corresponds to a single ATP hydrolysis irrespective of load. Although it was established that at high loads, a 1:1 coupling between the ATPase and power stroke existed, at lower loads, it was suggested that many steps may occur during one ATPase cycle. Finer et al. (1994) were able to identify a load dependence in their system. Unlike Ishijima *et al.*, this was concerned with a significant difference in the duration of single forces (high load) and displacements (low load) at 10μM and 2mM ATP. Finer *et al.* suggested that these may be due to altered ATP binding affinities at different loads.

Therefore, both groups confirm a step size which does not satisfy the constraints imposed by the current model of contraction, although they both highlight the importance upon load in the measurement of these parameters.

Using an optical trap system similar to that of Finer *et al.* (1994), Molloy *et al.* (Nature, in press) have recently demonstrated a working stoke of 5.5nm, a value that is consistent with the structural model for muscle contraction. Molloy *et al.* observed that to measure single molecule displacements, a low trap stiffness is required. As a consequence of this, the residual Brownian motion of the trapped beads, and therefore that of the actin filament, producing a distibution of displacements between -25nm and +30nm has to be acounted for in the data analysis.

Whereas Finer *et al.* (1994) predicted a working stroke size of 11-12nm by averaging only the obvious, positive displacements, Molloy took averages over the whole range of Brownian noise. The detection of single molecule steps among Brownian movements was made possible by the observation that when a crossbridge attaches to produce a displacement, an overall increase in the trap stiffness is manifested as a drop in the level of thermal noise. By subsequently performing a running variance analysis of the noise to identify these crossbridge attachments, he was able to measure a full range of displacements, even those that that moved the bead close to its resting position. These displacements gave a continuous distribution whose mean was shifted at about 5.5nm from a distribution representing the noise of the system alone. This mode of analysis would therefore be expected to redefine the working stroke sizes proposed by Finer *et al.* (1994) to magnitudes that would perhaps be more consistent with the current models for the action of the actomyosin crossbridge.

1.7 Aims

Drosophila melanogaster represents a powerful system for the *in vivo* study of actin. It has been used to extensively characterise the effects of a number of ACT88F mutations *in vivo* (Ball *et al.*, 1987; Drummond *et al.*, 1991a; Sparrow *et al.*, 1991a; 1991b; 1992). Despite the versatility of the *Drosophila* system for *in vivo* investigations, *in vitro* biochemical analyses have been limited to small scale G-actin binding and conformational studies (Drummond *et al.*, 1991a; 1991b; 1992; Hennessey *et al.*, 1991). Further analyses, such as the effect of these mutants upon actomyosin function, were prevented by the inability to obtain μg to mg quantities of pure protein. Although kinetic and *in vitro* motility analyses of two of the mutants, using material purified from whole flies, gave encouraging results (Anson *et al.*, 1995), the actin preparations used in this investigation were impure, containing the five other *Drosophila* actin isoforms.

One of the major aims of this thesis was to extend the study of the actomyosin interaction of existing *Drosophila* actin mutants by the *in vitro* motility analysis of pure ACT88F preparations. Additionally, an attempt was made to purify milligram

quantities of ACT88F, the success of which would improve the potential of the *Drosophila* system for studying the *in vitro* effects of actin mutations, subsequently making it a powerful rival to the yeast and *Dictyostelium* systems.

Two independent approaches were adopted to achieve these aims. The first was to express recombinant ACT88F in the yeast, *Saccharomyces cerevisiae*, and the second, to purify endogenous ACT88F actin, from *Drosophila melanogaster*. The latter strategy was tackled in two ways. The observation that *in vitro* motility assays require only nanogram quantities of actin prompted the development of a mini-actin isolation procedure to purify microgram quantities of pure ACT88F actin, from dissected IFMs alone, which would be sufficient for many motility assays. The second approach relies upon the charge differences between the *Drosophila* actin isoforms and the possibility of separating ACT88F from the other endogenous isoforms in whole fly actin preparations by anion exchange chromatography. The ultimate aim of the research presented in this thesis was to gain detailed insights into the interactions between actin and myosin, and the mechanisms of muscle contraction and the actomyosin motor by the analysis of actin mutants.

CHAPTER TWO: MATERIALS AND METHODS

2.1 DNA METHODS

2.1.1 Minipreparation of plasmid DNA

Extraction of plasmid DNA from bacteria utilised the alkaline lysis method of Birnboim (1983). The strain of interest was inoculated into 1.5ml of L-Broth [1% (w/v) tryptone, 0.5% (w/v) yeast extract (Difco), 1% (w/v) NaCl, 100μg/ml ampicillin, pH 7.2] and incubated overnight at 37°C and 250rpm on a platform shaker. The culture was then pelleted for 3 mins in a benchtop microcentrifuge.

The cell pellet was resuspended in 40μl of plasmid preparation mix [25mM Tris-Cl, 10mM EDTA, 15% (w/v) sucrose, 2mg/ml lysozyme, pH 8.0] and incubated on ice for 5 mins. 80μl of 0.2M NaOH, 1% (w/v) SDS was added to the tube, mixed, and this was incubated on ice for a further 5 mins. Next, 40μl of 3M NaAc pH 4.6 was added to each tube, mixed, and placed on ice again for a further 5 mins.

The sample was then spun for 5 mins, the supernatant removed and transferred to a fresh tube. This was extracted twice by adding an equal volume of phenol/chloroform/iso-amyl alcohol, (25:24:1) respectively, vortexing for 10 secs, and then spinning for 2 mins. After each spin, the upper aqueous phase was removed and transferred to a fresh tube, prior to the subsequent extraction step. The sample was then extracted once by adding an equal volume of chloroform/iso-amyl alcohol (24:1), vortexing and then spinning for 1 min.

After the aqueous phases was transferred to a fresh tube, 2 volumes of ice-cold 100% ethanol were added and the DNA precipitated at -80°C for 20 mins. The sample was then spun for 10 mins and the resultant pellet washed with 80% (v/v) ethanol. After dessicating the pellet, it was resuspended in water and stored at -20°C.

2.1.2 Restriction Digests

All restriction digests were carried out according to the enzyme manufacturers' instructions. Restriction enzymes were purchased from Gibco BRL, New England Biolabs, Boehringer Mannheim, Northumbria Biochemicals Limited, Pharmacia and Promega.

2.1.3 Blunt-ending of DNA 5' overhangs

End-filling was performed according to Maniatis *et al.*, (1982). Generally, 1mg of restricted DNA was made up to a final volume of 25µl with reagent mix [0.2mM dNTPs (Pharmacia), 10mM Tris-Cl pH 8.0, 5mM $MgCl_2$, 30mM NaCl]. 5 units of *E.coli* Klenow fragment of DNA polymerase I (Gibco BRL) was added to the mixture and incubated at 22°C for 25 mins. The reaction was stopped by the addition of 0.5µl of 500mM EDTA.

2.1.4 Agarose gel electrophoresis

50ml agarose gels containing 1% agarose (Seachem grade, Flowgen) in TEA buffer [40mM Tris-Cl, 2mM EDTA, 20mM NaOAc, 5.7% acetic acid] were made and 1µl of 10mg/ml ethidium bromide was added before the gel was poured. Samples were mixed with glycerol loading buffer [5% (v/v) glycerol, 10mM EDTA, 0.01% (w/v) bromophenol blue] prior to loading. A 1 Kb ladder (Gibco BRL) was used to estimate the size of the DNA fragments. Additionally, 1µl *Hind*III digested DNA aliquots were used to roughly estimate the DNA concentration. Following electrophoresis, with TEA as the running buffer, DNA was visualised using UV light.

2.1.5 Gel purification of DNA fragments

DNA bands were excised from agarose gels and the DNA was isolated using a Geneclean Kit (Bio 101) by following the manufacturer's protocol.

2.1.6 Ligation of DNA fragments

Ligations were performed according to the method of King & Blakesley (1986). Briefly, 200ng of vector DNA was mixed with a 3-fold molar excess of insert DNA and made up to a volume of 20µl in ligation buffer [50mM Tris-Cl, 5mM $MgCl_2$, 1mM rATP, 1mM DTT, 5% (w/v) PEG 8000, pH 7.6]. 1 unit of T4 DNA Ligase (Gibco BRL) was added and the mixture incubated overnight at 16°C.

2.2 Preparation of frozen competent cells for transformation

Frozen competent cells were prepared using the method of Hanahan (1985). All *E.coli* plasmid transformations used *DH1* competent cells whereas all *M13* plasmid transformations utilised *JM109* competent cells. An overnight of *DH1* in L-Broth [1% (w/v) tryptone, 0.5% (w/v) yeast extract, 1% (w/v) NaCl, pH 7.2] or *JM109* in 2YT [1.6% (w/v) tryptone, 1% (w/v) yeast extract, 0.5% (w/v) NaCl, pH 7.5] was prepared. 2.5mls of the overnight was added to 100mls SOB [2% tryptone, 0.5% Bacto yeast extract, 0.06% NaCl, 0.02%KCl, 10mM $MgCl_2$, 10mM $MgSO_4$, pH 6.8] and grown to a density of 6-9x10^7cells/ml at 37°C and 200rpm.

The culture was chilled on ice for 15 mins and then split into two 50ml polypropylene Oakridge tubes. The cells were pelleted by spinning in a Sorval at 2000rpm for 15 mins at 4°C. Each pellet was gently resuspended in 16.5ml of RF1 [100mM RbCl, 50mM $MnCl_2$, 30mM KOAc, 10mM $CaCl_2$, 15% (w/v) glycerol, pH 5.8] and again left on ice for 15 mins. The cells were then pelleted as above and each resuspended in 4ml of RF2 [10mM MOPS, 10mM RbCl, 75mM $CaCl_2$, 15% (w/v) glycerol, pH 6.8]. During a further incubation on ice for 15 mins, the cells were dispensed into 200µl aliquots, frozen in liquid nitrogen, and stored at -80°C.

For transformation, 1-10ng of DNA (in a maximum volume up to 20µl) was added to a 200µl aliquot of competent cells. After incubation on ice for one hour, the cells were heat-shocked at 42°C for 90 secs and then briefly cooled on ice.

For plasmids, the mixture was spread directly onto L-amp plates [L-Broth, 1.5% (w/v) agar] and incubated overnight at 37°C. For M13, the competent cell mixture was pipetted into 3ml of H-top [1% (w/v) tryptone, 0.8% (w/v) NaCl, 0.8% (w/v) agar] which also contained 1mM IPTG (Gibco BRL), 0.03% (w/v) X-gal (Gibco BRL) and a 1:60 dilution of a fresh *JM109* overnight. This mixture was then poured onto YT plates [0.8% (w/v) peptone, 0.5% (w/v) yeast extract, 0.5% (w/v) NaCl, 1.5% (w/v) agar] and incubated overnight at 37°C.

2.3 Preparation of single and double stranded DNA from *M13*

Following transformation of *M13* DNA into *JM109*, (see section 2.2), each plaque picked was placed into 1.5ml 2YT, (see section 2.2), containing a 1:40 dilution of a fresh *JM109* overnight, and was incubated for 5 hours at 37°C and 300rpm on a platform shaker. The culture was then spun in a microcentrifuge for 10 mins. The cell pellets were used to prepare double stranded DNA as described in section 2.1.1.

For single stranded DNA preparation, the 1.5ml supernatant was carefully removed to a tube containing 300µl phage buffer [2.5M NaCl, 20% (v/v) PEG8000] thoroughly mixed, and left on ice for 1hour. After spinning for 10mins, the phage DNA pellet was resuspended in 640µl TE buffer [10mM Tris-Cl, 1mM EDTA, pH 8.0]. The tube was then spun for 2 mins and the supernatant was transferred to a tube containing 160µl of phage buffer. After mixing thoroughly, the DNA was precipitated at room temperature for 30 mins.

After spinning again for 10 mins, the pellet was resuspended in 100µl TE buffer and mixed with 50µl phenol. This was left at room temperature for 15 mins after which 50µl of chloroform/iso-amyl alcohol, (24:1) respectively, was added and the mixture vortexed. The phases were separated by spinning for 5 mins and then removing the aqueous phase. The latter was then extracted sequentially with 100µl phenol/ chloroform/iso-amyl alcohol, (25:24:1) respectively, and then 100µl chloroform/iso-amyl alcohol, (24:1), respectively.

The DNA aqueous phase was ethanol precipitated by adding 1/10 volume 3M NaAc pH 5.2 and 2 volumes of 100% ethanol, and then incubating at -80°C for 20 mins. After spinning for 10 mins, the pellet was then washed with 80% (v/v) ethanol and dessicated. Upon resuspension with water, the DNA was quantified by running on an agarose gel with known amounts of single stranded DNA markers.

2.4 Site-directed Mutagenesis

Site-directed mutagenesis was performed using a "Muta-gene" *in vitro* mutagenesis kit (Biorad). The kit uses a modified version of the method of Kunkel (1985). The basic principle involves growing *M13* in *CJ236*, a *dut*, *ung* *E. coli* strain which produces an RNA template rich in uracil. This template is used to synthesise a normal second strand *in vitro*, which contains a desired mutation produced by using a mismatched oligonucleotide primer. This uracil rich M13 rf DNA is then transformed into a *JM109* host strain which subsequently replicates the mutant strand with a higher efficiency than the WT uracil rich strand therefore generating mainly mutant phage.

2.5 Sequencing

Sequencing was performed using the T7 Sequencing kit (Pharmacia) which is based on the dideoxy method of Sanger *et al.* (1977). Sequencing reactions were carried out according to the manufacturer's protocol. These samples were then electrophoresed for 4-12 hours at 55W constant power on a 0.5-1.5mm wedge shaped polyacrylamide gel [6% (w/v) acrylamide, 0.4% (w/v) bis-acrylamide, 50% (w/v) urea, 100mM Tris-Cl, 100mM boric acid, 2mM EDTA] which was polymerised by the addition of APS to 1% (v/v) and TEMED to 0.03% (v/v). Sequencing gels were pre-electrophoresed at 55W constant power for 30 mins before loading the samples. After running, gels were fixed in 5% (v/v) acetic acid, 5% (v/v) methanol for 30 mins and then dried down onto filter paper (Whatman) before autoradiography.

2.6 One dimensional polyacrylamide gel electrophoresis, 1D SDS-PAGE

SDS-PAGE (sodium dodecyl sulphate polyacrylamide gel electrophoresis) was performed according to the method of Laemmli (1970) using the BioRad Mini-Protean II gel electrophoresis system. Acrylamide gels [12.5% (w/v) acrylamide, 0.33% (w/v) *bis*-acrylamide, 0.1% (w/v) SDS, 0.37mM Tris-Cl, pH 8.8] were 0.75mm thick and approximately 3.5ml in volume and polymerised by the addition of APS to 0.03% (v/v) and TEMED to 0.04% (v/v). Overlaying this gel with propan-2-ol or water ensured the absence of air bubbles as well as an even surface. A stacking gel [3.75% (w/v) acrylamide, 0.1% *bis*-acrylamide, 0.1% (w/v) SDS, 0.125M Tris-Cl, pH 6.8] was also polymerised by the addition of APS to 0.03% (v/v) and TEMED to 0.06% (v/v).

Protein samples were prepared by adding 1/5 volume of a 5X sample buffer [0.31M Tris-Cl, 10% SDS, 25% (v/v) 2-mercaptoethanol, 50% glycerol, 0.01% bromophenol blue, pH 6.8] to each sample and then boiling the sample for 3 mins. Gels were electrophoresed in a running buffer [1.44% (w/v) glycine, 0.31% (w/v) Tris-Cl, 0.1% (w/v) SDS, pH 8.3] at 200V until the bromophenol blue front reached the bottom of the gel. Gels were then fixed and stained in staining solution [40% (v/v) methanol, 10% (v/v) acetic acid, 0.2% (w/v) Coomassie brilliant blue R] for 15 mins at 37°C and then destained in a 10% (v/v) acetic acid solution for 8 hours at RT.

2.7 Two dimensional gel electrophoresis, 2D PAGE

Two-dimensional gel electrophoresis was carried out according to the method of O'Farrel (1975) using the BioRad Mini-Protean II gel electrophoresis system. The first dimension isoelectric focusing tube gels [9.2M urea, 3.75% (w/v) acrylamide, 0.21% (w/v) *bis*-acrylamide, 2% (v/v) Triton X-100, 4% (v/v) ampholine 5-7 (Pharmacia), 1% (v/v) ampholine 3-10 (Pharmacia)] were polymerised upon the addition of APS to 0.01% (v/v) and TEMED to 0.08% (v/v). These were then overlaid with 1X sample loading buffer [9.5M urea, 2% (v/v) Triton X-100, 1.6% (v/v) ampholine 5-7, 0.4% (v/v) ampholine 3-10, 5% (v/v) 2-mercaptoethanol] for 15 mins at RT and then pre-focused for 200V, 300V and 400V for 10, 15 and 15 mins respectively, where the

anode buffer was 100mM H_3PO_4 and the cathode buffer 20mM NaOH. The buffers were then refreshed and samples were loaded into the tube gels.

Samples were prepared by the addition of 1/3 volume of a 3X sample loading buffer [6% (v/v) Triton X-100, 4.8% (v/v) ampholine 5-7, 1.2% (v/v) ampholine 3-10, 15% (v/v) 2-mercaptoethanol] and solid urea to a final concentration of 9.5M to each tube. After sample loading, the gels were electrophoresed at 500V for 10 mins and then 750V for 4 hours under constant current. After first dimensional electrophoresis, the tube gels were expelled into 5ml of equilibration buffer [0.125M Tris-Cl, 10% (v/v) glycerol, 4.6% (v/v) SDS, 2.5% (v/v) 2-mercaptoethanol, 0.01% (w/v) bromophenol blue, pH 6.8] and stored at -20°C until required.

The tube gels were allowed to stand in equilibration buffer for 30 mins at RT prior to second dimension gel electrophoresis which was performed as described in section 2.6 with the exception that the width of the gels was 1mm and the volume about 4mls.

2.8 Western Blotting

Gels for Western blotting were performed as described in section 2.6. However, after running, they were not fixed and stained as described, but soaked for 40 min in 250ml Western transfer buffer [25mM Tris-Cl, 150mM glycine, 20% (v/v) methanol, pH 8.3]. The gel was then laid onto a sheet of nitrocellulose and this was sandwiched between two sheets of filter paper, each of these components having being pre-soaked in transfer buffer. This assembly was then lowered into a BioRad Western gel tank filled with transfer buffer, with the nitrocellulose side facing the anode and transfer was performed for 75 mins at 250mA.

The nitrocellulose filter was removed, rinsed in transfer buffer and then stained in 200ml Ponceau S [0.2% (w/v) Ponceau S (Sigma), 3% (w/v) sulphosalicylic acid, 3% (w/v) TCA (tri-chloroacetic acid)] for 5-10 mins. Transferred proteins could be visualised after washing the filter in water. Once all stain had been removed from the filter by further rinses with water, it was washed for 20 mins in 100ml TBS [20mM

Tris-Cl, 0.5M NaCl, 0.01% (w/v) Thimerosal, 0.2% (v/v) Tween 20 (polyoxyethylenesorbitan monolaurate, Sigma), pH 7.5]. The filter was then blocked overnight at 4°C in 200ml blocking buffer [TBS + 5% (w/v) Marvel milk powder].

The filter was washed for 5X 5 min in 100ml TBS, the second and third TBS washes being separated by a single 5 min wash with 200ml 0.5M NaCl. It was then placed into a plastic bag containing 4ml of an antibody solution, prepared by diluting an actin antibody* into an antibody buffer [TBS + 1% Marvel]. The bag was sealed and hybridisation was allowed for 1 hour at RT. The filter was then washed as described above with the 6X 5 min washes, followed by hybridisation to the secondary antibody** in the same way as that for the primary antibody. In this case, the filter was incubated with 4ml of a 1:1000 dilution of the secondary antibody for 1 hour at RT. After washing the filter again in the aforementioned manner, the blot was developed using ECL (Amersham) according to the manufacturer's directions.

* The monoclonal and polyclonal actin antibodies, (gifts from Dr. Marie-Christine Lebart), were both raised in rabbit. The polyclonal actin antibody was raised against a cardiac actin and was diluted 1:25 before hybridisation to a filter. The *Drosophila* specific actin antibody was raised against a peptide sequence derived from the N-terminus of ACT88F and was diluted 1:80 into the antibody buffer prior to application to the filter.

** The secondary antibody possesses the horse-radish peroxidase (HRP) conjugate that enables its development by ECL.

CHAPTER THREE: THE EXPRESSION OF *DROSOPHILA* ACT88F ACTIN IN *SACCHAROMYCES CEREVISIAE*

3.1 Introduction

In vitro biochemical studies of actin generally require milligram quantities of protein. Two approaches can be followed to produce ACT88F actin in sufficient quantities for *in vitro* kinetic and motility assays that assess its interaction with myosin. The first involves the purification of endogenous ACT88F from its host, *Drosophila melanogaster*. Although milligrams of actin can be obtained by a modification of the standard actin preparation, (modified from Pardee and Spudich (1982) by Drummond, 1990), this preparation contains a mixture of up to six different *Drosophila* actin isoforms. To obtain pure ACT88F, these other endogenous isoforms have to be removed, possibly upon the basis of charge differences.

The second approach for generating pure ACT88F involves the heterologous expression of the *Act88F* gene in a suitable host. As described in section 1.5.2.1, the generation of recombinant actin in the commonly employed expression systems poses problems. Where the actin expressed in *E. coli* forms insoluble aggregates, over-expression in yeast results in host cell lethality. A report by Karlsson (1988) that moderate expression of actin was able to maintain the viability of a yeast host prompted an attempt to express *Act88F* in *Saccharomyces cerevisiae*.

3.1.1 A temperature-inducible actin expression system in *Saccharomyces cerevisiae*

The lethal phenotype generated by over-expression of actin in *Saccharomyces cerevisiae* is probably a consequence of an imbalance in the stoichiometries of the cytoskeletal proteins. Karlsson (1988) overcame this problem through the employment of a temperature inducible actin expression system. His more subtle approach generated moderate levels of a chicken β, non-muscle actin isoform which were

equivalent to those of the endogenous yeast actin and therefore sufficiently low enough to maintain host cell viability.

Karlsson's system is based on a temperature regulatable expression vector, pYC27, that incorporates sequences from both pBR322 and the 2μ plasmid (Waltan and Yarrington, unpublished), (see figure 3.1). The sequence elements derived from the 2μ plasmid ensure that the vector is maintained extrachromasomally upon transformation into a yeast host, therefore enabling the synchronous expression of recombinant and endogenous actins. These particular elements also mediate the stable inheritance of pYC27 during vegetative growth and induce its amplification within the cell to a copy number of 50-100. Heterologous expression in this system is under the control of the powerful, glucose-inducible, yeast *PGK* (phosphoglycerate kinase) gene promoter. In pYC27, this is situated upstream of a *Bgl*II restriction site into which the actin coding region is cloned. The expression vector also contains genes conferring ampicillin resistance and uracil prototrophy, which are used for selection purposes after transformation into *E.coli* and yeast respectively.

The temperature inducible element of this system is represented by an α2 binding site which is situated between the *PGK* promoter and the *Bgl*II site in the expression vector and is a DNA sequence that plays a role in the mating type regulation of the yeast cell. Cells can be either mating type a or α, depending upon the expression and repression states of the *mat a* and *mat α* loci. Host cells are *mat α* when an α2 repressor protein, encoded by the *HML* locus, binds to an α2 binding site in the promoters of *mat a* genes and subsequently represses their transcription. Conversely, repression of the *HML* locus by the *SIR* (Silent Information Regulatory) genes ensures the absence of the α2 binding protein, permitting *mat a* gene expression to generate *mat a* hosts.

The incorporation of this mechanism into the expression system involves transforming the expression construct into a *SIR3*^{ts} host. Switching between permissive and non-permissive temperatures governs the activity/inactivity of the *SIR* genes and therefore the absence/presence of the α2 binding protein respectively. At the permissive

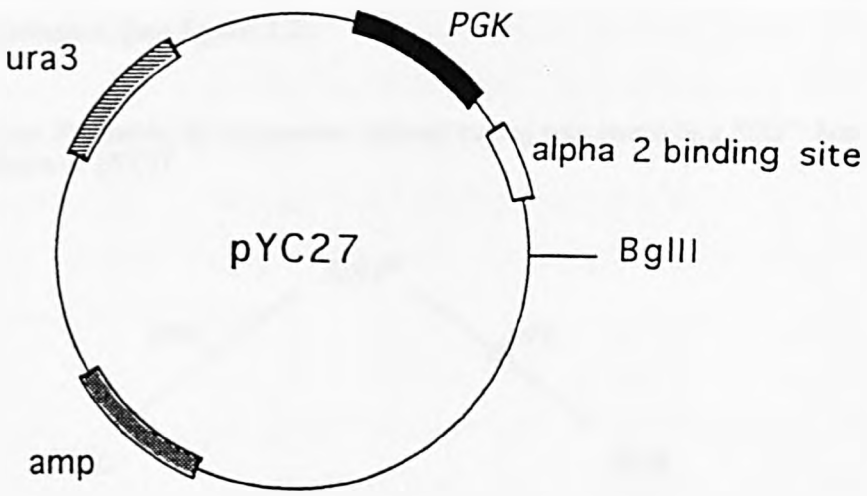

Figure 3.1. The pYC27 expression vector

temperature, (23°C), the absence of the repressor protein ensures that the α2 binding site on the vector is unprotected, enabling transcription to proceed unhindered through the actin gene. However, at the non-permissive temperature, (34°C), the α2 repressor protein is expressed normally, binds the α2 binding site on the vector and ultimately represses its expression, (see figure 3.2).

Figure 3.2 A scheme illustrating the temperature induced mating type switch in a *SIR3*^{ts} host that governs the expression of pYC27.

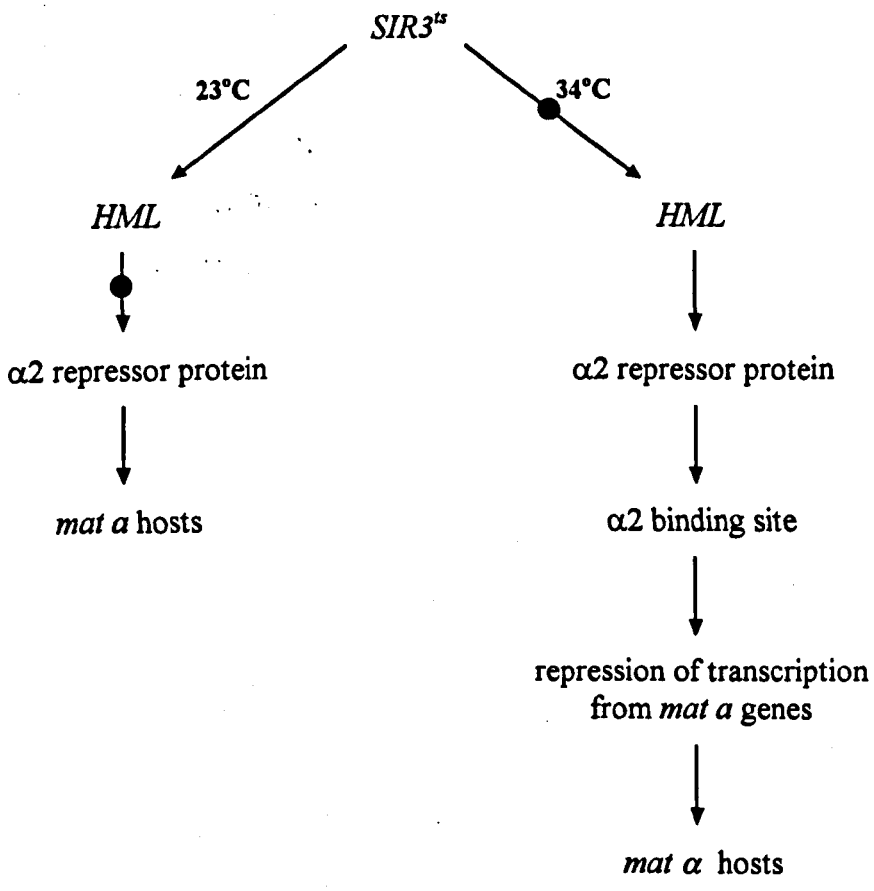

In bypassing the temperature regulation of this system, Aspenström and Karlsson (1991) found that constitutive expression also generated moderate actin levels which were not deleterious to host cell function. This observation predicted that the key for cell survival was not the inducibility of expression, but an intrinsic property of the gene sequence, promoter type and copy number combination. The association of a strong promoter and a high copy number, as seen in pYC27, would be expected to generate very high levels of protein. However, the surprisingly average yields during

constitutive expression highlight the importance of the heterologous gene sequence which will be discussed in detail in section 3.4.

For compatible expression of the chicken β-actin gene in this system, two modifications had to be made prior to its cloning into the expression vector. Firstly, since expression in this vector is under the control of the yeast *PGK* promoter, the 5' untranslated promoter region of this actin gene had to be precisely removed from the coding sequence. Cleavage at a natural *Nco*I restriction site spanning the initial ATG codon enabled the removal of the whole of the 5' untranslated region, except for a single base pair, from the actin gene.

The second necessary modification to the chicken β-actin gene sequence involved the removal of the four introns in the coding region. Intron exclusion was solely a precautionary measure to ensure that heterologous expression was unhindered by problems concerning the alternate intron splicing mechanisms seen in yeast, compared to those observed in higher eukaryotes.

Having satisfied these two criteria, the chicken β–actin gene was cloned into the expression vector. A *K923* yeast host strain, *(HMR trp1, MAT leu2, HMLα trp1, ura3, leu2, SIR* ^{u}, 23°C=a, 34°C=α), was then transformed with the expression plasmid according to the method of Ito (1983) with any transformants recovered upon the basis of uracil selection. These were then inoculated into a 12 litre fermentor culture which was subsequently incubated at the expressive temperature, (23°C). Aspenström and Karlsson (1991) were able to recover roughly 10mg of the chicken β-actin isoform.

3.1.2 ACT88F expression in *Saccharomyces cerevisiae*

A pre-requisite for actin expression and purification in this system is that the recombinant protein possesses a charge differential to that of yeast actin, such that its separation by anion exchange chromatography can be accomplished. In most cases, this is not a great problem since yeast actin intrinsically possesses a basic overall charge.

Before attempting to express the *Drosophila Act88F* gene in a yeast, the primary sequence of ACT88F was compared to that of yeast actin to establish whether these isoforms could be separated by a charge difference. The net charge of each protein was calculated by a simple addition and subtraction of the numbers of positively and negatively charged residues. Each basic residue, arginine, lysine and histidine, was assumed to have a single positive unit charge, (+1), and acidic residues, aspartic and glutamic acid, were assigned a single negative unit charge, (-1).

Table 3.1. This table lists the total number of each charged residue in the primary sequence of the isoforms listed. A final net charge value was obtained by the addition of these positive and negative charges.

	arginine	lysine	histidine	aspartic acid	glutamic acid	net charge
α skeletal	+18	+19	+9	-22	-28	-4
yeast	+18	+18	+10	-20	-27	-1
ACT88F	+18	+19	+9	-23	-26	-3
chicken β	+18	+19	+9	-23	-26	-3

These charge comparisons predict that recombinant ACT88F would have the same charge as chicken β-actin and would subsequently be separable from yeast actin upon the basis of the 2 charge unit difference, (see table 3.1).

3.1.3 Modifications of the *Act88F* gene

The *Act88F* gene was modified prior to its cloning into the expression vector to ensure its correct expression in this system. The first alteration regards the relatively unknown importance of actin N-terminal processing which is rarely complete for heterologous proteins and is virtually inessential in yeast. Karlsson (1988) showed that a recombinant Class I chicken β-actin isoform, like the endogenous Class I yeast isoform, was unprocessed but functional. True Class II actins, such as ACT88F, have not been previously expressed in yeast.

Cook *et al.* (1991) investigated the viability of a yeast actin isoform which had a cysteine residue inserted between positions Met0 and Asp1 at its N-terminus. It was found that this pseudo-Class II yeast actin isoform was 30-40% stably unprocessed *in*

vivo. In light of this information, and the apparent importance of the actin N-terminus in actomyosin interactions, I decided to express a pseudo-Class I ACT88F isoform rather than the conventional Class II ACT88F species, in yeast. An existing mutation in our laboratory, *ΔCys*, has the Cys2 codon deleted from its N-terminus, (see table 3.2). Expressing this mutant will hopefully ensure that like the other Class I alleles expressed in yeast, pseudo-Class I ACT88F will possess an unmodified N-terminus which is represented by completely acetylated methionine.

Table 3.2. Identities of the N-termini of the different actin isoforms expressed in yeast

Yeast actin (Class I)	Ac-Met-Asp-actin
Chicken βactin (Class I)	Ac-Met-Asp-actin
Drosophila ACT88F (Class II)	Ac-Met-Cys-Asp-actin (prediction)
pseudo-ACT88F (Class I)	Ac-Met-Asp-actin (prediction)

The second modification of the *Act88F* gene involves removal of the 5' promoter region of the gene prior to insertion into the expression vector. It was planned to splice away this region by restricting with *Nco*I at a site which spans the initial ATG codon. However, unlike the chicken β-actin gene, *Act88F* does not possess a natural *Nco*I site at its 5' end, (see table 3.3). Subsequently, an *Nco*I site was engineered at the 5' end of the gene by site-directed mutagenesis, (see figure 3.4).

Table 3.3. Nucleotide sequences at the 5' ends of the following actin genes

*Nco*I restriction site	5'-C$^{\nabla}$CATGG-3'

	-5 1 +5
Chicken β	5'----GCAGCCAGCCATGGATGATGATA---3'
Act88F	5'----AACTGCCAAGATGTGTGACGATG---3'
Act88FΔCys	5'----AACTGCCAAGATGGACGATGATG---3'

The final modification to the *Act88F* gene involved the removal of the short 61 base pair intron in the 3' end of the coding region, again for reasons analogous to those for the chicken β gene, (see figure 3.3). An intronless version of the *Act88F* gene was engineered by plasmid shuffling. The 3' untranslated region of *Act88F* was retained in

the final expression construct and a complete scheme for the cloning of this gene into the expression vector is outlined in figure 3.6.

3.2 Materials and Methods

Figure 3.3. A map of the *Act88F* gene sequence of *Drosophila melanogaster*

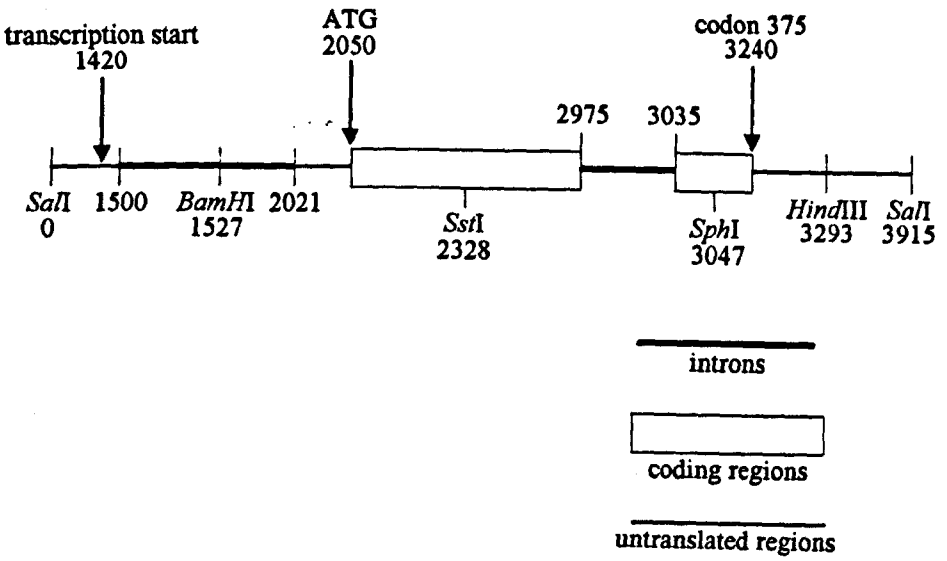

Figure 3.4. Site-directed mutagenesis of a *BamHI-SstI* fragment of the *Act88F* gene to create an *NcoI* restriction site spanning the initial ATG codon.

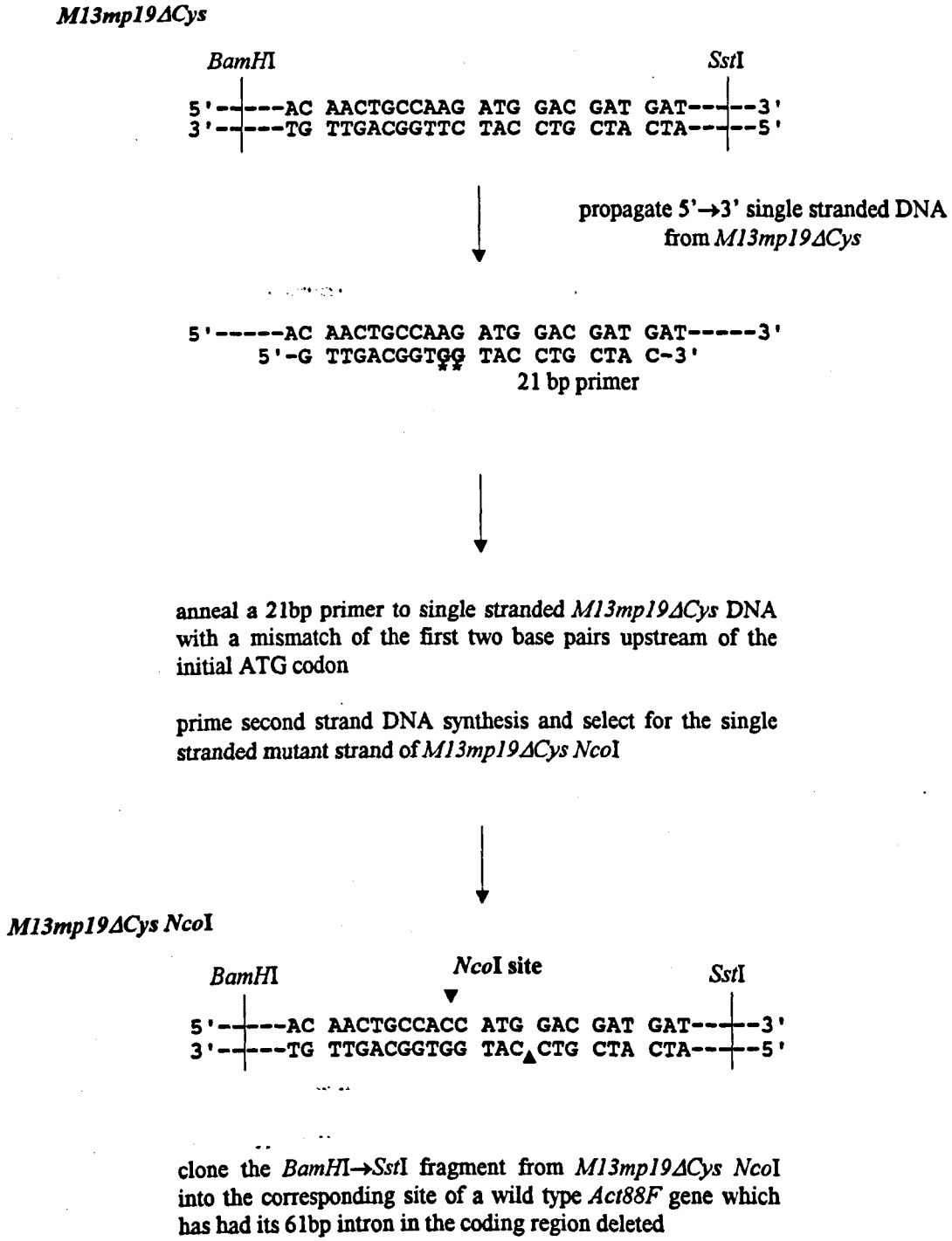

Figure 3.5. Removal of the 5' untranslated promoter region from the 5' end of the *Act88F* coding region

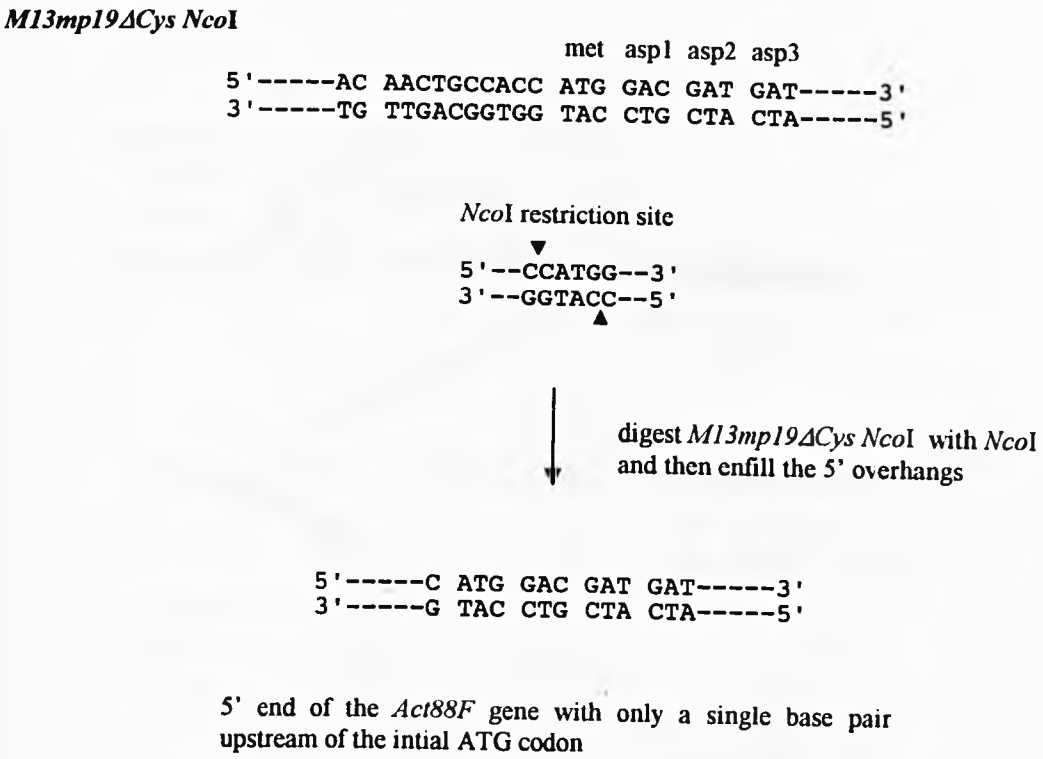

Figure 3.7 The sequence identity of the 5' promoter region of the *Act88F* gene immediately upstream of the initial ATG codon, after its insertion into the expression vector. The blocks denote the origin of the nucleotide sequence

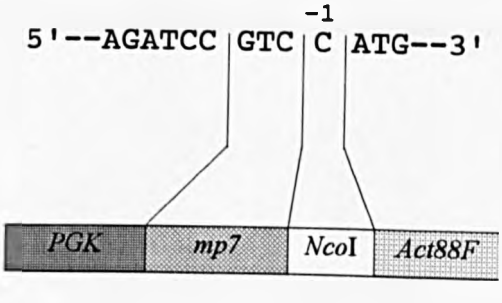

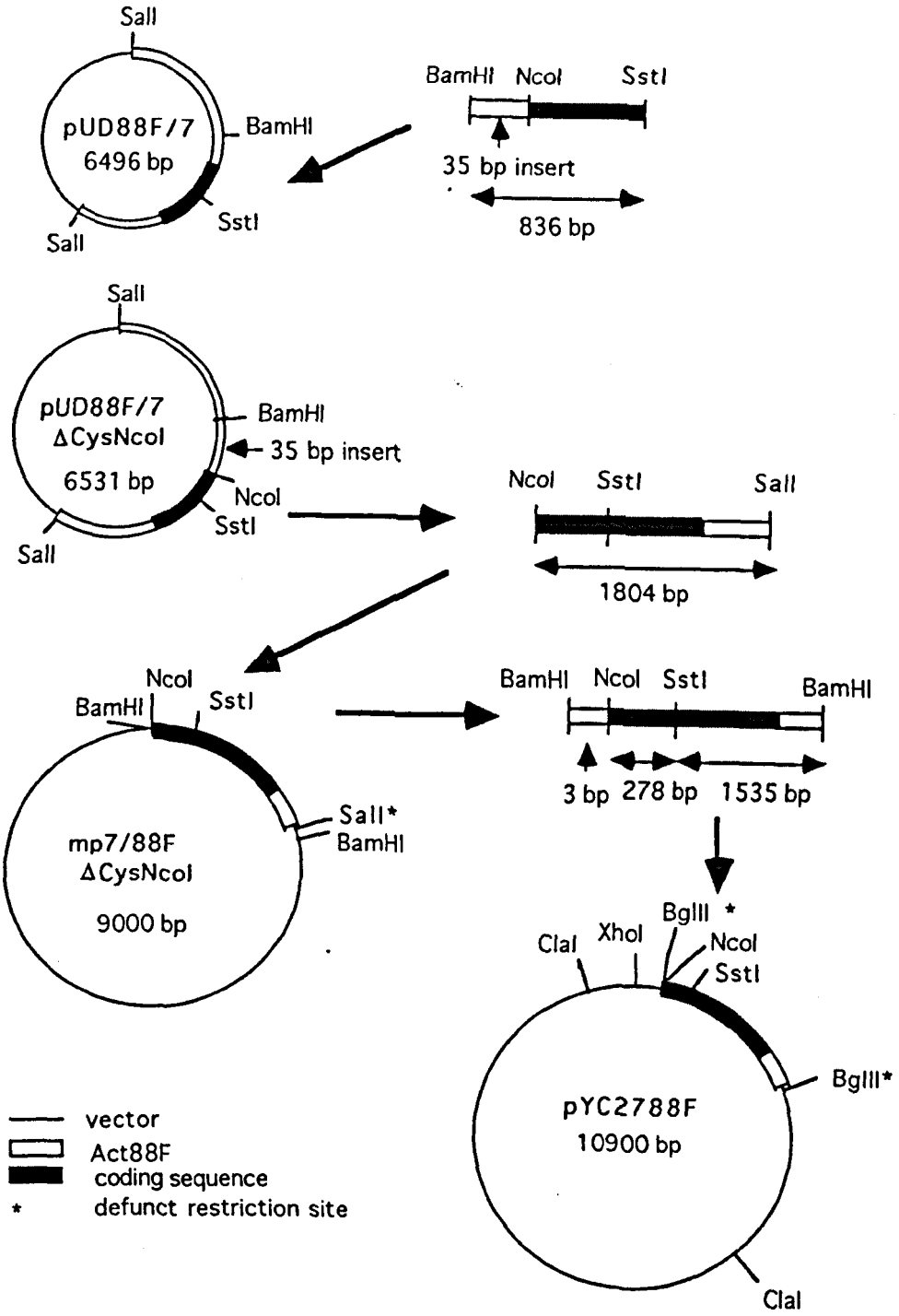

Figure 3.6 The cloning scheme used to insert the modified *Act88F* gene into the expression vector, pYC27.

3.2.1 Preparation of yeast competent cells

Yeast competent cells were prepared according to the lithium acetate based method of Ito (1983). 1ml of a fresh *K923* overnight was inoculated into 100ml of YEP-D [1.1% (w/v) yeast extract, 2.2% (w/v) bactopeptone, 0.16mM adenine sulphate, 2.2% (w/v) agar, 2% (w/v) glucose] and grown on a platform shaker to a cell density of 1-2X10^7 cells/ml, (OD_{600} =1.0), at 30°C and 250rpm. The culture was then split into two tubes and pelleted in a Sorval at 400g for 3 mins at 4°C. Each pellet was gently resuspended in 20ml of water and centrifuged again as above.

Each pellet was then resuspended in 1ml of Transformation buffer [10mM Tris-Cl, 1mM EDTA, 0.1M LiOAc, pH 7.6] and divided into 100µl aliquots. After incubation at 30°C for 60 mins, 50mg of sheared, phenol-extracted carrier DNA was added to each 100µl aliquot. For transformations, 1µg of plasmid DNA (in a maximum volume of 10µl) was mixed with each aliquot and incubated at 30°C for 30 mins. Next, 0.7ml PEG buffer [40% PEG4000, 10mM Tris-Cl, 1mM EDTA, 0.1M LiOAc, pH 7.6] was added to each tube, mixed gently, and then incubated at 30°C for 60 mins. The cells were then heat-shocked at 42°C for 5 mins and pulsed in a microcentrifuge for 10 secs.

Each pellet was resuspended in 100µl water and spread onto *ura*$^-$ plates [0.15% (w/v) yeast nitrogenous base without amino acids and ammonium sulphate (Difco), 0.5% (w/v) ammonium sulphate, 2% (w/v) glucose, 0.015% of the following amino acids: (L-histidine, L-arginine HCl, L-methionine, L-tyrosine, L-leucine, L-lysine HCl, L-phenylalanine, L-glutamic acid, L-aspartic acid, L-valine, L-threonine, L-serine, L-proline), 2% agar] which were incubated at 34°C for 2-3 days. Transformants appeared as small hemispherical colonies.

3.2.2 Growth of expression cultures

In order to analyse transformants for actin expression, the relevant strains were grown in a *ura*$^-$ medium, UYM [0.8% (w/v) yeast nitrogenous base without amino acids (Difco), 1.1% (w/v) casamino acid vitamin assay (Difco), 0.16mM adenine sulphate,

0.006% (w/v) tyrosine, 2% (w/v) glucose, 0.005% (w/v) tryptophan, 0.01% (w/v) leucine] to select for plasmid retention.

Firstly, an overnight of the transformed strain was grown in UYM at 34°C and 250rpm. This was subsequently diluted 1:100 into UYM and incubated at 34°C for 24 hours at 250rpm. This initiator culture was then diluted 1:10 into UYM and incubated at 23°C for another 24hours at 250rpm. For expression controls, untransformed *K923* were grown in exactly the same way as transformed *K923* strains, except for the final day of growth where the temperature was maintained at 34°C. After growth, the cells were divided into 50ml aliquots and harvested by spinning at 2000g for 20 mins at 4°C. The cell pellets were stored at -80°C prior to analysis for expression.

3.2.3 Preparation of DNaseI-Sepharose matrix

One of two grades of bovine pancreatic DNaseI (Sigma grades II and IV) were coupled to cyanogen-bromide activated sepharose 4B (Pharmacia) following the manufacturer's protocol. Grade II DNaseI was more selective but had a lower affinity for actin than Grade IV, (Roger Karlsson, pers. comm.). Approximately 10mg of DNaseI were coupled to 1g of Sepharose.

10mg of DNaseI was dissolved in 1ml of coupling buffer [0.1M $KHCO_3$, 0.5M KCl, 0.5mM $CaCl_2$, pH 8.3]. 1g of the Sepharose matrix was swelled by washing with 200ml 1mM HCl, (this and all subsequent washes were performed in a column with a sintered glass base), and then resuspended in 1ml coupling buffer. This was then added to a 25ml bottle containing the DNaseI and allowed to couple overnight at 4°C on a rotating windmill. The coupled matrix was then washed with 50ml coupling buffer and then placed in a 25ml bottle containing 10ml of blocking solution [1M ethanolamine]. Blocking was performed overnight at 4°C on a rotating windmill.

Next, the matrix was washed with 8 cycles of alternating pH. Each cycle consisted of a 50ml wash with acetate buffer [0.1M KOAc, 0.5M KCl, 0.5mM $CaCl_2$, pH 4.0] followed by a 50ml wash with Tris-Cl buffer [0.1M Tris-Cl, 0.5M KCl, 0.5mM $CaCl_2$,

pH 8.0]. The matrix was given a final wash with 50ml coupling buffer and stored at 4°C in 1/3 volume of coupling buffer containing 1mM NaN_3.

3.2.4 Analysis of yeast samples for the expression of recombinant actin

Buffers:

G-buffer: 5mM Tris-Cl, 0.1mM $CaCl_2$, 0.5mM ATP, 0.1mM NaN_3, 0.5mM DTT, pH 7.6.

Ethanol-based protease inhibitor* (EPI): 0.1M PMSF (phenylmethylsulphonyl fluoride), 0.01% (w/v) phenanthroline, (*made up in 100% ethanol).

Water-based protease inhibitors (WPI): 0.05% (w/v) leupeptin, 0.05% (w/v) pepstatin A, 0.05% (w/v) antipain, 10μM E64.

(Note: all protease inhibitor components were from Sigma)

Lysis buffer: G-buffer (-DTT supplement*) + 1/100 volume EPI + 1/500 volume WPI (lysis buffer is always prepared immediately before use)
* DTT prevents the protease inhibiting activity of PMSF.

Elution buffer: Lysis buffer + 2% (v/v) NP40 (Nonidet P40) + 2% (v/v) 2-mercaptoethanol.

For analysis of expression, each frozen yeast cell pellet harvested from 50ml of a yeast cell culture (see section 3.2.2) was thawed and 100μl of lysis buffer added to the cell suspension. This was then transferred to a 2ml Eppendorf tube to which an equal volume of glass beads, (212-300μm, acid-washed, Sigma), was added. The cells were then vortexed for 2X 2 mins with a brief period on ice between each vortex. Next, a further 1ml of lysis buffer was added to each tube and vortexed again for 1 min. After

centrifuging for 2 min at 13,000rpm and 4°C, the supernatant was removed carefully to avoid the inclusion of glass beads in the lysate.

This lysate was then applied to a mini DNaseI column, (10 ml BioRad mini columns), consisting of 200µl of a DNaseI-Sepharose matrix, as prepared in section 3.2.3, which had been pre-washed with 10ml G-buffer. After loading the lysate onto the column, the sample run-through was collected and reapplied to the matrix to ensure that sufficient actin had bound. The matrix was then washed with 10ml of G-buffer containing 10% (v/v) formamide, followed by a 10ml wash of G-buffer alone. Buffer was allowed to flow out of the column until only a 1ml volume remained above the surface of the matrix.

The 1ml retentate was then transferred from the mini-column into an Eppendorf tube using a long-nosed pasteur pipette and spun at 13,000rpm for 2 mins at 4°C. Upon the removal of the supernatant, 100µl of elution buffer was added to the sepharose pellet. Next, solid urea was added until the saturation point was reached. Centrifugation at 13,000rpm for 2 mins at 4°C was followed by removal of the supernatant to a fresh tube. This eluate was concentrated, (using 30,000 MW cut off Amicon micropure micro-centrifuge separators), and added to the appropriate sample buffer, (see sections 2.6 and 2.7).

3.3 Results

3.3.1 Site-directed mutagenesis of the *Act88F* gene to generate the *Nco*I restriction site

Generation of the *Nco*I site after site-directed mutagenesis of *Act88FΔCys* was verified by digesting *M13mp19ΔCys Nco*I DNA with *Nco*I. It cut once, as expected, yielding a fragment of the predicted size. Sequencing of both strands confirmed the presence of the base pair substitutions at positions -1 and -2, which define part of the *Nco*I restriction site. Sequencing also revealed two other changes represented by the

insertion of a 35bp sequence element and 3 consecutive bp changes in the 5' untranslated region of the *Act88F* gene, (see table 3.4).

Although the 35bp insert had not been encountered by Drummond (pers. comm.) in previous *in vitro* mutagenesis studies of the *Act88F* gene, two *Act88F* mutations, *M320* and *M342*, generated by whole fly mutagenesis, and subsequently some other versions of *Act88F* clones in our laboratory, were shown to possess an identical insert, (Sparrow, pers. comm.), (see table 3.4).

Table 3.4. A comparison of the *Act88FΔCys*, *Act88FΔCys NcoI* and *M320* gene sequences around the 35 base pair insert. Highlighted in bold are the 35bp inserts in the *M320* and *Act88FΔCys NcoI* sequences together with the other base changes identified after sequencing. A region of sequence duplication thought to represent the insertion site for a transposable element is underlined in the gene sequences that possess the 35bp insert.

Act88FΔCys	5'--TTTAAAGAATTGAGATGTAGGTGG.....
Act88FΔCys NcoI	5'--TTTAAAGAATTGAGATGTAGGTGG**GAGCTATAAAACTTTACATATAT**
M320	5'--TTTAAAGAATTGAGATGTAGGTGG**GAGCTATAAAACTTTACATATAT**
Act88FΔCys	.....GAGCTAACCGAGTGCACTTCCATCTCCCTTCCAGA
Act88FΔCys NcoI	**AATCGACAGATC**GAGCTAACCGAGTGCCACTCCATCTCCCTTCCAGA
M320	**AATCGACAGATC**GAGCTAACCGAGTGCACTTCCATCTCCCTTCCAGA
Act88FΔCys	TAAACAACTGCCAAG ATG ... GAC--3'
Act88FΔCys NcoI	TAAACAACTGCCACC ATG ... GAC--3'
M320	TAAACAACTGCCAAG ATG TGT GAC--3'

This insert was suspected to represent some form of *Drosophila* transposable element due to the fact that its ends create a 6 base pair target site duplication with the adjacent *Act88F* sequence, (see table 3.4). A data base search revealed that this 35 bp sequence showed no homology to a range of eukaryotic transposons and prokaryotic insertion sequences. Although the nature of this insert is not known, it does not affect the final *Act88F* expression construct. Due to its situation in a region lying upstream of the initial ATG codon, it will be spliced away from the coding region upon *NcoI* restriction, (see figure 3.6).

3.3.2 *Act88F* expression in yeast

3.3.2.1 Two dimensional gel analysis of expression

A *K923* host strain was transformed with the expression construct, *pYC27 88F*. A 100ml culture of this strain, *K923 88F*, was then grown at the expressive and non-expressive temperatures and analysed for actin expression as described in section 3.2.4, (see figure 3.8).

At the non-expressive temperature, a single spot at a molecular weight of 42KDa is visible, depicting the endogenous yeast actin isoform alone. Two spots, that both possess a molecular weight of 42KDa, can also be seen at the inducting temperature. One is clearly larger than the other and is predicted to be yeast actin because it migrates to a more basic pI. The smaller spot is not seen in the un-induced culture and is thought to represent the recombinant *Act88F* product since it migrates to the expected molecular weight and pI with respect to yeast actin. However, its levels are greatly reduced in comparison to those of the endogenous isoform.

3.3.2.2 Western blot analysis of expression

To verify whether the extra spot seen upon induction was truly recombinant ACT88F, Western blot analyses using a polyclonal and a monoclonal *Drosophila* specific actin antibody were performed upon the actin content of induced and non-expressive (control) cultures.

(i) Polyclonal actin antibody

A polyclonal actin antibody, (a gift of Dr. Marie-Christine Lebart), was hybridised to 2D gels of induced and control *K923 88F* cultures identical to those in section 3.3.2.1, (see figure 3.8). These blots show that the polyclonal actin antibody recognises both of the 42KDa spots in the induced culture, suggesting that the less intense, acidic spot is probably recombinant ACT88F.

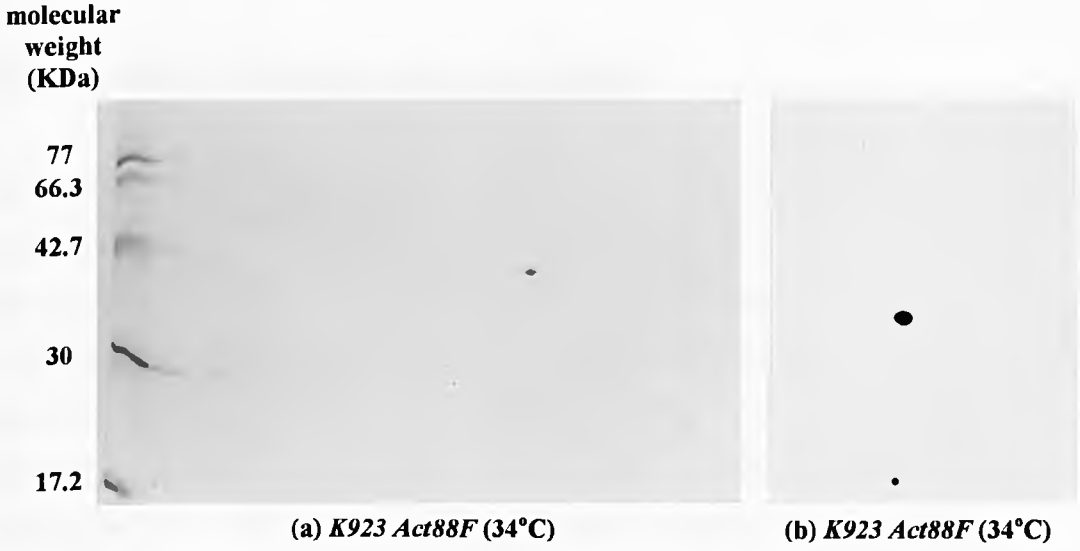

Figure 3.8 (a) and (c), 2D gels displaying the actin content of a *K923 Act88F* culture grown at the non-expressive, (34°C), and expressive , (23°C), temperatures respectively. A molecular weight marker is included in each. In (c) the large spots at a molecular weight of 66.2KDa and pI ranging from 5.4-5.6 represent a BSA marker that denotes the basic side of the gel. (b) and (d), Western blots of identical 2D gels that are shown in (a) and (c) respectively. A polyclonal actin antibody was raised in rabbit against a cardiac actin and diluted 1:25 before hybridisation to the filter. After the hybridisation of a secondary antibody possessing a HRP conjugate, the blot was developed by ECL.

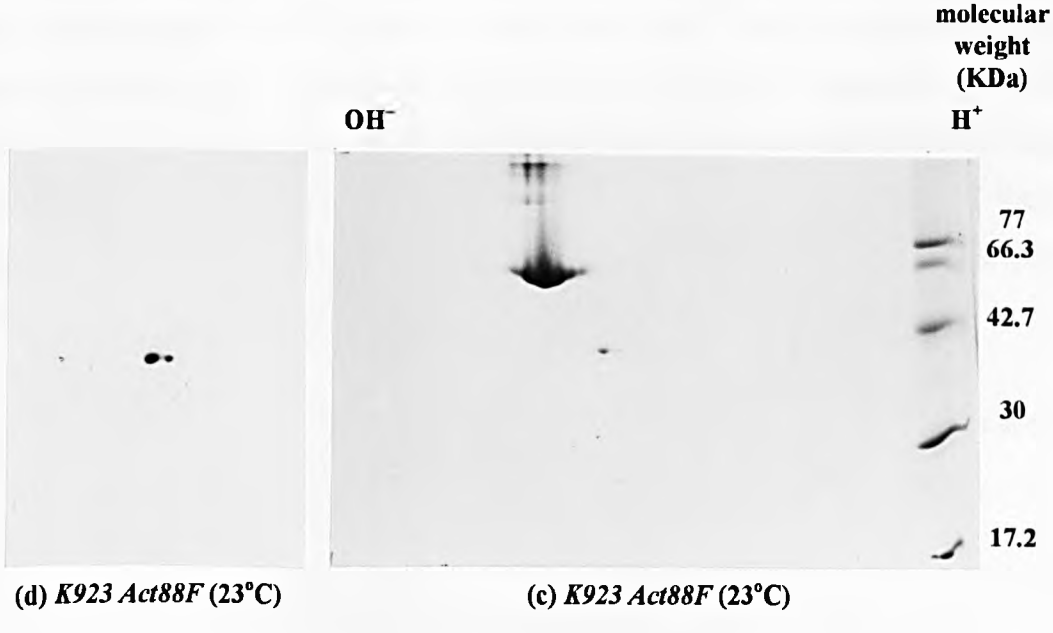

(ii) *Drosophila* actin specific monoclonal antibody

Due to the fact that the polyclonal actin antibody recognised both yeast and the recombinant actin, 1D gel analysis could not be used in Western analysis of actin expression. However, by using a *Drosophila*-specific anti-actin antibody, (again, a gift of Dr. Marie-Christine Lebart), the characterisation of expression from 1D gels representing actin extracts from induced and un-induced *K923 88F* cultures was achieved, (see figure 3.9). This blot shows that the recombinant protein found in induced cultures of *K923 88F* is a recombinant *Drosophila Act88F* isoform.

3.3.3 Mutant *Act88F* expression in yeast

Despite the low yields of recombinant ACT88F using flask cultures, an attempt to express existing *Act88F* mutations in this system was made in the hope that fermentor cultures would ultimately generate sufficient material for biochemical analyses. The six *Act88F* mutants, *G368E*, *E316K*, *E334K*, *E364K*, *G366D* and *V339I* were subsequently cloned into the expression vector and analysed for expression. Analysis of their overall charges with respect to yeast and *Act88F* actin revealed that the expression of the E→K mutations in this system would form a product that has an identical charge to that of yeast actin, (see table 3.1 in conjunction with table 3.5). This signified that 2D gel analysis of expression and ultimately separation of these recombinant proteins from endogenous yeast actin by anion exchange chromatography would probably not be possible.

Table 3.5. A comparison of the overall charges of yeast, *Act88F* and the mutant actins relative to one another.

Actin species	net charge
yeast	-1
Act88F	-3
G368E	-4
E316K	-1
E334K	-1
E364K	-1
G366D	-4
V339I	-3

Figure 3.9. (a) ID SDS-PAGE of different actin preparations visualised by Coomassie staining. Lanes 1 and 7 are molecular weight markers. Lane 2 represents the actin content of a *K923 Act88F* host strain grown at the expressive temperature, (23°C). Lane 3 represents the actin content of a *K923 Act88F* host strain grown at the non-expressive temperature, (34°C). Lane 4 is an actin extract from the thoraces of WT *Drosophila*, an ACT88F positive control. Lane 5 is an actin extract from the thoraces of *KM88 Drosophila*, an ACT79B positive control. Lane 6 is rabbit actin, a negative control. (b) A Western blot of an identical gel to the one in (a) using a *Drosophila* actin specific antibody raised in rabbit against a peptide homologous to the ACT88F N-terminus. This primary antibody was diluted 1:80 before hybridisation to the filter. After the hybridisation of a secondary antibody possessing a HRP conjugate, the blot was developed by ECL.

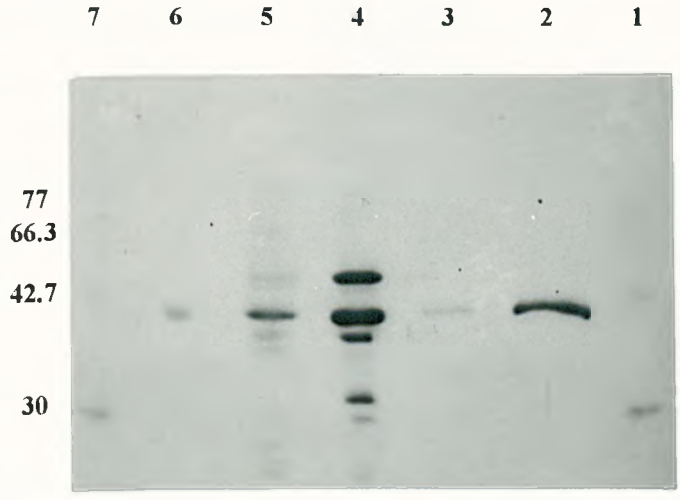

Conversely, the separation of the G→D mutant actins from the yeast isoform would be facilitated by the net increase in negative charge.

3.3.3.1 Analysis of mutant expression

Each of the aforementioned mutations was transformed into a *K923* host strain and these were then analysed for expression using 2D gel electrophoresis of their actin content, (see figure 3.11). These 2D gels clearly show that the three mutations *G368E*, *G366D* and *V339I* are expressed to similar levels to the wild type *Act88F* gene. As expected, the recombinant protein in the G→D mutations appeared to migrate at a more acidic pI than the V339I and WT actins, as established by comparing the distances from the yeast actin spot. As predicted, 2D gel analysis of the expression of the E→K mutations was not possible because the two proteins migrate to an identical pI, producing a single spot.

3.4 Discussion

The temperature-inducible actin expression system developed in *Saccharomyces cerevisiae* (Karlsson, 1988) enabled the generation of WT and mutant versions of a non-muscle, chicken β-actin isoform to levels equivalent to those of the endogenous yeast actin (Aspenström and Karlsson, 1991; Aspenström *et al.*, 1992a; 1992b; 1993). These moderate production levels were surprising considering that expression was mediated by a powerful *PGK* promoter coupled to a high copy number plasmid. The maintenance of host cell viability even under constitutive expression in this system subsequently led to the suggestion that the heterologous gene sequence may play a major role in determining the efficiency of expression (Aspenström and Karlsson, 1991). An attempt to express milligram quantities of the *Drosophila* ACT88F isoform in this system was only partially successful. Although flask cultures expressed both the WT and mutant recombinant actins, the amounts generated were much lower than those of the endogenous yeast isoform.

Figure 3.11. 2D gel electrophoresis representing induced yeast expression cultures of the *K923 Act88F* mutant strains, *G368E*, *E316K*, *E334K*, *E364K*, *G366D*, *V339I*. The proteins were separated first by isoelectric focusing over the pH range 3-10, (with pH 5-7 boosted), and then by SDS-PAGE. The gel was Coomassie stained to visualise the proteins. The gels are oriented with the anode to the right and the cathode to the left.

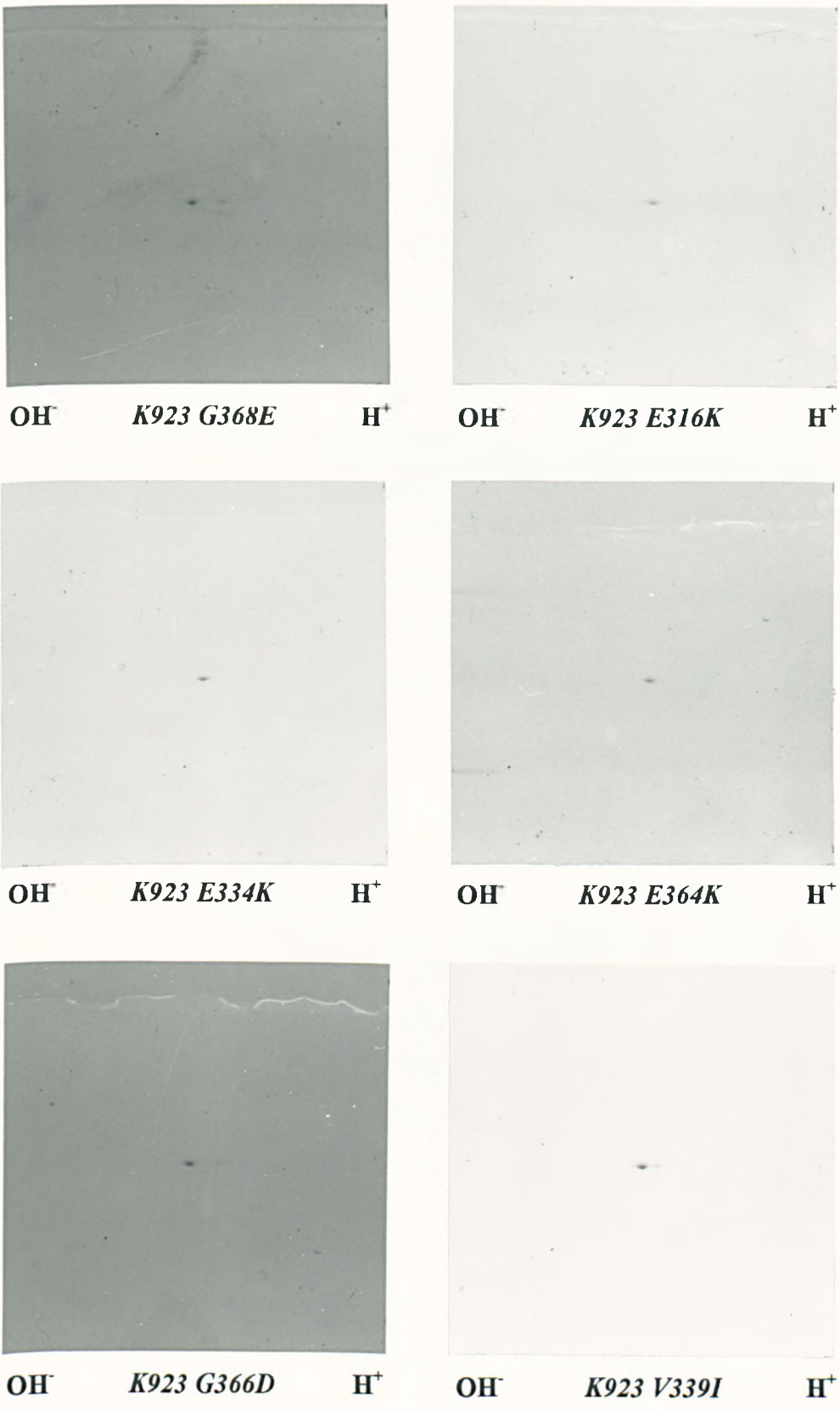

A number of factors, such as the growth conditions for expression and the tight transcriptional and translational regulation of eukaryotic genes, may be involved in the reduced production of ACT88F in yeast.

Karlsson (pers. comm.) stressed that the yield of recombinant actin per. host cell observed from flask expression was much lower than in fermentor cultures. This was illustrated by the recovery of 500mg of recombinant actin from a 12 litre flask culture (Karlsson, 1988) in comparison to 10mg from a 12 litre fermentor culture (Aspenström and Karlsson, 1991). Fermentor cultures permit a greater control of the parameters that maximise the aerobic activity of cells, thus preventing the culture from slipping into a slow, anaerobic growth phase. The ease in managing such factors as aeration, pH and glucose concentration in large scale fermentation argues that this is the better system for actin expression in yeast. The subsequent analysis of recombinant ACT88F expression from a 12 litre fermentor culture of *K923 88F* (performed by Dr. Roger Karlsson) confirmed the reduced levels of the *Drosophila* protein obtained using flask cultures and suggests that an inherent property of the *Act88F* gene, as opposed to the culture growth conditions, is responsible for the reduced expression of the recombinant gene product.

Yeast expression of human interferon alpha and calf chymosin genes (Mellor, 1985), under the control of a *PGK* promoter in a high copy number expression vector, generated levels of protein that were also lower than those predicted from the promoter/copy number combination employed. Although the basis for this reduced expression is not known, Mellor (1985) suggested that transcriptional inefficiency may be a crucial determinant. In an effort to minimise problems associated with transcription in yeast, modifications were made to the *Act88F* actin gene to render it compatible for expression in this system. In addition to the removal of the short intron in the coding region, the 5' untranslated region was removed so that expression would be under the control of the yeast *PGK* promoter without intervening *Drosophila* sequences. These changes were similar to those made to the chicken β-actin gene and therefore placed these heterologous genes under the control of identical promoters in the expression vector.

In higher eukaryotic genes, a conserved consensus region spanning the first five bases upstream of the initiator codon is thought to play an important part in the initiation of gene transcription. This consensus sequence, CCACC **ATG**, was identified by comparing 211 messenger RNA species from higher eukaryotic cells (Kozak, 1984). However, Sherman and Stewart (1982) proposed that where the exact base identity of this sequence immediately upstream of the initial ATG may not perform a vital role for transcription initiation in yeast, the overall base pair composition is an important factor.

Kingsman and Kingsman (1983) stated that an initiation region rich in A/T bases may be three times more proficient than a G/C region in initiating transcription. Since the identity of the extra base pairs in the chicken β and *Act88F* genes could modify their efficiency of translation, a comparison of their proximate bases revealed that they both had an unfavourable base composition for transcription initiation, (see table 3.6 and figure 3.7). These base pair additions may represent one of the factors that contributes to the overall reduction in the predicted levels of expression of the chicken β and *Act88F* genes.

Table 3.6. A comparison of the 5' promoter gene sequences of yeast *PGK*, yeast actin, chicken β and *Act88F*, immediately upstream of the initial ATG codon. The extra 4 base pairs upstream of the initial ATG in the *Act88F* and chicken β genes are highlighted in bold, (see figure 3.7).

gene	sequence
	-5 -1
yeast *PGK*	5'-ATATAAAACA ATG-3'
yeast actin	5'-TGAATTAACA ATG-3'
chicken β	5'-GCAGCCAGCC ATG-3'
Act88F	5'-AACTGCCAAG ATG-3'
Act88F/chicken β in pYC27	5'-AGATCCGTCC ATG-3'

The fact that *pYC27* chicken β and *pYC27 Act88F* were expressed to different levels, despite being under the control of identical promoters, suggests that the even lower comparative expression levels of the *Act88F* gene are probably not due to a reduction in the efficiency of transcription.

Unfavourable codon usage in heterologous genes may be another factor that reduces expression. There is a lot of controversy over whether rarely used, "sub-optimal" codons within a gene can reduce translational efficiency by slowing down the elongation process (Sharp and Li, 1986; Ernst and Kawashima, 1988; Sharp and Cowe, 1991). A comparative analysis of the codon usage in the *Act88F*, chicken β and yeast genes was performed in the hope of identifying unfavourable *Act88F* codons which would account for the reduced expression of this gene in yeast, (see table 3.9).

Synonymous codons are rarely employed at equal frequencies within a host genome. Prokaryotic and eukaryotic genes exhibit species-specific codon usage patterns that involve a marked preference for the employment of "optimal" synonym codons. This biased codon usage is mostly displayed in genes that are expressed to extremely high levels. For instance, the yeast *PGK*, *GAPH* (glyceraldehyde-3-phosphate dehydrogenase) and *ADH I* (alcohol dehydrogenase I) genes respectively utilise only 46, 29 and 33 of the 61 possible codon triplets, of which 25 are used almost exclusively in each.

The preference of yeast nuclear genes for particular codons is thought to correlate closely to the abundance of their isoacceptor tRNA species within the cell (Ikemura, 1982). Optimal codons found in highly expressed genes are preferentially translated by the most abundantly accessible tRNA molecules, thus ensuring that translational elongation and therefore efficiency is not limited. Yeast genes that are only expressed to low levels within the cell show a marked reduction in their codon bias, thus utilising a wider variety of the synonymous codons. Some of these codons are not found in highly expressed genes and this reflects the reduced frequency of their cognate tRNA molecules within the cell.

Codon frequency is a measure of the number of times a particular codon appears in the reading frame of a gene. Sharp and Cowe (1991) performed a cumulative codon frequency analysis of 575 yeast genes, which included those expressed to high and low levels, and enabled the identification of the overall species-specific codon bias shown by yeast, (see table 3.7). Through the comparison of the codon usage of 30 high and

low biased genes, the identities of the optimal and unfavourable codons was established. This analysis confirmed the presence of 22 ideal codons, (encoding 18 amino acids), originally described by Bennetzon and Hall (1982), in the majority of severely biased genes. From this thesis, as expected, 26 sub-optimal codons, (encoding 11 amino acids), were rarely employed in these genes and were designated as being unfavourable due to their frequency representing less than 5% of the total usage for a particular amino acid.

The codon usage of a particular organism is a measure of the mutational bias of its genome which could tend to either an A/T or a G/C rich composition. Whereas the former would favour triplets such as Phe, Tyr, Ile, Asn and Lys, a G/C rich content would exhibit mainly Pro, Arg, Ala and Gly codons. A subsequent nucleotide composition study was performed for the *Act88F*, chicken β and yeast *Act1*$^{+}$ genes in order to establish their underlying mutational bias, (see table 3.8).

Whereas the overall nucleotide composition of each gene is not notably different, the base identities at the third positions of codons in *Act88F*, yeast and to a lesser extent, chicken β–actin genes are biased. The yeast gene shows an A/T preference in contrast to the G/C bias of the *Act88F* gene and chicken β–actin genes. To assess whether their tendency towards a G/C content at the wobble position significantly affects their codon usage, the codon frequencies of the *Act88F* and chicken β–actin genes were compared to those of the 575 yeast genes, (see table 3.9).

Table 3.8 The overall and third position G/C content of the *Act88F*, chicken β and yeast *Act1*$^{+}$ genes. Values were calculated using a programme from Sharp and Cowe (1991). The contents are expressed as a fraction, with a value of 1 representing 100% G/C content and a value of 0 representing 100% A/T content. A value below 0.25 is significantly A/T biased.

	Act88F	chicken β	*Act1*$^{+}$
G/C content	0.595	0.533	0.439
G/C content at third position	0.767	0.593	0.378

Table 3.7. The central yeast column depicts the codon frequency derived from 575 yeast genes (Sharp and Cowe, 1991). The percentages in this table were recalculated from the RSCU (relative synonymous codon usage) values, ie. the ratio of the number of observed synonymous codons to the average for an amino acid. Flanking this central column are figures which represent the codon frequencies of 30 high and low bias yeast genes. The codons which are thought to be optimal and sub-optimal for translation in yeast are highlighted. The optimal codons were described in Sharp and Cowe (1991) and the sub-optimal synonymous codons were assigned as those that occur with a frequency that is less than 5% for a particular amino acid in a highly biased gene.

		low bias	yeast	high bias			low bias	yeast	high bias
Ala	GCU	25	43	77	Leu	UUA	21	27	11
	GCC	19	24	22.5		UUG	20	34	85
	GCA	35	24	0.5		CUU	14	11	0.5
	GCG	21	9	0		CUC	11	5	0
Arg	CGU	13	16	9		CUA	14	13	3
	CGC	11	5	0		CUG	20	10	0.5
	CGA	15	5	0	Met	AUG	100	100	100
	CGG	9	3	0	Phe	UUU	55	54	11
	AGA	31	53	91		UUC	45	46	89
	AGG	21	18	0	Pro	CCU	22	30	6
Asn	AAU	58	55	6		CCC	21	13	0.5
	AAC	42	45	94		CCA	35	47	93.5
Asp	GAU	39	62	57		CCG	22	10	0
	GAC	61	38	43	Ser	UCU	21	31	57
Cys	UGU	54	67	93		UCC	10	18	38
	UGC	46	33	7		UCA	22	19	1
Gln	CAA	57	73	98		UCG	15	9	0
	CAG	43	27	2		AGU	17	14	2
Glu	GAA	57	73	98		AGC	15	9	2
	GAG	43	27	2	Thr	ACU	25	38	48
Gly	GGU	29	59	98		ACC	19	24	51
	GGC	26	16	1.5		ACA	33	26	1
	GGA	29	16	0.5		ACG	23	12	0
	GGG	16	9	0	Trp	UGG	100	100	100
His	CAU	57	60	20	Tyr	UAU	54	51	6
	CAC	43	40	80		UAC	46	49	94
Ile	AUU	34	49	50	Val	GUU	24	43	55
	AUC	26	30	50		GUC	19	24	44
	AUA	40	21	0		GUA	29	17	0
Lys	AAA	55	53	10		GUG	28	16	1
	AAG	45	47	90	End	UAA	93	100	36

key	
optimal codons	
sub-optimal codons	

Table 3.9 A percentage comparison of the codon frequency of the *Act88F* and chicken β-actin genes with respect to a consensus codon usage table derived from 575 yeast genes (Sharp and Cowe, 1991). The predicted limiting codons in the *Act88F* and chicken β-actin genes are highlighted alongside the 26 sub-optimal codons in yeast. The limiting heterologous codons are assigned according to their frequency being twenty times greater, (ie. greater than 5%), than the frequency of the corresponding, synonymous codons in highly biased yeast genes.

		Act88F	yeast	chick β			*Act88F*	yeast	chick β
Ala	GCU	20	43	24	Leu	UUA	7	27	0
	GCC	67	24	66		UUG	11	34	4
	GCA	3	24	7		CUU	0	11	0
	GCG	10	9	3		CUC	4	5	26
Arg	CGU	33	16	32		CUA	0	13	4
	CGC	55	5	16		CUG	78	10	66
	CGA	6	5	0	Met	AUG	100	100	100
	CGG	0	3	0	Phe	UUU	8	54	8
	AGA	0	53	32		UUC	92	46	92
	AGG	6	18	20	Pro	CCU	11	30	32
Asn	AAU	11	55	33		CCC	63	13	42
	AAC	89	45	67		CCA	21	47	21
Asp	GAU	30	62	65		CCG	5	10	0
	GAC	70	38	35	Ser	UCU	4	31	36
Cys	UGU	14	67	33		UCC	40	18	36
	UGC	86	33	67		UCA	4	19	0
Gln	CAA	8	73	0		UCG	44	9	0
	CAG	92	27	100		AGU	4	14	0
Glu	GAA	0	73	27		AGC	4	9	28
	GAG	100	27	73	Thr	ACU	4	38	15
Gly	GGU	47	59	61		ACC	83	24	46
	GGC	37	16	29		ACA	0	26	35
	GGA	6	16	7		ACG	13	12	4
	GGG	0	9	3	Trp	UGG	100	100	100
His	CAU	22	60	33	Tyr	UAU	13	51	33
	CAC	78	40	67		UAC	87	49	67
Ile	AUU	20	49	36	Val	GUU	10	43	23
	AUC	80	30	64		GUC	19	24	23
	AUA	0	21	0		GUA	5	17	0
Lys	AAA	11	53	28		GUG	66	16	45
	AAG	89	47	72	End	UAA	100	100	100

key	
sub-optimal codons in yeast	
sub-optimal codons in *Act88F* and chicken β	

Although the codon usage of the *Act88F* and chicken β–actin genes revealed no significant differences in comparison to the overall usage derived from 575 yeast genes, the *Act88F* sequence has a greater codon usage bias than the chicken sequence. By assigning unfavourable codons in the *Act88F* and chicken β-actin genes as those that occur at a frequency twenty times greater, (over 5% higher), than those of their synonym codons in the highly expressed yeast genes, a codon frequency comparison of the 2 heterologous and the 30 highly expressed yeast genes identified a number of sub-optimal codons. These would almost certainly limit the high level expression of the chicken β and *Act88F* genes if codon usage was an influential factor in this process.

On the whole, of the 15 and 13 sub-optimal codons identified in the *Act88F* and chicken β coding sequences respectively, 11 involve the same synonymous codon, thus emphasising the codon bias of highly active yeast genes. Additionally, all of the unfavourable heterologous codons correspond to one of the 26 sub-optimal codons found in the highly expressed yeast genes, thus predicting their low level expression in a yeast host.

All of the limiting codons in the *Act88F* and chicken β–actin gene sequences, with the exception of Val GUA, have a G/C base at the third position of the codon triplet. The higher G/C content in *Act88F* compared to the chicken β-actin gene may account for the slightly higher frequencies of unfavourable codons in the former, (see table 3.9). These may define the codon bias that ultimately limits expression of ACT88F in yeast in comparison to the chicken β-actin isoform.

There are conflicting views about whether the codon usage of a particular gene affects its ultimate expression. Resynthesis of *E. coli* (Abate 1990) genes to replace sub-optimal codons with more favourable ones, and vice versa, in yeast (Hoekema, 1987) showed a relationship between unfavourable codons and low level expression. Conversely, Ernst and Kawashima (1988) found no correlation between a range of codon biases synthetically engineered into the same gene and the level of gene expression. Unfavourable codon usage may therefore not be such an important factor for heterologous expression.

If codon usage is a factor in the level of gene expression, then the moderate levels of the chicken β actin gene produced under the combined control of a strong *PGK* and high copy number 2μ plasmid, (see section 3.1.1), could be explained by its possession of the 13 sub-optimal codons described above. Conversely, if codon usage does not influence expression, it suggests that the major tRNA species, that normally favour the elongation of exactly complementary codons, are also able to translate heterologous triplets that are only complementary to the anticodon at the first two positions (Bennetzen and Hall, 1982). Although this selection of the tRNA species against wobble pairing would be thought to lower the translation rate of unfavourable codons, this may not be the case for expression under conditions which are optimal for growth.

It is not really known why the levels of the *Act88F* expression in this system are reduced. A suggestion that the instability of *Act88F* mRNA defines the reduced expression levels could be investigated by Northern blotting of chicken β-actin and *Act88F* RNA with specific probes to identify any deviations from the expected sizes and amounts of each transcript. Ultimately, the recovery of only a few micrograms of protein per litre indicates the current unsuitability of this system for the large scale expression of *Drosophila* ACT88F actin.

CHAPTER FOUR: ACT88F purification from *Drosophila melanogaster*

Biochemical and biophysical mutational studies on actin usually require milligram quantities of protein. Such quantities have only been obtained by the *Dictyostelium discoideum* and *Saccharomyces cerevisiae* "expression" systems. An effort to express the *Drosophila* ACT88F isoform in yeast showed that although recombinant protein expression was possible, the amounts generated were not sufficient for biochemical investigations, (see figure 3.8).

With the large number of ACT88F mutants available, and the effects of three of these on fibre mechanics (Drummond *et al.*, 1990; Sparrow *et al.*, 1991a; 1991b) attention was turned to the isolation of pure ACT88F from *Drosophila melanogaster*. This was plausible since a single fly has a wet weight of about 1 milligram, 20% of which is derived from the IFMs. In turn, the protein content of these muscles is represented by a tenth of the total IFM weight, corresponding to 20μg. With actin comprising 25% of this total protein content, one fly therefore possesses 5μg of ACT88F, a significant quantity of actin if purification from hundreds of flies is envisaged.

Drosophila melanogaster has been extensively used for the *in vivo* characterisation of a number of actin mutations, (see section 1.5.1.4 and 5.1.1), (Drummond *et al.*, 1991a; Sparrow *et al.*, 1991a; 1991b; 1992). However, its use as a system for generating large quantities of pure ACT88F is hindered by the presence of five other actin isoforms (Fyrberg *et al.*, 1983). Although the kinetic and biochemical studies of ACT88F preparations, "contaminated" with these mixed isoforms, has been able to characterise the effects of two ACT88F mutations (Anson *et al.*, 1995), the absolute consequences of these mutations may be diminished by the presence of the other *Drosophila* actin isoforms.

Two strategies were adopted to generate pure ACT88F from *Drosophila*. The first concerned the small scale, microgram purification of ACT88F from 10 pairs of dissected IFMs, which provides sufficient material for many *in vitro* motility assays.

The second procedure was developed to isolate milligram quantities of pure ACT88F from 10,000 flies, (equivalent to 10g wet weight).

4.1 A mini-actin purification scheme from flies

4.1.1 Introduction

4.1.1.1 Actin purification

Since the discovery of actin by Straub (1942) in rabbit skeletal muscle extracts, a great deal of work has concentrated upon developing various conditions that optimise the isolation of milligram quantities of pure, stable actin from skeletal muscle tissue. Pardee and Spudich (1982) incorporated the best of these specialisations into an actin purification scheme that is used by most researchers to date and is briefly outlined below.

The first stage involves the homogenisation of muscle tissue which facilitates actin extraction by exposing individual myofibrils. Myosin removal by depolymerisation and subsequent centrifugation is next performed by extracting the disrupted muscle tissue in a high salt buffer. The resulting, extracted myofibril pellet is then washed and dehydrated into an acetone powder, a procedure that denatures some proteins, including tropomyosin, and also enables the long term storage of actin in this crude form.

A low salt ACEX, (ACtin EXtraction buffer), buffer is used to depolymerise and extract the actin present in the acetone powder. This buffer is supplemented with ATP, whose role is to maintain the functional stability of actin monomers. Extracted actin is polymerised by the addition of KCl, Mg^{2+} and ATP to final concentrations of 50mM, 2mM and 1mM respectively to generate F-actin which is then isolated by high speed centrifugation. A following cycle of actin depolymerisation and repolymerisation, and the addition of KCl to a concentration of 0.6M, enhances the purity of actin (Spudich and Watt, 1971). The latter step is used specifically to "cut" tropomyosin and any

other thin filament associated proteins away from F-actin. Actin purity can be assessed by 1D SDS-PAGE and the final product is preferentially stored in the more stable F-actin form at -80°C.

4.1.1.2 Small scale purification of ACT88F from ten pairs of IFMs

The study of ACT88F using actin isolated from *Drosophila melanogaster* is complicated by the fact that this isoform co-purifies with the five other endogenous actin isoforms. However, ACT88F expression is restricted to the IFMs (Fyrberg *et al.*, 1983) and represents the sole actin isoform expressed in these tissues (Ball *et al.*, 1987). An actin preparation on these muscles alone would yield pure ACT88F. As outlined above, in theory, actin extracted from 200 flies would isolate one milligram of pure ACT88F, assuming that 100% recovery is possible. In reality, this sort of preparation is not feasible since the dissection of IFMs from this number of flies would be incredibly labour intensive. However, since only a few micrograms of actin is sufficient for the performance of many *in vitro* motility assays, the micro-purification protocol of ACT88F from a few *Drosophila* flight muscles was developed.

This is an abbreviated version of the Pardee and Spudich (1982) protocol and is used to purify actin from ten pairs of dissected IFMs. Since this actin preparation is dependent upon the polymerisation of actin, the low salt extraction of this small amount of starting material was limited to a 60µl volume such that the critical concentration for polymerisation could be surpassed. Ten flies will contain about 25µg of ACT88F, (half of the value quoted in section 4.1 because dissection of only one set of IFMs, the DLMs, is performed). A 1% recovery of actin would therefore generate an actin concentration of 0.25µg/60µl, (4.16µg/ml), which is exactly equal to the critical actin concentration for polymerisation, (ie. $A_{cc} = 0.1\mu M$ in the presence of Ca^{2+}, (4.2µg/ml), (Sheterline and Sparrow, 1994). With a greater than 10% actin extraction efficiency expected, polymerisation and therefore actin recovery using this mini-actin preparation was anticipated.

4.1.2 Materials and methods

4.1.2.1 Dissection of the IFMs

All manipulations were performed under a light microscope. Flies were anaesthetised using ether and the heads and abdomens were removed. The thoraces were then mounted into a Plasticine groove and a longitudinal slit down the dorsal midline was made using a fine tungsten needle. Split thoraces were then transferred to a transparent dish and immersed in cold YMG [20mM KPO_4, 50% (v/v) glycerol, 0.5% (v/v) Triton X-100, 2mM $MgCl_2$, 1mM DTT, 1mM NaN_3, pH 7.0].

With a pair of fine forceps, the thorax was held and cut in half along the dorsal longitudinal slit with microsurgical scissors. A fine tungsten needle was used to cut muscle attachments to the cuticle and tease the IFMs away. These were now stored in YMG at -20°C until needed.

4.1.2.2 Actin preparation buffers

High salt extraction buffer : 20mM KPO_4, 500mM KCl, pH 7.0.

ACEX buffer : 2mM Tris-Cl, 0.2mM $CaCl_2$, 0.2mM ATP, 1mM DTT, pH 8.0.

10X polymerisation buffer : 50mM Tris-Cl, 500mM KCl, 20mM $MgCl_2$, 10mM ATP, pH 8.0.

4.1.3 Results

4.1.3.1 The mini-actin preparation

All manipulations were carried out in Eppendorf tubes on ice, unless stated, and all spins, with the exception of the final one, were performed in a bench-top,

microcentrifuge at 13,000rpm for 2 mins. The mini-actin preparation is outlined in figure 4.1.

(i) Acetone powder preparation

The 10 pairs of muscles dissected in YMG were spun to a pellet. The supernatant was removed and the pellet homogenised in 500µl of the high salt buffer using a fine-tipped glass probe. After 2 mins extraction, the muscles were spun down and the supernatant again removed. As seen from figure 4.2, lane 2, a 20µl aliquot of this high salt wash contained a significant amount of extracted myosin.

The muscles were then resuspended and left to wash for 30 seconds in 1ml of double distilled water. The above time limit was strictly adhered to since prolonged exposure appears to extract actin and will therefore lower the final yield. After spinning the muscles into a pellet once more, they were washed once more in 1ml of water for the same limited period as before. Water washes were essential to dilute any salt remaining in the muscle pellet before the subsequent extraction of actin at low salt.

The muscles were then washed with 500µl of 50% acetone. No attempt was made to resuspend the material which formed a gelatinous pellet under these conditions. After spinning, the supernatant was removed and 500µl of 100% acetone was added. Again, no attempt to resuspend the pellet was made. The supernatant was removed after a further spin and the pellet was allowed to air dry at room temperature to form the stable acetone powder as described above.

(ii) Actin extraction and polymerisation

To extract actin, the acetone powder was homogenised in 30µl of ACEX using the fine glass probe and incubated for 45 mins at RT. This material was then spun and the actin supernatant carefully removed to a Beckman TL100 tube. The acetone powder was then re-extracted as above and the two 30µl aliquots were pooled. Analysis of this low salt extract, (figure 4.2, lane 4), revealed that actin was the most abundant protein. The

Figure 4.1. An outline of the different stages involved in the mini-actin preparation of pure ACT88F from the IFMs dissected from ten flies.

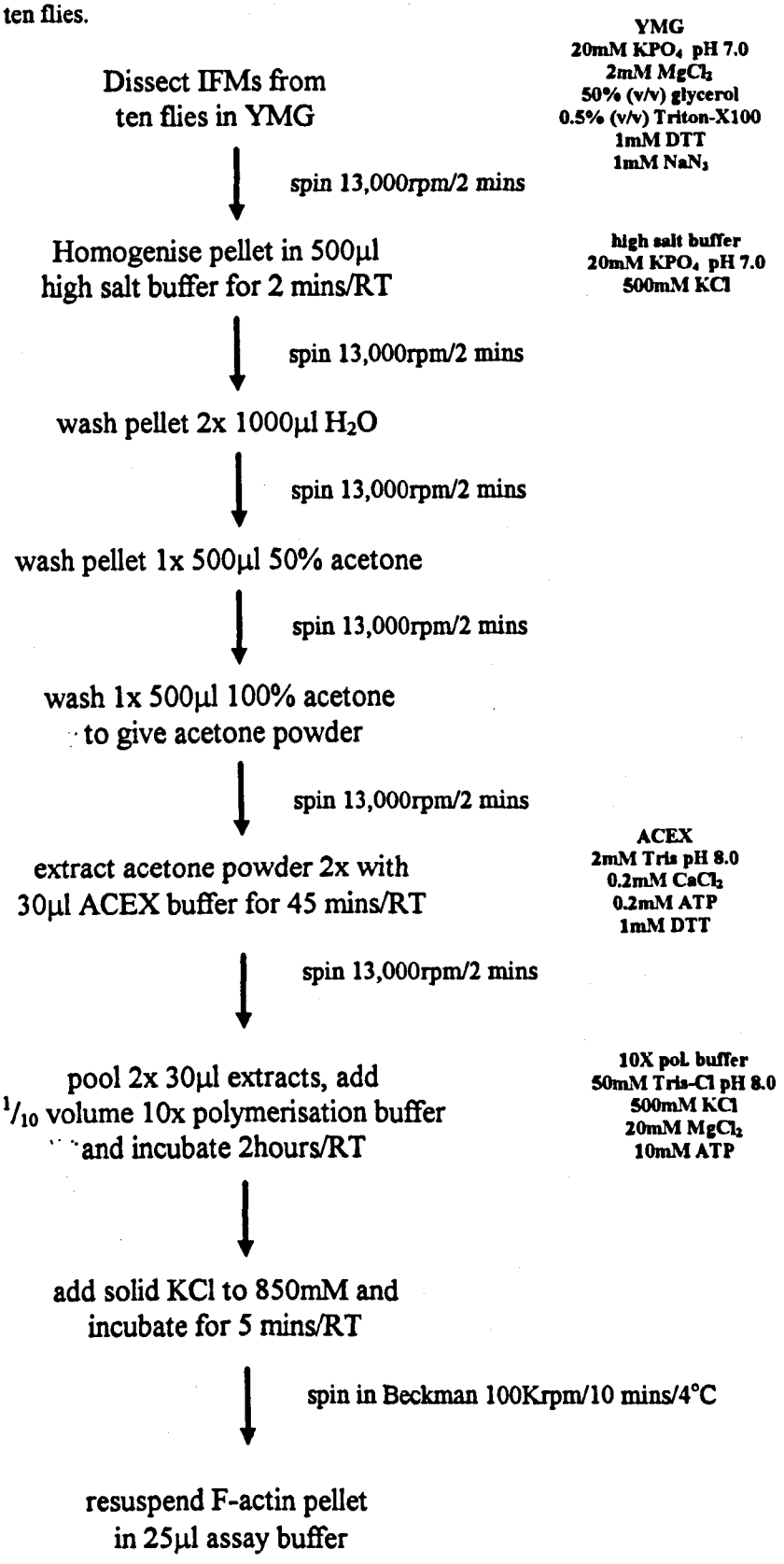

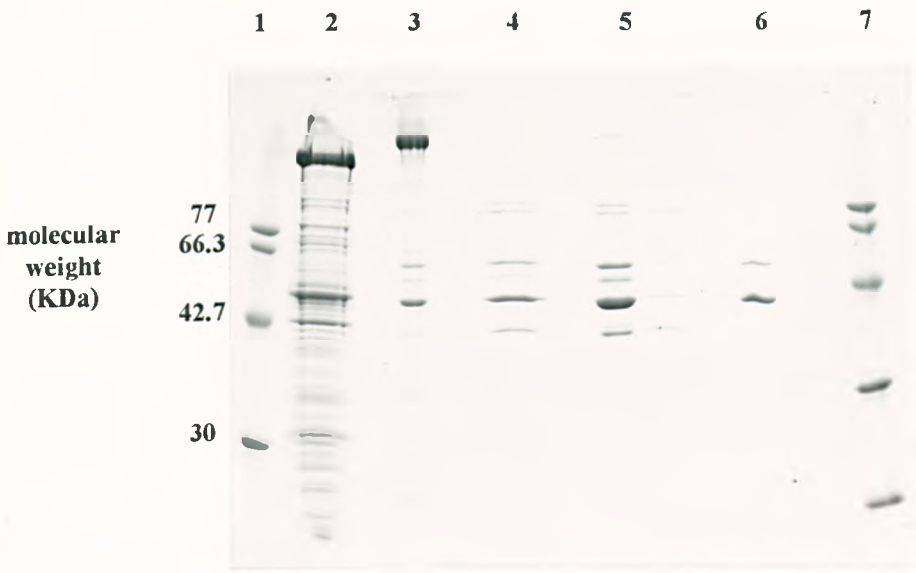

Figure 4.2. 1D SDS PAGE depicting the different stages of the mini-actin preparation. The proteins were run on a 12.5 % acrylamide gel with molecular weight markers, and visualised by Coomassie staining. Lanes 1 and 7 represent a molecular weight marker. Lane 2 is a high salt myosin extract; lane 3 a post extraction acetone powder; lane 4 an ACEX extract; lane 5 is an F-actin pellet purified without the KCl cut; lane 6 is the final F-actin pellet.

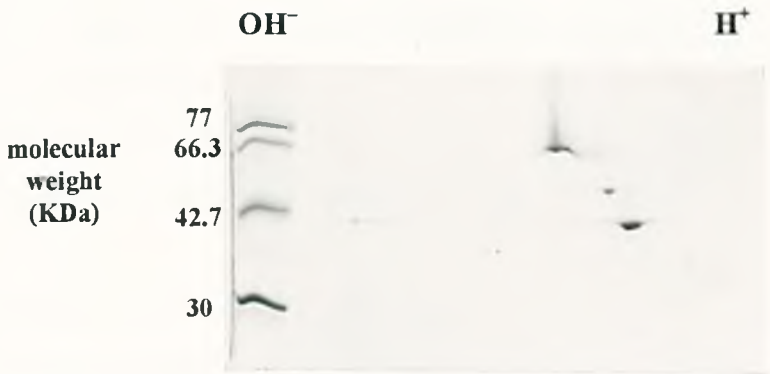

Figure 4.3. 2D gel of pure ACT88F purified by the mini-actin preparation from ten flies. Molecular weight and BSA markers are included, the latter to orient the basic side of the gel which is to the left. Two actin spots, ACT88F *mod*$^{+}$ and ACT88F *mod*$^{-}$ in order of increasing acidity migrate at the type III and type II positions respectively. The more basic 55KDa spot is arthrin.

protein content of the extracted acetone powder, (figure 4.2, lane 3), showed that a lot of actin and myosin remained in this pellet. The pooled actin extracts were polymerised for 90 mins at RT by the addition of one tenth of the volume of the 10X polymerisation buffer. A further cycle of depolymerisation/repolymerisation (Pardee and Spudich, 1982) was omitted to minimise losses from an already small amount of material.

(iii) ACT88F yields and purity

To assess whether removal of the thin filament associated proteins could be achieved by raising the KCl concentration prior to ultracentrifugation, two separate actin preparations were performed in tandem, one with added KCl and the other without. As seen from figure 4.2, (lanes 5 and 6), the addition of the KCl is essential for the isolation of pure ACT88F. Whereas the actin in the untreated extract co-sediments with a number of F-actin associated proteins, the latter are absent in the treated extract, indicating a highly pure ACT88F preparation. Subsequently, prior to ultracentrifugation, solid KCl was added to the polymerised extract to give a final concentration of 850mM KCl. A high speed spin at 100,000rpm was performed in a Beckman ultracentrifuge for 10 mins at 4°C.

From 1D SDS PAGE, it was estimated that 5μg of pure ACT88F can be recovered from ten pairs of dissected IFMs using this mini-actin preparation. Although this only represents a 20% recovery rate from the starting material, it provides enough material for many *in vitro* motility assays. The higher 55KDa band seen above the 43KDa actin band corresponds to arthrin, an ACT88F actin-ubiqutin complex that co-purifies with ACT88F actin (Bullard *et al.*, 1985; Ball *et al.*, 1987). An assessment of the purity of the isolated ACT88F actin was also made using 2D gel electrophoresis, (see figure 4.3). As expected for a pure ACT88F preparation, there were only two spots, corresponding to ACT88F *mod*$^+$ and ACT88F *mod*$^-$, with the former representing the more basic, mature form (Mahaffey *et al.*, 1985). Again, the higher 55KDa arthrin spot migrates to a more basic pI than the ACT88F isoforms.

Final F-actin pellets were resuspended in 25µl of ACEX, labelled with rhodamine-phalloidin, (see section 5.2.3), and then stored for up to 2 weeks in the dark at 4°C, prior to the *in vitro* motility assay.

4.2 The isolation of pure ACT88F from ten thousand flies

4.2.1 Introduction

The large scale actin extraction from *Drosophila melanogaster* developed by Drummond (unpublished, outlined in Anson *et al.*, 1995) was based upon procedures described by Saide *et al.* (1989), Pardee and Spudich (1982) and Szilagyi and Chen Lu (1982). From 100g of starting material, (100,000 flies), only 6mg of purified actin, containing more than one isoform, was attainable using this method. The observation that the mini-actin preparation, described above, gave a higher percentage recovery of actin prompted its direct scale-up to accommodate 10,000 whole flies as opposed to 10 pairs of IFMs. Subsequent actin preparations (Lawn and Sparrow, unpublished) gave yields of 5mg of relatively pure actin from 10g of whole flies. This ten-fold increase in yield over the Drummond actin preparation was almost equivalent, in terms of extraction efficiency, to the mini-actin preparation, although the latter extracted ACT88F alone as opposed to the six different *Drosophila* actin isoforms.

Despite the increased yields of actin from this scaled up isolation, the problem of removing ACT88F from the other "contaminating" actin isoforms remained. Any attempts to isolate ACT88F would have to exploit differences in the basic properties of these isoforms. As shown in table 1.3, adult *Drosophila* express six actin isoforms that exhibit distinct tissue-specific expression patterns (Fyrberg *et al.*, 1983). The two cytoplasmic isoforms, ACT42A and ACT5C, are expressed in undifferentiated cells while the two predominantly larval expressed actin isoforms, ACT87E and ACT57A, are found mainly in the adult intersegmental muscles. ACT88F and ACT79B are examples of two muscle-specific isoforms. ACT88F expression is restricted to the IFMs and that of ACT79B is localised to the thorax and the leg muscles. Each of these actin isoforms has the same molecular weight, but different pIs, the latter determined

by the 374 amino acids that they contain (Horovitch *et al.*, 1979; Fyrberg *et al.*, 1983).

A comparison of the primary sequences of these actins revealed a high degree of sequence homology that is exhibited by most actin isoforms. With reference to the ACT88F isoform, ACT42A represents the most divergent isoform with 18 amino acid differences, (95.2% sequence homology). ACT87E was the most similar isoform to ACT88F, displaying only 9 residue substitutions, (97.6% sequence homology).

The 2D gel electrophoresis of *Drosophila* actins revealed that they migrate as three distinct spots, types I, II and III, in order of increasing basicity, with pIs of 5.70, 5.77 and 5.84 respectively (Horvitch *et al.*, 1979; Fyrberg *et al.*, 1983), (see figure 4.4). The type I spot is believed to represent the ACT57A muscle specific actin isoform whilst the type II spot defines a mixture of five isoform species, the *Act88F*, *Act79B*, *Act42A*, *Act5C and Act87E* gene products (Fyrberg *et al.*, 1983). The ACT88F at the latter position is thought to be incompletely modified actin, *mod*$^-$, which is subsequently post-translationally modified to ACT88F *mod*$^+$ (Mahaffey *et al.*, 1985).

Although the exact nature of this modification is unknown, it clearly endows the ACT88F isoform with a more basic charge which is manifested by its migration to the type III position in 2D gels. An additional spot at 55KDa, that migrates to an even more basic pI than the type III spot, is arthrin, an ACT88F-ubiqutin conjugate (Ball *et al.*, 1987). Although the function of this protein is not known, it is predicted that 1 in every 7 actin monomers is stably ubiquitinated *in vivo*. Since 7 actin monomers represent the helical repeating unit of F-actin in muscle thin filaments, it suggests that the incorporation of arthrin into each unit may have some functional significance.

Since ACT88F has the most basic charge of the actin isoforms, an effort was made to isolate it from the other *Drosophila* isoforms by anion exchange chromatography. This separates proteins on the basis of charge differences which can be as small as that of a single charged amino acid. The binding affinity of a particular protein to the matrix is determined by a combination of its net charge and overall surface charge density. The

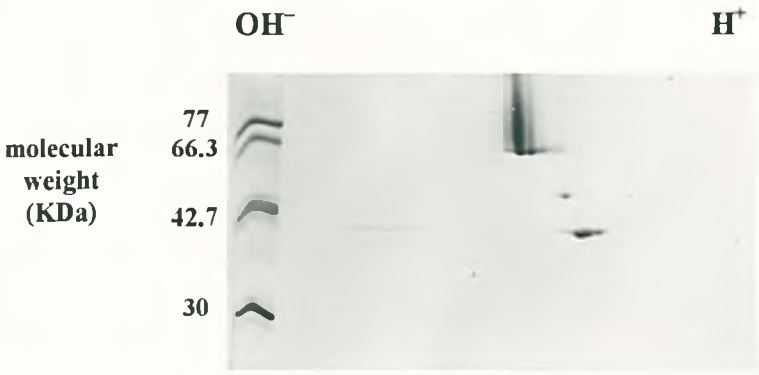

Figure 4.4. 2D gel of an actin preparation from whole flies. A molecular weight and BSA marker are also included, the latter running as a group of spots at a molecular weight of 66.2KDa and denoting the basic side of the gel which lies to the left. The three actin spots at 42KDa denote the six *Drosophila* isoforms. The type III, II and I spots are listed in order of increasing acidity. The single spot lying at 55KDa and a more basic pI to the three actin spots is arthrin, an actin-ubiquitin conjugate.

pH of the system also plays an important part. A pH above the isoelectric point of a protein endows it with a net negative charge and allows its binding to a anion exchanger. Conversely, at a pH below its isoelectric point, a net positive charge ensures that the protein will bind to an cation exchanger. Since proteins lose their activity outside a certain pH range, a strong ion exchanger, which remains charged over the pH range in which the protein is stable, has to be adopted. Actin has an isoelectric point around 5.5 and remains relatively stable at pHs between 7 and 8.5. Subsequently, an anion exchanger was used for the separation of the *Drosophila* actin isoform mixtures.

A number of chromatographic procedures are used to isolate recombinant actins from endogenous host cell isoforms. For instance, Sutoh *et al.* (1991) and Johara *et al.* (1993) express mutated *Dictyostelium 15* actins which have a charge differential in the recombinant protein that enables its subsequent isolation from the endogenous actins by anion exchange chromatography. Sutoh *et al.* (1991) employed a DEAE-5PW HPLC column that is a medium strength anion exchanger. Upon application of the mixed actin extracts to the column, the *Dictyostelium 15* recombinant and endogenous actins could be eluted off as separate peaks using a linear gradient of 0-500mM NaCl in a 20mM Tris-Cl, pH 8.0 buffer.

Karlsson (1988) developed a system for the expression and subsequent separation of a recombinant chicken β-actin from the endogenous isoform of *Saccharomyces cerevisiae* using hydroxyapatite chromatography. Although the mechanism of this matrix is not really understood, it was routinely employed by Karlsson's group to isolate many chicken β–actin mutations expressed in yeast (Aspenström and Karlsson, 1991; Aspenström *et al.*, 1992a; 1992b; 1993). The hydroxyapatite matrix used in this system was purchased from the Clarkson Chemical Company, USA. Application of the mixed actin preparation to the column was followed by elution of the actin with a linear gradient created by the mixing of buffer A (5mM KPO_4, 0.5mM DTT, pH 7.6) and buffer B (40mM KPO_4, 1.5M Glycine, 0.5mM DTT, pH 7.6).

The following sections will describe how anion exchange chromatography was applied to the problem of isolating the ACT88F isoform from the mixture of the other *Drosophila* actin isoforms.

4.2.2 Materials and methods

4.2.2.1 Actin preparation

Flies were grown and then stored at -20°C prior to the actin preparation. The method used to isolate actin was a scaled-up, slightly modified version of the mini-actin preparation described in the previous section. The actual isolation of actin from *Drosophila melanogaster* was performed in two stages. The first stage involved the formation of acetone powder from 50g, (50,000), flies. Since actin is stable in this form, acetone powder was stored at -20°C until the second stage of the preparation, where the extraction of actin was to be performed.

(i) Preparation of the acetone powder

All spins during the acetone powder preparation were performed in a Sorval at 13,000rpm for 20 mins at 4°C, unless stated otherwise. The 50g of flies were homogenised, according to the method of Saide *et al.* (1989), in 600ml of YMG, (see section 4.1.2.1), supplemented with 1mM DTT, 0.7μM pepstatin A, 0.5μM leupeptin, 2μM antipain, 0.1mg/ml soybean trypsin inhibitor and 0.5mM PMSF (the latter added immediately before use). The homogenate was then spun at room temperature and the supernatant removed. The myofibrillar pellet was resuspended in 600ml of the high salt extraction buffer, (see section 4.1.2.2). After stirring on ice for 10 mins, the mixture was spun once more.

After removal of the supernatant, the pellet was resuspended in 600ml of ice cold deionised water and spun immediately. This water wash was repeated once. The pellet was next resuspended in 6 volumes of ice cold 50% acetone by stirring on ice for 5 mins. This preparation was then spun in the Sorval at 13,000rpm for 5mins at 4°C,

after which the supernatant was removed and the pellet resuspended in 6 volumes of ice cold 100% acetone. After again stirring on ice for 5 mins, and spinning in the Sorval at 13,000rpm for 5 mins at 4°C, the supernatant was removed and the pellet allowed to air dry at room temperature overnight. From 50g of flies, a typical preparation yielded about 10g of acetone powder which was stored at -20°C indefinitely.

(ii) The extraction of actin from acetone powder

Actin extraction was performed upon 2g of acetone powder at a time. This was resuspended in 20ml of ACEX, (see section 4.1.2.2), and extracted at 4°C with occasional stirring. This mixture was then spun in a Sorval at 19,000rpm for 15 mins at 4°C. The supernatant, representing the actin extract, was removed and stored upon ice. The pellet was then re-extracted with 10ml of ACEX for 60 mins at 4°C. After spinning as before, the supernatant was removed and pooled with the initial extract. A tenth of the extract volume of 10X polymerisation buffer, (see section 4.1.2.2), was then added and polymerisation was allowed to proceed for 2 hours at 4°C.

After polymerisation, solid KCl was added to the F-actin extract to a final concentration of 800mM. After incubation for 10 mins at 37°C, this preparation was spun in a Beckman TL-100 at 90,000rpm for 20mins at 4°C. The pellet was finally resuspended in 3mls of ACEX and homogenised thoroughly. The actin stock was then dialysed for 24 hours with at least 3X 1 litre changes of ACEX. The optical density at A_{280}-A_{310}, with an extinction coefficient of 0.62/cm^2/mg, was used to estimate the molarity of the actin stock, which was subsequently diluted to a concentration of 1mg/ml with ACEX and stored at 4°C prior to use.

4.2.2.2 Preparation of the samples and buffers for anion exchange chromatography

All buffers were filtered through 0.45μM Millipore filters, thoroughly degassed and equilibrated to a temperature of 4°C before use. The mixed actin samples stored at 4°C

were sonicated for 3X 30 secs, (each burst being separated by 30 secs intervals on ice), in order to fragment any F-actin in the sample. These preparations were then spun in a Beckman TL-100 at 90,000 rpm for 20 mins at 4°C. The actin supernatant was removed and loaded onto the column within an hour.

4.2.2.3 Collection of the fractions after elution from the column

Since most anion exchangers do not bind ATP, all actin fractions were collected into Eppendorf tubes containing an amount of ATP that would produce a final concentration of 0.5mM.

4.2.2.4 Mono Q column purification

Prior to each run on a 1ml Mono Q anion exchange column, (Pharmacia), the column matrix was equilibrated with 10 volumes of the starting buffer. The sample was then loaded onto the column and washed with 5 column volumes of starting buffer. Next, the appropriate gradient was programmed into the FPLC controller and elution was initiated. All column equilibration, sample loading and elution gradient schemes were performed at a flow rate of 1ml/min and a temperature of 4°C. The gradient controller recorded the elution point of each peak and the fractions corresponding to each peak were automatically collected in either 200 or 300µl volumes by a fraction collector linked to the FPLC controller. At the end of a gradient programme, the column was washed with 5 volumes of the elution buffer alone to ensure that all bound material was released from the column. The mono Q column was then washed with 5 further column volumes of the starting buffer prior to the equilibration stage of the next run.

4.2.3 Results

Initial attempts to isolate ACT88F from the five other *Drosophila* actin isoforms employed the hydroxyapatite chromatography method of Karlsson (1988). However, during numerous, unsuccessful attempts at separation, only one run gave partial purification of ACT88F, (data not shown). Flow rates exceeding 0.1 ml/min caused the

hydroxyapatite columns to pack and block further buffer flow. In light of these problems, a more efficient chromatographic medium was sought for the isolation of ACT88F.

The Mono Q matrix is a strong anion exchanger that is analogous to the DEAE-5PW (Tosoh) FPLC column that was used by Sutoh *et al.* (1991) to resolve the *Dictyostelium* actin isoforms. This matrix is constituted from 10μM diameter beads that are coated with quaternary amine groups, (see Pharmacia handbook on ion exchange chromatography), and has a much better flow characterisation than DEAE-5PW. These columns were used in conjunction with an FPLC system (Pharmacia) and withstood flow rates of up to 2ml/min, effectively enabling isoform separation within minutes.

It was decided to release actin bound to the Mono Q column using a linear gradient from 0-500mM NaCl, an elution profile that was described by Sutoh *et al.*, (1991). However, where the latter study employed a pH of 8.0, the buffer pH in the present study was optimised for *Drosophila* actins prior to attempts at separation. Pharmacia recommend that for separation mediated by an anion exchanger, the pH of a buffer gradient should be at least 1 pH unit above the isoelectric point of the protein of interest. Additionally, at an ionic strength of 0.1M, proteins begin to dissociate from an ion exchanger when the buffer pH is at, or within, 0.5 pH units of their isoelectric point (Lampson and Tytell, 1965). An optimal pH is usually one that is a single pH unit above the isoelectric point, where the protein of interest is able to bind, but is easily released upon a slight increase in salt. Therefore, any differences in charge between individual proteins, which could be diminished at a higher starting pH, will be accentuated by the optimal pH.

Horovitch *et al.* (1979) and Fyrberg *et al.* (1983) demonstrated that *Drosophila* actin isoforms have a pI range between 5.7 and 5.84. A pH of 7.0 was chosen for the start and elution buffers since it was both sufficiently distant from the isoelectric point of the *Drosophila* actins to allow adequate binding to the matrix, and close enough to enable the differential binding affinity to, and consequently elution from the Mono Q matrix.

4.2.3.1 The Mono Q separation of the *Drosophila* actins

A pilot run was performed to test the Mono Q anion exchanger's ability to separate the ACT88F isoform from the mixture of *Drosophila* actins. Upon the application of a WT actin preparation to the column, it was eluted using a 10 min linear gradient of 0-500mM NaCl in 20mM Tris-Cl, pH 7.0. The resulting chromatogram possessed six individual peaks, (see figure 4.5). SDS-PAGE confirmed that the latter cluster of four were the only peaks that were protein-derived, corresponding to actin. These actin peaks eluted off the column between 300-450mM NaCl in the salt gradient.

The utilisation of a shallower, 30 min linear gradient from 0-500mM NaCl greatly enhanced separation of the four peaks, (see figure 4.6), allowing the individual protein content of each to be established by 1D and 2D gel electrophoresis, (see figure 4.7 and 4.8). The four actin peaks were labelled A, B, C and D, according to the order in which they were released from the Mono Q column, peak A therefore representing the first eluant, and peak D the last.

In anion exchange chromatography of a protein mixture, the most basic proteins normally elute from the column first. This was the case here; peak A was shown to contain arthrin alone, (see figure 4.7). Peaks A, B, C and D correspond well, both in their relative elution and magnitudes, with the charge positions and sizes of arthrin and the type III, II and I actin spots seen on 2D gels of the mixed *Drosophila* actins, (see figure 4.4). This correlation therefore predicts that peak B contains pure ACT88F *mod*$^+$. Similarly, peak C is thought to define the ACT79B, ACT88F *mod*$^-$, ACT87E, ACT42A and ACT5C isoforms whilst peak D contains the ACT57A isoform.

Samples from peaks B, C and D were analysed by 2D gel electrophoresis, (see figure 4.8, upper panel, #4, #9, #12). Instead of the single type I spot that would be expected for peak D, two major isoform spots were apparent. In contrast, each fraction from the top of peaks B and C migrated as a single spot, signifying that pure ACT88F could be isolated as peak B using the Mono Q anion exchanger.

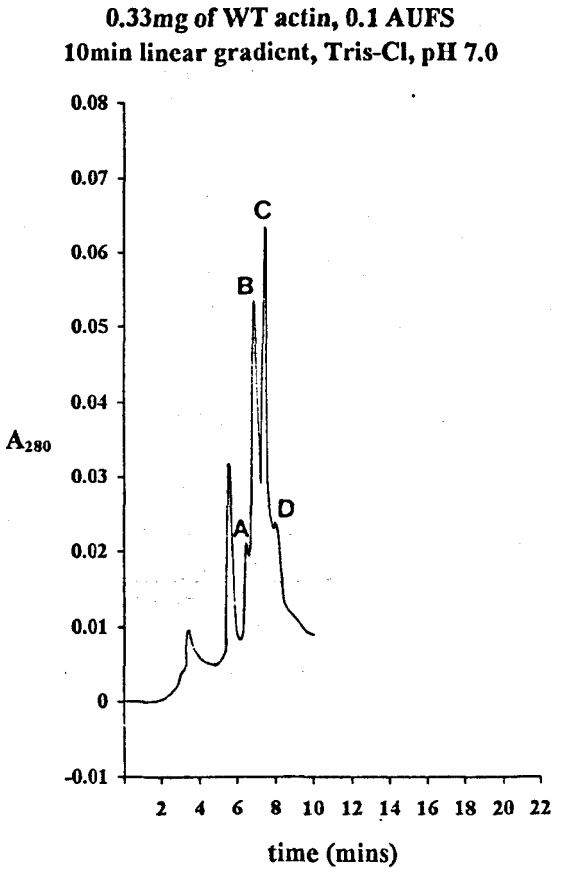

Figure 4.5. A chromatogram showing the elution of 0.33mg of WT actin from a Mono Q column using a 10 min linear gradient from 0-500mM NaCl in Tris-Cl, pH 7.0.

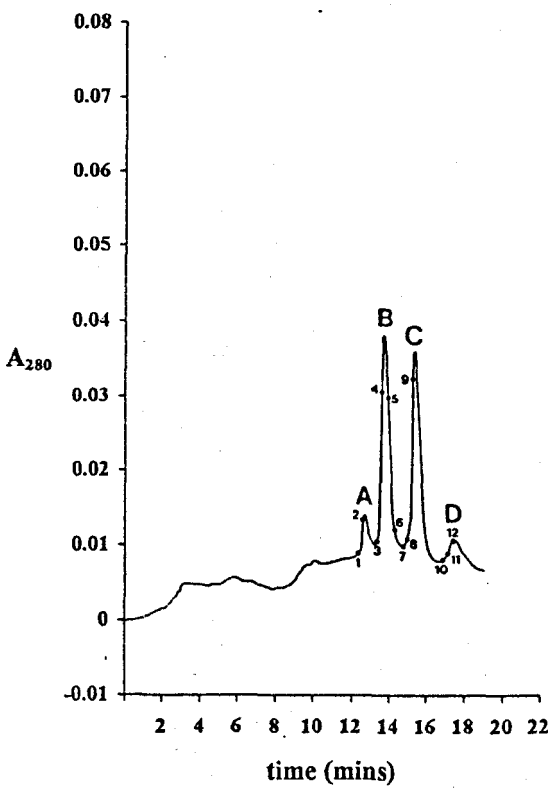

	peak A	peak B	peak C	peak D
WT actin	207mM NaCl	232mM NaCl	259mM NaCl	294mM NaCl

Figure 4.6. A chromatogram showing the elution of 0.2mg of WT actin from a Mono Q column using a 30 min linear gradient from 0-500mM NaCl in Tris-Cl, pH 7.0. The elution points, (mM NaCl), for each of the four actin peaks A, B, C and D are also shown.

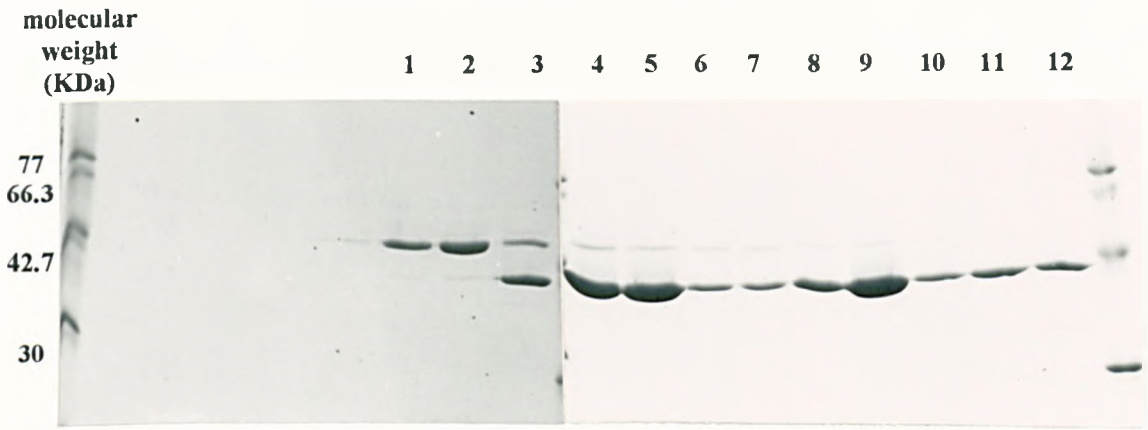

Figure 4.7. 1D SDS-PAGE of the fractions from a chromatographic run in which WT actin was eluted from a mono Q column with a linear gradient from 0-500mM NaCl in Tris-Cl, pH 7.0. Each lane number matches the fraction numbers shown in figure 4.6.

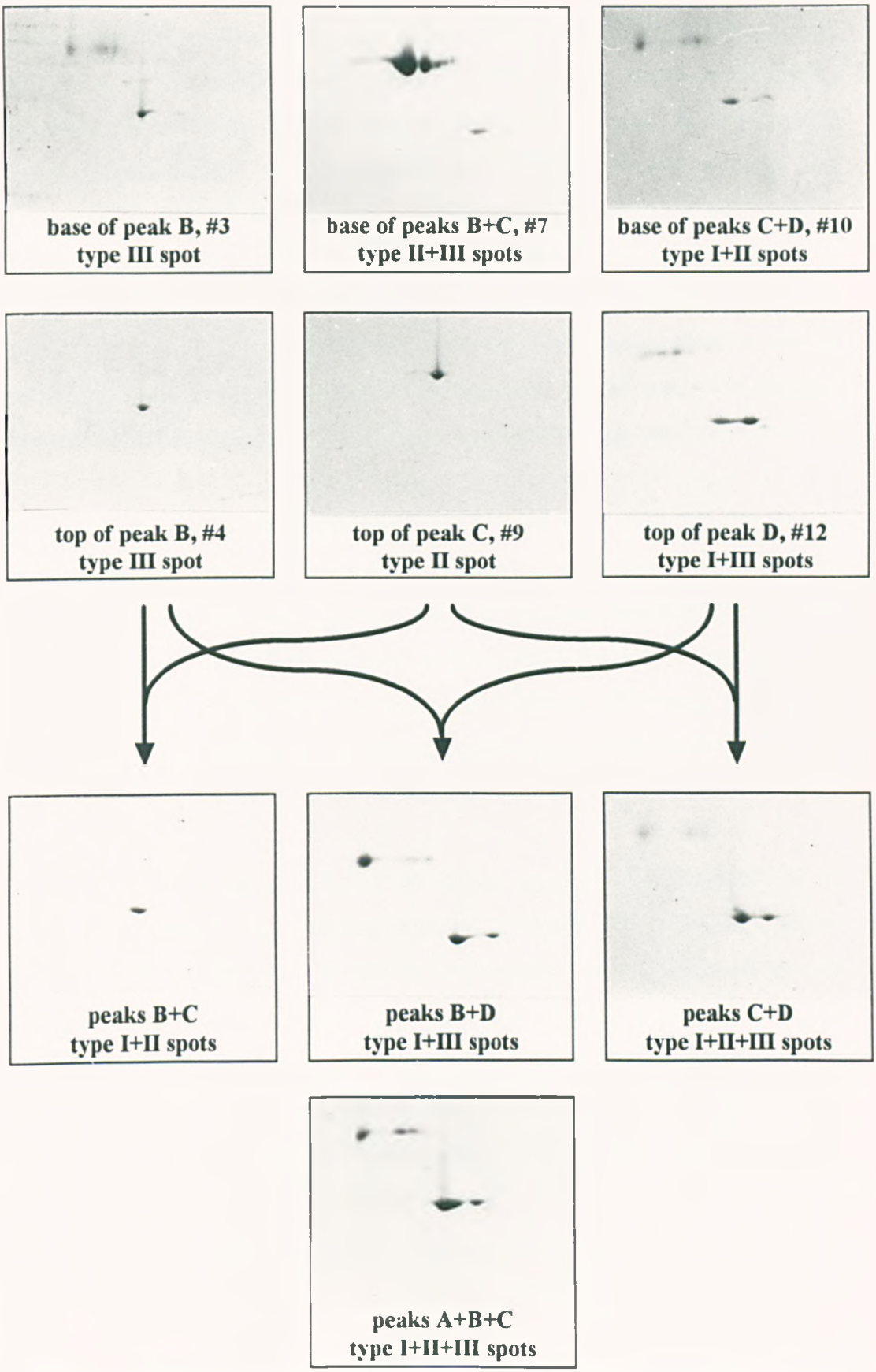

Figure 4.8. 2D gels representing the different fractions from a chromatographic run in which WT actin was eluted from a mono Q column using a linear gradient from 0-500mM NaCl in Tris-Cl, pH 7.0. The fractions are numbered according to their order of elution from the chromatogram in figure 4.6. Upper panel: Fractions from the top of peaks B (#4), C (#9) and D (#12) were each run on separate gels. Fractions from the base of each peak are also shown. Lower panel: 2D gels representing mixtures of the fractions from the tops of each peak.

One limitation of 2D gel electrophoresis is that it does not allow direct comparison of the charges of two individual protein samples in the absence of charge standards. Therefore, it could only be assumed that the single isoform spots from each peak would migrate to alternative isoelectric points. To prove that each spot represented an individual isoform, 2D gel electrophoresis of different combinations of peak samples was performed, (see figure 4.8, lower panel). This investigation showed that the actins in peaks B and C were clearly distinct isoforms. Interestingly, a combination of either peaks B or C with peak D revealed that one of the two isoform spots found in peak D coincided with either the type III or type II actin spot from peaks B and C respectively. The other peak D spot was therefore thought to be a conventional type I actin spot.

Additional 2D gel analysis of samples from the base of each peak, (see figure 4.8, upper panel, #3, #7, #10), revealed multiple isoforms, thus indirectly confirming the individuality of the actins in each peak as shown by the peak combination gels. This isoform heterogeneity in the base fractions signified that pure ACT88F could only be obtained from samples at the top of each peak. Subsequently, the overall resolution of the separations had to be improved in order to achieve large yields of completely pure ACT88F.

A further extension in the duration of the elution gradient duration was used to enhance peak resolution. Since the four actin peaks eluted off the column between 200mM and 300mM NaCl in a 30 min linear gradient, a new gradient profile was programmed in which the time taken to increase from 150mM to 300mM NaCl was lengthened from 9 min to 28 mins. A buffer pH 6.5, as opposed to pH 7.0, was used to try and enhance separation of the different peaks. Investigation into these and other factors that may increase the efficiency of separation is described below. The extended gradient run represented a three step elution profile. The initial phase involved an increase from 0-150mM NaCl over 5mins, followed by the less severe rise from 150-300mM NaCl, and the final phase producing an increase from 300-500mM NaCl in 5 mins.

The extended 28 min gradient from 0-500mM NaCl in MOPS, pH 6.5 revealed a greatly improved peak separation, (see figure 4.9). Whereas before, there was no real lag between the end of peak B and the start of peak C, a delay of about 90 seconds was apparent between these two peaks during the extended run. 1D SDS-PAGE and 2D gel electrophoresis was again performed to estimate the efficiency of isoform separation, (see figures 4.10 and 4.11).

Peaks B and C each constituted a single actin isoform with a distinct pI, (see figure 4.11, upper panel, #5, #10). The actin in peak D once again migrated as two spots, (see figure 4.11, upper panel, #14). Analysing a combination of peaks D and B showed that one of the two peak D spots co-migrated with the type III peak B actin spot, (see figure 4.11, lower panel). This was confirmed by the non-overlap of this peak D spot with the type II actin spot upon combination of peaks C and D. The enhanced isoform separation of the extended elution programme was emphasised by the fact that even the fractions at the bottoms of each peak constituted pure isoforms.

Using this optimised system, the complete isolation of the ACT88F isoform from a mixture of the *Drosophila* isoforms was now possible. The procedures that were used to optimise and ascertain the potential of Mono Q separation are described below.

4.2.3.2 Optimisation of the elution gradient profile for the separation of the *Drosophila* actin isoforms

A number of experimental factors such as pH, the binding capacity of the matrix, counter-ion identity, temperature and flow rate are expected to affect the resolution of ion exchange chromatography. All manipulations in this study were performed at 4°C and involved the application of a gradient from 0-500mM NaCl to the column. The effect of the gradient duration is analogous to the flow rate through a system. Both of these factors affect the dynamic capacity of a matrix. An increase in the flow rate or gradient duration will increase the dynamic capacity of the matrix and therefore enhance the efficiency of chromatographic separation as shown above for the extended gradient. Highlighted below are three chromatographic separations which investigate

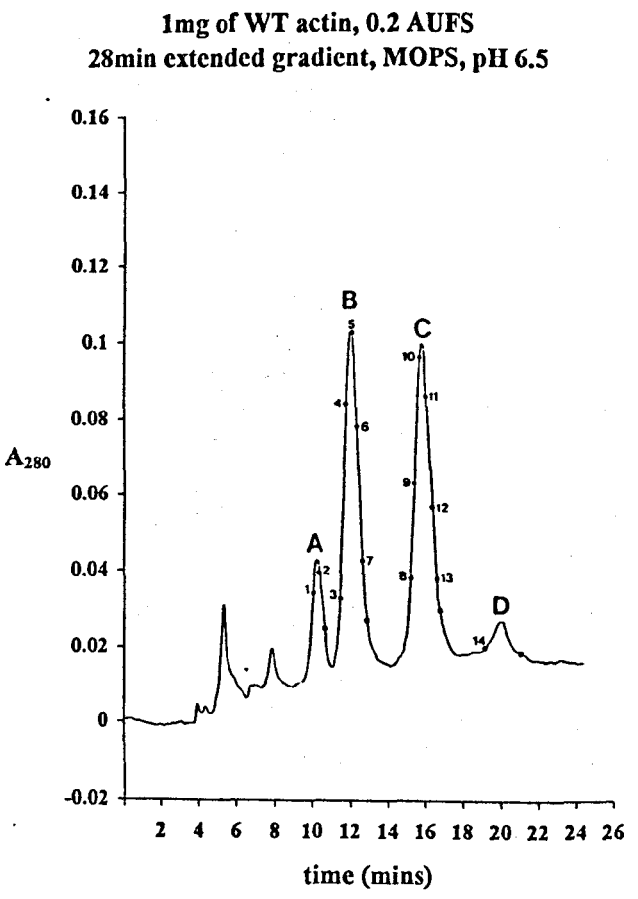

	peak A	peak B	peak C
WT actin	191mM NaCl	203mM NaCl	233mM NaCl

Figure 4.9. A chromatogram showing the elution of 1.0mg of WT actin from a Mono Q column using a 28 min extended gradient from 0-500mM NaCl in MOPS, pH 6.5. The elution points, (mM NaCl), for three of the four actin peaks A, B and C are also shown.

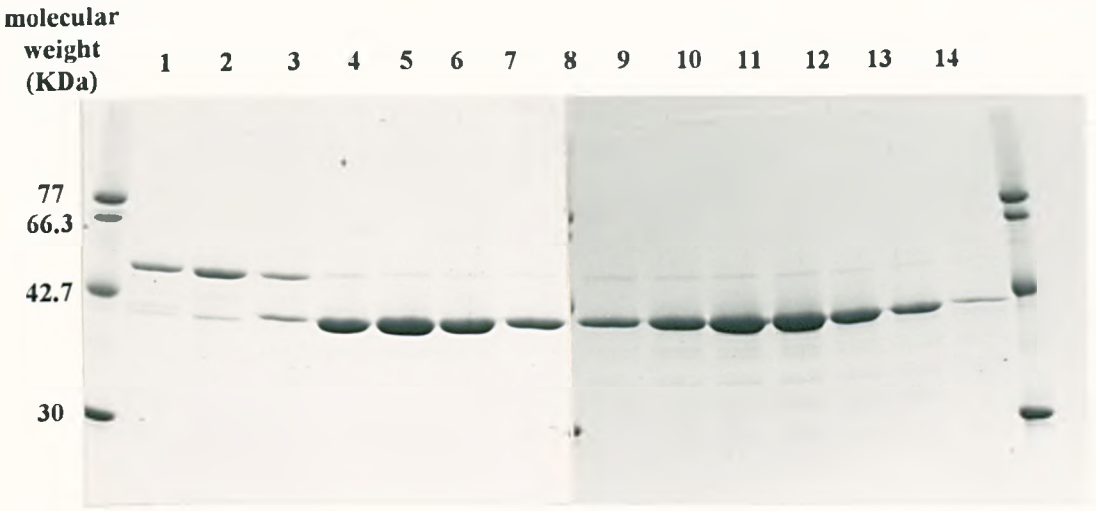

Figure 4.10. 1D SDS-PAGE of the fractions from a chromatographic run in which WT actin was eluted from a mono Q column with an extended gradient from 0-500mM NaCl in MOPS, pH 6.5. Each lane number matches the fraction numbers shown in figure 4.9.

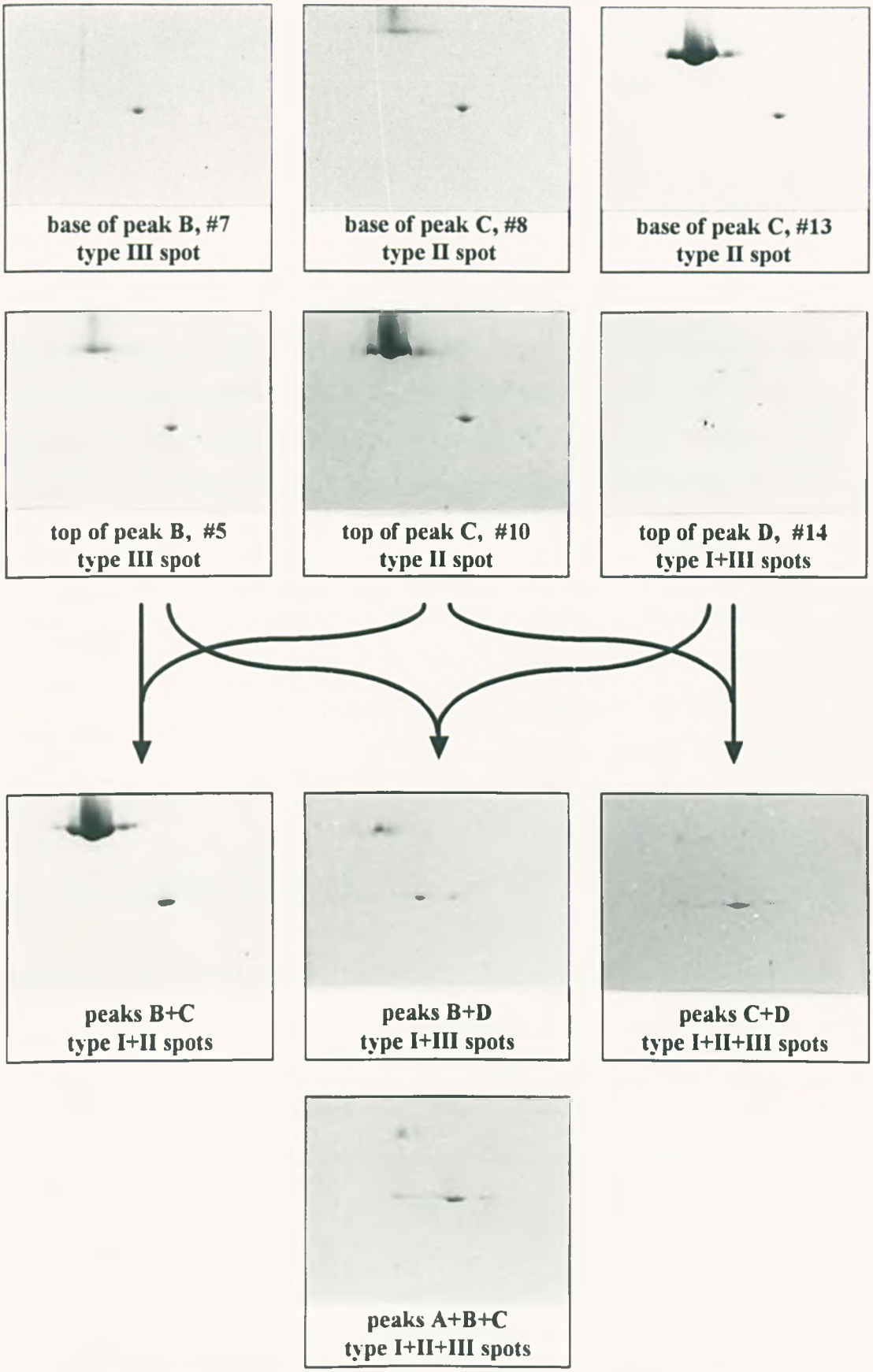

Figure 4.11. 2D gels representing the different fractions from a chromatographic run in which WT actin was eluted from a mono Q column using an extended gradient from 0-500mM NaCl in MOPS, pH 6.5. The fractions are numbered according to their order of elution from the chromatogram in figure 4.10. Upper panel: Fractions from the top of peaks B (#5), C (#10) and D (#14) were each run on separate gels. Fractions from the base of each peak are also shown. Lower panel: 2D gels representing mixtures of the fractions from the tops of each peak.

the effect of pH, the buffering agent and the matrix capacity upon the efficiency of anion exchange. In each case, these were compared to the gradient profile shown in figure 4.6.

(i) The effect of the buffering agent on chromatographic resolution at pH 7.0

The chromatogram shown in figure 4.6 was obtained through the application of a linear salt gradient in Tris-Cl, pH 7.0. Since Trizma is only active as a buffering agent over a pH range between 7.0-9.0, this base is working effectively at its buffering limit in this experiment. The effect of MOPS, a buffering agent that is active between a pH of 6.5 and 7.9, upon the separation of the *Drosophila* actins at pH 7.0 was evaluated, (see figure 4.12).

A 30 min linear gradient from 0-500mM NaCl in MOPS, pH 7.0 produced an elution profile that was essentially the same as that obtained for runs performed with Tris-Cl as the buffering agent, (see figures 4.6 and 4.12). This suggested that the nearness of Trizma to its buffering limit at a pH of 7.0 does not affect the resolution of separation of the actin isoforms.

(ii) The effect of pH on chromatographic resolution

A buffer with a pH of 7.0 was earlier predicted to promote a strong binding of the *Drosophila* actins to the anion exchanger without diminishing their capacity for displacement by low salt concentrations. Although this gave adequate resolution between the four different actin peaks, it was 1.2 units away from the predicted pIs of 5.7-5.84 for these isoforms. A pH of 6.5 was subsequently tested for its effect upon the separation of the *Drosophila* actins, (see figure 4.13).

This investigation revealed a chromatographic profile in which the relative elution points for each peak were very similar to those found for the run performed at pH 7.0, (see figures 4.6 and 4.13). Although this suggested that a pH of 7.0 was as effective as

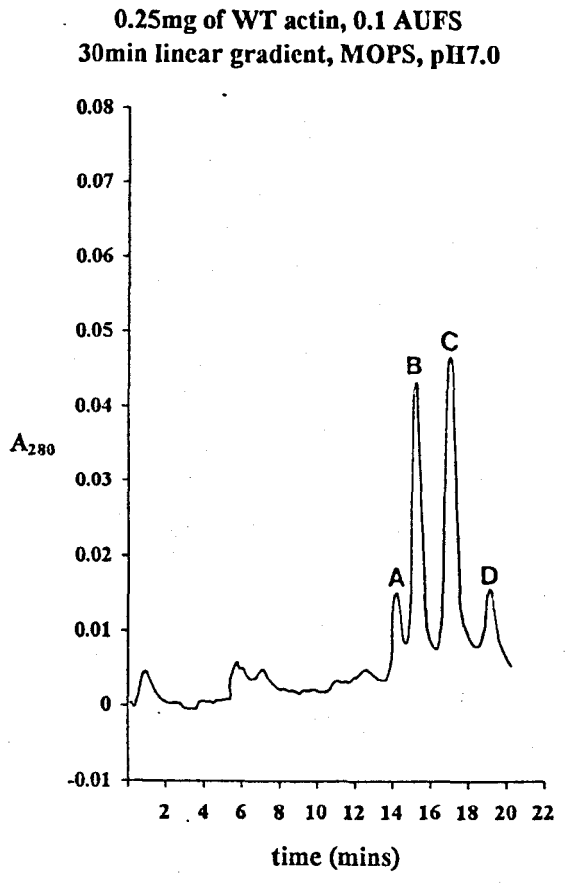

	peak A	peak B	peak C	peak D
WT actin	230mM NaCl	248mM NaCl	276mM NaCl	313mM NaCl

Figure 4.12. A chromatogram showing the elution of 0.25mg of WT actin from a Mono Q column using a 30 min linear gradient from 0-500mM NaCl in MOPS, pH 7.0. The elution points, (mM NaCl), for the four actin peaks A, B, C and D are also shown.

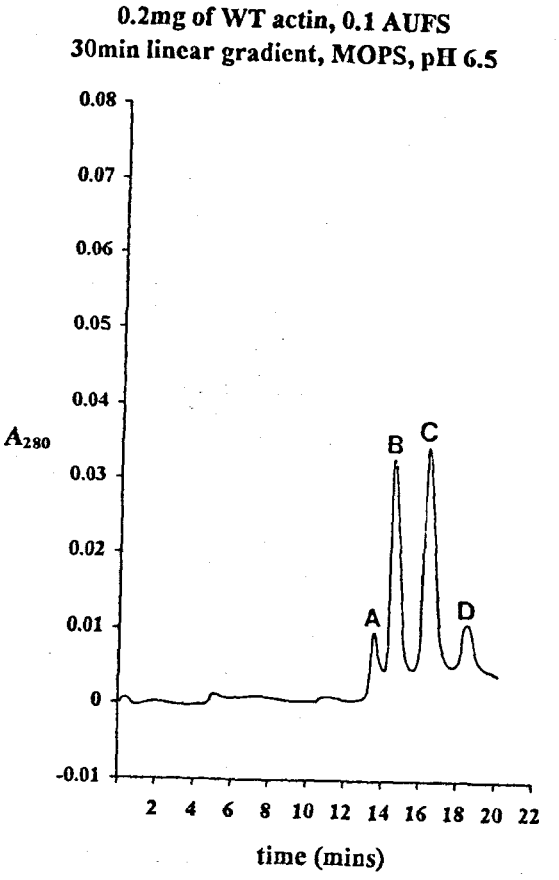

	peak A	peak B	peak C	peak D
WT actin	220mM NaCl	239mM NaCl	269mM NaCl	306mM NaCl

Figure 4.13. A chromatogram showing the elution of 0.20mg of WT actin from a Mono Q column using a 30 min linear gradient from 0-500mM NaCl in MOPS, pH 6.5. The elution points, (mM NaCl), for the four actin peaks A, B, C and D are also shown.

a pH of 6.5, the latter was employed in the optimised, extended gradient, (see figure 4.9).

(iii) The effect of sample loading capacity on chromatographic resolution

The binding capacity of an ion exchange matrix is determined by its ability to associate with counter-ions. The Mono Q matrix has an extremely high capacity in which a 1ml column is able to bind 25mg of protein. This is advantageous, both in terms of time and percentage recovery, since it enables the separation of milligram quantities of protein in one chromatographic run, (Pharmacia handbook) . There is a limit, however, where an increasing amount of sample loaded onto the column becomes detrimental to the resolution of peak separation. A run was performed in which 2mg of WT actin was applied to the column, followed by elution with a 30 min linear gradient of 0-500mM NaCl in Tris-Cl, pH 7.0, (see figure 4.14).

The separation of 2mg of *Drosophila* actin, representing almost a third of a large scale actin preparation generated a similar actin peak distribution to an identical run performed with 0.2mg of actin, (see figures 4.6 and 4.14). Although 2mg is nowhere near the binding capacity for the Mono Q matrix, the fact that this quantity did not curtail resolution indicated that hundreds of micrograms of ACT88F could be isolated during one column run. This therefore enables the separation of enough material for biochemical study using a single Mono Q run.

The aforementioned experiments helped to establish the conditions used to define the 28 min extended gradient from 0-500mM NaCl in MOPS, pH 6.5. Although this protocol is probably not optimised for maximal separation, it is routinely used to purify the ACT88F isoform from *Drosophila* actin preparations. A lower pH, in conjunction with a suitable buffering agent, or a doubling of the gradient time may further enhance the separation of the actin isoforms.

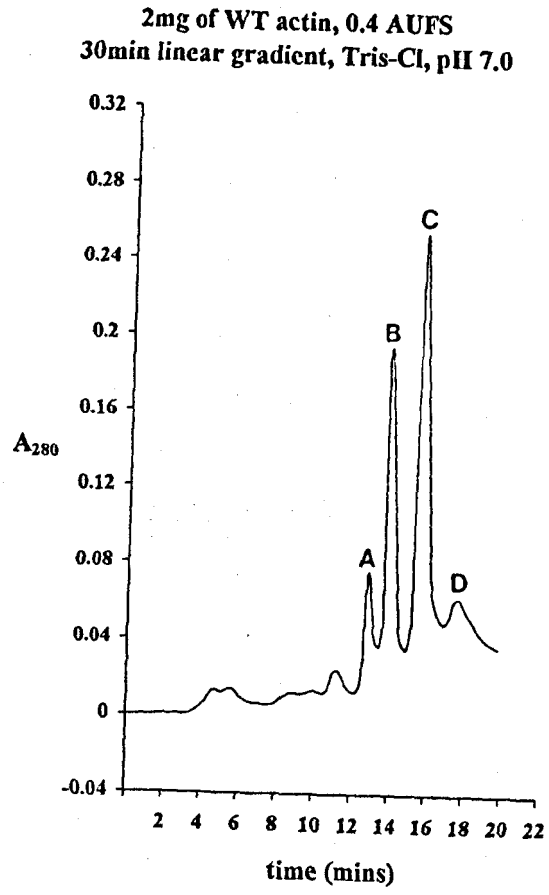

	peak A	peak B	peak C	peak D
WT actin	210mM NaCl	227mM NaCl	252mM NaCl	290mM NaCl

Figure 4.14. A chromatogram showing the elution of 2.0mg of WT actin from a Mono Q column using a 30 min linear gradient from 0-500mM NaCl in Tris-Cl, pH 7.0. The elution points, (mM NaCl), for the four actin peaks A, B, C and D are also shown.

4.2.3.3 The isolation of pure mutant ACT88F by anion exchange chromatography

The successful isolation of *Drosophila* WT ACT88F using anion exchange chromatography prompted the purification of mutant ACT88F isoforms in this system. As with the yeast and *Dictyostelium in vivo* "expression" systems, the choice of mutant actins that can be isolated is dependent upon their possession of a charge differential to that of the endogenous actins of the organism in question. Of the four ACT88F mutants available that form muscle in flies, (see section 5.1.1), only one, *G368E*, is incompatible for isolation in this system since its predicted isoelectric point coincides with that of the ACT79B isoform. The three other actin mutations, *E93K*, *E334K* and *E316K* all have an increased basicity with respect to the other *Drosophila* isoforms which enhances their separation in this system. The purification of the *E93K* and *E334K* mutations is described below.

The elution profile of *E93K* actin from the column upon the application of a 30 min linear gradient from 0-500mM NaCl in Tris-Cl, pH 7.0 displayed the four major peaks that are seen with WT actin, (see figure 4.15). As expected, the increased basic charge of *E93K*-ACT88F was manifested in the advanced elution of peaks A an B at lower salt concentrations in the gradient, (see figures 4.6 and 4.15). The unaltered elution positions of peaks C and D indirectly confirmed that peak B delineates the ACT88F *mod*$^+$ peak.

In addition to the 4 major actin peaks, two minor ones situated between peaks B and C were also distinguishable. These correspond to actin, (see figure 4.16), and were labelled as B(i) and B(ii), where the former lies on the shoulder of peak B and the latter immediately precedes peak C in the chromatogram. It was suspected that peak B(ii) may represent the *E93K*-ACT88F *mod*$^-$ isoform which would also be expected to elute from the column before its regular position at peak C due to an increased basic charge. As seen from the height of this peak, ACT88F *mod*$^-$ represents only a small fraction of the total *Drosophila* actin content and of the *Act88F* encoded proteins.

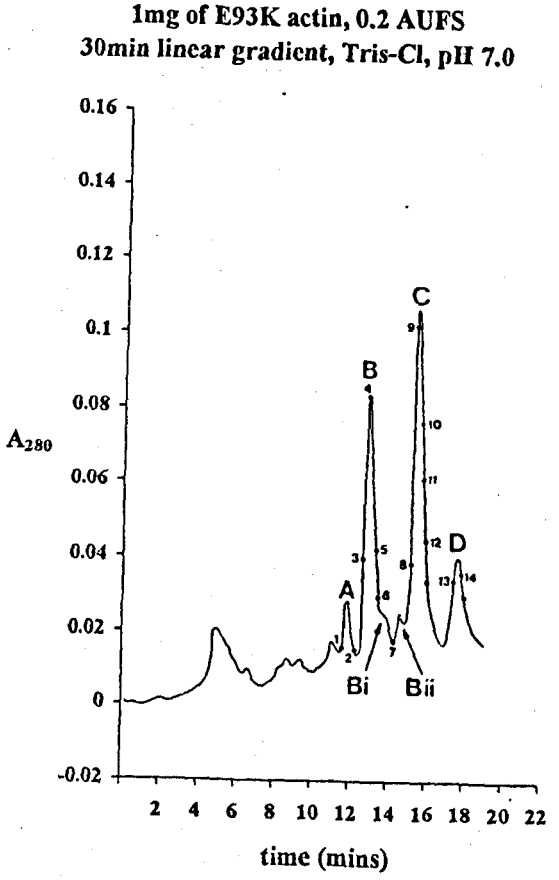

Figure 4.15. A chromatogram showing the elution of 1.0mg of E93K actin from a Mono Q column using a 30 min linear gradient from 0-500mM NaCl in Tris-Cl, pH 7.0. The elution points, (mM NaCl), for five of the six actin peaks A, B, B(ii), C and D are also shown.

	peak A	peak B	peak B(ii)	peak C	peak D
E93K actin	203mM NaCl	217mM NaCl	251mM NaCl	260mM NaCl	296mM NaCl

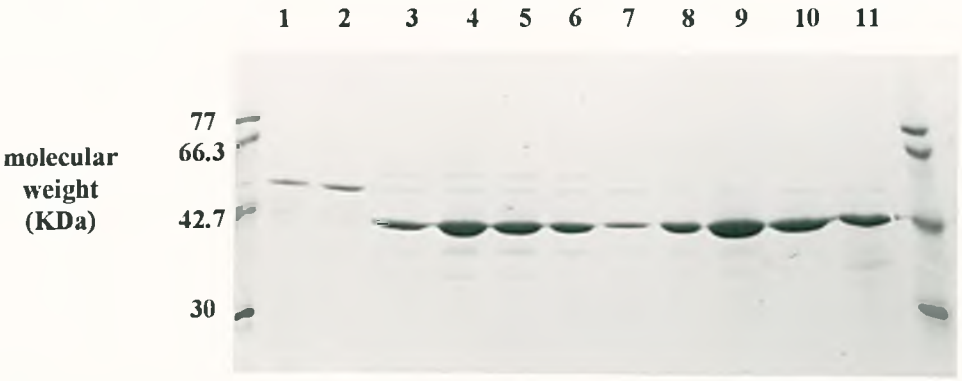

Figure 4.16(a). 1D SDS-PAGE of the fractions from a chromatographic run in which E93K actin was eluted from a mono Q column with a linear gradient from 0-500mM NaCl in Tris-Cl, pH 7.0. Each lane number matches the fraction numbers shown in figure 4.15 except for the omission of fractions 12, 13 and 14.

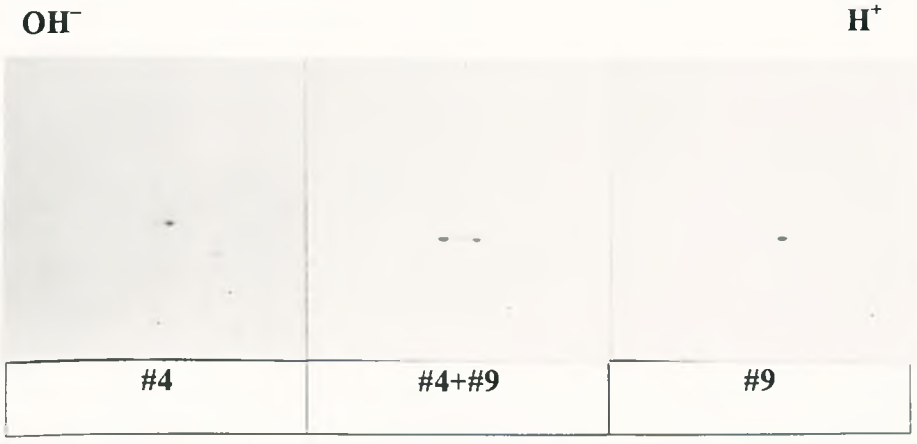

Figure 4.16(b). 2D gels representing the different fractions from a chromatographic run in which E93K actin was eluted from a mono Q column using a linear gradient from 0-500mM NaCl in Tris-Cl, pH 7.0. A sample from the top of peak B, (#4), and the top of peak C, (#9), representing E93K-ACT88F *mod*$^{+}$ and ACT79B respectively, were run on individual gels. #4+#9 represents a 2D gel of a mixture of these two samples. The anode is oriented to the right hand side.

Figure 4.16(c). A 2D gel showing an E93K actin preparation from whole flies using a scaled up version of the mini-actin protocol. Molecular weight and BSA markers are also shown, the latter being used to orient the basic side of the gel which lies to the left. The 55KDa arthrin and three actin spots, E93K-ACT88F *mod*$^{+}$, ACT79B and the cytoplasmic actins can be identified in order of increasing acidity.

The actin isoform identity of peak B(i) is unknown. However, the revelation of this actin peak, due to the earlier elution point of *E93K*-ACT88F *mod*$^+$, suggests that this isoform may constitute a small fraction of peak B in WT actin preparations, where its presence is obscured by the more abundant ACT88F *mod*$^+$ isoform. The earlier elution of peaks A and B during the separation of the *E334K* actins closely matched those of the *E93K* mutation, (see figure 4.17). The two minor peaks, B(i) and B(ii) were again apparent, although in different relative proportions to those seen for the *E93K* preparation. The latter difference may be generally attributed to the fact that the relative proportions of each of the actin isoforms varies in different actin preparations.

4.2.3.4 Anion exchange of the ACT88F null mutant, *KM88*

To establish that peak B(i) was not an artefact of the *E93K* and *E334K* actin mutations, the chromatographic profile of *KM88*, an ACT88F null was analysed, (see figures 4.18 and 4.19). Since an actin preparation from this mutant only contains ACT79B and cytoplasmic actin isoforms, elution would be expected to produce peaks C and D alone. Application of the extended elution gradient to a *KM88* sample revealed the presence of three individual peaks. The second and third peaks were depicted as the ACT79B and cytoplasmic isoforms respectively because they eluted off the column at concentrations corresponding to peaks C and D in the extended gradient run for WT actin, (see figure 4.9). The first peak was thought to portray the B(i) peak seen in the *E93K* run. Its elution at 203mM NaCl is identical to the position that peak B would elute from in a WT sample, (see figures 4.9 and 4.18). This signifies that peak B does not represent absolutely pure ACT88F. It also predicts that type III actin spots in 2D gels of whole fly actin preparations may constitute two, as opposed to one actin isoform.

4.2.4 Discussion

Drosophila melanogaster has been extensively used as a system for studying the *in vivo* effects of ACT88F mutants (Drummond *et al.*, 1991a; Sparrow *et al.*, 1991a; 1991b; 1992). However, although these and many other mutations were characterised

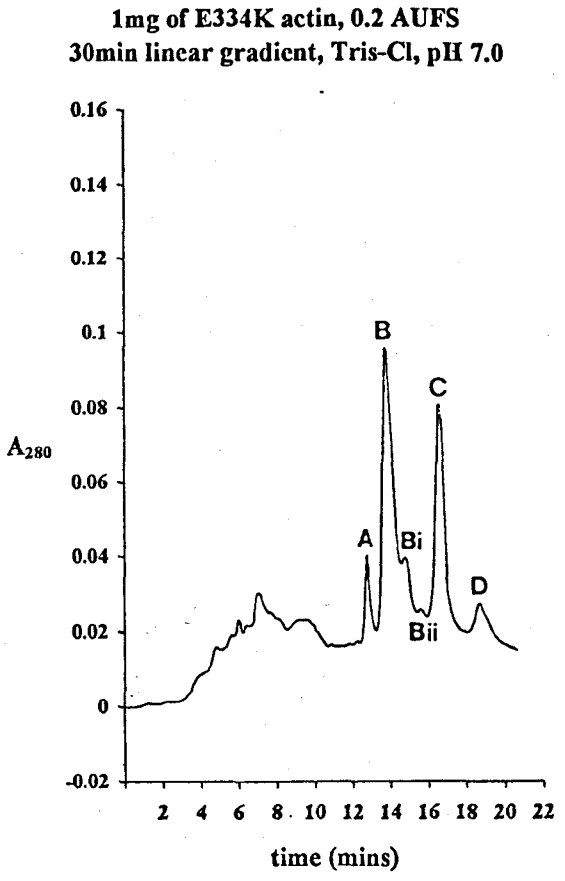

Figure 4.17. A chromatogram showing the elution of 1.0mg of E334K actin from a Mono Q column using a 30 min linear gradient from 0-500mM NaCl in Tris-Cl, pH 7.0. The elution points, (mM NaCl), for five of the six actin peaks A, B, B(i), C and D are also shown.

	peak A	peak B	peak B(i)	peak C	peak D
E334K actin	203mM NaCl	218mM NaCl	240mM NaCl	264mM NaCl	301mM NaCl

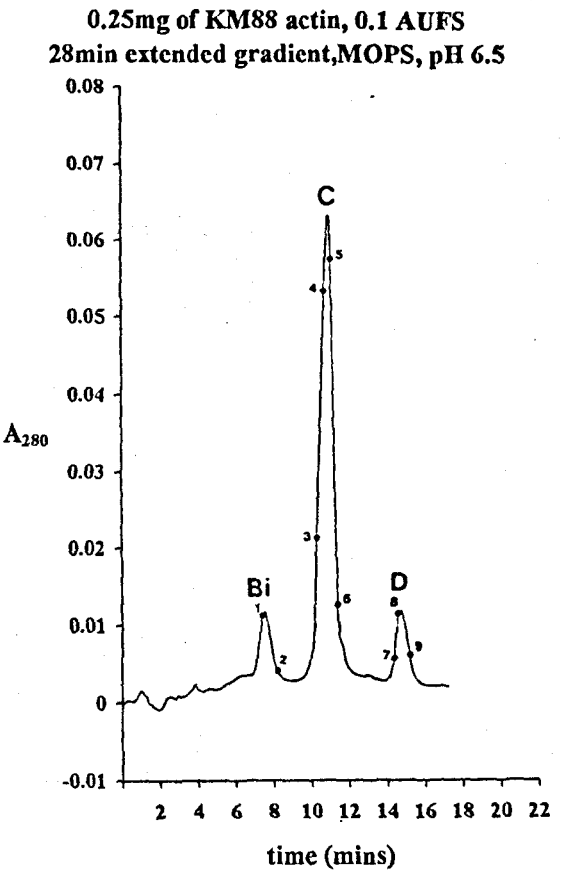

Figure 4.18. A chromatogram showing the elution of 0.25mg of KM88 actin from a Mono Q column using a 28 min extended gradient from 0-500mM NaCl in MOPS, pH 6.5. The elution points, (mM NaCl), for the three actin peaks, B(i), C and D are also shown.

	peak B(i)	peak C	peak D
KM88 actin	203mM NaCl	227mM NaCl	263mM NaCl

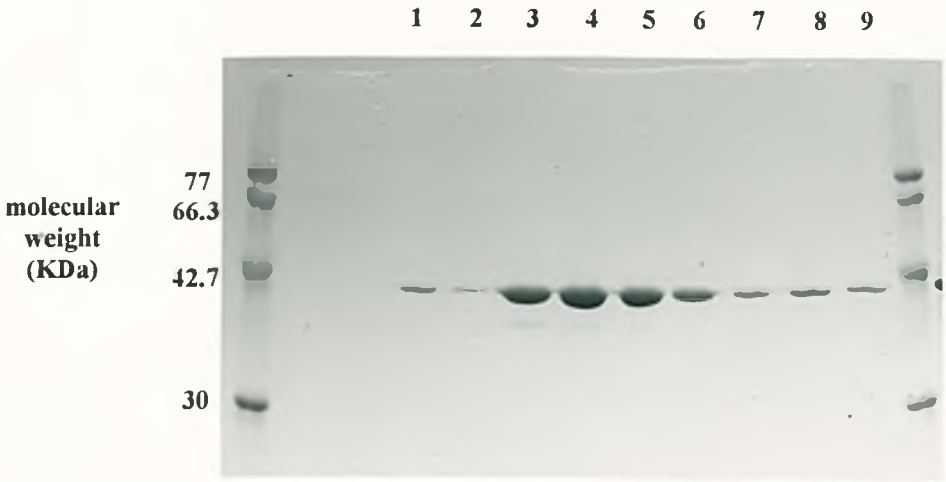

Figure 4.19. 1D SDS-PAGE of the fractions from a chromatographic run in which KM88 actin was eluted from a mono Q column with a 28 min extended gradient from 0-500mM NaCl in MOPS, pH 6.5. Each lane number matches the fraction numbers shown in figure 4.18

by various *in vitro* studies (Drummond *et al.*, 1991a; 1991b; 1992; Hennessey *et al.*, 1991) further biochemical analysis was limited by the inability to acquire sufficient quantities of pure mutant proteins. The aim of this work was to isolate pure ACT88F from *Drosophila* such that these additional studies could be performed.

The observation that only small quantities of actin are required for *in vitro* motility assays prompted the development of the mini-actin preparation. This was subsequently able to isolate about 5μg of pure ACT88F from 10 WT or mutant flies, providing enough material for many motility assays and *in vitro* force measurements using an optical trap (Molloy, unpublished).

By scaling up the mini-actin preparation, milligram quantities of the mixed actin isoforms could also be purified from thousands of flies, where ten thousand flies represents the population from 20 milk bottle cultures. Subjecting this large scale actin extract to anion exchange chromatography demonstrated that the different isoforms could be resolved into one arthrin and three major actin peaks. These corresponded directly to the four spots seen on 2D gel electrophoresis of the different *Drosophila* actin isoforms, (see figure 4.4), and predicted that peak B represented pure ACT88F.

Anson *et al.* (1995) estimated the percentage fraction of total actin that each of the *Drosophila* actin isoforms represented by performing gel densitometry on 2D gels showing the total actin of *E93K* mutant flies. This mutation causes the *E93K*-ACT88F *mod*$^-$ isoform to shift away from the type II position, such that the content of this and all of the other actins can be quantified, (see figure 4.16). Anson stated that the arthrin, ACT88F *mod*$^+$, ACT88F *mod*$^-$, ACT79B+ACT42A+ACT5C+ACT57E and ACT57A isoforms portray 5.9%, 24.8%, 10.7%, 34.1%, 24.5% of the total actin content respectively and suggested that the relative proportions of these would be about the same in different actin preparations.

The current study also enabled a direct measure of the proportion that each actin isoform represented of the total actin isolated. Although an accurate representation of the content of each isoform could be determined by comparing the square areas of

each peak, a simple comparison of the peak heights revealed that for almost every chromatographic run with different actin preparations for each genotype, the relative heights of analogous peaks were highly variable. This suggests that estimates of each actin isoform fraction from gel densitometry of an *E93K* preparation (Anson *et al.*, 1995) may not reflect the true amounts of these actins in different preparations. Since anion exchange chromatography provides a highly sensitive means for rapidly and accurately assessing the content of a mixture of proteins, it implied that the percentage fraction of each actin isoform may differ between individual actin preparations.

According to the conventional classification of the *Drosophila* actins, the type III actin spot seen in 2D gels is thought to represent pure ACT88F *mod*$^+$ (Mahaffey *et al.*, 1985). The subsequent isolation of peak B during the anion exchange chromatography of mixed *Drosophila* actin isoforms was therefore thought to be a pure ACT88F isoform. However, the presence of peak B(i) in *E93K*, *E334K* and *KM88* chromatograms suggests that peak B in WT runs is comprised of a major ACT88F *mod*$^+$ component and a minor amount of this unknown actin isoform. This protein is known to be encoded by a gene other than the *Act88F* gene since its charge is not affected by the *E93K* mutation and it is present in the *KM88* ACT88F null mutant.

In an attempt to identify which *Drosophila* actin constitutes peak B(i), variation in the primary sequences of each of the actin isoforms was analysed. Attention was focused upon the amino acid substitutions at charged positions. The net charge of each *Drosophila* actin isoform was predicted as described in section 3.1.2. Here, positively and negatively charged residues were assigned equivalent but opposite unit charges. The addition of these allowed an approximation of the relative net charge of each isoform, (see table 4.1).

This analysis revealed that out of all the amino acid substitutions between the six different actin isoforms, only two involved a non-conservative change at a charged position. Where residue Q263 was a histidine in ACT5C, Q360 in ACT57A was an aspartic acid.

Table 4.1. The total number of times a charge residue appears in the primary sequence is highlighted for each *Drosophila* actin isoform. Each basic residue is assigned a single positive unit charge, (+1), and each acidic residue is denoted a single negative unit charge, (-1). The addition of these unit charges provides an overall net charge for each actin isoform.

	arginine	lysine	histidine	aspartic acid	glutamic acid	net charge
ACT88F *mod*$^-$	18	19	9	23	26	-3*
ACT79B	18	19	9	21	28	-3
ACT42A	18	19	9	21	28	-3
ACT5C	18	19	10	21	28	-2
ACT87E	18	19	9	22	27	-3
ACT57A	18	19	9	22	28	-4

* note that this figure reflects the charge of ACT88F *mod*$^-$ isoform and does not account for the unknown modification that generates ACT88F *mod*$^+$ (Mahaffey *et al.*, 1985).

The sequence comparisons above suggest that all of these actin isoforms, with the exception of ACT5C and ACT57A, should constitute peak C and migrate to a type II position in 2D gels. Where ACT5C should migrate to a type III position, ACT57A is predicted to reside at a type I position. On the whole, these net charges were confirmed by a study in which fluorograms of ^{32}S-methionine labelled proteins on 2D gels showed that each of the *Drosophila* actins translated *in vitro* migrated as a major type II spot and a minor type III spot, except for ACT57A which translated to a major type I and a minor type II actin. The minor forms observed in this study were not expected to accumulate *in vivo* (Fyrberg *et al.*, 1983).

The only anomaly in the above comparison regards the ACT5C isoform. Whereas Fyrberg *et al.* (1983) predicted that this actin forms a stable type II product, sequence comparisons in the present study favour the possibility of ACT5C representing a type III actin. This discrepancy could be explained by the fact that since the Fyrberg *et al.* (1983) study, re-sequencing of the *Drosophila* actin genes (Sparrow and Fyrberg, unpublished) found differences in the nucleotide sequences. It was from the updated nucleotide sequences that the isoform charges from table 4.1 were predicted. It was therefore postulated that the ACT5C isoform may constitute peak B(i) and would consequently co-migrate with the ACT88F *mod*$^+$ isoform to the type III position on 2D gels of a whole *Drosophila* actin extract. Studies analysing the thoracic actin

content of ACT88F mutants demonstrated that destabilisation of their ACT88F actin produced 2D gels that lacked a type III actin spot (Lang *et al.*, 1981; Ball *et al.*, 1987), suggesting that the only type III actin product found in thoraces is encoded by the *Act88F* gene.

It is surprising that the proposed ACT5C, type III cytoplasmic actin has never been identified by the various studies that use 2D gel electrophoresis to visualise the *Drosophila* actins. This may reflect the lack of resolution of 2D gels in detecting small quantities of protein that are obscured by adjacent, highly abundant proteins. Two studies on *Drosophila* cell cultures did however provide some evidence for a type III actin that may not be related to the IFM specific actin III. Storti *et al.* (1978) and Horovitch *et al.* (1979) showed that fluorograms of 2D gels of different embryonic cell lines possessed a major type II and a minor type III actin spot. Additionally, they found that the type III product was not visible upon Coomassie staining and predicted, as Fyrberg *et al.* (1983), that this "generalised" product would be unstable *in vivo*.

There are no reports that *Drosophila* actins have previously been subjected to anion exchange chromatography. This may explain why the type III actin described as peak B(i), possibly corresponding to the ACT5C isoform, has not been previously identified. The enhanced sensitivity of ion exchange chromatography, coupled to the fact that it concentrates each protein fraction into a single peak, makes it a much better analytical tool. It clearly shows, in conjunction with mutant analysis, that that the type III spot on 2D gels of whole fly actin extracts contains two isoforms. Since this isoform is thought to be localised to the ovaries and the abdominal wall (Fyrberg *et al.*, 1983) it would not "contaminate" the actin preparations performed upon dissected IFMs which would therefore represent absolutely pure ACT88F.

The relative charges assigned to the *Drosophila* actins, (see table 4.1), match the expected type I, II or III positions on 2D gels described by Horovitch *et al.* (1979) and Fyrberg *et al.* (1983). The only exception is the ACT5C isoform. Its type III identity proposed in this study could be envisaged as a post-translational modification from a type II isoform (Fyrberg et al., 1983) to a more basic protein, in a manner analogous to

unknown modification to ACT88F. Peptide sequencing of the actin in peak B(i) could settle this inconsistency.

Anion exchange chromatography of a *Drosophila* actin preparation has therefore allowed the isolation of what was previously thought to represent pure ACT88F. The contaminating type III actin species represents less than 10% of the protein content of peak B when the heights of peaks B and B(i) are compared in the E93K chromatogram. Peak B therefore represents a relatively pure ACT88F isoform preparation that can be used to further the biochemical study of ACT88F mutations using assays that require upwards of 100μg of purified actin.

CHAPTER FIVE: THE *IN VITRO* MOTILITY ANALYSIS OF *DROSOPHILA* ACT88F MUTANTS

5.1 Introduction

5.1.1 Four ACT88F mutants of *Drosophila melanogaster*

In vitro motility assays enable direct observation of the effects of actin and myosin mutants upon actomyosin interactions and ultimately provide insights into the ways in which these two proteins interact within the contractile cycle. The *in vitro* motility of four *Drosophila* actin mutants, *G368E, E316K, E334K* and *E93K*, was tested under varying assay conditions. The previous extensive *in vitro* and *in vivo* characterisation of these mutants has demonstrated that their abnormal phenotypes could be due to defective interactions with myosin, as well as a number of other cytoskeletal proteins.

The *Act88F* actin mutants, *G368E, E316K* and *E334K* were all generated by the random *in vitro* mutagenesis of the *Act88F* gene (Drummond *et al.*, 1991a) and then transformed into the germline of an ACT88F null host strain, *KM88*, using P-element vectors (Drummond *et al.*, 1990; 1991a). The *E93K* mutation was isolated after chemical mutagenesis of flies by selection for a dominant flightlessness phenotype.

Examination of IFMs by electron microscopy revealed that each of the aforementioned mutants formed a discernible muscle structure, unlike three other *Act88F* mutants that had been introduced into *Drosophila* (Drummond *et al.*, 1991a). *G368E* and *E316K* caused only minor defects in muscle structure which were visible as disturbances to the thick and thin filament lattice at the periphery of the myofibrils. *E334K* and *E93K* IFMs displayed a greater degree of disruption. Electron microscopy of *E93K* IFMs showed that although myofibrils contained thick and thin filaments, there was an absence of Z-discs, and subsequently, sarcomeric structure (Sparrow *et al.*, 1991b). This myofibrillar disruption of *E93K* was attributed to a defective interaction with a Z-disc protein such as α–actinin. Although electron microscopy was not performed for

E334K, phase contrast microscopy of IFM myofibrils displayed a phenotype indistinguishable from that of *E93K*.

The IFMs of each of these mutants accumulated actin to levels equivalent to WT. However, all of these actin mutants were flightless, with the exception of *G368E*, which had a decreased flight ability and a 20% reduction in its wing beat frequency in comparison to WT (Drummond *et al.*, 1990; 1991a). Mechanical studies using demembranated IFM fibres showed that the rate constant for the delayed increase in tension following a quick stretch in activating solution was reduced by 30% for *G368E* and increased by a similar amount for *E316K* with respect to WT levels. Since these two mutations do not lie in any proposed myosin binding site (Rayment *et al.*, 1993b; Schröder *et al.*, 1993), their abnormal effects upon the actomyosin interaction were attributed to conformational changes in their actin monomer structures.

Initial biochemical studies utilised very small quantities of pure ACT88F proteins that had been transcribed and translated in an *in vitro* rabbit reticulocyte lysate system (Drummond *et al.*, 1991a; 1991b; 1992; Hennessey *et al.*, 1991). Subsequent investigations with these recombinant proteins suggested that *G368E*, *E316K* and *E334K* possessed a normal conformation *in vitro*, as assessed by their mobilities on non-denaturing gels (Drummond *et al.*, 1991b). Small scale binding assays revealed that the affinity of *E316K* and *E334K* for profilin was increased whereas that of *G368E* for ATP was reduced with respect to WT actin (Drummond *et al.*, 1992). Again, it was suggested that since these mutations do not lie near the proposed binding sites for ATP and profilin, long range conformational changes may exert significant effects upon ligand binding to these mutant actins.

Previous measurements of the activation of myosin ATPase and *in vitro* motility of *G368E* and *E316K* used material purified from whole flies (Anson *et al.*, 1995). These preparations contained six different *Drosophila* actin isoforms, of which ACT88F represented only 40%. These investigations established that *G368E* and *E316K* stimulated the myosin ATPase at levels equivalent to WT *Drosophila* actin. *In vitro* motility of these two mutations was tested on both rabbit skeletal muscle myosin and

HMM. The filament velocity of *G368E* was seen to decrease by 16% and 19% compared to WT over HMM and myosin substrates respectively. The *E316K* mutant exhibited WT filament velocities over a HMM surface but showed a 15% reduction over myosin.

5.1.2 Variation of the conditions during *in vitro* motility assays

Motility assays are normally performed under a set of standard conditions. These are optimised for maximal filament velocity with respect to their ATP content and ionic strength, the latter determining the stable binding of the actin filaments to the surface. Although the velocities of mutant filaments over a myosin substrate under standard conditions can provide a lot of information about the actomyosin interaction, more insights can be gained by performing the *in vitro* motility assay under different conditions that shift the equilibrium towards particular states of the crossbridge cycle.

5.1.3 Altering the ionic strength in the motility assay

In muscle, the affinities of the weakly bound states, M.ATP and M.ADP.Pi, (see figure 1.7), for actin are known to increase with decreasing ionic strength or temperature. Mechanical studies performed on skinned skeletal muscle fibres demonstrated that in relaxed muscle at physiological ionic strength, (0.17M), crossbridges exist predominantly in a weakly bound state (Brenner *et al.*, 1982). In low ionic strength buffers, (20mM), these weak crossbridges bind more tightly, and whereas before they offered little resistance to stretch, they could now be detected through measurements of increased fibre stiffness. Gulati and Podolsky (1981) demonstrated that ionic strength has a profound effect on isometric tension in skinned frog muscle fibres. Although the shortening velocity was unaffected between 100 and 260mM ionic strength, it started to decrease below 100mM and fell to 55% of its original value at 50mM ionic strength.

Takiguchi *et al.* (1990) varied KCl concentration in the *in vitro* motility assay to assess the effects of ionic strength on the movement of rabbit skeletal muscle actin over rabbit

skeletal muscle myosin, HMM and S1 coated surfaces. Using the standard motility assay, they sequentially perfused a buffer containing increasing concentrations of KCl into the same flow chamber and recorded velocity measurements at each point. By this protocol, they were able to show that moving actin filaments washed off the surface above a critical ionic strength termed the "wash off" point. At this ionic concentration, weak actomyosin binding was thought to be drastically reduced (Takiguchi *et al.*, 1990).

In vitro filament velocity rises steadily with an increase in ionic strength up to the critical wash off concentration, (see figure 5.4), (Takiguchi *et al.*, 1990; Harada *et al.*, 1987; Umemoto and Sellers, 1990; Vale and Fumio, 1990; Warshaw *et al.*, 1990; Homsher *et al.*,1992). The reduced velocities at low ionic strengths were attributed to an enhanced, weak actomyosin binding that may subsequently impart an internal resistance to actively stroking, strongly bound heads, thus retarding their action (Somlyo *et al.*, 1988; Sellers *et al.*, 1985; Warshaw *et al.*, 1990; Homsher *et al.*, 1992). The decline in the degree of this weak binding as the ionic strength is raised will reduce the effect of "internal load" upon stroking heads and therefore corresponds to the observed increase in filament velocity.

Although the *in vitro* assays confirm the ionic strength dependence of the velocity of shortening exhibited in work with muscle fibres, the "wash-off" phenomenon *in vitro* restricts velocity measurements to ionic strengths below a critical concentration which are much lower than those used in muscle studies. Uyeda *et al.* (1990) overcame this hurdle by including 0.7% methylcellulose in the assay buffer. This acts as a viscosity enhancing agent that mimics the action of weak actomyosin binding and minimises the lateral diffusion and displacement of actin filaments from the surface by Brownian motion. This subsequently enables observations of filament movements at ionic strengths above the critical concentration. Through the employment of methylcellulose, Homsher *et al.* (1992) showed that filament velocity increased from that of the previous critical concentration of 60mM up to 150mM ionic strength.

5.1.4 The effects of ATP on motility

Barany and Podolsky (1967) suggested that the shortening velocities of muscle from various sources correlated with their actin-activated myosin ATPase activities. By analogy, it was proposed that actin filament velocities in *in vitro* motility assays would also be proportional to the actin-activated ATPase activity of the myosin substrate surface, which in turn would match the corresponding activity measured in solution studies (Sheetz et al., 1983).

In vitro, Kron and Spudich (1986) found that the movement of actin filaments over a skeletal muscle myosin substrate was ATP dependent. In the absence of ATP, no motility was observed and actin filaments remained tightly bound to the surface in a rigor state. Movement was initiated upon the addition of ATP and filament velocity rose with an increase in the ATP concentration. A maximal filament velocity was reached at 100μM ATP, the saturating concentration, whilst the apparent half maximal velocity was around 50μM ATP.

A comparison of these motility values with the actin-activated myosin ATPases in solution, where the corresponding half maximal reaction velocity was 6μM (Moos 1973), suggested that filament velocity may not be directly linked to the kinetics of the actin-activated myosin ATPase in solution. An increase in K_m for the velocity of muscle shortening under zero load was also seen and estimated at approximately 200μM ATP (Cooke and Bialek, 1979). Moreover, Warshaw *et al.* (1990) confirmed the discrepancy between ATPase values by showing that phosphorylated smooth muscle myosin conveyed actin filaments at half maximal *in vitro* velocity at 29μM ATP, a concentration ten times greater than that required for the myosin ATPase activation in solution (Moos, 1973).

Measurements of the ATP dependence of velocity in the motility assay do not strictly follow an enzymatic reaction where catalysis is mediated by many molecules acting individually. During *in vitro* motility, many myosin heads are bound to a single actin filament and drive its movement effectively in concert. Subsequently, the co-operative

action of different, actively stroking heads may affect the kinetic parameters. Warshaw *et al.* (1990) described such an effect with reference to the uncoupling between filament velocity and the myosin ATPase activity in solution. This concerned the presence of a small number of damaged or "dead heads" on the myosin surface which behave periodically in a rigor-like manner, thus impeding the movement mediated by actively cycling crossbridges. Whereas a half maximal rate of hydrolysis in solution reflects the occupation of 50% of the myosin ATP binding sites, the analogous value in the motility assay is represented by the half maximal filament velocity. If *in vitro* filament movement occurs over a surface containing a few dead heads, movement will be retarded. Subsequently, a greater saturation of the myosin heads on the surface will be required to recover the lost velocity, therefore exaggerating the true values of K_m and V_{max} obtained from motility assays.

Kron and Spudich (1986), Umemoto *et al.* (1989), Umemoto and Sellers (1990) and Cook *et al.* (1993) have all proposed that filament velocity in the *in vitro* assays cannot be correlated directly with the steady state actin-activated myosin ATPase activity in solution because these two processes are limited by different steps in the ATPase kinetic cycle. Whereas the actin activated ATPase activity in solution is limited by the release of inorganic phosphate from the A.M.ADP.Pi complex, filament velocity has a kinetic limitation during ADP release from the AM.ADP complex (Siemankowski *et al.*, 1985).

5.1.5 Mutational analysis of actomyosin by the *in vitro* motility of actin mutants

Actomyosin interactions can be investigated by generating mutations in actin and then analysing them in terms of their S1 binding or myosin affinity, myosin ATPase activation and *in vitro* motility. Researchers have introduced specific mutations into a number of different actin genes including *Dictyostelium 15*, chicken β, yeast and *Drosophila* actins. In all of the investigations described below, myosin binding affinity, actin activated myosin ATPase activity and *in vitro* motility assays were performed with skeletal muscle myosin and its subfragments as the substrates. These studies therefore represent a heterogeneous analytical system in which the actomyosin

interaction of actins from different sources was examined. Actin isoforms which exhibit a high degree of sequence homology to the canonical actin sequence, namely that of skeletal muscle actin, will probably have the strongest affinity for skeletal muscle myosin, and therefore display the least phenotypic disruption.

There are a number of regions on the actin molecule that are involved in an interaction with myosin, (see section 1.4.1). Mutational analysis of the actomyosin interface to date has focused upon the primary ionic and the secondary contacts, both of which are thought to involve acidic residues in actin. To test the ionic dependence of these interfaces, mutagenesis has concentrated upon the generation of actins with a charge reversal (substitution of acidic residues with lysine or histidine), charge deletion/ neutralisation (in the case of the latter, substitution of acidic residues with alanine, asparagine or glutamine), or charge addition. The charge reversals are expected to generate more severe phenotypes than the latter classes of mutations. The following section describes the effects of these changes in specified parts of the molecule.

Table 5.11. The N-terminal primary amino acid sequences for four actin isoforms, together with their relative charges over the first nine amino acids, (10 in the case of the α-skeletal muscle actin).

actin isoform	1 2 3 4 5 6 7 8 9	net charge
α–skeletal	M C D E D E T T A L V	-4
yeast	M D S E V A A L V	-2
chicken β	M D D D I A A L V	-3
Dictyostelium 15	M D G E D V Q A L V	-3

5.1.5.1 The primary ionic actomyosin binding site

(i) The N-terminus

The actin N-terminus has been identified as playing a major role in actomyosin interactions (Sutoh *et al.*, 1982; Bertrand *et al.*, 1989). Since this region exhibits the greatest degree of sequence variation in the actin molecule, its diversity may define the basis for some of the observed differences in actomyosin interactions between actin isoforms. In general, most actin isoforms possess between two to four acidic residues at their N-termini. Skeletal muscle actins tend to have a greater negative charge than

cytoplasmic and non-muscle isoforms in this region, e.g. yeast and chicken β-actin respectively in the case of this overview, (see table 5.11).

Two charge reversal mutations *D3K/D4K* in chicken β-actin (Aspenström *et al.*, 1992b) and *D1H/D4H* in *Dictyostelium 15* actin (Sutoh *et al.*, 1991) were both shown to disrupt the actomyosin interaction. *D3K/D4K* was incapable of binding S1, had an abolished actin activated ATPase activity and displayed no *in vitro* motility. In contrast, *D1H/D4H* exhibited the normal arrowhead pattern upon S1 binding, a reduced myosin ATPase activation, which was attributed to a reduction in the V_{max} and not the K_m of the myosin ATPase, and a 79% reduction in *in vitro* filament velocity. These conflicting results were surprising in light of the fact that both mutations introduced a charge reversal into a similar region of the N-terminus, bestowing each mutant with the same overall charge in this area, (see table 5.1).

Two mutations in the chicken β-actin isoform, *D3Δ/D4Δ* and *D3A/D4A* (Aspenström *et al.*, 1992), a charge deletion and charge neutralisation respectively, were also shown to have their myosin ATPase activation abolished. The disruptive effects of these mutants were as expected, less severe than those of *D3K/D4K*, with *D3Δ/D4Δ* and *D3A/D4A* exhibiting a 63% and 34% reduction in filament velocity respectively and both generating distorted arrowhead binding patterns upon S1 decoration. A charge neutralisation *D2N/E4Q*, or a charge deletion *ΔDSE* mutation in yeast actin (Cook *et al.* 1992) produced similar effects to the chicken β-actin mutation, resulting in a large reduction in the actin activated myosin ATPase activity, and in the case of the former, a loss of *in vitro* motility.

Although the aforementioned are not identical mutations, the fact that charge neutralisation mutations in yeast and chicken β actin isoforms displayed more dramatic effects than charge reversals in *Dictyostelium 15* actin demonstrates the importance of actin isoform variation in the analysis of heterogeneous protein interactions. The identity of the actin isoform involved may be as much a contributing factor to the strength of the actomyosin disruption as the nature of the mutation itself. Since the N-terminal sequence of *Dictyostelium 15* actin suggests that it is a muscle-specific actin,

Table 5.1. The mutational analysis of actomyosin using the *in vitro* motility assay.

reference	actin isoform	charge mutation type	mutation	sequence at N-terminus	local charge	S1 decoration / binding affinity (% of WT)	ATPase activity (% of WT)	*in vitro* motility (% of WT)	rabbit substrate
Aspenström (1992)	chicken β	reversion	*D3K/D4K*	DKKIAALV	+1	no decoration	no ATPase	no motility	myosin
Sutoh (1991)	*Dictyostelium 15*	reversion	*D1H*	HGEDVQALV	-1	normal decoration	↓V_{max}	↓V_f , 69% WT	HMM
Sutoh (1991)	*Dictyostelium 15*	reversion	*D1H/D4H*	HGEHVQALV	+1	normal decoration	↓V_{max}	↓V_f , 21% WT	HMM
Aspenström (1992)	chicken β	deletion	*D3Δ/D4Δ*	DIAALV	-1	distorted decoration	no ATPase	↓V_f , 37% WT	myosin
Aspenström (1992)	chicken β	neutralisation	*D3A/D4A*	DAAIAALV	-1	distorted decoration	no ATPase	↓V_f, 66% WT	myosin
Cook (1992)	yeast	neutralisation	*D2N/E4Q*	MNSQVAALV	0	———	↓ 12.5% WT	no motility	myosin
Cook (1992)	yeast	deletion	*ΔDSE*	MVAALV	0	———	↓ 7% WT	———	myosin
Cook (1993)	yeast	addition	*4Ac*	MDEDEVAALV	-4	normal binding	↑300% WT	normal motility	myosin
Johara (1993)	*Dictyostelium 15*	reversion	*D24H/D25H*	———	+2	———	no ATPase	washed off in ATP	HMM
Miller/Reisler (1995)	yeast	neutralisation	*D24A/D25A*	———	0	↓binding 37% WT	↓↓↓ ATPase	washed off in ATP	HMM
(+0.7% MC)						normal binding	↓ATPase	normal motility	
Johara (1993)	*Dictyostelium 15*	reversion	*E99H/E100H*	———	+2	———	———	↓V_f, 17% WT	HMM
Miller/Reisler (1995)	yeast	neutralisation	*E99A/E100A*	———	0	↓binding 54% WT	↓↓↓ATPase	washed off in ATP	HMM
(+0.7% MC)						normal binding	↓ATPase	normal motility	

MC = methylcellulose
V_f = filament velocity

(see table 5.11), this isoform may therefore possess a greater overall affinity for rabbit skeletal muscle myosin. Subsequently, *Dictyostelium 15* actin may be more able to tolerate amino acid substitutions at the N-terminus than the two other non-muscle actin isoforms, thus minimising the disruption to its actomyosin interaction. In accordance with this observation is the fact that charge neutralisation mutants in yeast actin generate more dramatic effects in these assays than their analogous mutations in chicken β-actin. The predicted lower affinity of yeast actin is understandable considering this isoform's lower overall sequence homology and acidic N-terminal charge in comparison to that of the vertebrate actin isoform.

The yeast actin mutation *4Ac* possesses an N-terminus which incorporates 2 extra acidic residues so that it resembles a skeletal muscle N-terminus. Although this mutation did not affect *in vitro* motility, it enhanced the actin activated myosin ATPase activity threefold (Cook *et al.*, 1992). Despite this, the level of activation was still only 30% that of skeletal rabbit myosin activated by skeletal rabbit actin. These results suggest that maximal *in vitro* motility may only require at most four acidic residues in the N-terminus. An increase in the number of acidic residues in the actin N-terminus does not necessarily mean that myosin ATPase activation will be enhanced. The increase in ATPase activation seen in *4Ac* may be due to yeast actin possessing an intrinsic capacity for improvement in its ATPase activity since its N-terminus is less acidic than most isoforms. This particular mutation indirectly enables an assessment of how vital the unconserved residues in yeast actin are in influencing ATPase activation and *in vitro* motility. A yeast actin with a skeletal muscle actin N-terminus still has a reduced actin activated myosin ATPase with respect to rabbit actin.

(ii) Residues 24-25

These residues comprise the second half of the primary ionic binding site. A charge reversal mutation *D24H/D25H* in the *Dictyostelium 15* actin gene (Johara *et al.*, 1993) resulted in a total abolition of myosin ATPase activation. Mutant filaments were able to bind to the surface in rigor in the motility assay, but washed off upon the addition of ATP. The yeast charge neutralisation mutation *D24A/D25A* (Miller and Reisler, 1995)

exhibited similar properties to *D24H/D25H.* In addition to a greatly reduced myosin ATPase activation and the filaments washing off in the motility assay, this mutant was also shown to possess a reduced myosin binding affinity.

The effects of the mutations at residues D24/D25 closely resemble those at the N-terminus, strengthening the idea that both regions form part of the primary ionic interaction. Disruption of these sites may abolish or reduce the weak initial binding of actomyosin and subsequently diminish the overall affinity/formation of this complex. This would result in the aforementioned phenotypes; a loss or distortion of S1 decoration, a loss or reduction in the ATPase activation and absence of *in vitro* motility. These actomyosin disruptions were generally observed for most of the primary ionic binding site mutations.

Upon the inclusion of a viscosity enhancing agent, methylcellulose, in the assay buffer, the diffusion of *D24A/D25A* mutant filaments from the surface under Brownian motion was prevented. The severity of the previous *in vitro* phenotypes was reduced and mutant filaments exhibited an *in vitro* motility equivalent to that of WT. This observation suggests that the ionic interaction abolished by the *D24A/D25A* mutation is essential for the initial formation of the actomyosin complex. Without it, the overall actomyosin affinity and rigor complex formation is significantly reduced.

5.1.5.2 The secondary actomyosin binding site

The secondary actomyosin binding site involves the loop 91-100 in subdomain IA on actin. This contains three acidic residues, E93, E99 and E100 and it may, like the primary ionic binding site, be involved in initial contacts which stabilise the overall actomyosin complex. In order to test the ionic nature of this interface, mutagenic studies similar to those on the primary ionic interaction were performed. A charge reversal mutation of *Dictyostelium 15* actin, *E99H/E100H* (Johara *et al.*, 1993), generated actin filaments with reduced filament velocities. The effects of this mutation were similar to those of *D1H/D4H*, (*Dictyostelium*), (Sutoh *et al.*, 1991) and less

severe than those of *D24H/D25H*, (*Dictyostelium*), (Johara *et al.*, 1993) and *D3K/D4K*, (chicken β), (Aspenström *et al.*, 1992).

5.1.6 *In vitro* motility analysis of the ACT88F mutants *G368E*, *E316K*, *E334K* and *E93K*

The *in vitro* motility investigations of four ACT88F mutants, *G368E*, *E316K*, *E334K* and *E93K* were made using pure actin preparations from IFMs. As well as performing the assays under standard conditions, the concentrations of KCl and ATP were independently varied to further characterise these mutants. With respect to the KCl variation experiments, analyses were performed in either the presence or absence of ATP, thus enabling an investigation into the salt dependence of weak and strong actomyosin binding respectively. Finally, the *in vitro* motility of three different types of *E334K* and WT copolymers were measured to learn more about the mechanism of action of this mutant.

5.2 Materials and Methods for *in vitro* motility assays

5.2.1 Protein reagents

5.2.1.1 Rabbit skeletal muscle HMM preparation

Rabbit skeletal muscle myosin was prepared using a modification, made by Vassillis Kyrtatas (Thesis, York University, 1987), of the method of Margossian and Lowey (1982).

Rabbit skeletal muscle HMM was prepared by a method, (planned by Justin Molloy), similar to that of Margossian and Lowey (1982).

Method

The myosin stock prepared from the protocol above, and stored in glycerol, was precipitated by the addition of 10 volumes of cold deionised water. After spinning at 17,500g for 10 mins, the myosin pellet was dissolved in an equal volume of a high salt buffer [0.5M KCl, 20mM imidazole-HCl, 1mM DTT, 2mM $MgCl_2$, pH 6.5]. Proteolytic digestion was performed for 10 mins at 23°C after the addition of TLCK-treated α-chymotrypsin to a final concentration of 0.02mg/ml. The reaction was stopped by the addition of Bowman-Birk inhibitor to a final concentration of 0.04mg/ml. This mixture was then dialysed overnight in an ice cold dialysis buffer [0.1mM $NaHCO_3$, 0.1mM EGTA, 1mM DTT, pH 6.5] to precipitate undigested myosin. The undigested material was pelleted by centrifugation at 8,000g for 10 mins and the O.D. at A_{280}-A_{340} of the supernatant was taken to estimate the concentration. The sample was divided into 50-100µl aliquots which were drop frozen in liquid nitrogen.

5.2.1.2 Rabbit skeletal muscle actin preparation

Rabbit actin was prepared from acetone powder according to a modification, made by Vassillis Kyrtatas (Thesis, York University, 1987), of the procedure of Pardee and Spudich (1982).

5.2.2 Visualisation of actin filaments

A green light, (EF, 546FS10.25, excitation filter, Andover Corp., Salem, NH), from a mercury arc lamp was focused through a "hot mirror", (DM = 820DCSP, Omega Optical, Brattleboro, VT), into the microscope epifluorescence light path via a custom built port. Fluorescently labelled actin was visualised using an intensified CCD camera, ("Photon - P46036A", EEV, Chelmsford, U.K.), coupled to a barrier filter, (BF2 = LP590, Zeiss). Bright field illumination, (100W halogen lamp), was used to produce a high magnification video image, (CCD camera, P46310, EEV), and an Acroplan 100X,

2.5 N.A. objective and an Optovar 2.5X insert were used to obtain the desired image magnification.

5.2.3 Rhodamine-phalloidin labelling of actin filaments

Rhodamine-phalloidin, (Molecular Bioprobes, Inc.), was made as a 6.6μM solution in methanol. This was then divided into 2μl aliquots, each aliquot subsequently containing 12.3pmoles of rhodamine-phalloidin, (RMM rhodamine-phalloidin = 1305), and stored in the dark at -20°C. For optimal labelling, about 10pmoles of actin was added to each aliquot and stored on ice under darkened conditions.

5.2.4 Motility assay

The *in vitro* motility assays were performed generally according to the methods of Kron and Spudich (1986), Toyoshima *et al.* (1987) and Kishino and Yanagida (1988). All the assays performed in the present study utilised the same batch of rabbit skeletal muscle HMM substrate and were performed within a few days of each other. Observations of movement were carried out at a constant temperature of 23°C (+/- 0.5°C).

Prior to flow cell construction, a large No.1 coverslip, (50mm by 24mm), was coated on one surface with a thin, even layer of 0.1% nitrocellulose, (in amyl acetate), (Uyeda *et al.*, 1991). This was achieved by pipetting 5μl of the solution onto the coverslip, gently spreading the drop over the surface using the edge of an Eppendorf tip and then allowing the film to dry. Next, two parallel strips of Apiezon grease, approximately 20mm apart, were applied to one side of a clean microscope slide and the coverslip, nitrocellulose surface facing downwards, was placed onto the two strips of grease so that a cross-shaped flow cell was produced. The coverslip was then squashed onto the slide with a light, even pressure until the grease strip reached a constant width, thus producing an internal cell volume of around 50μl, (see figure 5.1).

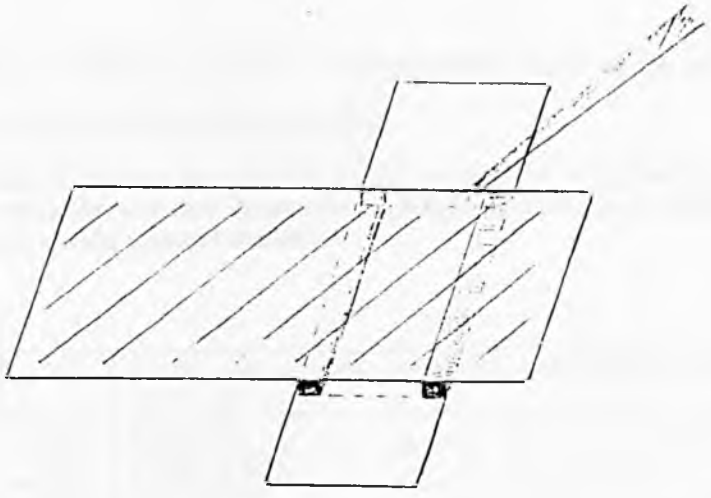

Figure 5.1. The *in vitro* motility flow cell which is constructed as described in section 5.5.4. An Eppendorf tip is shown to be coming in from the top right, perfusing assay buffer into the flow chamber.

5.2.4.1 Assay buffers

Different solutions, each a variation of (AB) + (supplement), have to be used for different stages of the assay, (see Table 5.2(a) and (b)).

Table 5.2. (a) The composition of the standard assay buffer and a list of the supplements. (b) The combinations of standard assay buffer with each supplement to produce the solutions required for the performance of the motility assay under standard conditions.

(a)

Standard assay buffer	(AB)	25mM Imidazole-HCl, 25mM KCl, 4mM $MgCl_2$, 1mM EGTA, pH 7.4
Supplements	(N)	2mM ATP
	(B)	0.5mg/ml BSA
	(D)*	20mM DTT
	(OS)*	0.02mg/ml catalase, 0.1mg/ml glucose oxidase, 3mg/ml glucose

* indicates the supplements that have to be added immediately prior to use

(b)

(AB--)	AB + D
(AB-)	AB + B + D + OS
(AB+)	AB + B + D + OS + N

To minimise oxidation during the motility assay, (AB) stock solution was degassed under vacuum immediately before use, (and before the addition of supplements). All solutions were then carefully transferred to syringes with wide bore needles and any air bubbles present were expelled, thus minimising the diffusion of oxygen into the solutions. These solutions could be stored on ice and used for two days, although it was preferable to start afresh each day.

5.2.4.2 Experimental procedure

The HMM made in section 5.2.1.2 was diluted in (AB--) to a concentration of about 40μg/ml on the day of the motility assay. The flow cell was then perfused with 80μl of the HMM solution by propping it up at an angle of 30° to the horizontal. The solution was applied to one side of the flow cell as a pool which flowed into and was drawn out of the other end of the cell by placing a piece of tissue over the cell exit. Care had to be taken to limit the withdrawal of infused liquid and thus prevent the introduction of air

bubbles into the flow chamber. The HMM solution was allowed to bind to the nitrocellulose coated inner surface of the cell for 1 min. Unbound motor protein was then removed by the perfusion of 80μl of (AB-). This contains 0.5mg/ml BSA which coated any remaining unbound areas of the nitrocellulose surface. (Since BSA would compete with HMM in the hydrophobic binding to the nitrocellulose surface, AB--, and not AB-, was used when HMM was initially infused into the chamber).

A 1:70 dilution of the actin filament stock, (5-10nM), (Umemoto and Sellers, 1990) was then perfused into the flow chamber and allowed to bind to the HMM surface for 1 min, or until a sufficient number of filaments bound per. frame was observed under fluorescence microscopy. Since actin filaments fragment upon the addition of (AB+), it was best to restrict the number of bound filaments at this stage, otherwise eventual movement would be almost impossible to track through a large number of moving filaments. Excess, unbound filaments were then removed from the surface by the addition of (AB-), leaving filaments stably bound in a rigor state.

Movement was initiated by the addition of (AB+), containing a saturating ATP concentration, and was observed by fluorescence microscopy, (see section 5.2.2). Although actin filaments started moving immediately upon the addition of (AB+), the movement was intermittent at first. After allowing the slide to equilibrate for 5 mins under unexposed fluorescence conditions, subsequent sliding was smooth and continuous. The average filament velocity for each genotype was calculated from the combined filament movements from three different assay slides.

5.2.4.3 Effects of KCl concentration on motility

This assay was performed according to the method of Takiguchi *et al.* (1990). *In vitro* actin filaments were bound in rigor to the HMM substrate in a buffer, (AB-KCl-), which lacks the 25mM KCl supplement, thus enabling equilibration at a basal ionic strength concentration. The rate of movement at different ionic strengths was determined by sequentially perfusing discrete, increasing concentrations of KCl, in AB+, (see table 5.3), into the same flow chamber, allowing the slide to equilibrate, and

then recording the movements of a number of filaments. The KCl concentration was raised in 5mM KCl increments. Velocities could only be recorded to levels up to 10mM KCl below the wash off point because filament motility became very unstable and impossible to track accurately around the critical concentration.

The wash off points for each genotype were identified as the lowest KCl concentration at which there were no filaments were seen to interact with the substrate surface. This was sometimes complicated by the presence of actin filaments that were "nailed" to the surface by dead heads. However, these were easily distinguishable from active filaments that were trying to interact with the surface. As with the standard assay measurements, the velocity measurements for each genotype were derived from a combination of movements from three independent flow cells.

Table 5.3. The buffers used for the initial equilibration and subsequent variation of KCl in the *in vitro* motility assay.

(AB-KCl-)	standard AB- except for the absence of 25mM KCl
(AB+KCl-)	standard AB+ except for the absence of 25mM KCl
(AB+KCl+)	standard AB+ except for a 100mM KCl content

Due to the fact that severe filament fragmentation occurs at lower ionic strengths, it was sometimes not possible to take velocity measurements through a full range of KCl concentrations from one slide alone. Subsequently, two or even three slides were used to obtain a full set of measurements, the extent of which varied with different genotypes.

5.2.4.4 Effects of KCl concentration in the absence of ATP

This assay was carried out in an identical manner to the KCl variation assays with the exception that increasing concentrations of KCl were added in (AB-) buffer, (see Table 5.4). The experiment was repeated twice for each genotype tested, with a single slide being used for each full range of KCl concentrations.

Table 5.4. The two buffers that were mixed to produce the different concentrations for the KCl variation assay in the absence of ATP.

(AB-KCl-)	standard (AB-) except for the absence of 25mM KCl
(AB-KCl+)	standard (AB-) except for a 2M KCl supplement

5.2.4.5 Variation of the ATP concentration in the motility assay

Discrete ATP concentrations in (AB) were sequentially titrated upwards on the same slide, with filament velocity measurements taken at each ATP concentration. A surface laden with actin filaments was washed initially with standard (AB-) and then the ATP concentration was increased through the range, 10μM, 25μM, 50μM, 75μM, 100μM and 2mM ATP.

At low ATP concentrations, extreme filament fragmentation prevented velocity measurements at a complete range of ATP concentrations to be taken from a single assay slide. Subsequently, three different assay slides, each representing two ATP concentrations, were used to define a full range. Two full ranges were analysed for each genotype, with the exception of the mutant *E93K* where only one was used.

5.2.5 *E334K*/WT copolymer formation

Three types of actin copolymer were generated, each differing in their relative distribution of mutant monomers throughout the cofilament. "Homogeneous" cofilaments possessing a 50:50 ratio of *E334K* and WT monomers were generated by mixing equal numbers of *E334K* and WT monomers and inducing polymerisation. Assuming that *E334K* and WT monomers displayed indiscriminate actin binding during copolymerisation, these cofilaments should possess an almost even distribution of mutant monomers throughout their length. Prochniewicz and Yanagida (1990) verified this kind of random copolymerisation by labelling a set of actin monomers with a fluorescent marker IAR, and mixing this set with one containing unlabelled monomers before inducing copolymerisation by the addition of salt. Fluorescence microscopy

revealed an even distribution of fluorescence intensity along these cofilaments, implicating the random distribution of the labelled and unlabeled monomers.

The two other *E334K*/WT copolymers, "segmented" and "block" copolymers, were generated by mixing WT and *E334K* homopolymer populations and then allowing them to anneal. Labelling WT filaments with substoichiometric ratios of rhodamine-phalloidin and *E334K* filaments with a slight molar excess, prior to annealing, enabled each homopolymer in a mixture to be distinguished upon the basis of the difference in their fluorescence intensity. Upon filament annealing, preceded by sonication in the case of segmented copolymers, individual monomer regions in either of the aforementioned cofilaments could be visualised as striations. Whereas segmented copolymers displayed short alternate stretches of *E334K* and WT monomers, block copolymers were composed of a single stretch of WT monomers annealed to the end of a single stretch of mutant monomers. In contrast, most researchers generate copolymers through alternative methods which involve polymerising a mixture of two populations of actin monomers which contains a defined proportion of each monomer type.

The percentages of *E334K* and WT monomers in individual block cofilaments were calculated from the filament lengths, (measured in Retrac, software written by Nic Carter). These were then compared to the type and filament velocity of the block cofilament being analysed, "type" referring to whether the *E334K* segment was situated towards the pointed or the barbed end of the actin filament.

5.2.6 "Tracking"

"Tracking" refers to the recording of an actin filament's path and velocity as it moves across the substrate surface. Filament movement was recorded onto videotape and a frame grabbing package (measured in Retrac) was used to generate image files representing 12 seconds of movement, with a capture rate of 0.45 frames per second. Only those filaments which displayed a smooth continuous sliding movement for periods greater than 3 seconds were "tracked" and their velocities recorded, (using

Retrac). The average velocity of each filament was calculated and then mean of the average velocities was determined for each genotype.

5.3 Results

5.3.1 Mutant ACT88F preparation

The mini-actin preparation, (see section 4.1.3.1), was used to recover about 5μg of WT and each of the *G368E*, *E316K*, *E93K* and *E334K* mutant actins which were then polymerised. It proved difficult to isolate *E334K* actin on several occasions despite a WT actin preparation in tandem producing expected yields of actin. Attempts to isolate actin from more flies, (20), in a smaller extraction volume, (25μl), did not solve this problem. Additionally, all *E93K* actin preparations were seen to generate bundled actin filaments, a property which hinders sliding and has been observed in other actin mutants. However, after a very brief sonication these actin bundles fragmented into filaments which were only a few μm long and moved well in the motility assay.

5.3.2 The *in vitro* sliding of rabbit and *Drosophila* actins under standard assay conditions (SAC)

Rabbit and each of the *Drosophila* mutant actins were seen to bind strongly to the HMM surface under rigor conditions in (AB-). Upon the addition of the standard assay buffer, rabbit, *WT*, *G368E* and *E316K* mutant filaments began to slide immediately, exhibiting smooth, stable movement.

Under Standard Assay Conditions, (SAC), WT *Drosophila* actin was seen to move 10% slower than rabbit actin in the motility assay, (see table 5.5). Additionally, whereas the *in vitro* velocity of *E316K* mutant actin was insignificantly reduced by 6% compared to WT, *G368E* showed a significant 35% reduction in motility, (see table 5.5). The velocity profiles, shown in 0.2μm/s histogram bins, (see figures 5.2 and 5.3), for rabbit and each of the *Drosophila* actins in the present study produced Gaussian velocity distributions unlike that seen in a *G368E* actin study by Anson *et al.* (1995).

Table 5.5. The *in vitro* filament velocities of rabbit and the *Drosophila* WT and mutant actins over a rabbit skeletal muscle HMM surface, under standard assay conditions, (23.5°C), where N represents the number of filaments from which the velocity was averaged for each genotype. The percentage reduction in motility, (%↓V_f), of the mutants with respect to WT filament velocity is also shown. Significant reductions in filament velocity in comparison to WT *Drosophila* actin are highlighted in grey.

	average filament velocity (μm/s±SD)	%↓V_f	N
rabbit	3.84±0.32μm/s		76
WT	3.47±0.30μm/s		144
G368E	2.26±0.25μm/s	35	95
E316K	3.27±0.31μm/s	6	171
E334K	no movement		
E93K	washed off the surface		

Under SAC, although *E334K* filaments appeared to maintain a stable rigor contact with the surface, they displayed no movement whatsoever. Furthermore, these bound filaments showed no signs of fragmentation, a process that occurs readily upon movement initiation by the addition of ATP.

Upon the perfusion of (AB+) into the flow cell, stably bound *E93K* filaments were observed to wash off the HMM surface and display Brownian movements in suspension in a manner similar to that described for other actin mutations. Some filaments would occasionally diffuse down to the surface and exhibit a very unstable interaction with the HMM substrate for a few seconds before drifting away again. For the brief period that they were attached, a few of these weakly bound filaments would attempt to slide, a behaviour which illustrated that these mutant filaments were capable of actomyosin-mediated force generation.

5.3.3 KCl variation experiments

5.3.3.1 The salt dependence of the weak binding states

The observation that *E93K* filaments washed off the substrate surface under SAC indicated that their myosin binding had been disrupted. Their *in vitro* motility was therefore studied at reduced ionic strengths where weak binding would be predicted to

Figure 5.2. Histograms showing the average *in vitro* velocities of the rabbit and WT *Drosophila* actin under standard assay conditions, plotted in 0.2μm/s bins.

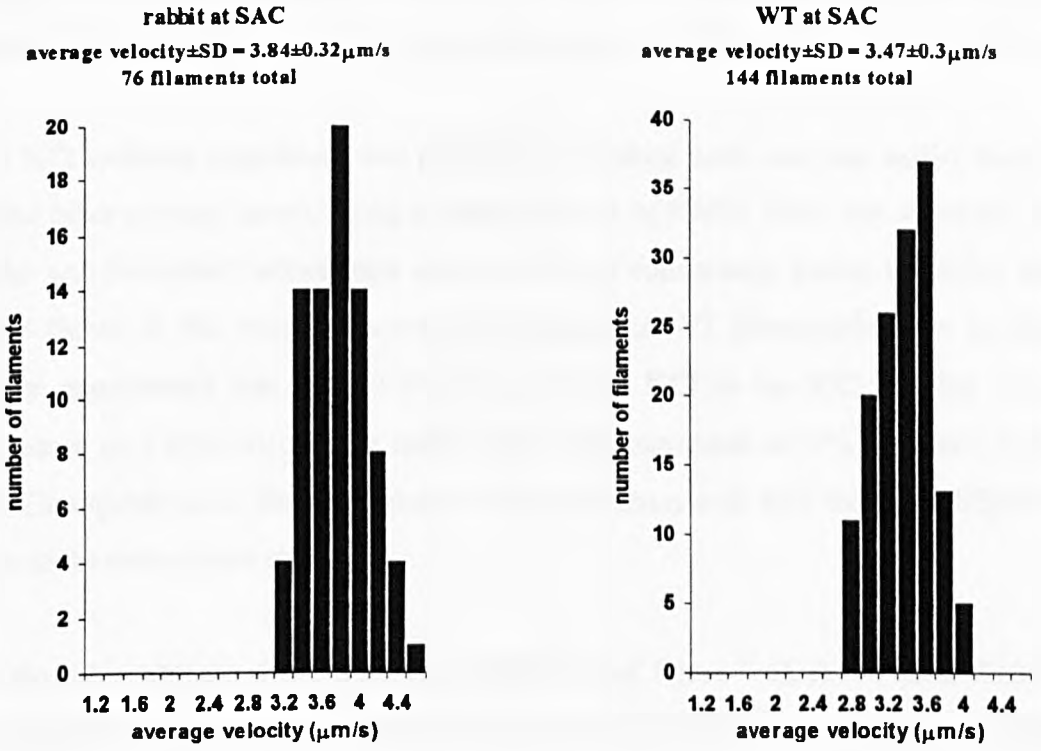

Figure 5.3. Histograms showing the average *in vitro* velocities of the *E316K* and *G368E* mutant actins under standard assay conditions, plotted in 0.2μm/s bins.

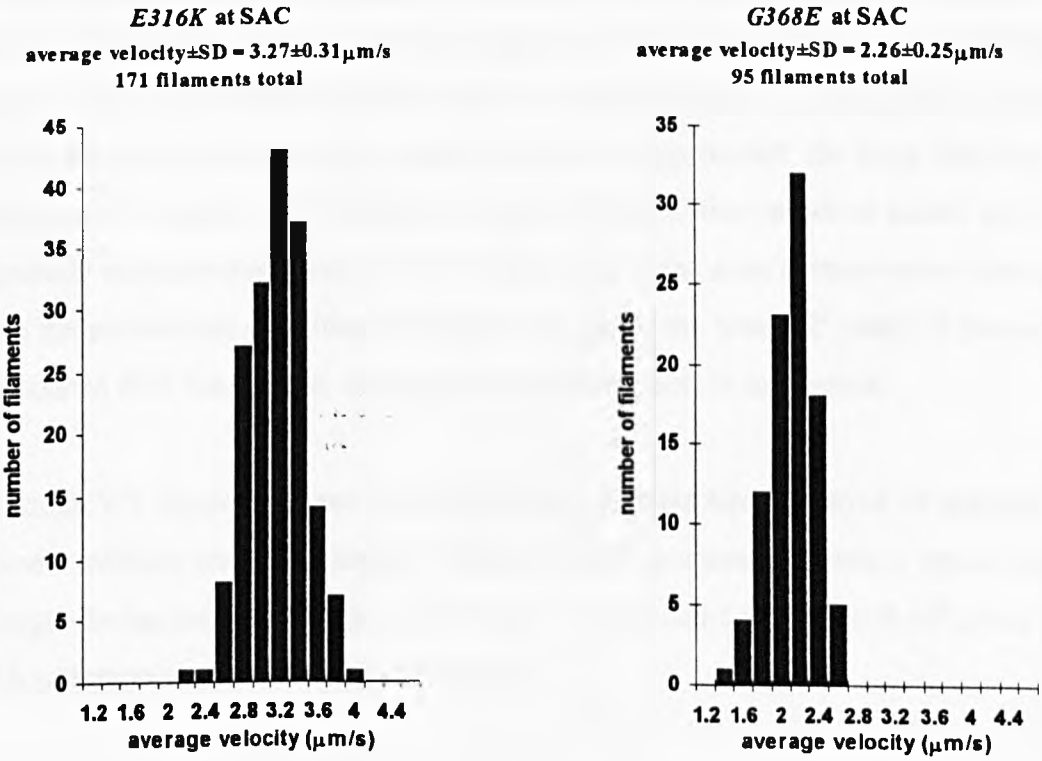

be stronger, allowing *E93K* filaments to interact and move over the myosin substrate. The *in vitro* filament movements of rabbit actin, WT *Drosophila* and the mutant actins, *G368E, E316K* and *E334K* were also determined at the different KCl concentrations.

The KCl variation experiment was performed for rabbit actin one year earlier than all of the other motility assays, using a different batch of HMM. Over this substrate, the rabbit and *Drosophila* actins were seen to move at consistently slower velocities than those shown in this study. However, the velocity of WT *Drosophila* actin in these earlier experiments was 2.43±0.59μm/s at 25mM KCl in the KCl motility assay, compared to 2.67±0.43μm/s for rabbit actin. This represents an 9% reduction in the WT *Drosophila* actin filament velocity which correlates well with the 10% difference seen in the more recent study.

As the ionic strength was raised, (see table 5.9 and figure 5.4), rabbit actin filament velocity increased up to a point just prior to the critical wash off concentration, (60mM KCl), at which a slight reduction in speed was seen. Although stable, continuous sliding was apparent at the lower KCl concentrations, a number of filaments washed off the surface as the ionic strength was raised. Under these conditions, although the velocity of attached filaments did not appear to be greatly affected, they displayed slightly unstable movements during which their anterior ends were often seen to detach from the surface. As the critical wash off point was approached, the large majority of filaments had washed off the substrate surface. The few that remained bound showed extremely unsteady movement in which many parts of the actin filament were detached from the surface and exhibiting Brownian activity. At the wash off point, all filaments dissociated from the surface, showing thermal movements in suspension.

Although WT *Drosophila* and each of the actin mutants also displayed an increase in filament velocity and characteristic changes in sliding associated with a rise in ionic strength during the motility assay, (see figure 5.5 and table 5.9), the wash off points for each genotype were different, (see table 5.6).

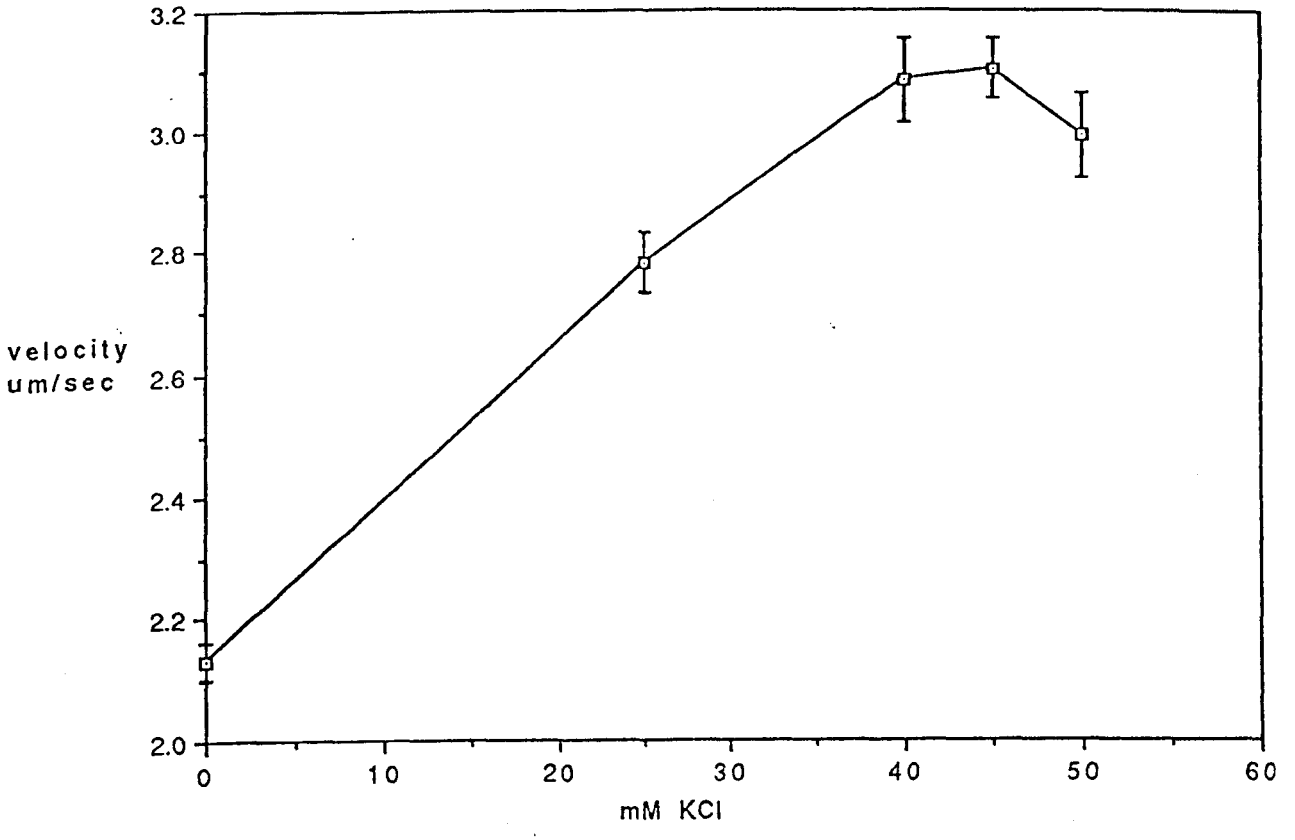

Figure 5.4. The KCl variation *in vitro* motility assay for rabbit actin. The KCl concentration was varied between 0-60mM KCl with rabbit actin washing off at 60mM KCl. Filament velocity is shown in μm/s together with the standard deviations.

The wash off point for WT *Drosophila* was 50mM KCl, 10mM KCl less than that of rabbit actin. This correlates with the reduced velocities of the *Drosophila* actins in comparison to rabbit actin, suggesting that the former have a lower affinity for the rabbit HMM substrate. Whereas the wash off point for *G368E* was unaltered with respect to WT actin in this assay, *E316K* showed a slight reduction and *E93K* and *E334K* a great reduction in the KCl concentrations that determined their wash off points.

Table 5.6. The KCl concentrations, (mM KCl), that define the critical wash off points for the rabbit, WT and mutant *Drosophila* actins, as determined using the KCl variation *in vitro* motility assay.

	wash off points
Rabbit	60mM KCl
WT	50mM KCl
G368E	50mM KCl
E316K	40mM KCl
E334K	30mM KCl
E93K	25mM KCl

The velocity reductions of the mutants in comparison to WT in the KCl variation assay were closely analogous to the reductions in mutant filament velocity under SAC. *G368E* mutant filaments displayed significant 26% and 28% reductions in motility with respect to WT at the 10mM and 25mM KCl conditions respectively, figures which are close to the 35% reduction obtained at SAC. The filament velocities of *E316K* at 10mM KCl were actually 6% higher than WT under the same condition. However, at 25mM KCl, the 4% decrease in velocity compared to WT matched the 6% reduction seen under SAC.

At reduced ionic strengths, *E93K* filaments were able to move *in vitro*, albeit, at a significantly reduced velocity which was 50% that of WT filaments, (see figure 5.5, figure 5.6 and table 5.9). However, as expected from observations under SAC, these mutant filaments washed off the surface as the KCl concentration was increased to 25mM, (see table 5.6).

Table 5.9. The filament velocities of rabbit, WT, *G368E*, *E316K* and *E93K* at different KCl concentrations *in vitro*. The average velocities, (μm/s±SD), are given for each KCl concentration at which movement was analysed and N = the number of filaments from which the velocity was averaged. The mean velocity for each genotype at each condition was derived from 3 individual assay slides.

	0mM KCl	5mM KCl	10mM KCl	15mM KCl	20mM KCl	25mM KCl	30mM KCl	35mM KCl	40mM KCl	45mM KCl	50mM KCl	60mM KCl
rabbit	2.12±0.22 N=60					2.67±0.43 N=51			2.87±0.41 N=36	3.14±0.32 N=24	3.00±0.42 N=24	WASH OFF
WT	2.25±0.18 N=23		2.69±0.30 N=129			3.11±0.37 N=67		2.90±0.32 N=32	2.65±0.37 N=13		WASH OFF	
G368E			2.00±0.23 N=59			2.24±0.30 N=86		2.17±0.27 N=39			WASH OFF	
E316K			2.85±0.29 N=117		3.00±0.27 N=127	2.98±0.28 N=215	2.69±0.32 N=88		WASH OFF			
E93K		1.22±0.23 N=119	1.34±0.20 N=95	1.43±0.14 N=66		WASH OFF						

Figure 5.5. The *in vitro* motility of WT, *G368E*, *E316K* and *E93K* actins at different KCl concentrations. The velocity values are taken from table 5.9 and are expressed as μm/s±SD

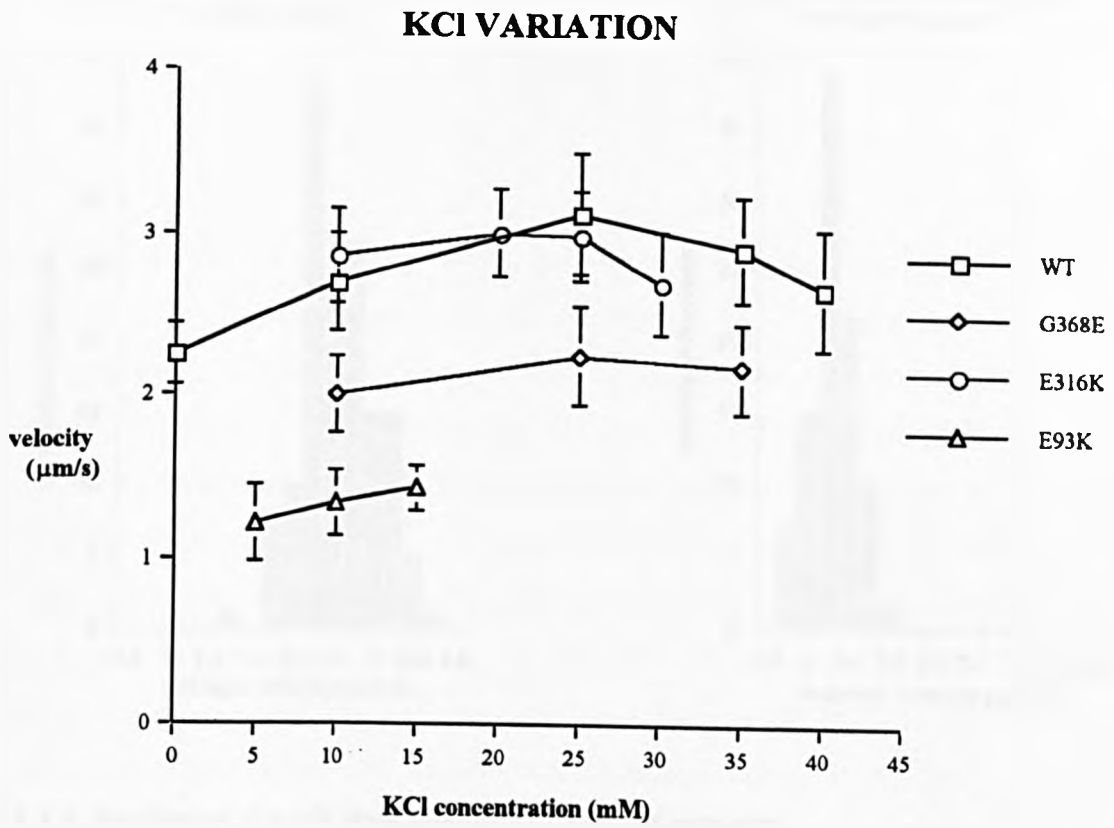

Consistent with their behaviour under standard assay conditions, *E334K* filaments did not move or fragment. At ionic strengths above those under SAC, *E334K* filaments began to display a slight unsteadiness upon the substrate surface which was reminiscent of WT filaments moving at 40mM KCl. The dissociation of *E334K* filaments at a wash off point of 30mM KCl, (see Table 5.6), suggested that their myosin binding is both salt and ATP dependent.

Figure 5.6. Histograms showing the average *in vitro* velocities of WT and *E93K* actins at 10mM KCl in the KCl variation motility assay, plotted in 0.2μm/s bins.

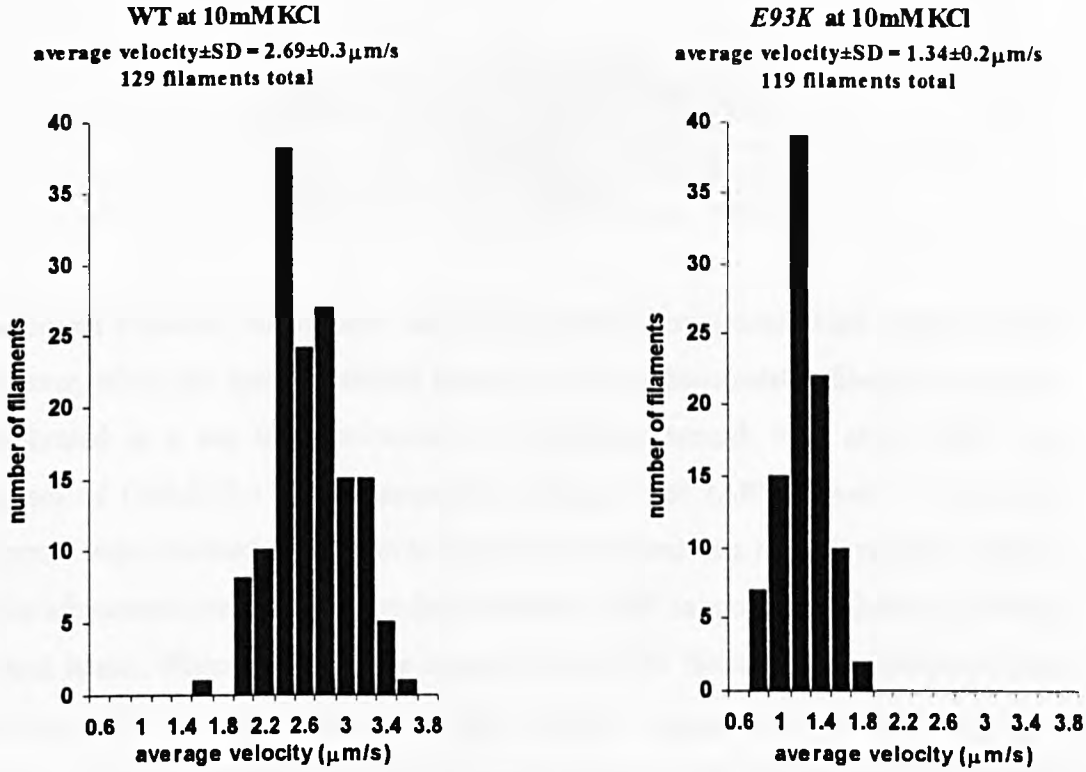

5.3.3.2 Studies of the salt dependence of the rigor complex

Whereas alterations of KCl concentration under SAC can be used to assess the effects of the mutants on weak actomyosin binding, varying the KCl concentration in the absence of ATP can be used to examine the comparative rigor binding strengths of different actins to HMM. Under the latter condition, rabbit, WT and *E93K* actins were not dissociatable from the HMM surface at salt concentrations below 2M, (see table 5.7). The filaments remained bound even when neat 4M KCl was flushed through the assay chamber. These concentrations would readily extract myosin from muscle, indicating the strong binding of the HMM substrate to the nitrocellulose-coated coverslip.

Table 5.7. The KCl wash off points for rabbit, WT, *E93K* and *E334K* from a HMM surface determined in the absence of ATP. Each genotype was tested twice for the full range of KCl concentrations from 100mM up to 4M KCl.

	Wash off point
rabbit	no wash off up to 4M KCl
WT	no wash off up to 4M KCl
E93K	no wash off up to 4M KCl
E334K	1M KCl

The bound filaments could have simply been stuck down onto dead myosin heads. However, when the same chambers laden with the undissociatable filaments were re-equilibrated in a salt free environment by flushing through with several flow cell volumes of (AB-KCl-) and subsequently perfused with (AB+), most of the bound filaments were released and began to move. This proved that the salt resistant binding of the aforementioned filaments in the absence of ATP cannot be attributed to binding to dead heads. When the assay was repeated for *E334K* filaments, they washed off the surface at salt concentrations approaching 1M KCl, suggesting that the strong rigor binding of these mutants may be weakened. This supports the proposal that *E334K* crossbridges may only be able to achieve a weakly bound state of some strength.

5.3.4 ATP dependence of *in vitro* filament velocity

The *in vitro* filament velocities of the *Drosophila* actins were measured at different ATP concentrations. Velocity measurements of WT, *G368E*, *E316K* and *E93K* filaments rose with increasing ATP concentrations from limiting conditions at 10μM ATP to saturating concentrations at 2mM, (see figure 5.7 and Table 5.10). At the lower ATP levels, the filament velocities for the *Drosophila* actins, ranging from 0.3-0.7μm/s, were hard to discern in real time.

Filaments moving at these low ATP concentrations exhibited severe fragmentation similar to that seen at low KCl concentrations. Under these limiting conditions, a high proportion of strongly bound heads are expected to be waiting to undergo their power strokes. However, since these can only "stroke" once other strongly bound heads

release the actin filament, they impart a great, internal, mechanical stress upon the moving filaments which facilitates their fragmentation.

Figure 5.7. The filament velocities, (μm/s), of WT, *G368E*, *E316K* and *E93K* at different ATP concentrations. The velocities are expressed as (μm/s±SD) and were taken from Table 5.10.

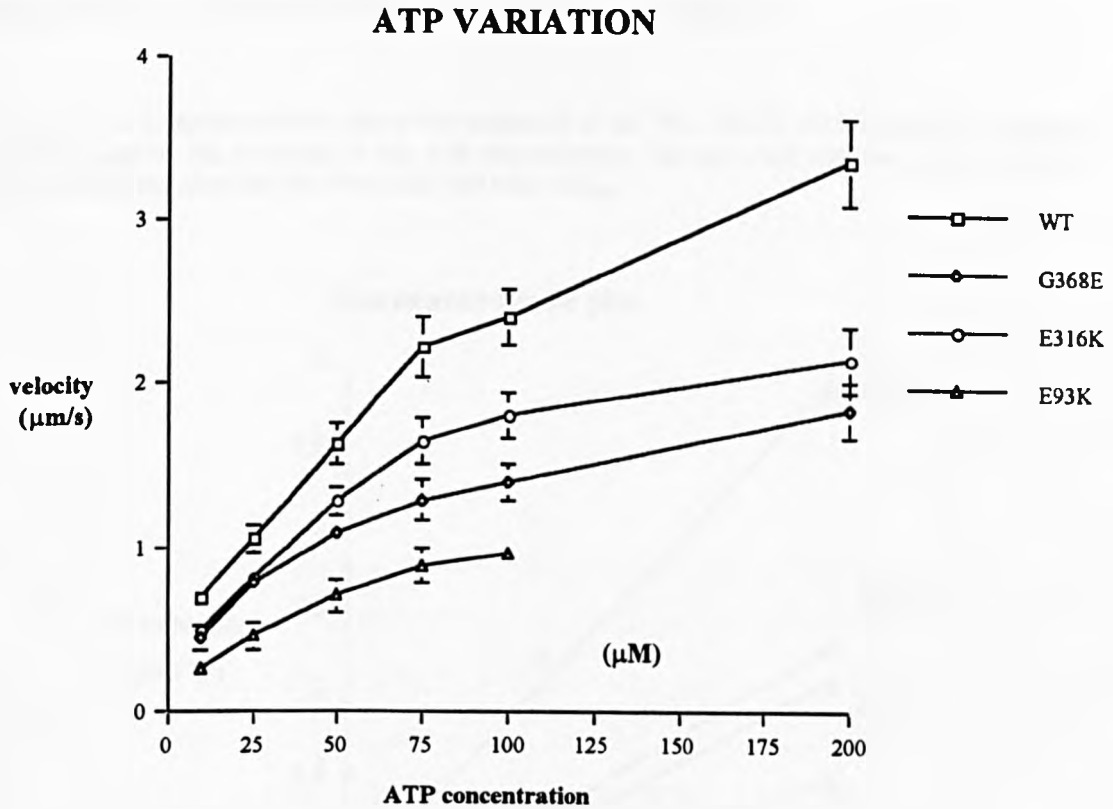

Table 5.10. The filament velocities for WT, *G368E*, *E316K* and *E93K* at different ATP concentrations. The average filament velocity, (μm/s±SD), is given for each ATP concentration at which movement was analysed. N denotes the number of filaments from which the mean velocity was derived. The velocity measurements for each ATP condition were taken from 2 separate assay slides, except for *E93K* where values were derived from a single slide for each concentration. Additionally, *E93K* movement was recorded in assay buffer conditions representing 10mM, as opposed to 25mM, ionic strength.

	10μM ATP	25μM ATP	50μM ATP	75μM ATP	100μM ATP	2mM ATP
WT	0.69±0.07 N=47	1.05±0.08 N=42	1.63±0.12 N=42	2.21±0.18 N=49	2.40±0.17 N=0.17	3.35±0.27 N=50
G368E	0.44±0.08 N=54	0.78±0.07 N=89	1.09±0.06 N=44	1.29±0.12 N=22	1.40±0.11 N=26	1.82±0.17 N=44
E316K	0.49±0.04 N=52	0.81±0.07 N=62	1.28±0.09 N=60	1.64±0.14 N=42	1.79±0.14 N=53	2.14±0.20 N=40
E93K	0.26±0.03 N=8	0.45±0.08 N=26	0.70±0.10 N=19	0.89±0.11 N=24	0.96±0.07 N=25	

The mutant filament velocities were all significantly slower than WT at each ATP concentration. Where *G368E* filaments showed a 26-46% reduction in their rate of movement, *E316K* and *E93K* exhibited a 21-36% and 62-67% reduction, respectively, in comparison to WT filament velocities throughout the range of ATP concentrations, (see table 5.10). On the whole, these percentage reductions in velocity were greater than those seen between the WT and mutant actins under SAC.

Figure 5.8 A Lineweaver-Burk plot of the reciprocal of the WT, *G368E*, *E316K* and *E93K* filament velocities against the reciprocal of the ATP concentration. The intercept with the *y*-axis represents $1/V_{max}$ whilst the intercept with the *x*-axis indicates $-1/K_{vel}$.

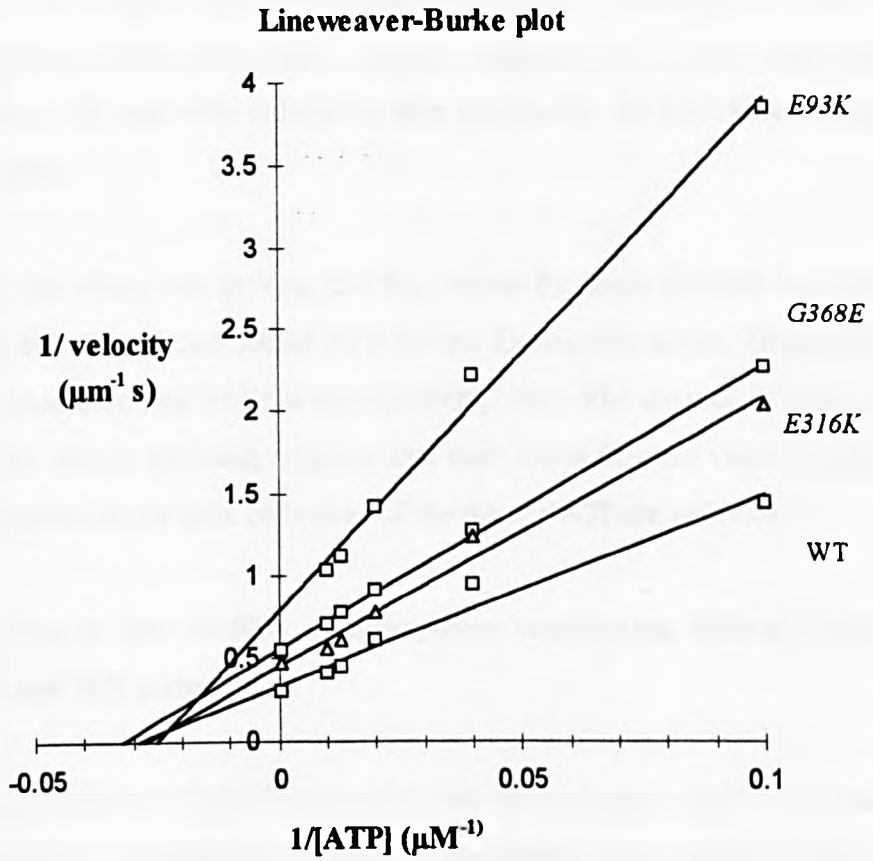

Table 5.8. The V_{max}, (μm/s), and K_{vel}, (μM), values for *WT*, *G368E*, *E316K* and *E93K* as derived from the Lineweaver-Burk plot. Also shown is the percentage reduction in velocity of each of the mutants with respect to WT velocity during ATP variation.

	Vmax (μm/s)	%↓V_f	K_{vel} (μM)
WT	2.94		34.23
G368E	1.80	39	31.04
E316K	2.22	25	36.19
E93K	1.27	57	39.48

Although the V_{max} values for WT and the mutants are significantly different, a Lineweaver-Burk plot of the filament velocities against the ATP concentrations enabled the K_{vel}, the ATP concentration that generates a half maximal filament velocity, to be determined, (see figure 5.8). Any differences in the K_{vel} values of WT and mutant actins subsequently allow a more accurate assessment of the effect of these mutants upon the myosin ATPase activity, (see table 5.8).

From the Lineweaver-Burk plot, the V_{max} values of the mutants are clearly lower than that for WT. The percentage velocity reductions of the mutants with respect to WT in this assay, (Table 5.8), were compared to the analogous reductions of the mutants under SAC, (10mM KCl for *E93K*), (see figure 5.6). Where the 39% and 57% reductions of *G368E* and *E93K* filament velocity in this assay were similar to the respective 35% and 50% reductions seen previously, the *E316K* reduction rose from 6% to 25%.

Despite the reductions in V_{max}, the K_{vel} values for these mutants were quite similar, ranging between 31 and 39μM ATP for the *Drosophila* actins. These figures are not unlike those described by Kron and Spudich (1986). The absence of changes in the K_{vel} values for mutant filaments suggests that their lower filament velocities cannot be due to a reduction in the actin activation of the myosin ATPase activities.

5.3.5 The *in vitro* motility of copolymers constituting different proportions of *E334K* and WT actin

Homopolymers of *E334K* actin did not move under SAC or when the KCl concentration was varied. To confirm the prediction made from the KCl experiments, (Table 5.7), that *E334K* may not be able to form a full strength rigor complex, an attempt was made to establish the effect that the copolymerisation of *E334K* and WT monomers would have on *in vitro* motility. If the static binding of an *E334K* filament is due to its crossbridge being locked in a rigor state, then *E334K*/WT copolymers would not be expected to move. Conversely, if these mutants are unable to form a full strength rigor complex, then *E334K*/WT copolymer movement will not be prevented

by the presence of *E334K* monomers. Subsequent investigations revealed that homogeneous, segmented and block copolymers, (see section 5.2.5), all moved under SAC.

Homogeneous copolymers displayed a sliding velocity that was insignificantly faster, (7%), than WT homopolymers under the same standard conditions, (see figure 5.9 and figure 5.2, the latter for the WT control). These copolymers also exhibited a slight instability upon the surface during movement which was not apparent in WT filaments. Subsequent *in vitro* motility analysis of homogenous *E334K*/WT copolymers, in which the KCl concentration was varied, showed that these cofilaments washed off the myosin surface at 45mM KCl, a slightly lower concentration than that for WT homopolymers, (data not shown).

After the mixing of two homopolymer populations of *E334K* and WT, each having a different fluorescent intensity, the distribution of each monomer type in "segmented" and "block" copolymers gave a striated appearance to the filaments under fluorescence microscopy. By measuring the length of each monomer block in a block copolymer from fluorescence images, the percentage content of *E334K* and WT monomers was estimated and correlated with the *in vitro* velocity of that particular block copolymer. This analysis could not be performed on the segmented copolymers because the runs of each monomer type were too short to measure accurately from the fluorescence images.

The even distribution of sonicated WT and *E334K* fragments in segmented copolymers was confirmed by the relatively uniform fluorescence of these filaments. This was also indicative of random copolymerisation and predicted that these cofilaments would effectively have a 50:50 content of WT and *E334K* monomers that had longer and more frequent consecutive runs of the different monomers than homogeneous copolymers. Segmented copolymers exhibited significantly slower, intermittent sliding under SAC in comparison to that of WT, (see figure 5.9). This comprised periods when the filament was held to the surface in a similar manner to that seen in interactions with dead heads.

E334K/WT block copolymer motility depends upon the identity of the monomer fraction at the pointed end of the filament, i.e. the anterior end of each moving filament. Most of the motile cofilaments possessed a WT block at their anterior end. These were termed "front-ended" block copolymers and displayed jerking movements which appeared to involve a physical wrenching of posterior *E334K* blocks from the surface so that motility could be initiated. During their movement, these posterior blocks were sometimes seen to be detached from the surface, exhibiting Brownian activity, whilst the actively attached anterior ends drove sliding. "Back-ended" *E334K*/WT block copolymers, possessing an *E334K* portion at their anterior ends, were rarely seen to move. Occasionally, such a filament with a short anterior *E334K* block became motile, its movement being propelled by the long WT posterior portion.

Figure 5.9. Histograms showing the average *in vitro* velocities, (plotted in 0.2μm/s bins), of the homogeneous and segmented *E334K*/WT copolymers under standard assay conditions.

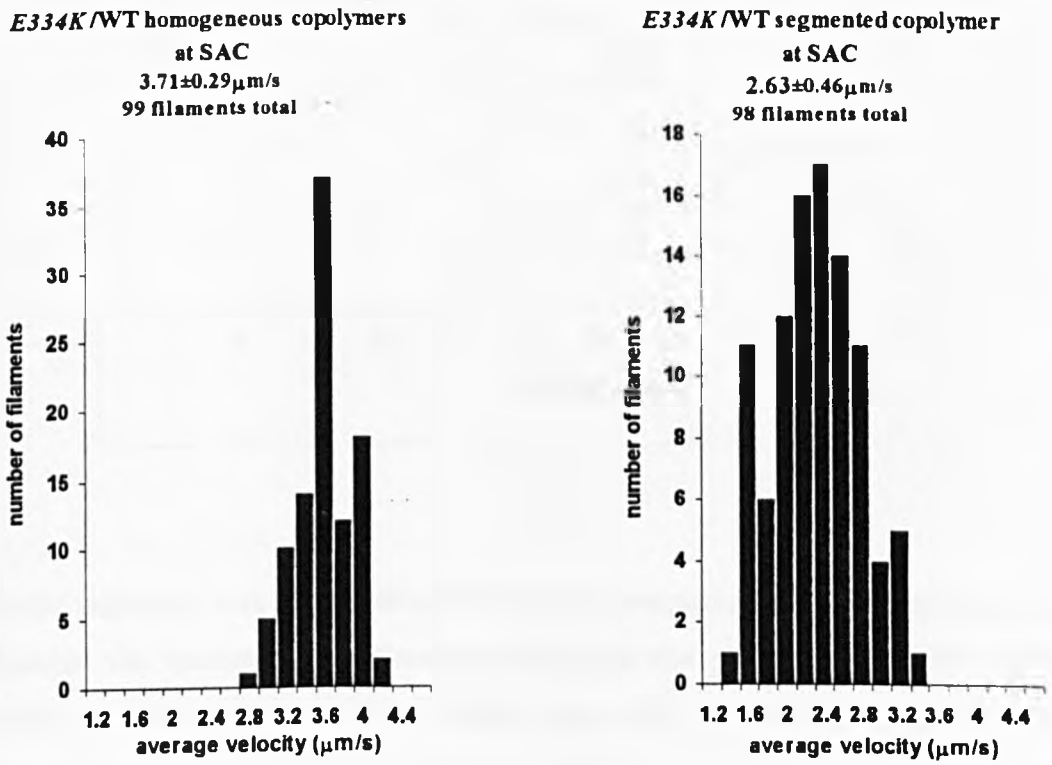

The *in vitro* filament velocities of 19 front-ended and 8 back-ended block cofilaments were recorded under SAC. The front-ended copolymers generally moved faster and

more frequently than the back-ended filaments. Additionally, front-ended cofilaments possessing short posterior *E334K* portions moved more quickly than those having long posterior *E334K* blocks and in the latter case, the posterior block could be so long that movement was totally inhibited. The percentage *E334K* content for each moving front and back-ended cofilament was determined and plotted against its corresponding filament velocity, (see figure 5.10).

Figure 5.10. The *in vitro* filament velocities for front and back-ended *E334K*/WT block copolymers. The percentage *E334K* content and filament velocity was recorded for each front and back-ended cofilament. The squares depict front-ended block copolymers and the triangles represent back-ended copolymers. A linear regression was performed for the front-ended copolymers alone.

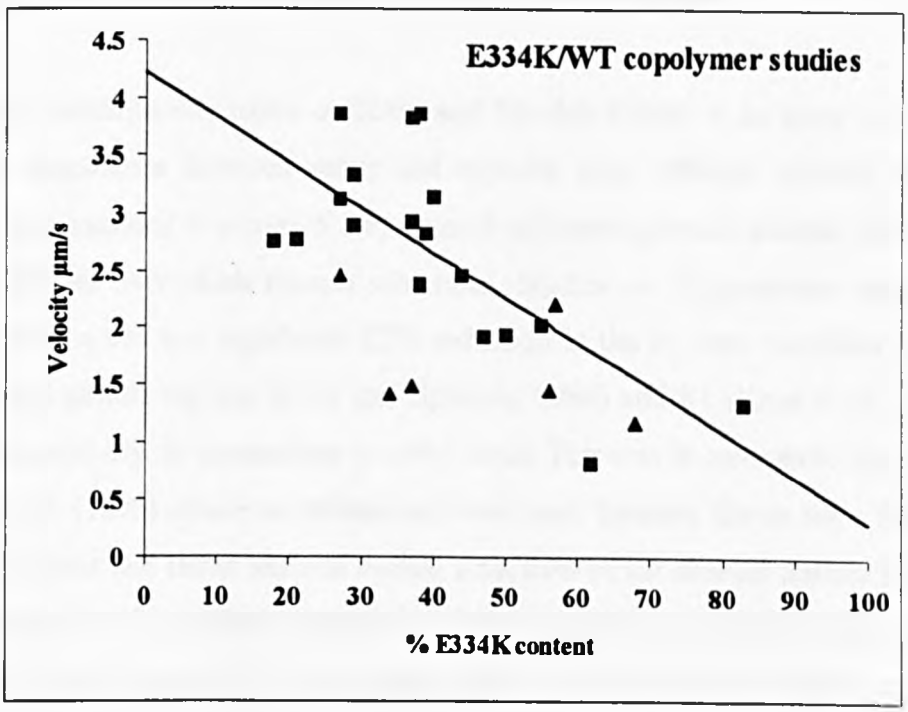

A linear regression was performed only for the front-ended *E334K*/WT copolymers. It illustrates the decrease in cofilament velocity as the percentage *E334K* content increases. Despite the lack of data points, the back-ended block copolymers also displayed lower filament velocities as their mutant monomer content increased. These features suggest that the *E334K* monomer blocks in a cofilament retard movement mediated by the WT blocks.

5.4 DISCUSSION

The *in vitro* motility assay is a versatile procedure that enables the measurement of movements generated by interactions between purified actin and myosin. In addition to analysis under standard assay conditions, variations of salt and ATP concentrations in the assay buffers can shift the equilibria to favour different states of the crossbridge cycle. The latter allow further characterisation of the effects of actin and myosin mutations which may ultimately provide insights into the mechanism of crossbridge action.

5.4.1 Rabbit actin versus *Drosophila* WT actin *in vitro* motility

The *in vitro* motility assay based on Kron and Spudich (1986) is an assay system in which the interactions between actins and myosins from different sources can be assessed. As mentioned in section 5.1.5, actins from heterogeneous sources each have discrete motilities over rabbit myosin substrates. Studies on *Dictyostelium* and yeast actin produced a 9% and significant 52% reduction in the *in vitro* motilities over a rabbit skeletal muscle myosin (Kron and Spudich, 1986) and S1 (Kron *et al.*, 1992) substrate respectively, in comparison to rabbit actin. This was in contrast to the report of Cook *et al.* (1993) where no differences were seen between the *in vitro* filament velocities of yeast and rabbit skeletal muscle actin over rabbit skeletal muscle myosin. The differences in the primary sequences of actin isoforms, particularly amino acid substitutions in the proposed myosin binding site, are thought to define the strength of their interactions with heterologous myosins, and therefore their *in vitro* motilities and myosin ATPase activation activities.

A comparison of the *in vitro* velocities of rabbit skeletal muscle and WT *Drosophila* actin filaments moving on rabbit skeletal muscle HMM revealed a 10% reduction in the motility of the *Drosophila* actin, (see section 5.3.2). This was similar to the previous finding of a 24% reduction in the movement of *Drosophila* actin filaments over rabbit HMM (Anson *et al.*, 1995). The difference in the reduction between these studies could be due to the fact that whereas the present study used pure ACT88F polymers,

Anson *et al.* (1995) used actin prepared from whole flies which contains different proportions of up to six actin isoforms. Additionally, the faster movements of both rabbit and *Drosophila* actins in Anson's system could be due to the increased temperature, (25°C), that they used, compared to that of 23°C for the present study.

The wash off point for rabbit actin occurs at a KCl concentration 10mM higher than that for WT *Drosophila* actin. This confirms the expected higher affinity of the rabbit actin for its rabbit HMM substrate. Overall, the WT ACT88F amino acid sequence is 92.3% homologous to that of rabbit skeletal muscle actin. Of the 29 differences in their primary sequences, only two reside within the proposed myosin binding site. These are Asp0, the first residue in the skeletal muscle isoform, that is absent in ACT88F, and a conservative substitution of Glu2 to aspartic acid in ACT88F. These two residues are both thought to be involved in the weak electrostatic binding and ATPase activation of myosin (Sutoh, 1982; Chaussepied and Morales, 1988; Cook *et al.*, 1993) and could explain the differences in velocity between the rabbit skeletal and *Drosophila* actin isoforms (this study; Anson *et al.*, 1995)

5.4.2 *In vitro* motility of the *G368E* and *E316K* actins

The mutations *G368E* and *E316K* do not affect residues within the proposed actomyosin interfaces. However, they were shown to affect muscle fibre kinetics (Sparrow *et al.*, 1991a; 1991b) and actomyosin interactions using whole actin preparations from mutant flies (Anson *et al.*, 1995). Where *E316K* filament velocity was not significantly reduced during *in vitro* motility under SAC, (↓6%), that of *G368E* showed a significant decrease of 35%. The slight decrease in the motility of pure *E316K* filaments found in the present study probably explains why Anson *et al.* (1995) found no effect upon the HMM mediated motility of mutant filaments containing a mixture of *E316K* actin copolymerised with other isoforms. The ACT88F mutant phenotypes in the latter cofilaments would be partially masked by the behaviour of the other constituent actin isoforms.

The similar KCl wash off concentrations for *G368E* and WT suggested that the weak actomyosin binding affinity of this mutant was unaffected. This contrasted with the observation that *G368E* had an increased K_d for S1 binding at 0.1M KCl (Anson *et al.*, 1995). The reduction in S1 binding was due to a two-fold increase in k_{off} and a small decrease in k_{on}. *G368E* had no effect upon the V_{max} and K_{app} (apparent actin concentration required for 50% activation of the myosin ATPase) values for the actin activated S1 ATPase activity (Anson *et al.*, 1995). This was corroborated by the results from this study which showed that *G368E* filaments had a K_{vel}, (the ATP concentration required to achieve half maximal filament velocity in the motility assay, supposedly through the activation of 50% of the bound myosin heads), similar to that of WT, (figure 5.8 and Table 5.8). This, coupled to the reduction in the V_{max} of *G368E* motility with respect to WT, (see figure 5.7), suggests that the lower *in vitro* velocities of *G368E* are not derived from changes in its ability to activate the myosin ATPase.

Since residue G368 is not in the proposed myosin binding site (Rayment *et al.*, 1993b; Schröder *et al.*, 1993) it is not obvious how it affects actomyosin kinetics. Anson *et al.* (1995) postulated that the disruption of a normal binding of this region of actin to one of the two essential myosin light chain isoforms, which has a 41 residue N-terminal extension, may result in this velocity reduction. Such a contact is normally seen for rabbit actin and has been proposed from EM reconstructions of S1-decorated F-actin (Milligan *et al.*, 1990), from chemical cross-linking (Sutoh, 1982) and nuclear magnetic resonance studies (Trayer *et al.*, 1987). Molecular graphics, (see figure 5.11), show that the glutamic acid side chain at position 368 in this mutant, which replaces Gly368 in ACT88F, (normally a serine in rabbit skeletal actin), sticks a charged group out into the solvent within the proposed light chain binding site. This could compromise the overall myosin interaction of *G368E* and generate the aforementioned phenotypes. Nevertheless, this hypothesis does not explain the *in vivo* effects of *G368E* since the *Drosophila* essential light chain isoforms do not possess an N-terminal extension.

E316K actin washed off at 40mM KCl, a slightly lower ionic strength than WT. Although this suggests a reduction in its weak actomyosin binding, Anson *et al.* (1995)

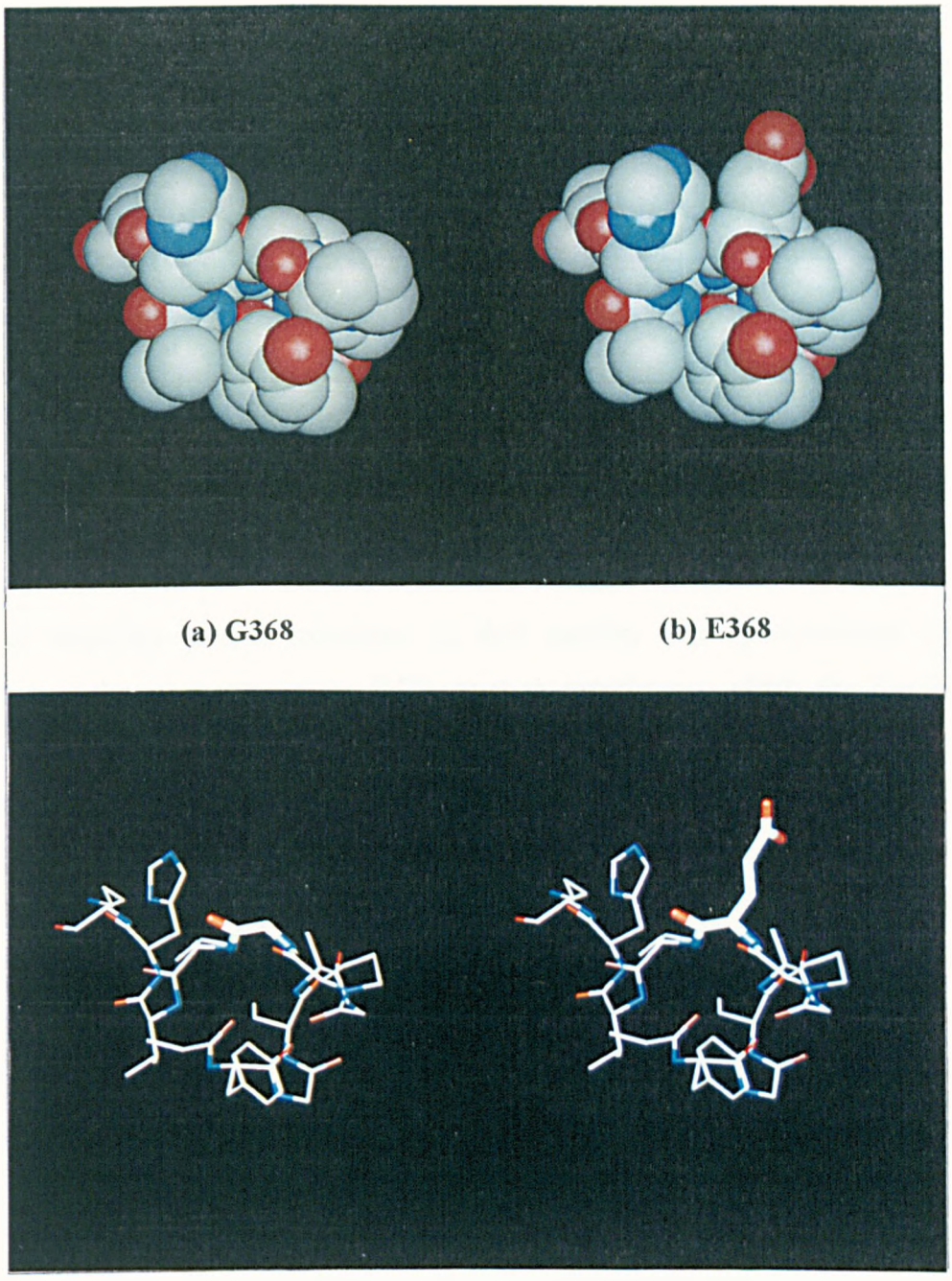

Figure 5.11. The *G368E* mutation. (a) Two molecular representations of the amino acids surrounding residue G368 in the rabbit skeletal muscle actin monomer, Kabsch *et al.*, (1990). (Note that residue 368 in rabbit skeletal muscle actin is normally serine). This set of residues lies on subdomain IA and the solvent is oriented towards the top of the model. The upper models are displayed as Van de Waals spheres whilst the lower models are shown in a ball and stick representation, with residue G368 exhibited in licorice style. (b) An identical representation as (a) but with residue G368 altered to E368.

showed that *E316K* had a normal S1 binding affinity. The movement of *E316K* filaments was not significantly reduced at low KCl concentrations, (see figure 5.5 and table 5.9). *E316K* had a similar K_{vel} and a slightly lower V_{max} value compared to WT, (see figure 5.8 and Table 5.8), suggesting that this mutation does not affect the actin-activation of the myosin ATPase.

The *in vitro* motility of *E316K* in the ATP experiments was reduced compared to movements under SAC, especially at the 2mM ATP condition where a 36%, as opposed to a 6%, reduction was observed. Although WT filament velocities in the ATP experiments approached those of WT filaments under SAC, each of the mutant genotypes displayed greater reductions in their motility. This phenomenon was reflected to a lesser degree in the KCl variation experiments where the filament velocities at 25mM KCl were slower than at the equivalent SAC. These reduced velocities could be attributed to the difference in the experimental design of the KCl and ATP variation experiments with respect to the SAC motility assays. Whereas a fresh slide was used each time for SAC measurements, during the KCl and ATP variation assays, a single slide was consistently exposed for longer periods to increasing ionic strength concentrations. This could produce a deterioration of the myosin surface which consequently reduces filament velocities. Therefore, the sequential titration protocol may not be the most appropriate approach for measuring *in vitro* motility under different assay conditions.

Residue E316 in actin is located some way from the proposed myosin binding sites. It lies on the back surface of subdomain IIA in the actin monomer, (see figure 5.12), and sticks out a basic, as opposed to an acidic side chain, into the solvent. Although *E316K* does not have a major effect upon actomyosin functions, an explanation for its action is not obvious. Drummond *et al.* (1991a) suggested that this mutation may act by generating long range conformational changes within the actin monomer.

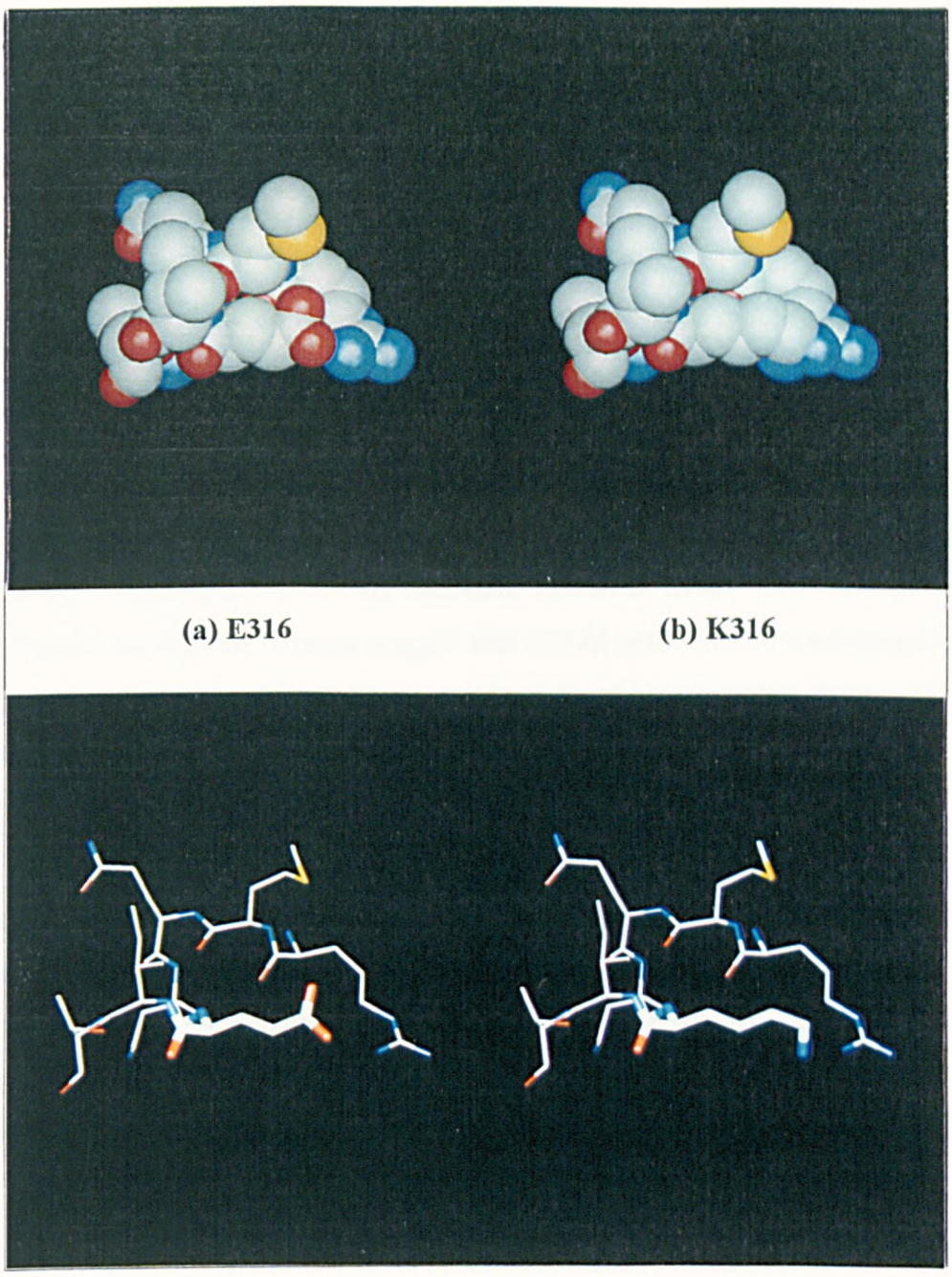

Figure 5.12. The *E316K* mutation. (a) Two molecular representations of the amino acids surrounding residue E316 in the rabbit skeletal muscle actin monomer, Kabsch *et al.*, (1990). This set of residues lies on the back surface of subdomain IIA with the solvent oriented towards the viewer. The upper models are displayed as Van de Waals spheres whilst the lower models are shown in a ball and stick representation, with residue E316 exhibited in licorice style. (b) An identical representation as (a) but with residue E316 altered to K316.

5.4.3 The *in vitro* motility of *E334K* actin

5.4.3.1 *E334K* homopolymers

The *E334K* filaments show no signs of movement in the *in vitro* motility assay under any conditions, including saturating ATP concentrations. Furthermore, no signs of filament fragmentation were seen upon the addition of ATP during *in vitro* motility at SAC. Even at low ATP and KCl concentrations, where a large number of strongly bound heads should be imposing a mechanical, shearing force upon the filaments that facilitates their disintegration, *E334K* filaments remained intact upon the myosin surface. These observations strongly suggest that *E334K* actin filaments are incapable of forming a strong contact with the myosin head that holds a tension during force generation and the subsequent power stoke event.

The lack of motility predicts that *E334K* F-actin could bind to myosin heads to form crossbridges that reside predominantly in either one of two states during the contractile cycle. The first constitutes a strong "rigor-like" contact which is not dissociatable by ATP and is therefore incapable of cycling and producing movement. The second alternative state resembles a weaker binding, actomyosin complex that is dissociatable by ATP, but unable to form the strong crossbridge contact that mediates the power stroke.

Residue E334 lies in a short loop on the surface of subdomain IIA of the actin monomer, (see figure 5.13). The lysine side-chain in this mutation is seen to protrude further from the surface than the substituted glutamic acid side-chain. This appears to significantly alter the surface charge in this region of the monomer which is proposed as one of the strong myosin binding sites (Rayment *et al.*, 1993b). Charge reversal at this position could therefore hinder the formation of a strong actomyosin contact and keep the *E334K* filaments in weakly bound crossbridge states.

E334K filaments were dissociatable by ATP at higher ionic strengths in the KCl experiments, (see table 5.6). This could not be achieved by a crossbridge locked in a

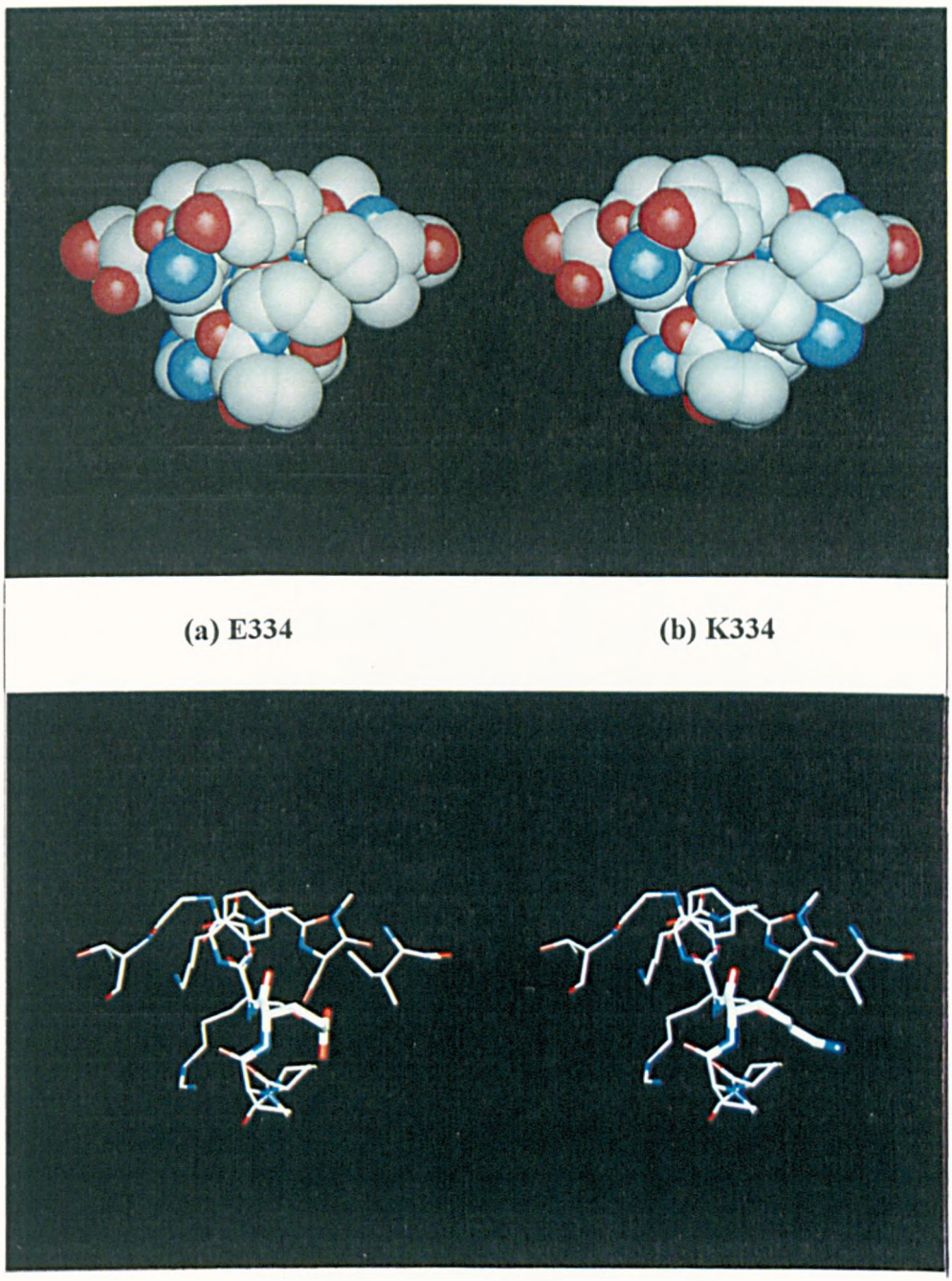

Figure 5.13. The *E334K* mutation. (a) Two molecular representations of the amino acids surrounding residue E334 in the rabbit skeletal muscle actin monomer, Kabsch *et al.*, (1990). This set of residues lies on the surface of subdomain IIA, near to the junction with subdomain IA, with the solvent oriented towards to the right of the model. The upper models are displayed as Van de Waals spheres whilst the lower models are shown in a ball and stick representation, with residue E334 exhibited in licorice style. (b) An identical representation as (a) but with residue E334 altered to K334.

strong rigor linkage and supports the contention that *E334K* crossbridges may be predominantly in one of the weaker states of the crossbridge cycle. The fact that *E334K* filaments also wash off at a lower ionic strengths than WT suggests that the strong myosin binding contact involving residue E334 is partly ionic in nature and may be weakened or abolished in this mutant.

If *E334K* filaments are restricted to the formation of one of the weak, initial, electrostatic contacts, then they would not be expected to form any semblance of a stronger contact, (A.M.ADP.Pi, A.M.ADP*.Pi or A.M.ADP, see section 1.4), and would subsequently wash off at the same ionic strength in the KCl variation assays performed with and without ATP present. The observation that these filaments did not wash off at 30mM KCl in the ATP independent KCl variation assay therefore implies that these mutant actins are able to form a relatively strong complex of some sort. The wash off of *E334K* filaments in the latter assay at 1M KCl, a concentration at which WT filaments were still stably bound to the HMM surface, additionally concludes that *E334K* is not able to form a full strength rigor contact with the myosin head. This would corroborate the proposal that the *E334K* "pre-rigor" crossbridge is unable to hold tension during force generation and undergo a power stroke.

5.4.3.2 *E334K*/WT copolymers

In vitro motility assays have been used to assess the effects of proteolytic cleavage, chemical crosslinking and mutagenesis upon the actomyosin crossbridge. These have been used to identify changes in actin and myosin that either abolish or severely inhibit filament movement. Copolymer studies have been generally used to characterise further the behaviour of these modified actin and myosin components by polymerising them into filaments with varying ratios of unmodified monomers. Their effects upon copolymer *in vitro* motility can subsequently be used to gauge the actions of the disrupted crossbridges upon those of unmodified crossbridges (Prochniewicz and Yanagida, 1990; Prochniewicz *et al.*, 1993; Schwyter *et al.*, 1990; Warshaw *et al.*, 1990). Most modified actins and myosins generate crossbridges that have negative effects upon copolymer *in vitro* motility. For the sake of this study, this negative effect

will be generally termed as "connectivity". The mechanism and severity of connectivity is dependent upon the nature of the modification and two "extremes" of action are described below.

Skeletal muscle myosins can be chemically modified by NEM or pPDM treatment to generate crossbridges that are unable to hydrolyse ATP, and therefore cycle (Pemrick and Weber, 1976). Whereas NEM favours the formation of a tight binding of myosin to actin, pPDM generates a weakly bound crossbridge state. The effect of these strongly and weakly bound crossbridge analogues can be assessed by the *in vitro* motility analysis of their copolymers with untreated myosins. If a modified monomer had no negative effect upon *in vitro* motility, the cofilament velocity would be equal to that of unmodified homopolymers, (i.e. filaments constituting unmodified monomers alone), (see figure 5.14A).

Copolymers of unmodified rabbit skeletal muscle myosin possessing a content of NEM-myosin greater than, or equal to, 1% conveyed no *in vitro* motility (Warshaw *et al.*, 1990). Additionally, when the proportion of NEM-myosin was reduced to less than 1%, cofilament-mediated velocity was indistinguishable from that of unmodified homopolymers, (see figure 5.14B). This represents one extreme of connectivity and suggests that NEM-myosin forms a rigor-like crossbridge of which only small amounts are sufficient to abolish movement mediated by unmodified crossbridges.

One example of the weak extremity of connectivity was demonstrated by copolymers of pPDM myosin with phosphorylated smooth muscle monomers (Warshaw *et al.*, 1990). Here, a modified monomer content below 75% did not affect the actin filament velocity over cofilaments. Above this percentage, actin filament velocity was gradually reduced to a minimum, but not abolished, at about 90% of a pPDM-myosin monomer content, (see figure 5.14C).

Figure 5.14. A representation of the "connectivity" effect upon the *in vitro* motility of copolymers constituting unmodified monomers and different percentages of weakly and strongly bound crossbridge analogues. (A) depicts the effect of modified monomers that do not affect copolymer motility at all. (B) shows the effect of the severe connectivity of NEM-myosin crossbridges, (for clarity, the steepness and the intercept with the *x*-axis, of the curve representing the Warshaw *et al.* (1990) data are less exaggerated). (C) describes the mild connectivity of weakly bound pPDM myosin crossbridges (Warshaw *et al.*, 1990). (D) denotes the connectivity of copolymers possessing chemically crosslinked actin monomers (Prochniewicz and Yanagida, 1990; Prochniewicz *et al.*, 1993).

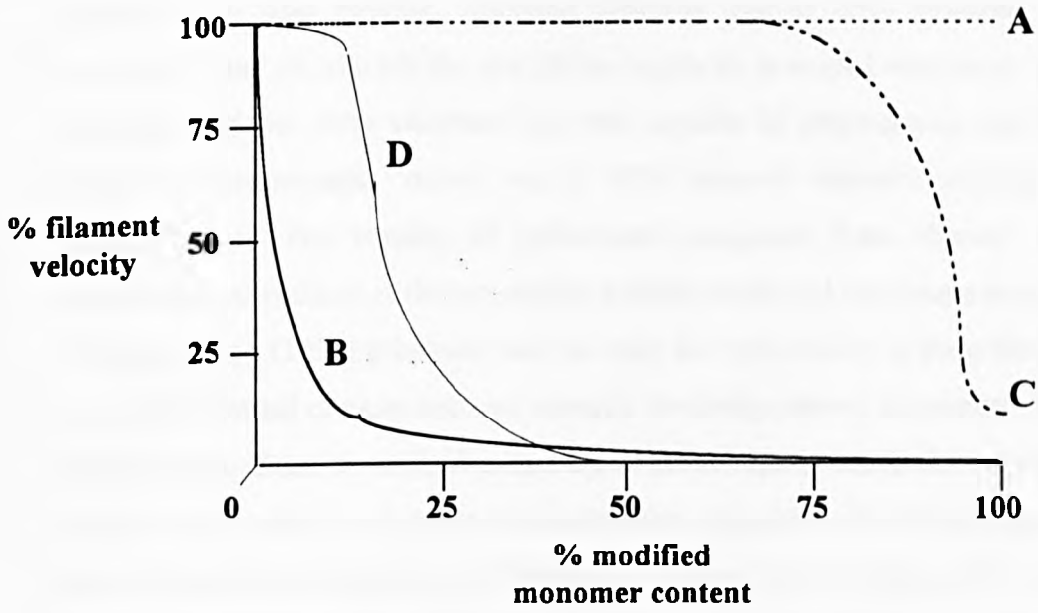

E334K/WT segmented and block copolymers exhibited some degree of connectivity as seen by a reduction in their *in vitro* filament velocities compared to WT homopolymers. Since the mechanisms of copolymer retardation vary for the different types of modifications, a brief overview of the alternate forms will hopefully help to establish the underlying behaviour shown by the *E334K* monomers.

Prochniewicz and Yanagida (1990) and Prochniewicz *et al.* (1993) investigated the *in vitro* motility of copolymers containing chemically crosslinked, (EDC or glutaraldehyde), and unmodified actin monomers. Homopolymers of these modified monomers were unable to move. These two agents were thought to abolish movement by introducing artificial, inter-monomeric contacts into the F-actin which would distort the actin helices, making them incapable of a correct actomyosin interaction, and consequently movement. The *in vitro* copolymer filament velocity decreased as the percentage of crosslinked monomers increased up to a 50% level, at which point,

movement was totally inhibited, (see figure 5.14, D). The "connectivity" effect seen in these copolymers was attributed to the altered intrafilament interactions of the modified monomers distorting the myosin binding sites on adjacent, unmodified monomers and therefore generating the aberrant copolymer properties.

Schwyter *et al.* (1990) addressed the effect of subtilisin cleaved actin monomers upon copolymer *in vitro* motility. Although subtilisin cleaves actin monomers between residues 47 and 48, the 36KDa and 9KDa fragments remained associated, apparently retaining a global actin structure that was capable of polymerising into filaments. Cleaved homopolymers moved at a 30% reduced filament velocity to WT homopolymers. The motility of cofilaments composed from cleaved and intact monomers was reduced as the percentage content of cleaved monomers was increased. Schwyter *et al.* (1990) proposed that the basis for connectivity in these filaments was due to the internal motions between contacts involving cleaved monomers. Since actin filaments may function as rigid cables upon which myosin heads form loaded spring complexes that drive movement upon relaxation, alterations in the actin:actin contact sites by proteolytic cleavage may disrupt or reduce filament rigidity. The subsequent dissipation of the spring energy in filaments containing cleaved monomers would subsequently reduce *in vitro* velocities.

The above studies concluded that the modified monomers in the copolymers alter the actin filament structure by interfering with neighbouring, inter-monomeric bonds. Since residue E334 resides in an actomyosin and not an actin-actin interface, it is likely that filament structure will be unaffected. It is more probable that *E334K* copolymer connectivity has a very different basis and is due to the formation of distorted crossbridges which exert restrictive effects upon other crossbridges in the same filament.

Warshaw *et al.* (1990) used the *in vitro* motility of actin filaments over myosin filaments and cofilaments to study the effect of phosphorylation upon smooth muscle myosin. They proposed that two mechanically distinct crossbridge populations, represented by phosphorylated smooth muscle myosin (psm) and dephosphorylated

smooth muscle myosin (**dpsm**), can interact mechanically in cofilaments to modulate filament velocity.

Homopolymers of non-cycling dpsm displayed no ATPase activity and though able to bind, did not support the movement of actin filaments. Copolymers of psm and dpsm had actin-activated ATPase activities that were linearly dependent upon the percentage of psm in the cofilament. This linearity was not apparent during *in vitro* motility where only >60% dpsm content began to reduce actin filament velocity. In copolymers of psm and dpsm, the non-cycling dpsm crossbridges were thought to impose an internal load, or connectivity, upon cycling psm crossbridges, subsequently reducing the degree of filament movement conveyed by the latter in a non-linear manner.

This mechanical impedance imposed by one crossbridge population upon another was also demonstrated by copolymers of smooth and skeletal muscle myosin (**sm**). Again, although a linear relationship was observed for the actin activated myosin ATPase activities of these copolymers, a non-linear dependence of filament velocity upon the percentage of the slower cycling crossbridge was apparent (Warshaw *et al.*, 1990).

Warshaw *et al.* (1990) concluded that dpsm crossbridges are weakly attached crossbridges which both quantitatively and qualitatively resemble the PDM-myosin bridges mentioned earlier, (see figure 5.14). Somlyo *et al.* (1988) postulated that the rates of attachment and detachment of crossbridges are strain dependent, i.e. when weakly bound crossbridges are strained as the filament moves, their kinetics are altered in such a way that they become more tightly bound and subsequently retard movement by faster cycling crossbridges. In this case, "connectivity" between different crossbridges can be visualised as an internal load imposed upon the faster cycling crossbridges by the weaker bound crossbridges.

Homsher *et al.* (1992) addressed the question of whether weakly bound crossbridges do indeed reduce filament velocity by imposing a strain dependent internal load. He attempted to increase the number of weakly bound crossbridges in a filament using ATPγs, an analogue of ATP which binds S1 heads with an equal affinity but is

hydrolysed some 500 times slower. The binding of ATPγs therefore increases the proportion of crossbridges that are weakly bound. Filament velocities were measured in the presence of equimolar ratios of ATP/ATPγs. Homsher argued that since this would effectively double the number of weakly bound crossbridges found with ATP alone, a sharp decrease in filament velocity would therefore be expected. A reduction of <14% in velocity was seen, increasing to 22% with a fivefold molar excess of ATPγs.

The lack of proportionality between the number of weakly attached crossbridges and filament velocity suggests that weakly bound states do not impose an internal load upon the faster cycling crossbridges. One possible explanation suggested by Homsher *et al.* for this discrepancy was that ATPγs dissociates rigor actomyosin complexes approximately 10-20% as efficiently as ATP. This would therefore lead to an overestimation of the number of weakly bound crossbridges present in this experiment.

The characterisation of the *E334K* mutant with the three types of copolymer, (see section 5.2.5), demonstrated that they do not display a connectivity indicative of strongly bound, "rigor-like" heads. Homogeneous copolymers possessing a 50% *E334K* content showed no signs of connectivity and were able to move at WT *in vitro* filament velocities under SAC. Since *E334K* crossbridges are incapable of generating movement, it must be assumed that copolymer motility is due to the WT monomers.

Segmented *E334K*/WT copolymers are basically alternate versions of homogeneous copolymers in that are predicted to have longer and more frequent, consecutive stretches of either mutant and WT monomers. Their reduced velocity in comparison to the homogeneous copolymers suggested that the longer *E334K* stretches restrain movement generated by cycling WT monomers through the formation of many more pre-rigor binding contacts with the surface. Unlike the homogeneous copolymers, the effects of these contacts are not diminished due to the presence of interspersed WT monomers.

"Block" copolymers had reduced *in vitro* velocities compared to the corresponding homogeneous and segmented copolymers. In this case, movement was dependent upon the type of actin in the block at the pointed end of the filament. The movement of front-ended copolymers was faster than that of WT back-ended cofilaments when the *E334K* proportion in the polymer was below 50% under SAC, (see figure 5.10). This difference was explained by the fact that actin filaments are analogous to semi-flexible rods (Yanagida *et al.*, 1984). This predicts that the action of WT-front-ended block copolymers pulling a filament taut is likely to be more efficient in producing movement than the pushing of a semi-flexible rod by WT-back-ended copolymers.

By determining the percentage of E334K monomers in the copolymer that is required to reduce filament movement, the strength of its connectivity can be estimated. The *E334K* crosssbridge appears to be acting in a manner more similar to the weakly bound dpsm and PDM-myosin crossbridges than the NEM-sm situation described in the above studies. The fact that a 50% content of dpsm in a dpsm/sm copolymer, and *E334K* in a homogeneous copolymer, did not inhibit movement suggests that their crossbridges may exhibit a similar degree of connectivity. However, the limited analysis of *E334K*/WT copolymer motility showed that a linear relationship between the *E334K* content in a copolymer and *in vitro* movement could be fitted, where a 30% *E334K* content began to reduce filament velocity. Comparison of this figure to the 60% dpsm that begins to reduce dpsm/psm cofilament movement proposes that the *E334K* monomers may in fact exert a stronger connectivity effect.

The *E334K* and dpsm copolymer studies were similar in that by altering actin and myosin respectively, they were able to generate actomyosin crossbridges which had a similar connectivity. However, these copolymer studies used to determine this negative crossbridge activity were not directly comparable since they generated copolymers that were intrinsically different. Where the dpsm monomers in myosin cofilaments were interspersed with psm monomers even at high percentages of the former, the *E334K*/WT actin block copolymers were constituted from a single stretch of *E334K* monomers annealed to the end of a stretch of WT monomers. As seen from the

difference between the filament velocities of homogeneous and segmented copolymers, the different distributions may affect the severity of connectivity.

In conclusion, the *E334K* is probably incapable of forming a rigor complex that mediates the power stroke. Rather, it seems to form a pre-rigor complex of moderate strength that involves a number of the actomyosin contacts, thus providing a strong binding that retards the motility produced by WT crossbridges in block copolymers. Although the strength of this binding has not been estimated, it is presumed that this mutant crossbridge may be locked, or only cycles up to the A.M.ADP.Pi or A.M.ADP.Pi* states in the crossbridge cycle. Studies of the ATPase activity of these mutants would help to establish whether or not *E334K* crossbridges were cycling up to, or locked, in one of these states. Additionally, the investigation of *E334K* actin filaments in an optical trap would be able to quantify the "connective" strength of this crossbridge. The fact that a single amino acid substitution can have such a devastating effect upon *in vitro* motility underlines the effectiveness of using actin mutants to study the details of the actomyosin interactions.

5.4.4 *E93K*

Although the *E93K Drosophila* mutant forms disrupted IFM myofibrillar structures (Sparrow *et al.*, 1991b) which are similar to those of *E334K* (Drummond *et al.*, 1991a), the mini-actin preparation enabled the isolation of pure F-actin sufficient for many motility assays. However, observation of fluorescently labelled *E93K* F-actin revealed dense, bundled structures containing large numbers of actin filaments. These were seen consistently in most *E93K* actin preparations. This type of actin filament bundling was first reported by Cook *et al.* (1992) in two yeast N-terminal actin mutations, *D2N/E4Q* and *ΔDSE*. Two other yeast actin mutations, *D24A/D25A* and *E99A/E100A* (Miller and Reisler, 1995) and a *Dictyostelium 15* actin mutant, *E99H/E100H* (Johara *et al.*, 1993) also formed filament bundles upon polymerisation. The mechanism(s) of this bundling remains unknown.

Although the F-actin bundling of the aforementioned actin mutations prevented biochemical analyses such as the measurement of their myosin ATPase activation, *in vitro* motility of *E93K* actin in this report was made possible by briefly sonicating the bundles prior to use. This generated single, short filaments which were seen to reanneal into filament bundles after a period of a few hours. Consequently, sonication was performed immediately before motility analysis.

The *E93K* mutation causes a charge reversal that lies at the end of a loop involved in the interaction of the so-called secondary binding to a flexible polypeptide loop in the myosin head. The change of Glu93 to a lysine results in an amino group protruding from the surface of the monomer, (see figure 5.15). Although rigor crossbridges had been seen in electron micrographs of *E93K* IFMs (Sparrow *et al.*, 1991b) and *E93K* filaments displayed a stable, rigor contact with the myosin surface, (this study), the expectation that this mutation would affect the secondary, and subsequently overall actomyosin interaction was fulfilled when *E93K* filaments washed off the myosin substrate surface upon the addition of ATP in the motility assay.

Three mutations, *D24H/D25H* (Johara *et al.*, 1993), *D24A/D25A* and *E99A/E100A* (Miller and Reisler, 1995) in *Dictyostelium* and yeast actin respectively, also washed off the surface during the *in vitro* motility assay upon the addition of ATP, (see table 5.1). The mutations at residues 24 and 25 lie in a region of actin which is involved in electrostatic contacts with the N-terminus of actin (Kabsch *et al.*, 1991; Rayment *et al.*, 1993b; Schröder *et al.*, 1993; Uyeda *et al.*, 1994). If formation of the rigor complex involves a sequential increase in the number of the proposed actomyosin binding sites that are occupied, it is not surprising that a charge reversal at residues D24 and D25 disrupts the weak, initial collision contacts, resulting in a loss of overall actomyosin binding.

The *E93K* mutation in this study, and *E99A/E100A* both lie in the proposed secondary actomyosin binding site (Rayment *et al.*, 1993b; Milligan *et al.*, 1990) which is thought to stabilise the overall contact of the myosin head to two actin monomers. The fact that both *E93K* and *E99A/E100A* actin filaments are unable to interact with the myosin

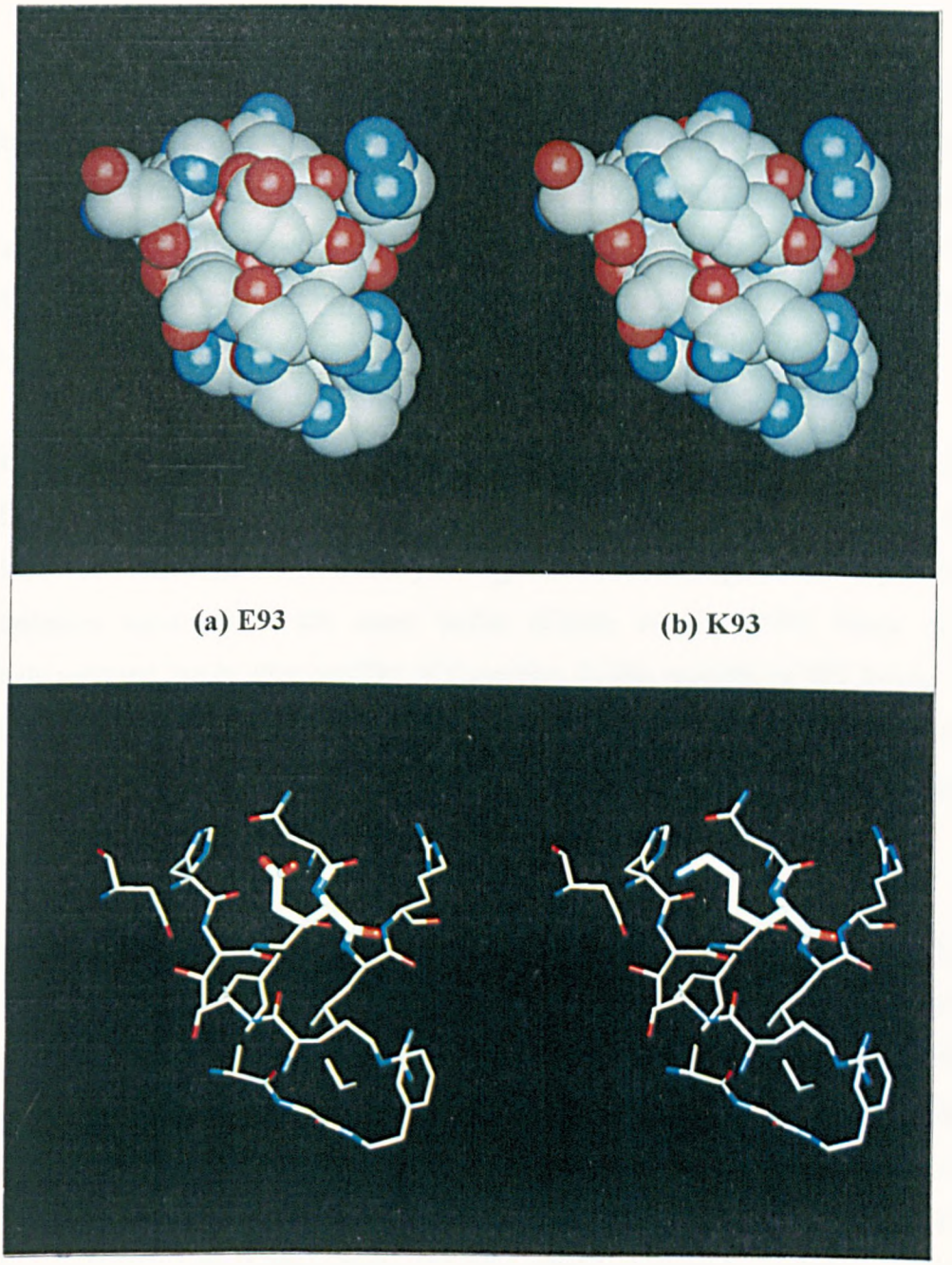

Figure 5.15. The *E93K* mutation. (a) Two molecular representations of the amino acids surrounding residue E93 in the rabbit skeletal muscle actin monomer, Kabsch *et al.*, (1990). This set of residues lies on a surface loop in subdomain IA with the solvent oriented to the top of the model. The upper models are displayed as Van de Waals spheres whilst the lower models are shown in a ball and stick representation, with residue E93 exhibited in licorice style. (b) An identical representation as (a) but with residue E93 altered to K93.

surface under SAC in the motility assay suggests that the secondary binding interaction may also represent early stages in the formation of the actomyosin complex and is ionic in nature. These observations additionally support the prediction of Rayment *et al.* (1993) that secondary binding involves the contacts between residues E93, E99 and E100 on actin with five basic resdiues on a flexible loop, 567-578, in the myosin lower 50KDa domain.

To test whether disruption of the initial, ionic binding of the *D24A/D25A* and *E99A/E100A* yeast actin mutants was responsible for the wash off during the motility assay, Miller and Reisler (1995) artificially strengthened this binding by including 0.7% methylcellulose substitute in the assay buffer (Uyeda *et al.*, 1990). Since this completely restored the *in vitro* motility of these two double mutants to WT levels, it implied that the purpose of the initial, electrostatic actomyosin interactions may be to enhance the formation of the actin and myosin collision complex as the first step towards the stronger binding states later in the crossbridge cycle.

To establish whether the *E93K* mutation simply affected the actomyosin interaction by disrupting the initial formation of the A.M.ATP collision complex, an attempt was made to strengthen, rather than substitute for, the ionic binding between actin and myosin. Reports that a reduction in ionic strength enhances weak actomyosin binding (Brenner *et al.*, 1982) led to motility assays at reduced ionic strengths. Movement of *E93K* filaments was subsequently observed at ionic concentrations below those under standard conditions, confirming that, in this, *E93K* behaved similarly to the *D24A/D25A* and *E99A/E100A* yeast actin mutants.

Smooth, stable sliding of *E93K* filaments was detected between 0-15mM KCl and as the KCl concentration was increased, the filaments, as expected, washed off at 25mM KCl, (see figure 5.5 and table 5.6). *E93K* filament velocity was about half that of WT over the range of KCl concentrations investigated. This was unlike the observations of Miller and Reisler (1995) where the sliding velocities of the *D24A/D25A* and *E99A/E100A* yeast actin mutants were restored to WT levels.

To investigate whether reduced *E93K* filament velocities were due to an inability to activate the myosin ATPase, the movement of this mutation under different ATP concentrations was measured, (see figure 5.8 and table 5.8). The K_{vel} for myosins interacting with *E93K* actin filaments was almost equivalent to WT, supporting the conclusion that the reduction in *E93K* filament velocity at lower ionic strengths is not due to an inability to activate the myosin ATPase. In the absence of ATP, the attempted dissociation of the *E93K* rigor complex with KCl showed an equivalent behaviour to that of WT actin, suggesting that *E93K* may form a full strength rigor complex. However, this is not direct information on the strong binding states during movement in the motility assay.

One possible explanation for the reduction of *E93K in vitro* motility is that the actual stroke size mediated by an *E93K* crossbridge may be smaller than that of WT. However, Molloy *et al.* (1995), (and in preparation), have demonstrated that the working stroke for single *E93K* and WT crossbridges is 5.5nm, (see section 1.6.7). However, the fact that the optical trap measurements were made from a single crossbridge under unloaded conditions does not reflect the circumstances pertaining during *in vitro* motility, where many crossbridges may produce a partial load on the actin filament. This leads to the proposal that if the working stroke of a single crossbridge was measured under partially loaded conditions, a reduction in its size may become apparent.

Using an optical trap to measure the force of a single crossbridge under strain, a situation that is more representative of conditions in the motility assay, Molloy (unpublished) have shown that a single *E93K* crossbridge can produce only 75% of the force generated by a WT crossbridge. The reduction in force production under load suggests that a reduced *E93K* crossbridge stiffness may play an important role in filament velocity determination.

Residue E93 lies in the proposed secondary actomyosin contact site which is thought to stabilise the binding of a single myosin head to two adjacent actin monomers. The *E93K* mutation may weaken this stabilising component such that the subsequent

overall strong actomyosin binding is reduced. Upon tension generation, an increased crossbridge compliancy may lead to the inefficient transmission of force, and subsequently, a smaller working stroke. This compliancy could be manifested in a slipping of the strong hydrophobic contacts upon the commencement of the power stroke, or alternatively, a premature dissociation of actomyosin upon the onset of the power stroke which is facilitated by the loss of the secondary contact upon tension generation, (see figure 5.16).

One caveat in this theory reflects the behaviour of the secondary myosin binding mutation, *E99A/E100A* in yeast (Miller and Reisler, 1995). This does not introduce a compliance into its crossbridge since it displays WT filament velocities in the presence of methylcellulose. This difference could be a consequence of a charge neutralisation in the yeast actin gene imposing less severe effects upon the actomyosin interaction than a charge reversal in the *Drosophila Act88F* gene.

Unlike *E93K*, the *Dictyostelium 15* reversal mutation *E99H/E100H* (Johara *et al.*, 1993) did not appear to lose its weak binding capacity during *in vitro* motility. Nevertheless, this secondary binding mutation exhibited a reduced filament velocity during the motility assay which may also implicate an increased crossbridge compliance. Both these mutations therefore predict that the loop 91-100 on actin is involved in a secondary contact with the myosin head that stabilises the overall strong binding complex such that efficient force transmission can be mediated.

The *in vitro* motility assays are valuable tools that are used to assess aspects of the actomyosin interactions of modified actins and myosins. Since these assays represent movement mediated by actin and myosin alone, they enable an investigation into the details of the mechanochemical transduction process without complications that are due to the effects of accessory thick or thin filament associated proteins. Although the motility assay is not entirely representative of the situation seen in muscle or other actomyosin processes *in vivo*, it can provide valuable insights into the causes of aberrant actomyosin interactions. In the case of the *Drosophila* actin mutations studied above, the results showed that both *G368E* and *E316K*, lying outside the known

Figure 5.16. A cartoon representation of the possible action of the *E93K* crossbridge. The loss of the secondary binding upon tension generation in *E93K* postulates that the onset of the power stroke is facilitated. Subsequently, although the myosin head is proposed to undergo its normal conformational change, the increased compliancy in the *E93K* crossbridge manifests itself as a reduction in the *in vitro* filament velocity.

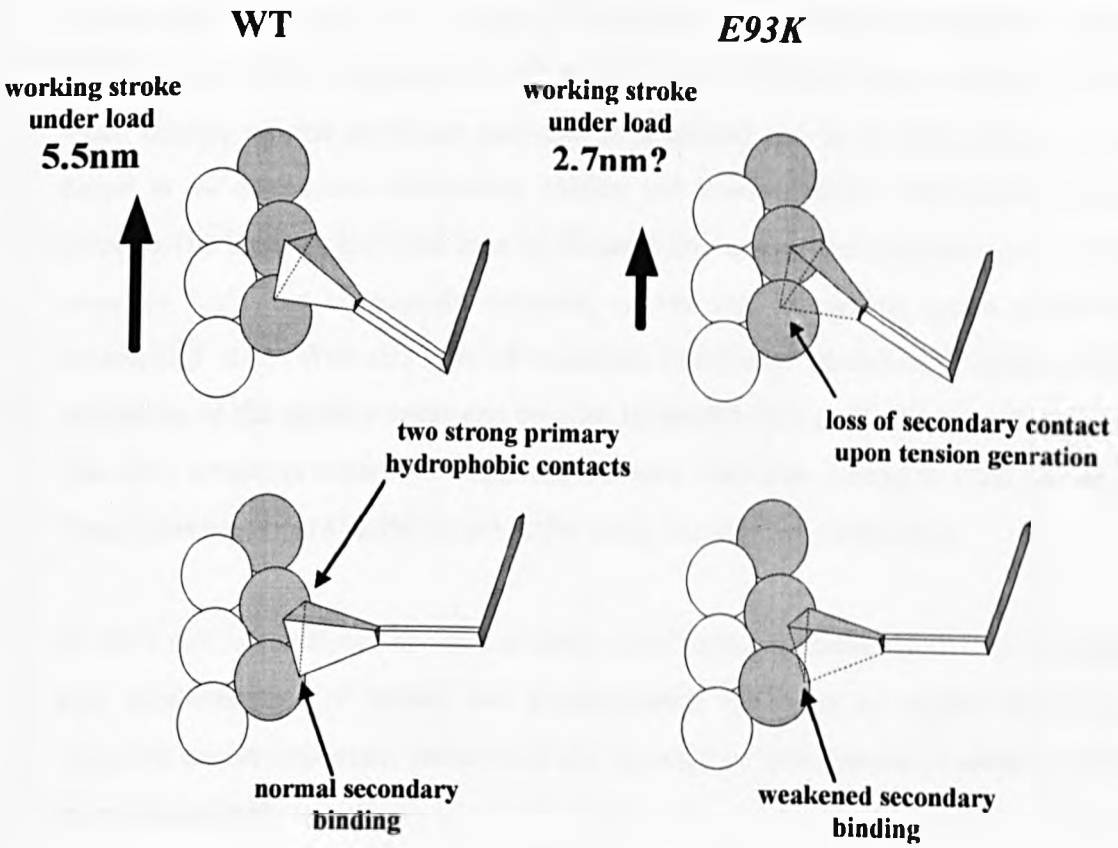

myosin binding sites, can affect the actomyosin interaction. Their effects were not as severe as those of the *E334K* and *E93K* myosin binding site mutations.

As seen from the mutant analysis in this study, the motility assay can loosely diagnose the basis for a particular actin mutant phenotype from the recognition of three different "crossbridge symptoms". For example, the first describes the actin filament wash off seen under standard conditions in the motility assay. This generally suggests that the weak binding of that particular mutation is abolished and is, in most cases, the only defect in the actomyosin interaction, (Miller and Reisler, 1995). The second indicator involves the binding, but total loss of filament movement and proposes that the actin mutation locks the actomyosin complex, or restricts its cycling up to a particular crossbridge state. With this type of mutation, copolymer studies and variation of the conditions of the motility assay can be used to identify this particular crossbridge state. The third symptom regards the reduced filament velocities during *in vitro* movement. These phenotypes are harder to prescribe using the motility assay alone.

In vitro motility analyses at various assay conditions, in conjunction with the optical trap measurements of forces and displacements mediated by single crossbridges, therefore enable important features of the actomyosin interactions of these mutations to be ascertained.

CHAPTER SIX: SUMMARY

One of the major aims of present day muscle and motor protein research is to elucidate the mechanisms of the mechanochemical transduction that drives eukaryotic motile processes. In the past, this has been tackled through the biochemical and kinetic characterisation of muscles and muscle proteins. Mutational analysis is an important tool for investigating the functional interactions and cellular roles of the myosin motor protein and its complementary cytoskeletal polymer, actin. One of the main aims of this thesis was to develop and use new technologies to extend the knowledge of existing ACT88F *Drosophila* actin mutations in terms of their actomyosin behavior.

Drosophila melanogaster represents a unique system for studying the actomyosin mechanism, allowing the examination of *in vivo* effects of actin mutations at the striated muscle level. A number of site-directed mutants in the IFM specific *Act88F* gene of *Drosophila* were subsequently tested for their effects upon muscle structure and function (Drummond *et al.*, 1990; 1991a; Sparrow *et al.*, 1991a; 1991b; 1992). Although these *in vivo* phenotypes were partially complemented by *in vitro* mutant G-actin ligand binding and conformational studies (Drummond *et al.*, 1991a; 1991b; 1992; Hennessey *et al.*, 1991) a more extensive *in vitro* biochemical analysis, in terms of F-actin based and actomyosin kinetic studies, has to be performed so that the role of actin in mechanochemical transduction can be investigated.

The traditional *E. coli* and *Saccharomyces cerevisiae* protein expression systems are not entirely suited for the generation of recombinant actin (Frankel and Leinwand, 1990; Huffaker *et al.*, 1987). An attempt was made to express milligram quantities of recombinant ACT88F in *Saccharomyces cerevisiae* according to the method of Karlsson (1988). Although both mutant and WT forms of *Drosophila* actin could be generated, the yields were not great enough to merit further exploitation of this system.

The next effort to obtain pure ACT88F involved isolation from the host organism. A number of researchers use this approach to isolate endogenous mutant actins from

hosts such as *Saccharomyces* and *Dictyostelium* (Cook *et al.*, 1991; 1992; Sutoh *et al.*, 1991; Johara *et al.*, 1991). With the exception of yeast, this route is fraught with complications that involve the separation of the actin of interest from the other endogenous isoforms upon the basis of charge differences.

Since ACT88F *mod*$^+$ is the most basic of the *Drosophila* actin isoforms (Mahaffey *et al.*, 1995), anion exchange chromatography was used to isolate milligram quantities of pure ACT88F from a mixed actin preparation from 10,000 flies, (10g). One unexpected drawback was indirectly discovered by the increased sensitivity of this chromatographic procedure. Where peak B, (see section 4.2.3.1), analogous to a type III actin spot on a 2D gel (Fyrberg *et al.*, 1983), was thought to contain ACT88F *mod*$^+$ alone, an extra actin isoform, encoded by a gene other than *Act88F*, was also present. This actin is predicted to be the ACT5C isoform upon the basis of its primary sequence, (see table 4.1), and represented about 10% of the total actin in peak B of an *E93K* chromatographic separation. Despite this "contamination", the recovery of large yields of a relatively pure ACT88F preparation using anion exchange chromatography opens the way for a whole range of *in vitro* biochemical analyses of this protein and its mutant forms.

The *in vitro* motility assay (Kron and Spudich, 1986) is a relatively new addition to the arsenal of procedures used to investigate actomyosin interactions. Over the last decade, it has made major contributions in the analysis of the action of various actin mutants by allowing a direct, real-time visualisation of the movement generated by their interactions with myosin. Since motility assays require only nanogram quantities of protein, a mini-actin preparation protocol was developed to isolate the pure ACT88F content of ten pairs of *Drosophila* flight muscles. This material was sufficient for many motility assays and was used for the extensive *in vitro* motility characterisation of four *Drosophila* ACT88F mutants.

The *Drosophila* system is a powerful alternative to yeast and *Dictyostelium* because the effects of actin mutations upon muscle assembly, structure and function can also be determined. Its main drawback regards the more complex procedures necessary for the

transformation of mutant alleles into its genome. The subsequent recovery and mapping of introduced mutations in this organism also involves a longer time-scale than the yeast systems of Johannes and Gallwitz (1991) and Wertman *et al.* (1992) where the rapid screening for actin mutants with disruptive phenotypes is possible. Additionally, although the cultivation of thousands of flies for actin preparations is relatively simple and inexpensive, the major disadvantage regards the labour intensive management of the flies. Despite these limitations however, once a mutation has been introduced into flies, it can be extensively and easily characterised in terms of its *in vitro* and *in vivo* behaviour.

The role of actin in actomyosin motor function represents just one of its many biological interactions within the eukaryotic cell. A lot of work initially attempted to map the actomyosin binding sites through cross-linking, biochemical and immunochemical studies (Sutoh *et al.*, 1982; Das Gupta and Reisler 1992). These subsequently implicated the involvement of sequences 1-7, 18-29 and 90-101 in the actin monomer. Sutoh *et al.* (1991) assessed the role of the N-terminal component in actomyosin function by looking at the effects of N-terminal *Dictyostelium* actin mutants upon the myosin ATPase activity and *in vitro* motility. This study was one of the first investigations that combined mutagenic and *in vitro* motility approaches to examine the actomyosin interaction, (see section 5.1.5).

The rapid expansion of structural information over the last few years, which includes the solution of the crystal structures for actin (Kabsch *et al.* 1990; McLaughlin *et al.*, 1993; Schutt *et al.*, 1993), S1 (Rayment *et al.*, 1993a; Xie *et al.*, 1994), the F-actin filament model (Holmes *et al.*, 1990; Lorenz *et al.*, 1993) and the S1.F-actin complex (Rayment *et al.*, 1993b; Schröeder *et al.*, 1993) has enabled molecular geneticists to find their bearings, so to speak, and led to the generation of rational mutations that will be used to answer specific questions about the mechanism of mechanochemical coupling.

Although the structural data do not specify the exact interactions involved in the actomyosin interface, the routine *in vitro* motility analysis of actin mutations is now

used to identify regions of actin that interact with the myosin motor (Aspenström *et al.*, 1992a; Sutoh *et al.*, 1991; Cook *et al.*, 1993; Johara *et al.*, 1993; Miller and Reisler, 1995), (see section 5.1.5). The double mutants at residues E99/E100 (Johara *et al.*, 1993; Miller *et al.*, 1995) lie in a loop that includes the *E93K* mutation. These mutations all show similarites in their behaviour during the *in vitro* motility assay, confirming that the loop 91-100 is probably involved in a secondary interaction with myosin.

As well as corroborating the electrostatic myosin binding sites previously established by biochemical analyses, *in vitro* motility assays can use mutants to probe other regions of actin involved in actomyosin motor functions. This was highlighted in this study using a mutation, *E334K*, that is thought to reside in one of the strong stereo-specific myosin contacts (Rayment *et al.*, 1993b) and had a dramatic effect upon the actomyosin force generation. Although the crystal structures allow molecular geneticists to almost pinpoint residues which, when mutated, will have an effect upon actomyosin function, there are cases where actin mutations affect functions by long range conformational effects upon distantly located ligand binding sites (Drummond *et al.*, 1992). This was partially seen in this study with the mild effects upon *in vitro* motile behavior of the *E316K* ACT88F mutant.

The *in vitro* motility of myosin mutations in *Dictyostelium discoideum* is also used to investigate actomyosin-based mechanochemical transduction. *Dictyostelium* is an example of a powerful system that has been used to study the *in vivo* and *in vitro* effects of both *Dictyostelium* actin and myosin mutants (Sutoh *et al.*,1991; Johara *et al.*, 1993; De Lozanne and Spudich, 1987; Manstein *et al.*, 1989; Kubalek *et al.*, 1992; Itakura *et al.*, 1993; Ruppel *et al.*, 1994; Uyeda *et al.*, 1993; 1994). The more recent *Dictyostelium* myosin mutations were engineered specifically to investigate features of the Rayment *et al.* (1993b) structural model for muscle contraction. The proposal that the myosin molecule acts as a lever arm that drives movement by swinging through an arc of approximately 5nm was investigated by performing the *in vitro* motility of a genetically shortened myosin fragment. Analysis of these truncated myosins revealed

drastic reductions in actin filament velocity which corroborated the Rayment *et al.* model (Itakura *et al.*, 1993; Uyeda *et al.*,1993).

Additional studies probed the effects of the myosin surface loop, 626-647, in determining the actin activated ATPase activity (Uyeda et al., 1994). By substituting this *Dictyostelium* surface loop with the corresponding loops from skeletal muscle, α-cardiac, β-cardiac and chicken smooth muscle myosin, the ATPase activities of the subsequent chimaeric myosins were seen to reflect those of the myosin species from which the inserts were derived. This combination of *in vitro* motility, mutagenesis and structural biology used in the *Dictyostelium* system highlights the great strength of this organism for the study of the myosin molecular motor.

Considerable advances within the field of actomyosin over the last two years concern the advent of laser trap technology which provides the exciting opportunity to witness for the first time, forces and displacements that are produced by single crossbridge interactions (Finer *et al.*, 1994; Ishijima *et al.*, 1994; Molloy *et al.*, in press). The strength of applying *in vitro* motility and optical traps to actin and myosin mutations was demonstrated in the *E93K* mutant investigation. The fact that this mutant actin washes off under standard assay conditions and moves at reduced velocities in the motility assay, combined to its normal working storke size and reduced force under load in optical trap measuements, predicts that it introduces a compliancy into the crossbridge. Future mutagenic investigations using the optical trap will hopefully provide valuable insights into the mechanism of actomyosin based movement.

The aims of this thesis have been fullfilled. Through the development of the mini-actin preparation from IFMs, the exciting effects of two ACT88F mutations using the motility assay have been identified. Additionally, the ability to isolate almost pure ACT88F from whole flies makes *Drosophila* a powerful organism for the study of mutant actins *in vitro* as well as its previous unique strengths for the study of mutant muscle fibres.

REFERENCES

Abate C., Luk D., Gentz R., Ranscher III F.J. & Curran T. (1990) Expression and purification of the leucine zipper and DNA-binding domains of *fos* and *jun*: both *fos* and *jun* contact DNA directly. *Proc. Natl. Acad. Sci. USA* **87**, 1032-1036.

Adams R.J. and Pollard T.D. (1986) Propulsion of organelles isolated from *Acanthamoeba* along actin filaments by myosin I. *Nature* (*London*) **322**, 754-756.

Adelstein R.S. & Eisenberg E. (1980) Regulation and kinetics of the actin-myosin-ATP interaction. *Ann Rev. Biochem.* **49**, 921-956.

Aebi U., Millonig R., Salvo H. & Engel A. (1986) The three-dimensional structure of the actin filament revisited. *Ann. N.Y. Acad. Sci.* **483**, 100-119.

Aktories K. (1989) ADP-ribosylation of actin by Clostridial toxins. *J. Cell Biol.* **109**, 1385-1387.

Aktories K. (1990) ADP-ribosylation of actin. *J. Mus. Res. Cell Motility.* **11**, 95-97.

Alonso S., Minty A., Bourlet Y. & Buckingham M. (1986) Comparison of three actin-coding sequences in the mouse; evolutionary relationships between the actin genes of warm-blooded vertebrates. *J. Mol. Evol.* **23**, 11-22.

Anson M., Drummond D.R., Geeves M.A., Hennessey E.S., Ritchie M.D. & Sparrow J.C. (1995) Actomyosin kinetics and *in vitro* motility of wild-type *Drosophila* actin and the effects of two mutations in the *Act88F* gene. *Biophys. J.* **68**, 1991-2003.

Applegate D. & Reisler E. (1983) Protease-sensitive regions in myosin subfragment 1. *Proc. Natl. Acad. Sci. USA* **80**, 7109-7112.

Armatruda J.F., Cannon J.F., Tatchell K., Hug C. & Cooper J.A. (1990) Disruption of the actin cytoskeleton in yeast capping protein mutants. *Nature* **344**, 352-354.

Aspenström P. & Karlsson R. (1991) Interference with myosin subfragment-1 binding by site-directed mutagenesis of actin. *Eur. J. Biochem.* **200**, 35-41.

Aspenström P., Engkvist H., Lindberg U. & Karlsson R. (1992a) Characterization of yeast-expressed beta-actins, site-specifically mutated at the tumor-related residue Gly245. *Eur. J. Biochem.* **207**, 315-320.

Aspenström P., Lindberg U. & Karlsson R. (1992b) Site-specific amino-terminal mutants of yeast-expressed beta-actin. Characterization of the interaction with myosin and tropomyosin. *FEBS Letts.* **303**, 59-63.

Aspenström P., Schutt C.E., Lindberg U. & Karlsson R. (1993) Mutations in beta-actin: influence on polymer formation and on interactions with myosin and profilin. *FEBS Letts.* **329**, 163-170.

Ball E., Karlik C.C., Beall C.J., Saville D., Sparrow J.C., Bullard B. & Fyrberg E.A. (1987) Arthrin, a myofibrillar protein of insect flight muscle, is an actin-ubiquitin conjugate. *Cell* **51**, 221-228.

Barany M. and Podolsky R.J. (1967) ATPase activity of myosin correlated with speed of muscle shortening. *J. Gen. Physiol.* **50**, 197-218.

Bennetzen J.L. & Hall B.D. (1982) Codon selection in yeast. *J. Biol. Chem.* **257**, 3026-3031.

Bertrand R., Chaussepeid P., Audemard E. & Kassab R. (1989) Functional characterization of skeletal F-actin labelled on the NH_2-terminal segment of residues 1-28. *Eur. J. Biochem.* **181**, 747-754.

Birnboim H.C. (1983) A rapid alkaline extraction method for the isolation of plasmid DNA. *Meths. Enzymol.* **100**, 243-255.

Bloom G.S., Wagner M.C., Pfister K.K. & Brady S.T. (1988) Native structure and physical properties of bovine brain kinesin and identification of the ATP-binding subunit polypeptide. *Biochemistry* **27**, 3409-3416.

Bloom G.S. and Endow S.A. (1994) *Protein profile*, Motor Proteins **1**. Kinesins.

Bork P., Sander C. & Valencis A. (1992) An ATPase domain common to prokatyotic cell cycle proteins, sugar kinases, actin, and hsp70 heat shock proteins. *Proc. Natl. Acad. Sci. USA.* **89**, 7290-7294.

Bremer A., Millonig R.C., Sutterlin R., Engel A., Pollard T. & Aebi U. (1991) The structural basis for the intrinsic disorder of the F-actin filament: the lateral slipping model. *J. Cell Biol.* **115**, 689-703.

Bremer A. & Aebi U. (1992) The structure of the F-actin filament and the actin molecule. *Curr. Opin. Cell Biol.* **4**, 20-26.

Brenner B., Schoenberg M., Chalovich J.M., Greene L.E. & Eisenberg E. (1982) Evidence for cross-bridge attachment in relaxed muscle at low ionic strength. *Proc. Natl. Acad. Sci. USA.* **79**, 7288-7291.

Bullard B., Bell J., Craig R. & Leonard K. (1985) Arthrin: a new actin-like protein in insect flight muscle. *J. Mol. Biol.* **182**, 443-454.

Burke M. & Reisler E. (1977) Effect of nucleotide binding on the proximity of the essential sulphydryl groups of myosin: chemical probing of movement of residues during conformational transitions. *Biochemistry* **16**, 5559-5565.

Burton K. (1992) Myosin step size: estimates from motility assays and shortening of muscle. *J. Mus. Res. Cell Motil.* **13**, 590-607.

Carlier M. Pantaloni D. & Korn E.D. (1984) Steady state length distribution of F-actin under controlled fragmentation and mechanism of length redistribution following fragmentation. *J. Biol. Chem.* **259**, 9987-9991.

Carlier M.F., Pantaloni D. & Korn E.D. (1986) Fluorescence measurements of the binding of cations to high-affinity and low-affinity sites on ATP G-actin. *J. Biol. Chem.* **261**, 10778-10784.

Carlier M.F., Pantaloni D. & Korn E.D. (1987) The mechanism of ATP hydrolysis accompanying the polymerization of Mg-actin and Ca-actin. *J. Biol. Chem.* **262**, 3052-3059.

Carlier M.F. (1989) Role of nucleotide hydrolysis in the dynamics of actin filaments and microtubules. *Int. Rev. Cytol.* **115**, 139-170.

Carlier M. (1991) Actin: Protein structure and filament dynamics. *J. Biol. Chem.* **266**, 1-4.

Chausspied P., Morales M.F. & Kassab R. (1988) The myosin SH2-50KDa fragment crosslink: location and consequences. *Biochemistry* **27**, 1778-1785.

Chen J.C.W. & Kamiya N. (1975) Localisation of myosin in internodal cell of *Nitella* as suggested by differential treatment with N-ethyl-maleimide. *Cell Struct. Func.* **1**, 1-9.

Chen X., Cook R.K. & Rubenstein P.A. (1993) Yeast actin with a mutation in the "hydrophobic plug" between domains 3 and 4 (*L266D*) displays a cold-sensitive polymerization defect. *J. Cell Biol.* **123**, 1185-1195.

Chen X. & Rubenstein P.A. (1995) A mutation in an ATP-binding loop of *Saccharomyces cerevisiae* actin (*S14A*) causes a temperature-sentitive phenotype *in vivo* and *in vitro*. *J. Biol. Chem.* **270**, 11406-11414.

Cheney R.E. & Mooseker M.S. (1992) Unconventional myosins. *Curr. Opin. Cell Biol.* **4**, 27-35.

Clayton J.D. (1994) Thesis, University of York.

Collins K. & Matsudaira P. (1991) Differential regulation of vertebrate myosin I and II. *J. Cell Sci.* **14** (suppl), 11-16.

Cook R.K., Sheff D.R. & Rubenstein P.A. (1991) Unusual metabolism of the yeast actin amino terminus. *J. Biol. Chem.* **5**, 16825-16833.

Cook R.K., Blake W.T. & Rubenstein P.A. (1992) Removal of the amino-terminal acidic residues of yeast actin: studied *in vitro* and *in vivo*. *J. Biol Chem.* **267**, 9430-9436.

Cook R.K., Root D., Miller C., Reisler E. & Rubenstein P.A. (1993) Enhanced stimulation of myosin subfragment 1 ATPase activity by addition of negatively charged residues to the yeast actin NH_2 terminus. *J. Biol. Chem.* **268**, 2410-2415.

Cooke R. & Bialek W. (1979) Contraction of glycerinated muscle fibers as a function of the ATP concentration. *Biophys. J.* **28**, 241-258.

Cooke R. (1986) The mechanism of muscle contraction. *C.R.C. Crit. Rev. Biochem.* **21**, 53-118.

Craig R., Szent-Gyorgyi A.G., Beese L., Flicker P., Vibert P. & Cohen C. (1980) Electron microscopy of thin filaments decorated with a Ca^{2+}-regulated myosin. *J. Mol. Biol.* **140**, 35-55.

Craig R., Greene L.E. & Eisenberg E. (1985) Structure of the actin-myosin complex in the presence of ATP. *Proc. Natl. Acad. Sci. USA* **82**, 3247-3251.

Cripps R.M., Ball E., Stark M., Lawn A. & Sparrow J.C. (1994) Recovery of dominant, autosomal flightless mutants of *Drosophila melanogaster* and identification of a new gene required for normal muscle structure and function. *Genetics* **137**, 151-164.

Cupples C.G. & Pearlman R.E. (1986) Isolation and characterisation of the actin gene from *Tetrahymena thermophila*. *Proc. Natl. Acad. Sci. USA* **83**, 5160-5164.

DasGupta G. & Reisler E. (1992) Actomyosin interaction in the presence of ATP and the N-terminal segment of actin. *Biochemistry* **31**, 1836-1841.

De Lozanne A. & Spudich J.A. (1987) Disruption of the *Dictyostelium* myosin heavy chain gene by homologous recombination. *Science* **236**, 1086-1091.

Drummond D.R., Peckham M., Sparrow J.C. & White D.C.S. (1990) Alteration in crossbridge kinetics caused by mutations in actin. *Nature* (*London*) **348**, 440-442.

Drummond D.R., Hennessey E.S. & Sparrow J.C. (1991a) Characterisation of missense mutations in the *Act88F* gene of *Drosophila melanogaster*. *Mol. gen. Genet.* **226**, 70-80.

Drummond D.R., Hennessey E.S. & Sparrow J.C. (1991b) Stability of mutant actins. *Biochem. J.* **274**, 301-303.

Drummond D.R., Hennessey E.S. and Sparrow J.C. (1992) The binding of mutant actins to profilin, ATP and DNase I. *Eur J. Biochem.* **209**, 71-179.

Egelman E.H., Francis N. & DeRosier D.J. (1982) F-actin is a helix with a random variable twist. *Nature* **298**, 131-135.

Egelman E.H. (1985) The structure of F-actin. *J. Mus. Res. Cell Motil.* **6**, 129-151.

Egelman E.H. (1992) Two key questions raised by an atomic model for F-actin. *Curr. Opin. Struct. Biol.* **2**, 286-292.

Egelman E.H. & DeRosier D.J. (1992) Image analysis shows that variations in actin crossover spacings are random, not compensatory. *Biophys. J.* **63**, 1299-1305.

Eisenberg E. & Green L.E. (1980) The relation of muscle biochemistry to muscle physiology. *Ann. Rev. Physiol.* **42**, 293-309.

Elliot A. & Offer G. (1978) Shape and flexibility of the myosin molecule. *J. Mol. Biol.* **123**, 505-519.

Endow S.A. & Hatsumi M. (1991) A multimember kinesin gene family in *Drosophila*. *Proc. Natl. Acad. Sci. USA* **88**, 4424-4427.

Ernst J.F. and Kawashima E. (1988) Variations in codon usage are not correlated with heterologous gene expression in *Saccharomyces cerevisiae* and *Eschericia coli*. *J. Biotech.* **7**, 1-10.

Faulstich H., Zobeley S., Rinnerthaler G. & Small J.V. (1988) Fluorescent phallotoxins as probes for filamentous actin. *J. Mus. Res. Cell Motility*. **9**, 370-383.

Faulstich H., Zobeley S., Heintz D. & Drewes G. (1993) Probing the phalloidin binding site of actin. *FEBS Letts* **318**, 218-222.

Files J.G., Carr S. & Hirsh D. (1983) Actin gene family of *Caenorhabditis elegans*. *J. Mol. Biol.* **164**, 355-375.

Finer J.F., Simmons R.M. & Spudich J.A. (1994) Single myosin molecule mechanics: Piconewton forces and nanometre steps. *Nature* **368**, 113-119.

Fisher A.J., Smith C.A., Thoden J., Smith R., Sutoh K., Holden H.M. & Rayment I. (1995) Structural studies of myosin:nucleotide complexes: A revised model for the molecular basis of muscle contraction. *Biophysical journal* **68**, 19s-28s.

Flaherty K. M., McKay D.B., Kabsch W. & Holmes K.C. (1991) Similarity of the three-dimensional structures of actin and the ATPase fragment of a 70-KDa heat shock cognate protein. *Proc. Natl. Acad. Sci. USA*. **88**, 5041-5045.

Frado L. & Craig R. (1992) Electron microscopy of the actin-myosin head complex in the presence of ATP. *J. Mol. Biol.* **223**, 391-397.

Frankel S., Condeelis J. & Leinwand L. (1990) Expression of actin in *E. coli*.. Aggregation, solubilization and functional analysis. *J. Biol. Chem.* **265**, 17980-17987.

Fyrberg E.A., Mahaffey J.W., Bond B.J. & Davidson, N. (1983) Transcripts of the six *Drosophila* actin genes accumulate in a stage and tissue-specific manner. *Cell* **33**, 115-123.

Gallwitz D. & Sures I. (1980) Structure of a split yeast gene in *Saccharomyces cerevisiae*. *Proc. Natl. Sci. USA*. 77, 2546-2550.

Gao Y., Thomas J.O., Chow R.L., Lee G.H. & Cowan N.J. (1992) A cytoplasmic chaperonin that catalyses beta-actin folding. *Cell* **69**, 1043-1050.

Geeves M.A. (1991) The dynamics of actin and myosin association and the crossbridge model of muscle contraction. *Biochem. J.* **274**, 1-14.

Gershman L.C., Selden L.A. & Estes J.E. (1986) Higher affinity binding of divalent cation to actin monomer is much stronger than previously reported. *Biochem. Biophys. Res. Comm.* **135**, 607-614.

Goldman Y.E. (1987) Kinetics of actomyosin ATPase in muscle fibers. *Ann. Rev. Physiol.* **49**, 637-654.

Goodson H.V. & Spudich J.A. (1993) Molecular evolution of the myosin family: Relationships derived from comparisons of amino acid sequences. *Proc. Natl. Acad. Sci.* **90**, 659-663.

Gulati J. & Podolsky R.J. (1981) Isotonic contraction of skinned muscle fibers on a slow time base. *J. Gen. Physiol.* **78**, 233-257.

Haarer B.K., Lillie S.H., Adams A.E.M., Magdolen V., Bandlow W. & Brown S.S. (1990) Purification of profilin from *Saccharomyces cerevisiae* and analysis of profilin deficient cells. *J. Cell Biol.* **110**, 105-114.

Hammer J.A. & Jung G. (1991) Molecular cloning of myosin I heavy chain genes. *J. Cell Sci.* **14** (suppl), 37-40.

Hanahan D. (1985) Transformations. *DNA Cloning vol.* I: a practical approach. IRL Press, Oxford, 109-135.

Harada Y., Noguchi A., Kishino A. & Yanagida T. (1987) Sliding movement of single actin filaments over one-headed myosin filaments. *Nature* **326**, 805-808.

Harada Y. & Yanadiga T. (1988) Direct observation of molecular motility by light microscopy. *Cell Motil. Cytoskeleton* **10**, 71-76.

Harada Y., Sakurada K., Aoki T., Thomas D.D. & Yanagida T. (1990) Mechanochemical coupling in actomyosin energy transduction studied by *in vitro* movement assay. *J. Mol. Biol.* **216**, 49-68.

Harrington W.F. & Rogers M.F. (1984) Myosin. *Ann. Rev. Biochem.* **53**, 35-73.

Hennessey E.S., Drummond D.R. & Sparrow J.C. (1991) Post-translational processing of the amino terminus affects actin function. *Eur. J. Biochem.* **197**, 345-352.

Hennessey E.S., Drummond D.R. & Sparrow J.C. (1993) Molecular genetics of actin function. *Biochem. J.* **282**, 657-671.

Herman I.M. (1993) Actin isoforms. *Curr. Opin Cell. Biol.* **5**, 48-55.

Higashi-Fujime S. (1980) Active movement *in vitro* of bundles of microfilaments isolated from *Nitella* cell. *J. Cell Biol.* **87**, 569-578.

Higashi-Fujime S. (1982) Active movement of bundles of actin and myosin filaments from muscle: A simple model for cell motility. *Cold Spring Harbour Symp. Quant. Biol.* **46**, 69-75.

Higashi-Fujime S. (1985) Unidirectional sliding of myosin filaments along the bundle of F-actin filaments spontaneously formed during superprecipitation. *J. Cell Biol.* **101**, 2335-2344.

Hightower R.C. & Meagher R.B. (1986) The molecular evolution of actin. *Genetics* **114**, 315-332.

Hirokawa N., Pfister K.K., Yorifuji H., Wagner M.C., Brady S.T. & Bloom G.S. (1989) Submolecular domains of bovine brain kinesin identified by electron microscopy and monoclonal antibody decoration. *Cell* **56**, 867-878.

Hiromi Y. & Hotta Y. (1985) Actin gene mutations in the *Drosophila*: heat shock activation in the indirect flight muscles. *EMBO J.* **4**, 1681-1687.

Hirono M., Endoh H., Okada N., Numata O. & Watanabe Y. (1987) *Tetrahymena* actin-cloning and sequencing of the *Tetrahymena* actin gene and identification of its gene product. *J. Mol. Biol.* **194**, 181-192.

Hoekema A., Kastelein R.A., Vasser M. & De Boer H.A. (1987) Codon replacement in the *PGK* gene of *Saccharomyces cerevisiae*: experimental approach to study the role of biased codon usage in gene expression. *Mol Cell Biol.* **7**, 2914-2924.

Holmes K.C., Popp C.D., Gebhard W. & Kabsch W. (1990) Atomic model for the actin filament. *Nature* **347**, 44-49.

Holmes K.C. & Kabsch W. (1991) Muscle proteins: Actin. *Curr. Opin. Struct. Biol.* **1**, 270-280.

Homsher E., Wang F. & Sellers J.R. (1992) Factors affecting movement of F-actin filaments propelled by skeletal muscle heavy meromyosin. *J. Physiol.* **262**, C714-C723.

Honda H., Nagashima H. & Asakura S. (1986) Directional movement of F-actin *in vitro*. *J. Mol. Biol.* **191**, 131-133.

Horovitch S.J., Storti R.V., Rich A. & Pardue M.L. (1979) Multiple actins in *Drosophila melanogaster*. *J. Cell Biol.* **82**, 86-92.

Huffaker T.C., Hoyt M.A. & Botstein D.A. (1987) Genetic analysis of the yeast cytoskeleton. *Ann. Rev Gen.* **21**, 259-284.

Huxley A.F. & Niedergerke R. C. (1954) Structural changes in muscle during contraction. *Nature* **173**, 971-972.

Huxley H.E. & Hanson J. (1954) Changes in muscle during contraction and stretch and their structural interpretation. *Nature* **173**, 973-997.

Huxley H.E. (1963) Electron microscope studies on the structure of natural and synthetic protein filaments from striated muscle. *J. Mol. Biol.* **7**, 281-308.

Huxley H. E. (1969) The mechanism of muscular contraction. *Science* **164**, 1356-1366.

Huxley H.E. (1990) Sliding filaments and molecular motile systems. *J. Biol. Chem.* **265**, 8347-8350.

Hynes T.R., Block S.M., White B.T. & Spudich J.A. (1987) Movement of myosin fragments *in vitro*: Domains involved in force production. *Cell* **48**, 953-963.

Ikemura T. (1982) Correlation between the abundance of yeast transfer RNAs and the occurrence of the respective codons in protein genes. *J. Mol. Biol.* **158**, 573-597.

Ishijima A., Doi T., Sakurada K. & Yanagida T. (1991) Sub-piconewton force fluctuations of actomyosin *in vitro*. *Nature* **352**, 301-306.

Ishijima A., Harada Y., Kojima H., Funatsu T., Higuchi H. & Yanagida T. (1994) Single-molecule analysis of the actomyosin motor using nano-manipulation. *Biochem. Biophys. Res. Comm.* **199**, 1957-1063.

Itakura S., Yamakawa H., Toyoshima Y.Y., Ishijima A., Kojima T., Harada Y., Yanagida T., Wakabayashi T. & Sutoh K. (1993) Force-generating domain of myosin motor. *Biochem. Biophys. Res. Comm.* **3**, 1504-1510.

Ito H., Fukuda Y., Murata K. & Kimura A. (1983) Transformation of intact yeast cells treated with alkali cations. *J Bacteriol.* **153**, 163-168.

Johannes F.J. & Gallwitz D. (1991) Site-directed mutagenesis of the yeast actin gene: a test for function *in vivo*. *EMBO J.* **10**, 3951-3958.

Johara M., Toyoshima Y.Y., Ishijima A., Kojima H., Yanagida T. & Sutoh K. (1993) Charge-reversion mutagenesis of *Dictyostelium* actin to map the surface recognized by myosin during ATP-driven sliding motion. *Proc. Natl. Acad. Sci.* **90**, 2127-2131.

Kabsch W., Mannherz H.G., Suck D., Pai E.F. & Holmes K.C. (1990) Atomic structure of the actin:DNase I complex. *Nature* (*London*) **347**, 37-44.

Kabsch W. & Vanderkerckhove J. (1992) Structure and function of actin. *Annu Rev. Biophys. Biomol. Struct.* **21**, 49-76.

Kamiya N. & Kuroda K. (1956) Velocity distribution of the protoplasmic streaming in *Nitella* cells. *Bot. Mag.* **69**, 544-554.

Karlsson R. (1988) Expression of chicken beta-actin in *Saccharomyces cerevisiae*. *Gene* **68**, 249-257.

Karlsson R., Aspenström P.A. & Bystrom A.S. (1991) A chicken beta-actin gene can complement a disruption of the *Saccharomyces cerevisiae* ACT1 gene. *Mol. Cell Biol.* **11**, 213-217.

Kersey Y.M., Helper P.K., Palevitz B.A. & Wessels N.K. (1976) Polarity of actin filaments in *Characean* algae. *Proc. Natl. Acad. Sci. USA* **73**, 165-167.

King P.V. & Blakesey R.W. (1986) Optimising DNA ligations for transformation. *BRL Focus* **8**, 397-406.

Kingsman S.M. & Kingsman A.J., Dobson M.J., & Roberts N.A. (1985) Heterologous gene expression in *Saccharomyces cerevisiae*. *Biotech. and Genetic Engineering reviews* **3**, 377-416.

Kinosita K., Ishiwata S., Yoshimura H., Asai H. & Ikegami A. (1984) Submicrosecond and microsecond rotational motions of myosin head in solution and in myosin synthetic filaments as revealed by time-resolved optical anisotropy decay measurements. *Biochemistry* **23**, 5963-5975.

Kishino A. & Yanagida T. (1988) Force measurements by micromanipulation of a single actin filament by glass needles. *Nature* **334**, 74-76.

Korn E.D. (1982) Actin polymerization and its regulation by proteins from nonmuscle cells. *Physiol. Rev.* **62**, 672-737.

Kozak M. (1984) Compilation and analysis of sequences upstream from the translational start site in eukaryotic messenger RNAs. *Nucl. Acid Res.* **12**, 857-872.

Kron S.J. & Spudich J.A. (1986) Fluorescent actin filaments move on myosin fixed to a glass surface. *Proc. Natl. Acad. Sci. USA* **83**, 6272-6276.

Kron S.J., Drubin D.G., Botstein D. & Spudich J.A. (1992) Yeast actin filaments display ATP-dependent sliding movement over surfaces coated with rabbit muscle myosin. *Proc. Natl. Acad. Sci. USA* **89**, 4466-4470.

Kubalek F.W., Uyeda T.Q.P. & Spudich J.A. (1992) A *Dictyostelium* myosin II lacking a proximal 58-kD portion of the tail is functional *in vivo* and *in vitro*. *Mol. Biol. Cell* **3**, 1455-1462.

Kunkel T.A. (1985) Rapid and efficient site-specific mutagenesis without phenotypic selection. *Proc. Natl. Acad. Sci. USA* **82**, 488-492.

Kuznetsov S.A., Langford G.M., Weiss D.M. (1992) Actin-dependent organelle movement in squid axoplasm. *Nature* **356**, 722-725.

Kyrtatas V. (1987) Thesis, University of York.

Laemmli U.K. (1970) Cleavage of structural proteins during the assembly of the head of bacteriophage T4. *Nature* (*London*) **227**, 680-685.

Lampson G.P. & Tytell A.A. (1965) A simple method for estimating isoelectric points. *Anal. Biochem.* **11**, 374-377.

Lang. A.B., Wyss C. & Eppenberger H.M. (1981) Lack of actin III in fibrillar flight muscle of flightless *Drosophila* mutant *raised. Nature* **291**, 506-508.

Lazarides E. & Lindberg U. (1974) Actin is the naturally occuring inhibitor of deoxyribonuclease I. *Proc Natl. Acad. Sci. USA* **71**, 4742-4746.

Lillie S.H. & Brown S.S. (1992) Suppression of a myosin defect by a kinesin-related gene. *Nature* **356**, 358-361.

Liu Z., Zhu Z., Roberg K., Faras A.J., Guise K.S., Kapuscinski A.R. & Hackett P.B. (1989) The beta-actin gene of carp (*Ctenopharyngodon idella). Nuc. Acids Res.* **17**, 5850.

Lorenz M., Popp D. & Holmes K.C. (1993) Refinement of the F-actin model against X-ray fiber diffraction data by the use of a directed mutation algorithm. *J. Mol. Biol.* **234**, 826-836.

Lowey S. & Cohen C. (1962) Studies on the structure of Myosin. *J. Mol.Biol.* **4**, 293-308.

Lowey S., Cohen C., Weeds A.G. & Baker H. (1969) Substructure of the myosin molecule. *J. Mol. Biol.* **42**, 1-29.

Lymn R.W. & Taylor E.W. (1971) Mechanism of adenosine triphosphate hydrolysis by actomyosin. *Biochemistry* **10**, 4617-4624.

Magdolen V., Drubin D.G., Mages G. & Bandlow W. (1993) High levels of profilin suppress the lethality caused by overproduction of actin in yeast cells. *FEBS letts.* **1**, 41-47.

Mahaffey J.W., Coutu M.D., Fyrberg E.A. & Inwood W. (1985) The flightless *Drosophila* mutant *raised* has two distinct genetic lesions affecting accumulation of myofibrillar proteins in flight muscles. *Cell* **40**, 101-110.

Maniatis T., Fritsch E.F. & Sambrook J. (1982) Molecular cloning a laboratory manual. *Cold Spring Harbour Laboratory.*

Manstein D.T., Ruppel K.M. & Spudich J.A. (1989) Expression and characterization of a functional myosin head fragment in *Dictyostelium discoideum. Science* **240**, 656-658.

Margossian S.S. & Lowey S. (1982) Preparation of myosin and its subfragments from rabbit skeletal muscle. *Methods Enzymol.* **85**, 55-71.

McLaughlin P.J., Gooch J.T., Mannherz H.G., & Weeds A.G. (1993) Structure of the gelsolin segment 1-actin complex and the mechanism of filament severing. *Nature* (*London*) **364**, 685-692.

McNally E., Sohn R., Frankel S. & Leinwand L. (1991) Expression of myosin and actin in *Escherichia coli. Meths Enzymol.* **196**, 368-389.

Meagher R.B. (1991) Divergence and differential expression of actin gene families in higher plants. *Int. Rev. Cytol.* **125**, 139-163.

Mellor J., Dobson M.J., Roberts N.A., Kingsman A.M. & Kingsman S.M. (1985) Factors affecting heterologous gene expression in *Saccharomyces cerevisiae*. *Gene* **32**, 215-226.

Miller C.J. & Reisler E. (1995) Role of charged amino acid pairs in subdomain-1 of actin in interactions with myosin. *Biochemistry* **34**, 2694-2700.

Milligan R. A. & Flicker P. F. (1987) Structural relationships of actin, myosin, and tropomyosin revealed by cryo-electron microscopy. *J. Cell Biol.* **105**, 29-39.

Milligan R.A., Whittaker M. & Safer D. (1990) Molecular structure of F-actin and location of surface binding sites. *Nature* (*London*) **348**, 217-221.

Miyanishi T., Toyoshima C., Wakabayashi T. & Matsuda G. (1988) Electron microscopic study on the location of 23 kDa and 50 kDa fragments in skeletal myosin head. *J. Biochem.* **103**, 458-462.

Molloy J.E., Burns J.E., Sparrow J.C., Tregear R.T., Kendrick Jones J. & White D.C.S. (1995) Single-molecule mechanics of heavy meromyosin and S1 interacting with rabbit or *Drosophila* actins using optical tweezers. *Biophys. J.* **68**, 298s-305s.

Moore P.B., Huxley H.E. & DeRosier D.J. (1970) Three-dimensional reconstruction of F-actin, thin filaments and decorated thin filaments. *J. Mol. Biol.* **50**, 279-295.

Moos C. (1973) Actin activation of heavy meromyosin and subfragment-1 ATPases; Steady state kinetics studies. *Cold Spring Harbour Symp. Quant. Biol.* **37**, 137-143.

Mooseker M. (1993) A multitude of myosins. *Current Biology* **3**, 245-248.

Mornet D., Bertrand R., Pantel P., Audemard E. & Kassab R. (1981) Structure of the Actin-Myosin interface. *Nature* **292**, 301-306.

Muller C.W. & Schultz G.E. (1992) Structure of the complex between adenylate kinase from *Escherichia coli* and the inhibitor Ap5A refined at 1.9Å resolution. *J. Mol. Biol.* **224**, 159-177.

Nagashima H. (1986) Active movement of synthetic filaments observed by dark-field light microscopy. *J. Biochem.* **100**, 1023-1029.

Ng R. & Abelson J. (1980) Isolation and sequence of the gene for actin in *Saccharomyces cerevisiae. Proc. Natl. Acad. Sci. USA* **77**, 3912-3916.

Novick P. & Botstein D. (1985) Phenotypic analysis of temperature sensitive yeast actin mutants. *Cell* **40**, 405-416.

O' Farrel P.H. (1975) High resolution two-dimensional electrophoresis of proteins. *J. Biol. Chem.* **250**, 4007-4021.

Pai E.F., Krengel U., Petsko G.A., Goody R.S., Kabsch W. & Wittinghofer F. (1990) Refined structure of the triphosphate conformation of *H-ras-p21* at 1.35Å resolution: implications for the mechanism of GTP hydrolysis. *EMBO J.* **9**, 2351-2359.

Pardee J.D. & Spudich J.A. (1982) Purification of muscle actin. *Meth. Cell Biol.* **24**, 271-289.

Pardo J.V., Pittenger M.F. & Craig S.W. (1983) Subcellular sorting of isoactins-selective association of gamma actin with skeletal muscle mitochondria. *Cell* **32**, 1093-1103.

Pemrick S. & Weber A. (1976) Mechansim of inhibition of relaxation by N-ethyl maleimide treatment of myosin. *Biochemistry* **15**, 5193-5198.

Pharmacia handbook, Anion Exchange chromatography.

Pollard T.D. & Korn E.D. (1973) *Acanthamoeba* myosin I. Isolation from *Acanthamoeba castellanii* of an enzyme similar to muscle myosin. *J. Biol. Chem.* **248**, 4682-4690.

Pollard T.D. (1981) Cytoplasmic contractile proteins. *J. Cell Biol.* **91**, 156s-165s.

Pollard T.D. (1984) Polymerisation of ADP-actin. *J. Cell. Biol.* **99**, 769-777.

Pollard T.D. (1986) Actin and actin-binding proteins. A critical evaluation of mechanisms and functions. *Ann Rev. Biochem.* **55**, 987-1035.

Pollard T.D. (1990) Actin. *Curr. Opin. Cell Biol.* **2**, 33-40.

Pollard T.D., Doberstein S.K. & Zot H.G. (1991) Myosin-1. *Annu. Rev. Physiol.* **53**, 653-681.

Ponte P., Gunning P., Blau H. & Kedes L. (1983) Messenger RNAs for the single copy human sarcomeric alpha actin gene and for the multiple copy cytoskeletal beta and gamma actin genes. *Mol. Cell Biol.* **3**, 1783-1791.

Prochniewicz E. & Yanagida T. (1990) Inhibition of sliding movement of F-actin by crosslinking emphasizes the role of actin structure in the mechanism of motility. *J. Mol. Biol.* **216**, 761-772.

Prochniewicz E., Katayama E., Yanagida T. & Thomas D.D. (1993) Cooperativity in F-actin: Chemical modifications of actin monomers affect the functional interactions of myosin with unmodified monomers in the same actin filament. *Biophys. J.* **65**, 113-123.

Rayment I., Rypniewski W.R., Schmidt-Base K., Smith R., Tomchick D.R., Benning M.M., Winkelmann D.A., Wesenberg G. & Holden H.M. (1993a) Three-dimensional structure of myosin subfragment-1: a molecular motor. *Science* **261**, 50-58.

Rayment I., Holden H.M., Whittaker M., Yohn C.B., Lorenz M., Holmes K.C. & Milligan R.A. (1993b) Structure of the actin-myosin complex and its implications for muscle contraction. *Science* **261**, 58-65.

Reedy M.C., Beall C.J. & Fyrberg E.A. (1989) Formation of reverse rigor chevrons by myosin heads. *Nature* (*London*) **339**, 481-483.

Reedy M.K., Holmes K.C. & Treager R.T. (1965) Induced Changes in orientation of the cross-bridges of glycerinated insect flight muscle. *Nature* (*London*) **207**, 1276-1280.

Rich S.A. & Estes J.E. (1976) Detection of conformational changes in actin by proteolytic digestion: evidence for a new monomeric species. *J. Mol Biol.* **104**, 777-792.

Romans P. & Firtel R. A. (1985) Organization of the actin multigene family of *Dictyostelium discoideum* and analysis of variability in the protein coding regions. *J. Mol. Biol.* **186**, 321-335.

Rouayrenc J.F. & Travers F. (1981) The first step in the polymerisation of actin. *Eur. J. Biochem.* **116**, 73-77.

Rubenstein P.A. (1990) The functional importance of multiple actin isoforms. *BioEssays* **12**, 309-315.

Rubin G.M. & Spralding A.C. (1982) Genetic transformation of *Drosophila* with transposable element vectors. *Science* **218**, 348-353.

Ruppel K.M., Uyeda T.Q.P. & Spudich J.A. (1994) Role of highly conserved lysine 130 of myosin motor domain. *J. Biol. Chem.* **29**, 18773-18780.

Saide J.D., Chin-Bow S., Hogan-Sheldon J., Busquets-Turner L., Vigoreaux J.O.M., Valgiersdottir K. & Pardue M.L. (1989) Characterisation of components of Z-bands in the fibrillar flight muscle of *Drosophila melangaster. J. Cell Biol.* **109**, 2157-2167.

Sanchez F., Tobin S.L., Rdest U., Zulauf E. & McCarthy B.J. (1993) Two *Drosophila* actin genes in detail. Gene structure, protein structure and transcription during development. *J. Mol. Biol.* **163**, 533-551.

Sanger F., Nicklen S. & Coulson A.R. (1977) DNA sequencing with chain-terminating inhibitors. *Proc. Nat. Acad. Sci. USA* **74**, 5463-5467.

Sawin K.E. & Endow S.A. (1993) Meiosis, mitosis and microtubule motors. *Bioessays* **15**, 399-407.

Schröder R.R., Manstein D.J., Jahn W., Holden H., Rayment I., Holmes K.C., & Spudich J.A. (1993) Three-dimensional atomic model of F-actin decorated with *Dictyostelium* myosin S1. *Nature* (*London*) **364**, 171-174.

Schutt C.E. & Lindberg U. (1992) Actin as the generator of tension during muscle contraction. *Proc. Natl. Acad. Sci.* USA **89**, 319-323.

Schutt C.E., Myslik J.C., Rozycki M.D., Goonesekere N.C.W. & Lindberg U. (1993) The structure of crystalline profilin-*B*-actin. *Nature* (*London*) **365**, 810-816.

Schwyter D.H., Kron S.J., Toyoshima Y.Y., Spudich J.A. & Reisler E. (1990) Subtilisin cleavage of actin inhibits *in vitro* sliding movement of actin filaments over myosin. *J. Cell Biol.* **111**, 465-470.

Sellers J.R., Spudich J.A. & Sheetz M.P. (1985) Light chain phosphorylation regulates the movement of smooth muscle myosin on actin filaments. *J. Cell Biol.* **101**, 1897-1902.

Sellers J.R. & Kachar B. (1990) Polarity and velocity of sliding filaments: Control of direction by actin and of speed by myosin. *Science* **249**, 406-408.

Sellers J.R. (1985) Mechanism of the phosphorylation-dependent regulation of smooth muscle heavy meromyosin. *J. Biol. Chem.* **260**, 15815-15819.

Sellers J.R. & Homsher E. (1991) A giant step for myosin. *Current Biology* **1**, 347-349.

Selve N. & Wegner A. (1986) Rate of treadmilling of actin filaments *in vitro*. *J. Mol. Biol.* **187**, 627-631.

Sharp P.M. & Li W.H. (1986) Codon usage in regulatory genes in *Eschericia coli* does not reflect selection for rare codons. *Nuc. Acids Res.* **14**, 7737-7749.

Sharp P.M. & Cowe. E. (1991) Synonymous codon usage in *Saccharomyces cerevisiae*. *Yeast* **7**, 657-678.

Sheetz M.P., Block S.M. & Spudich J.A. (1983) Myosin movement *in vitro*: A quantitative assay using oriented actin cables from *Nitella. Meths. in Enzymology* **134**, 531-544.

Sheetz M.P. & Spudich J.A. (1983) Movement of myosin-coated fluorescent beads on actin cables *in vitro*. *Nature* **303**, 31-35.

Sheetz M.P., Chasan R. & Spudich J.A. (1984) ATP-dependent movement of myosin *in vitro*: Characterization of a quantitative assay. *J. Cell Biol.* **99**, 1867-1871.

Sherman F. & Stewart J.W. (1982) Mutations altering initiation of translation of yeast iso-1-cytochrome C: contrast between eukaryotic and prokaryotic initiation process. *The Molecular Biology of the Yeast Saccharomyces cerevisiae* **2**.

Sheterline P. & Sparrow J.C. (1994) Actin. *Protein Profile* **1.**

Sheterline P., Clayton J.D. & Sparrow J.C. (1995) Actin. *Protein Profile* **2**.

Shortle D., Haber J.E. & Botstein D. (1982) Lethal disruption of the yeast actin gene by integrative DNA transformation. *Science* **217**, 371-373.

Shortle D., Novick P. & Botstein D. (1984) Construction and genetic characterisation of temperature-sensitive mutant alleles of the yeast actin gene. *Proc. Natl. Acad. Sci. USA* **81**, 4889-4893.

Siemankowski R.F., Wiseman M.O. & White H.D. (1985) ADP dissociation from actomyosin subfragment 1 is sufficiently slow to limit the unloaded shortening velocity in vertebrate muscle. *Proc. Natl. Acad. Sci. USA* **82**, 658-662.

Somlyo A. V., Goldman Y., Fugimori T., Bond M., Trentham D. & Somlyo A.P. (1988) Cross-bridge kinetics, cooperativity, and negatively strained cross-bridges in vertebrate smooth muscle. *J. Gen. Physiol.* **91**,165-192.

Sparrow J.C., Drummond D.R., Peckham M., Hennessey E.S. & White D.C.S. (1991a) Protein engineering and the study of muscle contraction in *Drosophila* flight muscles. *J. Cell Sci.* **14**, 73-78.

Sparrow J.C., Reedy M., Ball E., Kyrtatas V., Molloy J.E., Durston J., Hennessey E.S. & White D.C.S. (1991b) Functional and ultrastructural effects of a missense mutation in the indirect flight muscle-specific actin gene of *Drosophila melanogaster*. *J. Mol. Biol.* **222**, 963-982.

Sparrow J.C, Drummond D.R., Hennessey E.S., Clayton J.D. & Lindegaard F.B. (1992) *Drosophila* actin mutants and the study of myofibrillar assembly and function. *Soc. Exp. Biol. Symp.* **46**, 111-129.

Spradling A.C. & Rubin G.M. (1982) Transposition of cloned P element into *Drosophila* gemline chromosomes. *Science* **218**, 341-347.

Spudich J.A., Kron S.J. & Sheetz M.P. (1985) Movement of myosin-coated beads on oriented filaments reconstituted from purified actin. *Nature* **315**, 584-586.

Storti R.V., Horovitch S.J., Scott M.P., Rich A. & Pardue M.L. (1978) Myogenesis in primary cell cultures from *Drosophila melanogaster*: protein synthesis and actin heterogeneity during development. *Cell* **13**, 589-594.

Straub F.B. (1942) Actin. *Stud. Univ. Szeged* **2**, 3-15.

Strzelecka-Golaszewska H., Moraczewska J., Khaitlina S.Y. & Moosakowska M. (1993) Localization of the tightly bound divalent-cation-dependent conformation changes in G-actin using limited proteolytic digestion. *Eur. J. Biochem* **211**, 731-742.

Sutoh K. (1982) Identification of myosin-binding sites on the actin sequence. *Biochemistry* **21**, 3654-3661.

Sutoh K., Ando M., Sutoh K. & Toyoshima Y.Y. (1991) Site-directed mutations of *Dictyostelium* actin: Distruption of a negative charge cluster at the N terminus. *Proc. Natl. Acad. Sci. USA*. **88**, 7711-7714.

Svoboda K., Schmidt C.F., Schnapp B.J. & Block S.M. (1993) Direct observation of kinesin stepping by optical trapping interferometry. *Nature* **365**, 721-727.

Svoboda K. & Block S.M. (1994) Force and velocity measured for single kinesin molecules. *Cell* **77**, 773-784.

Szent-Gyorgi A. (1951) *"Chemistry in muscular contraction" Acad. Press New York 2nd. ed.*, 72-82.

Szilagyi L., Balint M., Streter F.A. & Gergley J. (1979) Photoaffinity labelling with an ATP analog of the N-terminal peptide of myosin. *J. Biochem. Biophys. Res. Comm.* **87**, 936-945.

Szilagyi L. & Lu R. C. (1982) Changes of lysine reactivities of actin in complex with myosin subfragment-1, tropomyosin and troponin. *Biochem. Biophys. Acta* **709**, 204-211.

Takiguchi K., Hayashi H., Kurimoto E. & Higashi-Fujime S. (1990) *In vitro* motility of skeletal muscle myosin and its proteolytic fragments. *J. Biochem.* **107**, 671-679.

Taylor E.W. (1979) Mechanism of actomyosin ATPase and the problem of muscle contraction. *CRC Crit. Rev. Biochem.* **6**, 103-164.

Titus M.A. (1993) Myosins. *Curr. Opin. Cell Biol.* **5**, 77-81.

Toyoshima Y.Y., Kron S.J., McNally E.M., Niebling K.R., Toyoshima C. & Spudich J.A. (1987) Myosin subfragment-1 is sufficient to move actin filaments *in vitro*. *Nature* **328**, 536-539.

Toyoshima Y.Y., Toyoshima C. & Spudich J.A. (1989) Bidirectional movement of actin filaments along tracks of myosin heads. *Nature* **341**, 154-156.

Toyoshima Y.Y., Kron S.J. & Spudich J.A. (1990) The myosin step size: Measurement of the unit displacement per. ATP hydrolyzed in an *in vitro* assay. *Proc. Natl. Sci. USA* **87**, 7130-7134.

Toyoshima Y.Y. (1993) How are myosin fragments bound to nitrocellulose film? Mechanism of myofilament sliding in muscle contraction. *Plenum Press, New York.*

Trayer I.P., Trayer H.R. & Levine B.A. (1987) Evidence that the N-terminal region of A1-light chain of myosin interacts directly with the C-terminal region of actin. A proton magnetic resonance study. *Eur. J. Biochem.* **164**, 259-267.

Umemoto S., Bengur A.R., & Sellers J.R. (1989) Effect of multiple phosphorylations of smooth muscle and cytoplasmic myosins on movement in an *in vitro* motility assay. *J. Biol. Chem.* **264**, 1431-1436.

Umemoto S. & Sellers J.R. (1990) Characterization of *in vitro* motility assays using smooth muscle and cytoplasmic myosins. *J. Biol. Chem.* **265**, 14864-14869.

Uyeda T.Q.P., Kron S.J. & Spudich J.A. (1990) Myosin step size estimation from slow sliding movement of actin over low densities of heavy meromyosin. *J. Mol. Biol.* **214**, 699-710.

Uyeda T.Q.P., Warrick H.M., Kron S.J. & Spudich J.A. (1991) Quantized velocities at low myosin densities in an *in vitro* motility assay. *Nature* **352**, 307-311.

Uyeda T.Q.P. & Spudich J.A. (1993) A functional recombinant myosin II lacking a regulatory light chain-binding site. *Science* **262**, 1867-1870.

Uyeda T.Q.P., Ruppel K.M. & Spudich J.A. (1994) Enzymatic activities correlate with chimaeric substitutions at the actin-binding face of myosin. *Nature* **368**, 567-569.

Vale R.D. & Fumio O. (1990) Protein motors and Maxwell's demons: Does mechanochemical transduction involve a thermal ratchet? *Adv. Biophys.* **26**, 97-134.

Vanderkerckhove J. & Weber K. (1978) Mammalian cytoplasmic actins are the products of at least two genes and differ in primary structure in at least 25 identified positions from sleletal muscle actins. *Proc. Natl. Acad. Sci. USA* **75**, 1106-1110.

Vanderkerckhove J., Leavitt J., Kakunaga T. & Weber K. (1980) Coexpression of a mutant beta-actin and the two normal beta and gamma-cytoplasmic actins in a stably transformed human fibroblast cell line. *Cell* **22**, 893-899.

Vandekerckhove J. & Weber K. (1980) Vegetative *Dictyostelium* cells containing 17 actin genes express a single major actin. *Nature* (*London*) **284**, 475-477.

Vanderkerckhove J. & Weber K. (1984) Chordate muscle actins differ forom invertebrate muscle actins. The evolution of the different vertebrate muscle actins. *J. Mol. Biol.* **179**, 391-413.

Waechter F. & Engel J. (1977) Association kinetics and binding constants of nucleoside triphosphates with G-actin. *Eur. J. Biochem.* **105**, 2811-2816.

Warshaw D.M., Desrosiers J.M., Work S.S. & Trybus K.M. (1990) Smooth muscle myosin cross-bridge interactions modulate actin filament sliding velocity *in vitro*. *J. Cell Biol.* **111**, 453-463.

Waterston R.H., Hirsh D. & Lane T.R. (1984) Dominant mutations affecting muscle structure in *Caenorhabditis elegans* that map near the actin gene cluster. *J. Mol. Biol.* **180**, 473-496.

Wegner A. (1976) Head to tail polymerisation of actin. *J. Mol. Biol.* **108**, 139-150.

Wells J.A. & Yount R.G. (1982) Chemical modification of myosin by active-site trapping of metal-nucleotides with thiol crosslinking reagents. *Meths. Enzymology* **85**, 93-116.

Wertman K.F., Drubin D.G. & Botstein D. (1992) Systematic mutational analysis of the yeast *ACT1* gene. *Genetics* **132**, 337-350.

Winkelmann D.A. & Lowey S. (1986) Probing Myosin head structure with monoclonal antibodies. *J. Mol. Biol.* **188**, 595-612.

Xie X., Harrison D.H., Schlichting I., Sweet R.M., Kalabokis V.N., Szent-Gyorgyi A.G. & Cohen C. (1994) Structure of the regulatory domain of scallop myosin at 2.8Å resolution. *Nature* **368**, 306-368.

Yanadiga T., Nakase M., Nishiyama K & Oosawa F. (1984) Direct observation of motion of single F-actin filaments in the presence of myosin. *Nature* **307**, 58-60.

Yanagida T., Arata T. & Oosawa F. (1985) Sliding of actin filament induced by a myosin crossbridge during one ATP hydrolysis cycle. *Nature* **316**, 366-369.

Yang J.T., Laymon R.A. & Goldstein S.B. (1989) A three-domain structure of kinesin heavy chain revealed by DNA sequence and microtubule binding analyses. *Cell* **56**, 879-889.

Yang J.T., Saxton W.M., Stewart R.J., Raff E.C. & Goldstein S.B. (1990) Evidence that the head of kinesin is sufficient for force generation and motiliy *in vitro. Science* **249**, 42-47.

Yano M. (1978) Observation of steady streamings in a solution of Mg-ATP and acto-heavy meromyosin from rabbit skeletal muscle. *J. Biochem.* **83**, 1203-1204.

Yano M., Yamamoto Y. & Shimizu H. (1982) An actomyosin motor. *Nature* **299**, 557-559.